TRACE CHEMICAL ANALYSIS AND MOLECULAR DYNAMICS UTILISING ULTRAINTENSE FEMTOSECOND LASERS

Paul Graham

Submitted as a thesis for the degree of *Doctor of Philosophy* (Ph.D)

University of Glasgow

Department of Physics and Astronomy

November 2000

ProQuest LLC.
789 East Eisenhower Parkway
P.O. Box 1346
Ann Arbor, MI 48106 – 1346

The long unmeasured pulse of time moves everything. There is nothing hidden that it cannot bring to light, nothing once known that may become unknown. Nothing is impossible.

- Sophocles, Electra

The most beautiful and deepest experience a man can have is the sense of the mysterious. It is the underlying principle of religion as well as of all serious endeavour in art and in science

- Albert Einstein, 1932

The mind is not a vessel to be filled, but a fire to be kindled

- Plutarch

Do not go where the path may lead, go instead where there is no path and leave a trail

- Ralph Waldo Emerson

I had the ambition to go not only farther than man had gone before, but to go as far as it was possible to go

- Captain Cook

To Mum and Dad

- *for everything*

ACKNOWLEDGEMENTS

Further to the thesis dedication, I would like to take this opportunity to express my thanks to the following for their support and assistance:

- My family who have guided and supported me throughout my life and continue to encourage and show me the path

- My supervisors Dr. Ken Ledingham and Dr. Ravi Singhal, who were always there for discussions, advice and help whenever I needed it

- The post-docs within the LIS group, Drs. Hankin and Fang for useful discussions and advice and Mr. McCanny for technical assistance

- Colleagues at RAL, especially Dr. A.J Langley, Dr. P.F Taday and Mr. E. Divall for their excellent support in experiments and imparting their knowledge about the laser system

- The E.P.S.R.C. for a Ph.D studentship

- Miss MacIntyre for her assistance

- My brother Ryan who is always with me, and sister Selena who is much treasured

- Some of my former school teachers who have made an indelible impression on me and who were more than mere teachers

- All my friends, especially Stuart and Steve, who have helped to keep me sane

CONTENTS

ABSTRACT

This thesis is presented for the award of a Ph.D in laser and chemical physics. The principal doctrine of the work seeks to investigate the dynamical response of a variety of small molecules (CS_2, CO_2, N_2O, CH_3I, etc.) in an intense (typically 10^{16} W cm^{-2}) femtosecond (10^{-15} s) linearly polarised laser pulse. The resulting ions are detected in a linear time-of-flight (TOF) mass spectrometer. The polarisation vector of the laser light is rotated with respect to the TOF spectrometer axis and the ion yield measured. In this way the preferred direction of ejection of fragment ions can be determined and the mechanisms responsible can be deduced.

The other experimental investigation concerns using short-pulse (femtosecond duration) intense laser pulses to sensitively and unambiguously detect molecules of interest (dangerous and environmentally sensitive species). By increasing both the intensity and reducing the duration of the laser light the method, termed femtosecond laser mass spectrometry (FLMS), is shown to be a universal and powerful analytical tool. The sensitivity is achieved via complete ionisation of all species within the ionisation region of the laser pulse and unambiguous identification is achieved via rapid by-passing of dissociative states of the parent species.

THESIS SUMMARY

The work presented herein was undertaken at the prestigious Rutherford Appleton research laboratory (RAL) in Didcot, Oxfordshire. During the course of the work the performance of the femtosecond laser facility at RAL was updated, with a view to increase laser intensity and improve experimental capabilities for users. The laser was 'coupled' to a linear time-of-flight (TOF) mass spectrometer, in order to detect ions that result from the interaction of molecules studied with the laser beam. As mentioned in the abstract, the experiments concerned both the molecular dynamics of this interaction, as well as a demonstration of the universality, sensitivity and unambiguity of identification of the FLMS technique at sufficiently high laser intensities and short pulse durations.

The first chapter in the thesis focuses on presenting to the reader not only the concepts that will be needed to interpret and understand the later results chapters, but also to review the concepts and theories that have developed from previous work in the field of intense laser/matter interactions. The main source of information and inspiration for this chapter has come from the author's extensive survey of the literature.

The second chapter details the experimental apparatus, layout and techniques. The chapter starts off with a thorough description of short-pulse lasers in general and their origins and evolution. The separate constituent components of femtosecond lasers are then explained, before describing the RAL femtosecond laser system in detail. The optical layout in the target chamber and the TOF spectrometer are then described along with an explanation of experimental techniques adopted to acquire data.

The results chapters 3 to 6, present data obtained during various experimental runs at RAL over the course of the author's Ph.D training (3 years) and conclusions based on these results. Chapter 3 is unique in these experimental chapters in that it is mainly concerned with chemical analysis and identification using intense ultra-short laser pulses; whereas chapters 4, 5 and 6 are more to do with the mechanisms involved when various

small molecules interact with such pulses. In particular, the origin of the preferred direction of ejection of fragment ions produced as a consequence of Coulomb explosion of the parent transient ion.

The final chapter looks to the future for inspiration and tries to conjecture the further development and evolution of this exciting line of research. This includes suggestions for future experiments and possible applications that may arise from this.

The experimental work in the thesis was mainly carried out in the context of a team effort between the LIS group and the workers at RAL. The LIS group were solely responsible for setting up the target area and performing the experiments, with the author heavily involved in this; whilst the RAL workers were mainly responsible for maintaining the laser performance and providing us with what was needed for the experiments to be successful. The author also received first-hand knowledge of the operation of the laser, whenever possible. The author also had the opportunity to organise, design and perform experiments, especially those in chapter 3 and 5.

The research work required for chapters 1, 2 and 7, as well as the analysis and interpretation of the results presented in chapters 3 to 6 were completely the work of the author.

PUBLICATIONS AND PRESENTATIONS

PAPERS

[1] **Dissociative ionisation and angular distributions of CS_2 and its ions**

P. Graham, K.W.D. Ledingham, R.P. Singhal, D.J. Smith, S. Wang, T. McCanny, H.S. Kilic, A.J. Langley, P.F. Taday and C. Kosmidis

1998 9th Int. Symp. Resonance Ionisation Spectroscopy (RIS '98) Conf. Proc. (AIP Conf. Proc. 454) ed. J C Vickerman, I Lyon, N P Lockyer and J E Parks (Woodbury, NY: American Institute of Physics) p 331

[2] **An investigation of the angular distributions of fragment ions arising from the linear CS_2 and CO_2 molecules**

P. Graham, K.W.D. Ledingham, R.P. Singhal, T. McCanny, S.M. Hankin, X. Fang, D.J. Smith, C. Kosmidis, P. Tzallas, A.J. Langley and P.F. Taday

1999 J. Phys. B: At. Mol. Opt. Phys., **32**, 5557-5574

[3] **The angular distributions of fragment ions from labelled and unlabelled N_2O in intense laser fields**

P. Graham, K.W.D. Ledingham, R.P. Singhal, T. McCanny, S.M. Hankin, X. Fang, P. Tzallas, C. Kosmidis, P.F. Taday and A.J. Langley

2000 J. Phys. B: At. Mol. Opt. Phys., **33**, 3779-3794

[4] **The behaviour of polyatomic molecules in intense laser beams**

K.W.D. Ledingham, R.P. Singhal, D.J. Smith, T. McCanny, **P. Graham**, H.S. Kilic, W.X. Peng, S.L Wang, A.J. Langley, P.F. Taday and C. Kosmidis

1998 J. Phys. Chem., **102**, 3002-3005

[5] **Dissociation ionisation and angular distributions of CS_2 using ultraintense laser beams**

P. Graham, K.W.D. Ledingham, R.P. Singhal, D.J. Smith, T. McCanny, A.J. Langley, P.F. Taday

1998 Rutherford Annual Report 1997-1998, RAL Report no. RAL-TR 1998-080, 117-118

[6] **An investigation of polyatomic molecules in intense infrared laser beams**

K.W.D. Ledingham, R.P. Singhal, D.J. Smith, T. McCanny, **P. Graham**, H.S. Kilic, W.X. Peng, S.L Wang, A.J. Langley, P.F. Taday and C. Kosmidis

1998 Rutherford Annual Report 1997-1998, RAL Report no. RAL-TR 1998-080, 101-103

[7] **Vulcan used as a plasma accelerator for nuclear reactions**

K.W.D. Ledingham, T. McCanny, **P. Graham**, X. Fang, R.P. Singhal, J. Magill, A.J. Creswell, D.C.W. Sanderson, R. Allott, B. Kennedy, D. Neely, P.A. Norreys, M. Santala, E. Clark, M. Zepf, I. Watts, K. Krushelnick, M. Tatarakis, A.E. Dangor, A. Machecek, J.S. Wark

1998 Rutherford Annual Report 1997-1998, RAL Report no. RAL-TR 1998-080, 41-43

[8] **Laser induced nuclear reactions**

K.W.D. Ledingham, T. McCanny, **P. Graham**, X. Fang, R.P. Singhal, J. Magill, A.J. Creswell, D.C.W. Sanderson, R. Allott, D. Neely, P.A. Norreys, M. Santala, E. Clark, M. Zepf, I. Watts, K. Krushelnick, M. Tatarakis, A.E. Dangor, A. Machecek, J.S. Wark

1998 9th Int. Symp. Resonance Ionisation Spectroscopy (RIS '98) Conf. Proc. (AIP Conf. Proc. 454) ed. J C Vickerman, I Lyon, N P Lockyer and J E Parks (Woodbury, NY: American Institute of Physics) p 331

[9] **Multiply charged ions from aromatic molecules following irradiation in intense laser fields**

K.W.D. Ledingham, D.J. Smith, R.P. Singhal, T. McCanny, **P. Graham**, H.S. Kilic, W.X. Peng, A.J. Langley, P.F. Taday and C. Kosmidis

1999 J. Phys. Chem., **103**, 2952-2963

[10] **Observation of a highly directional gamma-ray beam from ultrashort, ultraintense laser pulse interaction with solids**

P.A. Norreys, M. Santala, E. Clark, M. Zepf, I. Watts, F.N. Beg, K. Krushelnick, M. Tatarakis, A.E. Dangor, X. Fang, **P. Graham**, T. McCanny, R.P. Singhal, K.W.D. Ledingham, A.J. Creswell, D.C.W. Sanderson, J. Magill, A. Machecek, J.S. Wark, R. Allott, B. Kennedy, D. Neely

1999 Physics of Plasmas, **6**, 2150

[11] **Laser induced fission and nuclear reactions**

R.P. Singhal, K.W.D. Ledingham, T. McCanny, **P. Graham**, X. Fang, J. Magill, A.J. Creswell, D.C.W. Sanderson, R. Allott, D. Neely, P.A. Norreys, M. Santala, E. Clark, M. Zepf, I. Watts, K. Krushelnick, M. Tatarakis, A.E. Dangor, A. Machecek, J.S. Wark

Third international workshop on the fast ignition of fusion targets
1999 Technical Report RAL-TR-1998-085 January 1999

[12] **The onset of Coulomb explosion in polyatomic molecules**

D.J. Smith, K.W.D. Ledingham, R.P. Singhal, T. McCanny, **P. Graham**, H.S. Kilic, P. Tzallas, C. Kosmidis, A.J. Langley, P.F. Taday

1999 Rapid Commun. Mass Spectrom., **13**, 1366-1373

[13] **Uniform molecular analysis using femtosecond laser mass spectrometry**

X. Fang, K.W.D. Ledingham, **P. Graham**, D.J. Smith, T. McCanny, R.P. Singhal, A.J. Langley, P.F. Taday

1999 Rapid Commun. Mass Spectrom., **13**, 1390-1397

[14] **Unusual fragmentation patterns from dissociation of some small molecules**

P. Graham, X. Fang, K.W.D. Ledingham, R.P. Singhal, T. McCanny, D.J. Smith, C. Kosmidis, P. Tzallas, A.J. Langley, P.F. Taday

Accepted for publication: Laser and Particle Beams, **18**, no.3

[15] **Unusual angular distribution anisotropies of fragment ions from the dissociation of N_2O and H_2S**

P. Graham, K.W.D. Ledingham, R.P. Singhal, T. McCanny, X. Fang, A.J. Langley, P.F. Taday, C. Kosmidis, P. Tzallas,

1999 Rutherford Annual Report 1998-1999, RAL Report no. RAL-TR 1999-062, 89-91

[16] **On the multielectron disociative ionisation of some cyclic aromatic molecules induced by strong laser fields**

P. Tzallas, C. Kosmidis, K.W.D. Ledingham, R.P. Singhal, **P. Graham**, T. McCanny, S.M. Hankin, P.F. Taday, A.J. Langley

2000 J. Phys. Chem. (Accepted for publication)

[17] **Coulomb explosion in aromatic molecules and their deuterated derivatives**

P. Tzallas, C. Kosmidis, **P. Graham**, K.W.D. Ledingham, T. McCanny, R.P. Singhal, S.M. Hankin, P.F. Taday, A.J. Langley

2000 Chem. Phys. Lett. (Accepted for publication)

[18] **Uniform molecular analysis using femtosecond laser mass spectrometry**

X. Fang, K.W.D. Ledingham, **P. Graham**, D.J. Smith, T. McCanny, R.P. Singhal, A.J. Langley, P.F. Taday

1999 Rutherford Annual Report 1998-1999, RAL Report no. RAL-TR 1999-062, 85-88

[19] **An investigation of the angular distributions of fragment ions from Coulomb explosion of the linear CS_2 molecule**

P. Graham, K.W.D. Ledingham, R.P. Singhal, T. McCanny, S.M. Hankin, X. Fang, D.J. Smith, C. Kosmidis, P. Tzallas, P.F. Taday, A.J. Langley

1999 Rutherford Annual Report 1998-1999, RAL Report no. RAL-TR 1999-062, 95-98

[20] **The angular distributions of fragment ions arising from tetrahedral CH_3I**

P. Graham, K.W.D. Ledingham, R.P. Singhal, T. McCanny, S.M. Hankin, X. Fang, P.F. Taday, A.J. Langley, C. Kosmidis, P. Tzallas

2000 Rutherford Annual Report 1999-2000, RAL Report no. RAL-TR 2000

[21] **Angular distributions of fragment ions arising from tetrahedral CH_3I and isomer identification using intense laser fields**

P. Graham, K.W.D. Ledingham, R.P. Singhal, S.M. Hankin, T. McCanny, X. Fang, P.F. Taday, A.J. Langley, C. Kosmidis

Submitted to Laser and Particle Beams (ULIA-2 Conf. Proc.)

[22] **On the fragment ion angular distributions arising from a tetrahedral molecule**

P. Graham, K.W.D. Ledingham, R.P. Singhal, S.M. Hankin, T. McCanny, X. Fang, P.F. Taday, A.J. Langley, C. Kosmidis

Submited to J. Phys. B: At. Mol. Opt. Phys.

POSTERS

[1] **The ionisation and photofragmentation of CS_2 using intense laser beams**

P. Graham, K.W.D. Ledingham, R.P. Singhal, D.J. Smith, S. Wang, T. McCanny, A.J. Langley and P.F. Taday

Presented at the 9th International symposium on **Resonance Ionisation Spectroscopy** (RIS '98), 21st-25th June, UMIST, Manchester, 1998
Presented at the **1st Symposium on Physics Research and R&D** (PRR&D '98) CLRC Rutherford Appleton Laboratory, Chilton, Didcot, Oxon., 13th November, 1998

[2] **Some unusual angular distributions of small molecules**

P. Graham, K.W.D. Ledingham, R.P. Singhal, T. McCanny, A.J. Langley and P.F. Taday

Presented at the **1st Ultraintense Laser Interactions and Applications** (ULIA-1) International EuroConference, Elounda, Crete, Greece, May 7 - 11, 1999;

[3] **Fragment ion angular distributions from N_2O**

P. Graham, K.W.D. Ledingham, R.P. Singhal, T. McCanny, A.J. Langley and P.F. Taday

Presented at the **2nd Symposium on Physics Research and R&D** (PRR&D '99) CLRC Rutherford Appleton Laboratory, Chilton, Didcot, Oxon., 12th November, 1999;
Presented at the **Scottish chapter meeting of the Laser and Electro-Optics Society** (LEOS 2000) St. Andrews University, St. Andrews, Fife, Scotland, 23rd August, 2000

[4] **Investigation of quantitative analysis of atoms and molecules using femtosecond laser mass spectrometry**

X. Fang, K.W.D. Ledingham, **P. Graham**, T. McCanny, R.P. Singhal, S.M Hankin, A.J. Langley and P.F. Taday

Presented at the **2nd Symposium on Physics Research and R&D** (PRR&D '99) CLRC Rutherford Appleton Laboratory, Chilton, Didcot, Oxon., 12th November, 1999

TALKS

"Fragment ion distributions from tetrahedral CH_3I subjected to intense femtosecond laser beams"

P. Graham, K.W.D. Ledingham, R.P. Singhal, T. McCanny, S.M. Hankin, X. Fang, P.F. Taday, A.J. Langley, C. Kosmidis

Presented at the **2nd Ultraintense Laser Interactions and Applications** (ULIA-2) International EuroConference, Pisa, Italia, 28th September-03rd October, 2000

LIST OF FIGURES AND TABLES

Chapter 1

Chapter 2

Chapter 3

Chapter 1

Introduction and background Theory

1.1 Chapter Overview

This chapter focuses on discussing the relevant research that has been carried out in the field of intense laser/matter interactions utilising femtosecond lasers. A discussion of the important concepts and principles involved and the motivation behind performing the experiments detailed in later chapters, will be given. This will facilitate the interpretation of the experimental results and will set an overall context in which some conclusions can be drawn from the results presented.

1.2 Molecular responses to intense laser fields

All results presented in this thesis are obtained from experiments performed utilising the intense (~ 10^{15}-10^{16} W cm^{-2}) femtosecond (1fs = 10^{-15} s) Ti:S laser situated at the Rutherford Appleton Laboratory (RAL) in Didcot, Oxfordshire (see chapter 2). Thus, as the bandwidth from a femtosecond laser is much greater than the rovibrational levels in a molecular system, resonance effects can be neglected. Furthermore, at the high laser intensities used here, perturbation theory no longer applies and the laser field/molecule system must be described semi-quantum mechanically. Described below are various effects that the electromagnetic field of an ultraintense laser may induce upon a molecular system.

1.2.1 Multiphoton and Tunneling ionisation

When atomic or molecular (gas-phase) samples are subjected to a femtosecond laser field, the valence electrons may be stripped off to form ions. This process may be repeated several times to produce highly-charged ions that are usually unstable. The cross-sections for photons from the laser to eject electrons are very small and decrease progressively the more electrons that are being stripped off. However, the photon flux at laser intensities of the order of 10^{15}-10^{16} W cm^{-2} is sufficiently high that all molecules in the laser/matter interaction region attain highly-charged states. Depending on the ionisation mechanism, electrons may be stripped off one-by-one (sequential ionisation) or simultaneously (non-sequential ionisation). This largely depends on the laser pulse duration and intensity as well as on the ionised system itself.

For long laser pulse durations and smaller intensities, the ionisation will proceed in a multi-photon process. This is shown in figure 1.1. It is best to think of this in terms of a large number of photons impinging on the molecules in the interaction region. The photon flux is such that the molecule absorbs several photons at the operating wavelength of the laser (here at infrared), which may induce it first to an excited state and then to the continuum state. The ionisation rate may be calculated using a rate

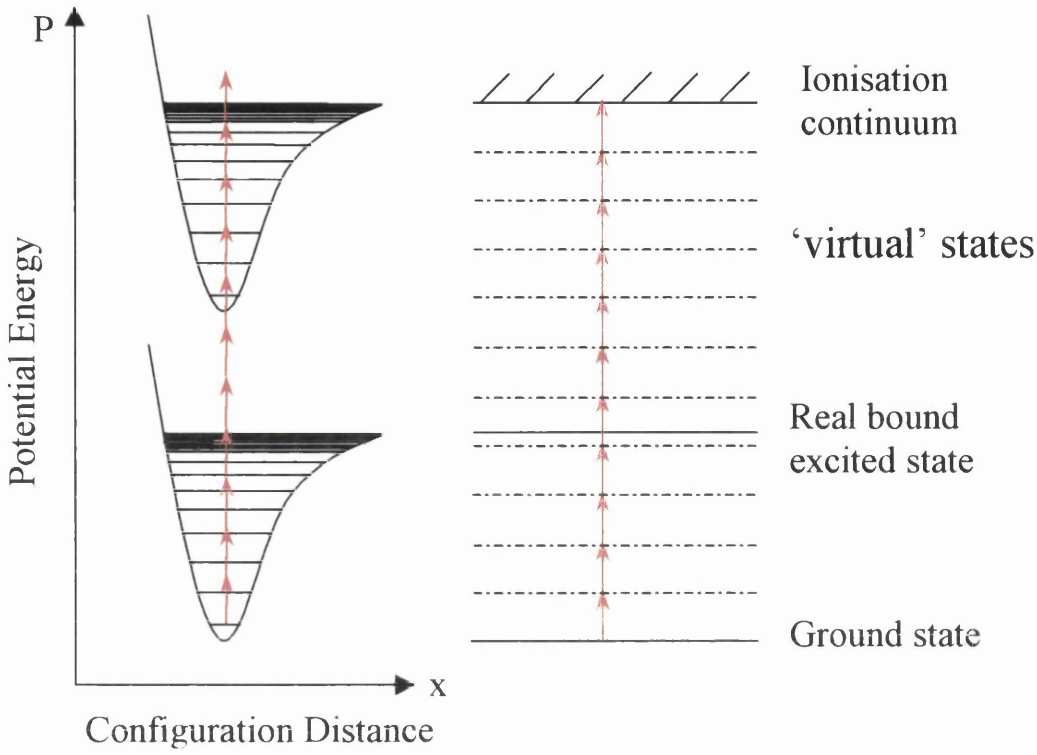

Figure 1.1 Pictorial representation of multiphoton ionisation (MPI)

equation model [1], as long as the photon absorption and ionisation cross-sections as well as intermediate-state lifetimes are known. When using femtosecond lasers, the intermediate states do not necessarily have to exist but may be 'virtual' states. This is due to the femtosecond pulse duration being much shorter than the virtual state lifetimes and so a rapid up-pumping through virtual states is possible. This property has been manipulated to facilitate trace chemical detection of various thermally labile molecules, which are of environmental concern [2, 3].

At longer wavelengths and higher intensities the multi-photon description breaks down and a tunnel ionisation picture begins to dominate. In this mechanism it is better to think of the laser electric field strength superimposed onto the molecular potential energy surface. This is shown in figure 1.2. In the tunneling regime, the laser field strength is sufficient to lower the barrier to ionisation such that the electron can tunnel through to the continuum. The rate of ionisation has been modeled with varying degrees of success. The Ammosov-Delone-Krainov (ADK) model accurately fits experimental results for strong-field ionisation in atomic systems [4-6] and small molecules near their equilibrium configuration [7, 8]. Several theories exist for molecular systems undergoing tunneling [9, 10].

The criterion for distinguishing MPI from tunneling ionisation is the Keldysh [11] adiabaticity parameter, γ. It is the ratio of the angular frequency of the optical laser field to the tunneling rate through the barrier at the peak field strength. It is given by [12]:

$$\gamma = \frac{\omega_L}{\omega_T} = \sqrt{\frac{E_0}{2U_p}} = \left[\frac{E_0}{1.87\times10^{-19} I\lambda^2}\right]^{1/2} \qquad \text{(Eq. 1.1)}$$

where ω_L is the laser field angular frequency, ω_T is the tunneling rate at peak field strength, E_0 is the field-free binding energy of the electron (in eV), I is the laser intensity (in W cm^{-2}), λ is the laser light wavelength (in μm) and U_p is the ponderomotive potential of the laser (in eV). The ponderomotive potential is equivalent

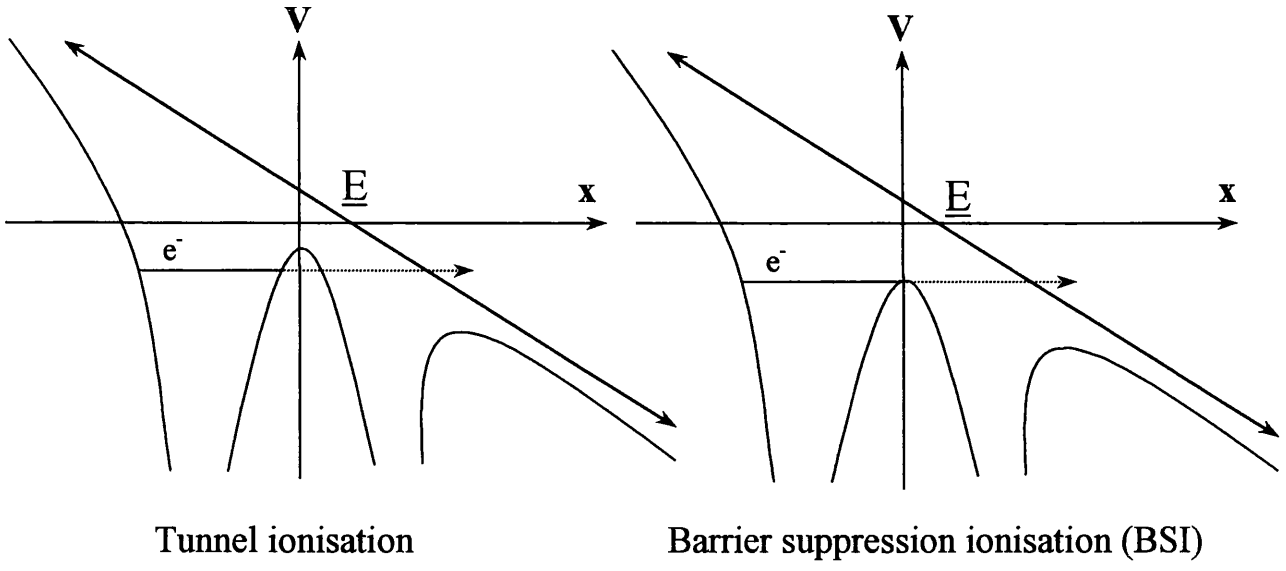

Figure 1.2 Pictorial representation of the tunneling ionisation mechanism

to the average kinetic energy imparted to an electron in the laser field, and is given by [13, 14]:

$$U_P = \frac{I}{4\omega_L^2} = \frac{e^2E^2}{4m_e\omega_L^2} = 9.33\times10^{-14} I\lambda^2 \qquad \text{(Eq. 1.2)}$$

where I is the laser intensity, E is the peak electric field amplitude, and e and m_e are the electronic charge and mass, respectively. The first term is integrated over time and space, but is conventionally written as above. For $\gamma \leq 0.5$, a tunneling regime is dominant, and for $\gamma > 1$, a MPI process is dominant. For even greater laser field strengths (and longer wavelengths), the barrier to ionisation can be completely suppressed leading to a barrier suppression ionisation (BSI) model [15], figure 1.2.

At the other extreme, the maximum intensity an atom or molecule can withstand and not be ionised is given by [13]:

$$I_{thr} = \frac{cE}{2}\left[\frac{4\pi E}{e^3}\right]^2 \frac{E_0^4}{16} \qquad \text{(Eq. 1.3)}$$

where E_0 is the ionisation potential and c is the speed of light in free-space. An intensity that is slightly higher than this value will be sufficient to strip the first valence electron from the atom/molecular system at the laser pulse peak. As the intensity rises still further, more electrons can be stripped off on the rising-edge of the pulse in addition to the pulse peak.

The development of ultraintense lasers of femtosecond pulse duration can generate electric field strengths of comparable magnitude to those that bind atoms together. Therefore, the barrier to ionisation is lowered sufficiently that either electrons can pass directly over, termed barrier suppression ionisation (BSI) [15], or else can tunnel through the barrier to the continuum (tunnel ionisation). Therefore, binding electrons can be ejected. This will lead to a molecular photo-dissociation process in the singly-

charged parent. Furthermore, the Coulombic repulsion between 2-or-more charged ions that comprise the multiply-charged parent will also lead to dissociation via a Coulomb explosion process. This model is termed multi-electron dissociative ionisation (MEDI) [16, 17].

1.2.2 Molecular photodissociation

Molecular interactions with an intense laser are more complicated than such interactions with an atomic system, as the molecule has more degrees of freedom, i.e rotational and vibrational. When a molecule is ionised, the ions may become unstable and fragment. This process is largely molecule specific, with some molecular ions possessing an unbound potential, particularly for highly charged states. The matter is further complicated by curve-crossings, which place the ions in a bound state in the dissociative limit. Depending on the laser field strength, the curve-crossings may be avoided via the Stark shift. This is shown in figure 1.3. The laser-induced Stark shift is given by the dot product: $U_S = \pm\mu.E$, where E is the electric field and μ is the sum of induced and permanent electric dipole moments, and results in the lower energy curve being shifted down in energy and the upper level shifting upwards in energy.

Two possible theories have been advanced for the ionisation mechanism. One is the 'shake-off' model, whereby an electron is ejected sufficiently rapidly that the molecule loses another in its wake. High charge-states may be achieved in this manner, leading to highly ionised parent or fragment ions. An alternative model is electron rescattering, in which an electron is ejected during the first half of the optical cycle of the laser pulse and is turned round back towards the same molecule where it originated from during the second half of the cycle. Here it may collide with the molecule and strip a further electron from it. This can only occur with a linearly polarised light pulse, since for circular or elliptical polarisation, the electron misses the molecule. Both these processes may be classed as non-sequential ionisation, occurring within one optical cycle. Both of these mechanisms are represented pictorially in figure 1.4.

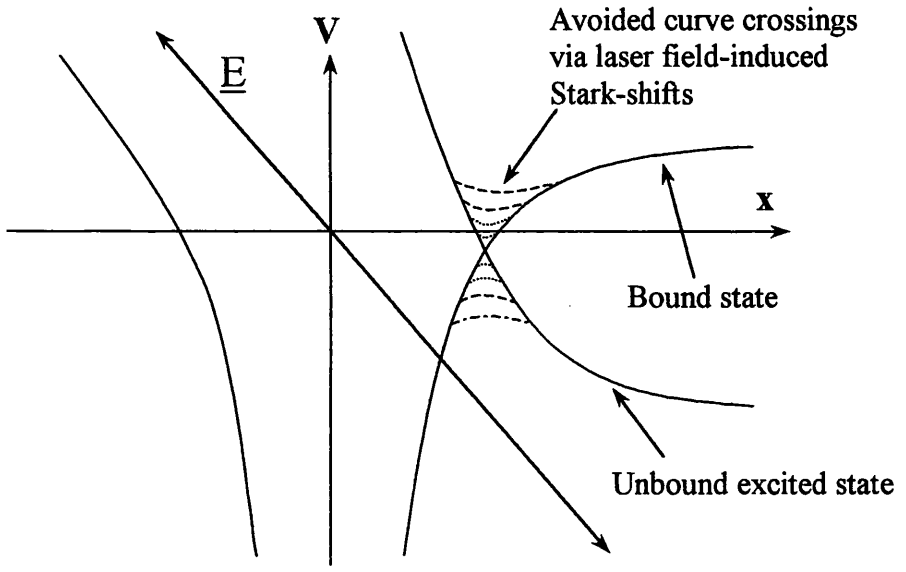

Figure 1.3 Diagram showing potential energy curves and avoided curve-crossings, via laser-induced Stark-shifts

a)

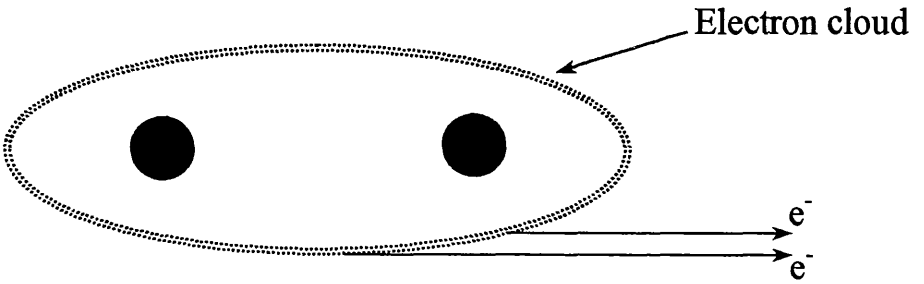

'shake-off' model of electron ejection to produce multiply ionised molecular ions

b)

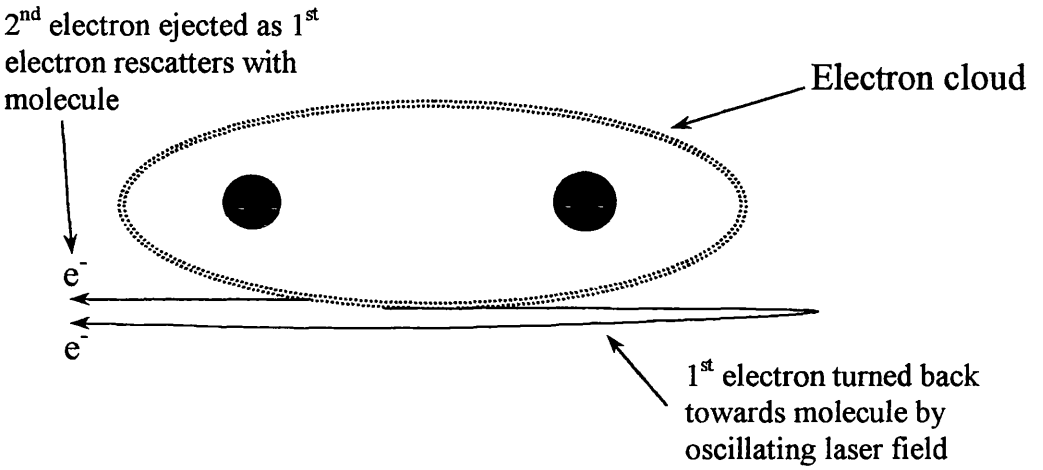

're-scatter' model of electron ejection, whereby the 1st electron re-scatters with molecule to eject further electrons

Figure 1.4 Pictorial representation of a) the 'shake-off' and b) electron re-scattering mechanism of electron ionisation

Utilising femtosecond laser pulses allows the ionisation to proceed very rapidly before significant dissociation can take place. This has been termed a 'ladder-climbing' process. This is in contrast to results obtained using nanosecond lasers, where dissociation usually precedes ionisation of the molecule and 'ladder-switching' results [2, 3]. The various ionisation stages may take place via vertical transitions (Franck-Condon principle, i.e. the molecular internuclear separation remains at the equilibrium distance), to Coulomb potential curves as shown in figure 1.5. This is an diabatic process, which means that the molecule does not have sufficient time to adjust itself to the energy it is subjected to in the interaction with the laser pulse. This is a kind of vibrational trapping process [12]; i.e. the vibrational degree of freedom cannot change significantly from the small oscillations about the equilibrium. This may be the case particularly for rigid molecules with double and triple bonds such as nitrous oxide N≡N=O [18-20], or an inherently rigid structure such as benzene [21].

The alternative to this model is the charge-resonance-enhanced ionisation (CREI) [14] or MEDI mechanism [22]. In this picture, the parent precursor is able to attain a singly or doubly ionised state. During the course of this ionisation, the molecule undergoes a adiabatic elongation to typically twice the equilibrium bond length [23]. At this lengthened internuclear separation, which is often termed the critical distance R_c, the ionisation rate increases significantly such that highly ionised transient states of the molecule are attained. This enhancement of the ionisation rate is achieved through a lowering of the barrier and hence the electrons may escape over the top, similar to the BSI mechanism, figure 1.6. The enhancement of the dissociative ionisation only occurs for those molecules that have their main geometric axis (or molecular bonds) oriented collinearly with the polarisation vector of a linearly polarised laser beam [18, 24, 25]. If the molecular axis and polarisation vector are orthogonal to each other, the ionisation is 'atom-like' with an effective ionisation potential equal to the energy needed to ionise in this configuration. This elongation to large internuclear separation has been observed previously, principally in molecular hydrogen where it is termed 'bond-softening'. This bond-softening process was recently resolved on a sub-pulse-duration time-scale by Posthumus et al. [26], where it was concluded that it occurred on the falling-edge of the

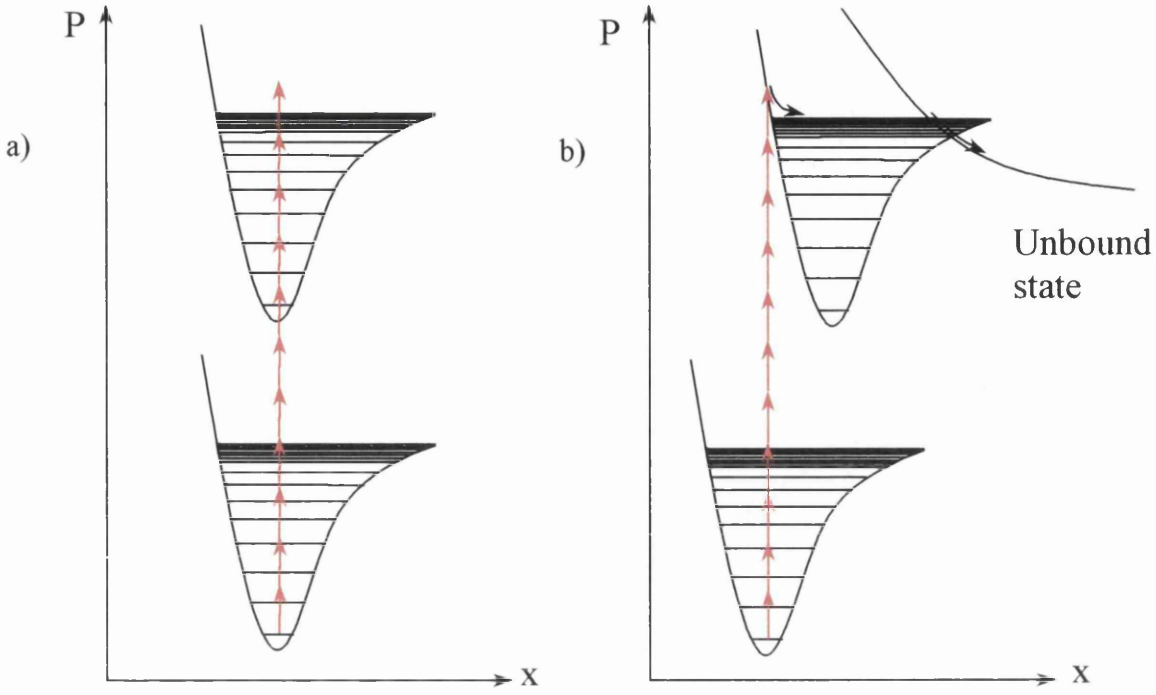

Ionisation at equilibrium internuclear distance (Franck-Condon principle)

Ionisation of elongated molecule, possibly exciting to unbound state of molecular ion

Figure 1.5 Ionisation taking place at a) the Franck-Condon regime and b) elongated configurations

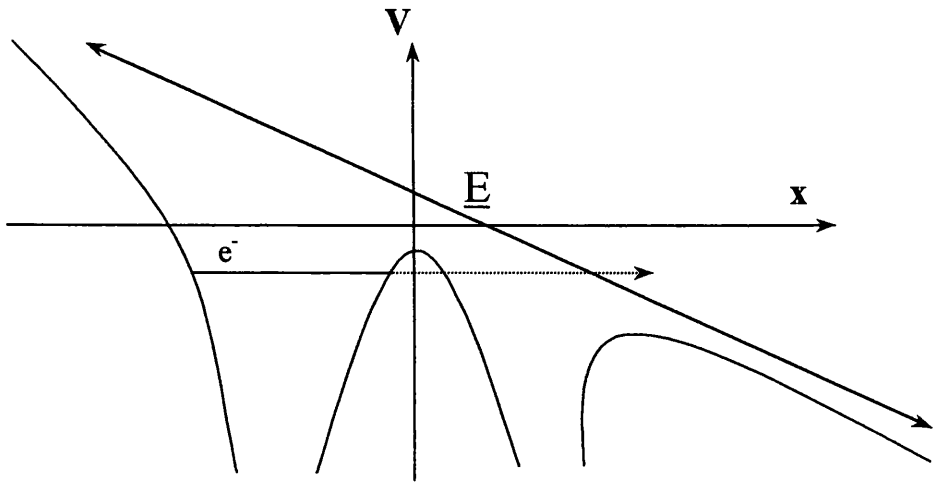

Tunnel ionisation at equilibrium internuclear distance

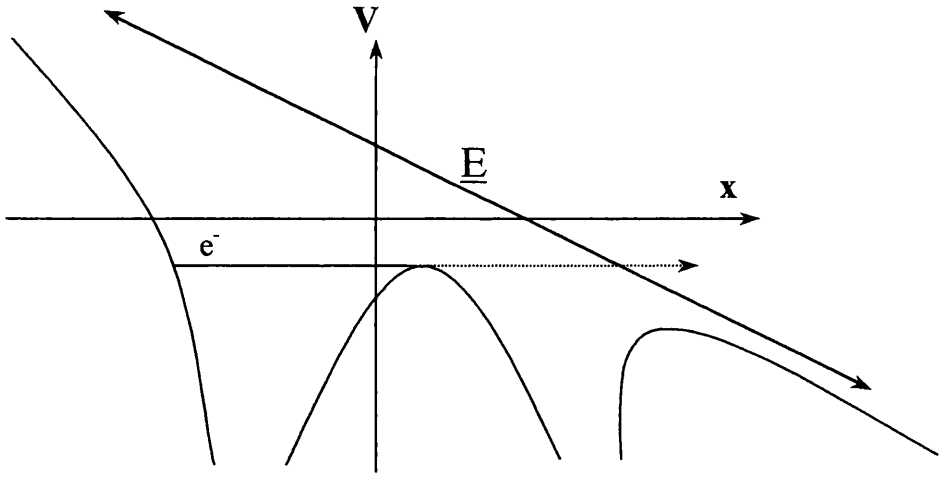

Barrier suppression ionisation at elongated molecular configuration

Figure 1.6 Diagram showing that the electron can escape over the barrier to ionisation when the molecular bond stretches to a 'critical' internuclear distance

pulse whereas Coulomb explosion occurred on the rising-edge of the laser pulse. There is some experimental evidence it occurs for some small molecules such as N_2, H_2O and CO_2 [27, 28]. Molecular elongation was not observed for N_2O [18], CS_2 [24] and CH_3I [29], or benzene [21], however.

The critical internuclear distance is determined by calculating the fragment ion kinetic energy release and comparing with the energy that would be released assuming dissociation along a purely Coulombic potential at the equilibrium internuclear distance. The experimental kinetic energy values are determined from the splitting observed in fragment ion peaks in mass spectra. The splitting arises due to the Coulomb explosion of multiply-charged parent ions along the time-of-flight (TOF) mass spectrometer axis, which give rise to fragment ions that travel initially forward towards and initially backwards away from the detector situated at the end of the drift-tube (see chapter 2). An extraction field applied between two electrodes is able to turn the backward travelling fragments around towards the detector and the difference in time-of-flight between the fragment ions results in the split mass peak. The calculation of the kinetic energy is shown in the appendix to chapter 5. There is a possibility that ejected electrons can 'screen' the exploding fragment ions, but this is not thought to significantly affect the Coulomb repulsion.

The experimental evidence of CREI is hence the comparison of the kinetic energy to the Coulomb energy, which has been shown to be a constant value. It is typically half the Coulomb energy, independent of charge-state of the molecule and laser parameters [30].

However, if laser pulses are used that have rise times that are fast compared with the nuclear vibrational period, then the electrons will be stripped off in a time-scale that is short in comparison to the vibrational frequency of the nuclear wave function. The fragment ions will be hence imparted with energies near the Coulomb value. Pulses with longer rise times will lead to fragmentation nearer the critical distance. The internuclear distance at which the molecule will dissociate will also, to some extent, depend on the molecular structure. For example, it has been determined that the energy

of fragment ions arising from nitrous oxide N_2O [18, 19] and from benzene [21] is close to the Coulomb value and hence the molecule dissociates at the equilibrium internuclear distance. The dissociation occurring at the equilibrium internuclear distances for both nitrous oxide and benzene may be due to the double and triple bonds in N_2O and the inherently rigid structure of the benzene ring. These features may make it difficult to ionise bonding electrons and hence the molecules do not change their structure significantly prior to dissociation.

1.2.3 Molecular alignment and enhanced ionisation

1.2.3.1 Photofragment ion angular distribution

When an intense linearly polarised light beam illuminates a molecule, its structure may be distorted somewhat when the laser electric field is superimposed on the molecular potential, as shown in figure 1.2. As electrons are stripped off from the molecule as the laser intensity increases, the electronic structure becomes more polarised along the field direction, inducing a polarisability in the molecule. This polarisation of electronic charge within the molecule is responsible for the resulting induced dipole moment, which is given by the product of the charge of the ion and the internuclear distance, i.e. $\mathbf{p} = q\mathbf{l}$. This dipole moment couples to the laser electric field and is described by the interaction potential $V_\theta(\theta)$, given by [31]:

$$V_\theta(\theta) = -(1/2)\varepsilon^2\left(\alpha_{//}\cos^2(\theta) + \alpha_\perp \sin^2(\theta)\right) \qquad \text{(Eq 1.4)}$$

where ε is the average electric field strength, $\alpha_{//}$ and $\alpha_\perp$ are the parallel and perpendicular components of the molecular polarisability, respectively and θ is the angle between the polarisation vector and the molecular bond. The field thus exerts a torque on the molecule that *tends* to align the molecular axis in the field direction. This torque is given by $\Gamma = p\varepsilon\sin(\theta)$. Thus, molecular alignment is governed by the

interaction of the laser electric field vector with the molecular polarizability, the anisotropy of which arises from the laser-induced dipole moment.

This alignment of molecules with the polarisation vector of an intense laser pulse is general for both polar and non-polar molecules. However, since the permanent dipole moment has a $\cos(\theta)$ dependence it averages out over the laser cycle and plays no role in the alignment process. The laser-induced dipole moment on the other hand, has a $\cos^2(\theta)$ dependence, and as Eq. 1.4 shows, is responsible for aligning the molecule with the field.

The alignment of both polar and non-polar molecules in strong non-resonant laser fields has been studied both experimentally and theoretically [31-42]. A formula that has been previously used in semi-quantum mechanical treatments [31, 32] of the aligning of molecules is:

$$I(\theta) = (1/4\pi)[1 + \beta P_2 \cos(\theta)] \qquad \text{(Eq. 1.5)}$$

where $I(\theta)$ is the ion-signal as a function of angle between the laser field and molecular axis, $P_2\cos(\theta)$ is the second-order Legendre polynomial and β is a parameter of anisotropy whose value tends to +2 for excitation parallel to the field and (–1) for a perpendicular excitation. For an oblate molecule, i.e. one in which $\alpha_{//} > \alpha_{\perp}$, the molecule aligns along the field, while a prolate molecule ($\alpha_{//} < \alpha_{\perp}$) will align orthogonally to the laser field.

Since the polarisability of the molecule will increase as the ionisation-state of the transient molecule increases, the signature that the molecule is actually aligning in the laser field is that the anisotropy parameter increases with charge-state. If the angular distributions of fragment ions are plotted, they can be fitted to a Gaussian or $\cos^n(\theta)$ function [43]. The resulting increase in torque on molecules with multiple charge-state will tend to align them more strongly with the field. This will be apparent as a narrowing in the ion angular distribution, as n will increase in this case. For laser-

induced alignment of H_2 for example, Posthumus et al. [43] show a good fit to the experimental data using n = 22. The time required to align a small molecule in such an intense laser field will become shorter than the field-free rotational time for the molecule, as the torque increases. Hence it may be possible to control the alignment and orientation of some small molecules using an intense linearly polarised fs laser field. Due to an increase in the moment of inertia associated with larger molecules, it may be unlikely that the molecule has sufficient time to align within a fs laser pulse even at high laser intensities.

The polarisability of a molecule will also be increased if it elongates in the laser field, before fragmenting. Therefore, the aligning torque will be stronger at this extended internuclear distance, as the induced dipole moment will be greater. This is particularly so at the critical internuclear distance, at which the ionisation-rate is a maximum. The enhancement of the ionisation hence leads to higher ionisation-states and a further increase of the aligning effect, via a concomitant increase in the molecular polarisability.

A further effect that may account for the anisotropy of fragment ions arising from the Coulomb explosion of highly-charged transient parent ions, is the dependence of ionisation rates upon the angle made between the polarisation vector of a linearly-polarised laser pulse and the molecular axis. As mentioned above, the ionisation and dissociation of a linear molecule will be more efficient if the laser field orientation is along the molecular bond axis, whereas the ionisation is 'atom-like' when the field orientation is perpendicular with respect to the molecular axis. On the rising-edge of the laser pulse, those molecules that are oriented orthogonally to the laser field are unlikely to be ionised past the first or second ionisation stage. As such, the dissociation process, if it occurs, will give rise to low kinetic energy fragment ions and neutrals. This is the origin of the isotropy component of modestly charged fragment ion angular distributions. Once all the molecules in the interaction region reach the singly- or doubly-ionised state, the laser field strength is no longer sufficient to strip further electrons off from molecules in the orthogonal orientation, as then the barrier to

ionisation becomes insurmountable and the tunneling probability is infinitesimal. One would need to increase the laser intensity considerably (greater than 10^{16} W cm^{-2} used in the experiments detailed in later chapters) to reach higher ionisation states and this may lead to the molecule Coulomb exploding into high kinetic energy fragment ions perpendicularly to the laser field. This angle-dependent ionisation-rate hence leads to anisotropic angular distributions for the higher charge state fragment ions resulting from the Coulomb explosion of the highly ionised transient parent molecule.

The ionisation-enhancement mechanism may not be the whole story for lighter molecules subjected to ultraintense (> 10^{15} W cm^{-2}) laser pulses, as it is unable to account for this small narrowing observed in some fragment ion distributions. This is because the enhancement of the ionisation when the polarisation is collinear with the molecule would be similar for all charge-states of the precursor molecule. The threshold intensity required to reach a particular ionisation stage as a function of the internuclear distance is very similar for all angles between the polarisation vector and the molecular axis. The minimum intensity required for ionisation is a minimum at similar internuclear distances, of approximately twice the equilibrium distance, figure 1.7. Therefore, the conclusion is that at near peak intensity of an ultraintense laser pulse, the lighter molecules tend to align with the laser electric field prior to fragmenting and the higher the ionisation-stage reached before fragmenting, the more tightly it will be aligned. This will be evident in a narrowing of fragment ions arising from Coulomb explosion of these molecules along the bond/polarisation vector orientation. The alignment of several diatomics were studied by Schmidt et al. [41] using two pulse durations of 130fs and 2ps and 395, 610 and 790nm wavelengths and at laser intensities of 10^{15} and 2×10^{16} W cm^{-2}. Their results show that the degree of alignment depends on the number of photons required to reach the ionisation stage of the parent under consideration and that alignment is greater the more highly ionised the transient parent ion is prior to Coulomb exploding.

If the polarisation is not collinear the molecule cannot achieve the ionisation-state it would otherwise achieve. If the polarisation is neither collinear nor orthogonal to the

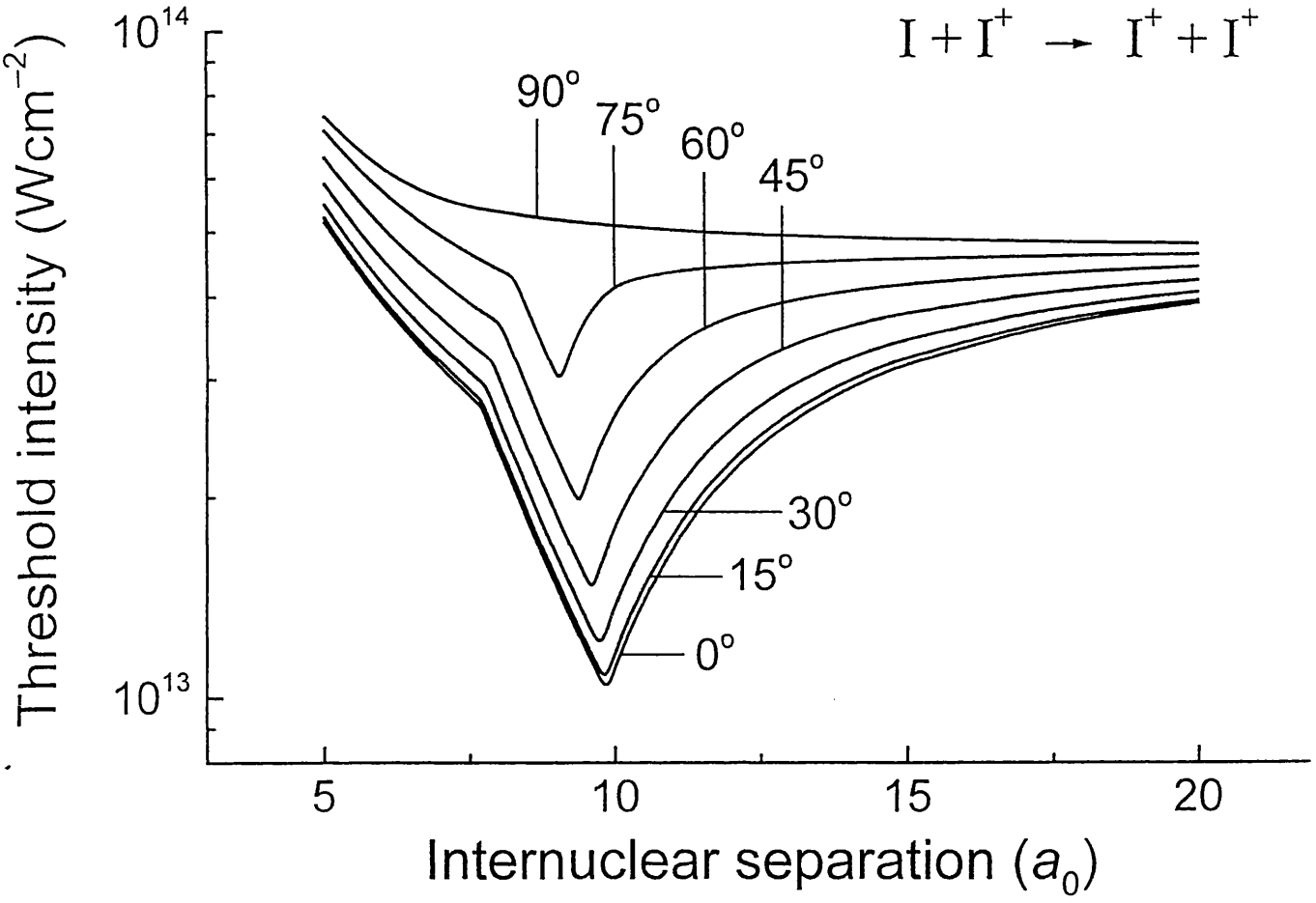

Figure 1.7 Threshold laser intensity as a function of internuclear separation for varying angle between the molecular axis and electric field of the laser field.

Reproduced by kind permission from Professor K. Codling

molecular axis, the laser intensity component along the molecular axis may be sufficient to enhance the dissociative ionisation. This may be the cause of the counter-intuitive broadening of I^{2+} ion distributions with increasing laser intensity [43] that leads to the conclusion of a geometric alignment, or enhancement of ionisation when the molecule is collinear with the laser field, rather than dynamic alignment of the I_2 molecule [25].

Several pump-probe experiments have been performed to elucidate the origin of fragment ion angular anisotropies [45-48]. The earlier studies (Ca. 1992) concluded that the pump-probe results indicated that the fragment ion anisotropies were (at least partially) as a result of laser-induced alignment of the precursor molecule. This was prior to the realisation that the ionisation rate could be dependent on the initial orientation of the molecule with respect to the laser field. The double-pulse measurements with both H_2 and I_2 concluded that the laser pulse duration and intensity were sufficient to align the lighter H_2 molecule. The anisotropy from Coulomb explosion of the heavier I_2 diatomic molecule, however, was a result of the enhanced ionisation rate when the linear polarisation was collinear with the molecular axis.

An elegant set of experiments to determine the degree of alignment of several molecules (I_2, ICl, CS_2, CH_3I and C_6H_5I) was performed by Larsen et al. [48], in which the molecules are seeded in a supersonic beam (to reduce the rovibrational temperature). The molecules are aligned by an intense, non-resonant ns linearly-polarised laser field from a Nd:YAG and probed utilising two fs laser beams delayed with respect to one another. The fragment ions produced are detected using mass-selective two-dimensional imaging. The alignment of the molecules is probed while the ns laser field is applied. The first femtosecond pulse dissociates the neutral molecule, then the second delayed femtosecond laser pulse ionises the resulting fragment atoms. The pump and probe pulses are polarised perpendicularly to the detector. The advantage of this technique is that all the molecules interacting with the ns Nd:YAG laser are aligned prior to ionisation and dissociation and so the anisotropy observed is unambiguously interpreted as an alignment with the Nd:YAG laser field. The degree of alignment depends on the intensity of the Nd:YAG laser, which is still sufficiently low

to ensure no ionisation or dissociation of the molecules. The degree of alignment of neutral Iodine molecules was controlled by increasing the Nd:YAG alignment laser intensity or by lowering the initial rotational energy of the molecules [48]. Since the aligning field is non-resonant, the technique is non-selective, as shown by the varied selection of molecules that were analysed, and is applicable to both polar and non-polar molecules.

1.2.3.2 Controlling molecular alignment and orientation in stereochemical reactions

The alignment and orientation of molecules, using both electrostatic techniques for polar molecules and laser-induced dipole moments for both polar and non-polar molecules, was investigated by Friedrich and Herschbach [49]. The advantage of the former methods, such as electric hexapole focussing or strong dc electrical field orientation, is that they are able to orient the electric dipole of the molecules, i.e. arrange polar molecules in a head vs. tail order. This initial order in the orientation of molecules can play an important role in reactions. In a hetronuclear diatomic for example, the bond will be initially compressed or stretched by an oscillating infrared laser pulse, and this effect was used to control the photofragment angular distributions using a two-pulse arrangement [50]. The advantages of a laser-induced alignment is that it does not interact with the permanent dipole so is applicable to all molecules with anisotropic polarisability and the degree of alignment achieved can be larger.

The molecular alignment utilising intense non-resonant laser fields also lends itself to coherent control techniques [50-52]. These control processes include coherent quantum control of multiphoton transitions by using custom-shaped femtosecond pulses (using frequency resolved optical gating (FROG) [53] techniques to achieve the desired spectral properties of the pulse. FROG is an optical technique closely related to autocorrelation techniques. The geometric set-up is similar, but provides additional information on pulse frequency and phase vs. time. This allows for pulse manipulation and shaping, as desired). Absorption of a coherent superposition of a fundamental laser frequency phase-locked with one of its harmonics can induce complex interference

effects between different pathways in atomic or molecular photo-processes, thereby permitting the coherent optical control of chemical reactions. By controlling the molecular alignment with a linearly polarised intense laser beam, the possibility of controlling the evolution of many chemical reactions (stereochemistry) is opened up and this has implications in many fields of application.

Stereochemical reactions have already been demonstrated. For example, a NO molecule is able to form a chemical bond with a Pt surface more efficiently if the molecule approaches with the N atom pointing towards the surface compared to being oriented in the other direction [54]. The emission of N_2 as a molecular beam after N_2O impinges on a CS surface is found to be more efficient when the N_2O is oriented such that it approaches with its O atom towards the surface [55]. In the dissociation of I_2, two different dissociation channels could be accessed when laser radiation of 485nm was used. The branching ratio between these two channels was controlled by aligning the molecules prior to the interaction with the 485nm laser pulse [56]. Similar results were also obtained by Larsen et al. [51]. The rate of the reaction Li+HF $\rightarrow$ LiF+H has been shown to be dependent on the relative orientation of the molecule HF to the Li atom [57]. A recent experiment by Posthumus et al. [47] using pump-probe techniques showed that the alignment of the light H_2 molecule with an intense 50fs pulse was possible, but not so for the I_2 molecule. In order to probe the degree of alignment, an increase of the laser intensity is required. Then however, the alignment was difficult to distinguish from the enhanced dissociative ionisation. It was however concluded that, as long as the intensity was below the threshold for dissociative ionisation to occur then a polarisable molecule would be aligned within the intense fs laser pulse.

The control of the degree of ionisation/dissociation achieved [58-60] as well as molecular trapping can be realised by alignment and reflecting (i.e. repelling or attracting) molecules with light, which can be done simultaneously [61]. This effect may lead to 'molecular wave-guiding' along the low-intensity axis of a TEM_{01} (doughnut) mode laser. Molecular trapping could also lead to an evaporative cooling of all molecules in a trap [31, 62] to a lower temperature achievable in molecular

ensembles by conventional means by cooling vibrational and rotational degrees of freedom. Increasing the focus of the lasers comprising the trap can then increase the trapped ensemble density. The very low velocities of the trapped cooled molecules would also enable investigation of chemical reactions in which the deBroglie wavelength would have a significant effect [62] and hence to a 'molecular laser' [63]. Furthermore, if the orientation (head vs. tail configuration) as well as alignment could be controlled, this would have significant impact in the field of medicine as well as allow the processing of materials with pre-determined optical and mechanical properties, in similar fashion to the examples detailed above. This was shown to be achievable theoretically, by combining laser-induced alignment with electrostatic fields, as well as control of the alignment in two orthogonal planes, by Friedrich et al. [49].

The previous work detailed above demonstrates the feasibility of controlling chemical reactions to produce a desired end product. A main aim of the present work was to elucidate the mechanism behind the photofragment ion distributions arising from Coulomb explosions of several triatomic molecules in ultraintense ($\sim 10^{15}$-10^{16} W cm^{-2}), ultrashort (50fs) linearly polarised laser pulses. The information obtained from these polarisation-dependent laser/matter investigations of the mass, charge and kinetic energies of fragment ions also allows the elucidation of the transient state of the parent *prior* to the Coulomb explosion process, such as the precursor ionisation state, bond lengths and angles. These results serve to explain the processes involved in the interaction for experimental conditions hitherto unobtainable, until recent developments in intense fs laser pulse generation outlined in the next chapter.

1.3 Trace chemical detection and identification

Laser mass spectrometry permits sensitive detection and analysis of both atoms and molecules and has become an important analytical tool in many areas of application [64-67]. Coupled with a time-of-flight (TOF) mass spectrometer, femtosecond laser ionisation of atomic or molecular samples can provide high levels of sensitivity of

detection. Together with observation of the intact parent ion for unambiguous identification it is clear that femtosecond laser mass spectrometry (FLMS) is a very powerful analytical technique. Taking advantage of resonance levels in the atomic or molecular system, which the laser can excite further enhances the sensitivity, by careful choice of the exciting laser wavelength. This is termed resonance-enhanced ionisation. The resonance-enhanced ionisation technique also lends itself to selectivity, if this is required for a particular application, as only those atoms or molecules that the laser wavelength can resonantly excite will be efficiently detected. As Haefliger and Zenobi point out however, the claim of selectivity of resonance–enhanced multiphoton ionisation (REMPI) to identify and distinguish different isomers at room temperature is in doubt [68]. The resonance-enhancement can only be performed with ns lasers however, as the bandwidth is too broad to excite resonantly using fs laser pulses. Chemical detection can also be performed off-resonance however, and sensitivities of a sub-ppm level are routinely achieved.

Molecular fragmentation can compete with ionisation however, due to extra degrees of freedom and complexity associated with molecules, as compared with atomic systems. This is particularly so with large and thermally labile molecules. It has been shown [69] that if a molecule has a dissociation energy less than 6 eV, then it will dissociate before it can ionise when irradiated by picosecond or longer-duration pulses. This will lead to a 'ladder-switching' mechanism, shown in figure 1.8, i.e. dissociation will precede ionisation (DI), as the molecular states that the laser excites have short lifetimes compared with the pulse duration. This motivated the development of utilising femtosecond generated laser pulses to analyse chemical samples. The resonance excitation is lost with fs pulses, but the molecule undergoes rapid up-pumping to the ionisation continuum, where it then may dissociate (ID) as more photons are absorbed. This is termed 'ladder-climbing' and is shown in figure 1.8. The pulse duration is short compared to the excited state lifetimes. Since the pulse durations are extremely short, this increases the laser intensity, so the molecule may absorb many photons simultaneously. The molecule will hence achieve a highly ionised state, which may be excited and fragment, giving highly-charged fragment ions.

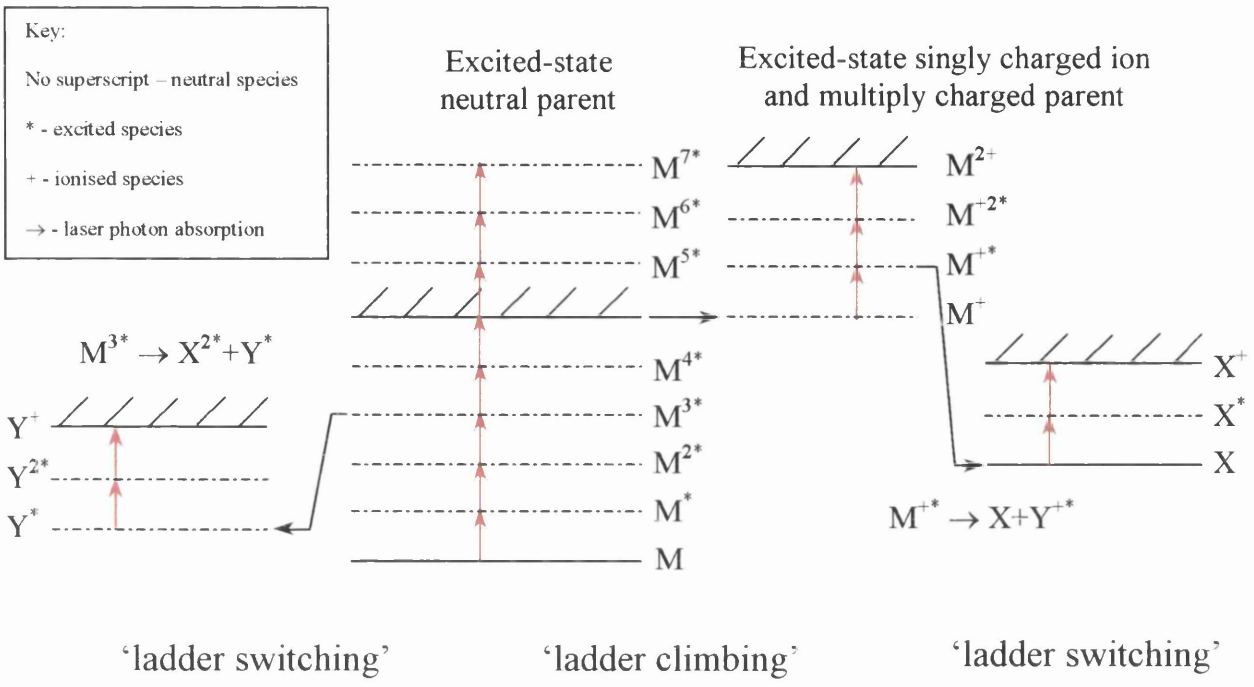

Figure 1.8 Schematic showing the ladder climbing and ladder switching mechanisms

Since some parent molecules will survive fragmentation, this obviously aids in their detection and identification. The fragment ions, on the other hand, whose kinetic energies may be calculated, aid in the determination of the parent molecular structure prior to the fragmentation process. In analytical work, however, it is the former property of FLMS that is most important. Furthermore, the FLMS has been shown to be quite general in application to both large and small molecules [3, 70-73].

For quantitative chemical and surface analysis Becker and He et al. [74-77] have studied gas-phase samples (Ar, Kr, NO, Xe, N_2 and O_2) and solid samples (SiO_2, GaAs, SiC and C1154 alloy) by post-ionising ablated neutrals. These experiments were performed at a laser intensity in the range of (10^{14}–10^{15}) W cm^{-2}, 35ps pulses at a wavelength of 532nm, together with a TOF. With the ps pulse duration they were still able to identify the sample under consideration. They also were able to test the sensitivity of their technique by counting the ion yield of the sample and comparing this with a known amount of a calibrant sample, typically Ar gas. This was done by calculating a relative sensitivity factor (RSF) for the particular sample under investigation. The RSF is given by:

$$RSF(A) = \frac{I_A/[A]}{I_B/[B]} \qquad \text{(Eq. 1.6)}$$

where I_A and I_B are the summed ion signal intensities of species A and the calibrant species B, respectively, over all charge-states observed in the mass spectra and [A] and [B] are the concentrations of A and B present in the mixture sample. In these experiments they were able to achieve RSF values close to unity for all species. This shows that by saturating the ionisation in the laser/matter interaction region with sufficiently high laser intensities, uniform ion yields were achieved for various species with widely differing ionisation potentials. This demonstrates the uniformity of the detection technique. It was indicated that ionisation was multiphoton, although at the highest intensities used, tunneling became prominent.

Similar results were obtained at a higher laser intensity region of 10^{15}-10^{16} W cm^{-2} by the Glasgow group [70] with various gas-phase samples, to extend the technique to high-intensity non-resonance conditions and further prove the general applicability and sensitivity of FLMS. It is possible to extend this technique to solid-phase samples of interest such as semiconductors or environmental samples, as both Ledingham et al. [78] and He and Becker et al. have done. The experiments were performed using Ar as the calibrant, as the ionisation characteristics of this chemical with increasing intensities are well understood. Looking at Eq. 1.6, if the concentrations are made to be equal in the mixture [A] = [B], then the RSF is simply given by:

$$RSF(A) = \frac{I_A}{I_B} \qquad \text{(Eq. 1.7)}$$

and I_A and I_B are proportional to the photo-ion yields, which are given by the area under the ion peak in the mass spectra. The sample and calibrant were mixed in a 'mixing manifold' and were left awhile to ensure complete mixing. All charge-states are summed together. All fragment ions are included in the parent ion count, since they must arise from parent molecules that have fragmented. The fragment ions must be weighted with their stoichiometric ratios occurring in the molecule of interest.

The results obtained (see chapter 3) show that by using femtosecond lasers at high intensities the FLMS technique can not only identify the sample of interest via the detectable parent ion, but that the technique is also sensitive. By saturating the ionisation of various chemicals: CO, CH_4, NO, NO_2, H_2S, N_2O, CO_2, N_2, CH_3I, CS_2, C_6H_6 and C_7H_8 with widely differing ionisation potentials, the technique is shown to be uniform as the RSF values approached unity for all samples studied. However, for the liquid-phase samples such as CS_2 and CH_3I, separate mass spectra were required for the sample and calibrant in order to achieve this result. The challenge of obtaining sensitive trace chemical detection of a large variety of chemical samples has thus been met by FLMS. By using intense femtosecond laser pulses, the ionisation is 100% efficient in a well-defined interaction region for all samples studied, regardless of their

very different relative ionisation potentials. This is due to the field intensity being sufficient at (10^{15}-10^{16}) W cm^{-2} to induce either tunneling or barrier suppression ionisation (BSI) in all atoms/molecules in the focal spot (1st Airy disc) of the laser. Hence, ionisation to at least singly-charged ions is saturated, i.e. *all* atoms/molecules in the region undergo ejection of at least one of their valence electrons.

The experiments detailed above show that with developments in intense femtosecond laser pulse generation to make the lasers even smaller and cheaper than present, the technique of FLMS could be applied in varying applications. These include the detection of unknown environmentally important chemicals such as explosives [2], car exhaust particulates [79], earth samples [3], water samples, and even fumes from petrol pumps, foodstuffs and drugs of abuse. Of particular environmental concern at present, especially in the context of increasing reported cases of asthma, are what are known as polycyclic aromatic hydrocarbons (PAH), a family of molecules built up from fused benzene rings. These are emitted as a result of incomplete combustion of organic matter, particularly in diesel engines where they can form on soot particles. It has been established that most PAHs are carcinogenic, mutagenic, teratogenic and have immunotoxic effects on both animals and humans. Furthermore, the reaction products that can form in photosynthesis with other atmospheric pollutants can be even more toxic than the original PAH [80, 81].

References

[1] Singhal RP, Land AP, Ledingham KWD, Towrie M 1989 J. Anal. At. Spectrom., **4**, 599; Zakheim DS and Johnson PM 1980 Chem. Phys., **46**, 263

[2] Ledingham KWD, Smith DJ, Singhal RP, McCanny T, Graham P, Kilic HS, Peng WX, Langley AJ, Taday PF, Kosmidis C 1999 J. Phys. Chem., **103**, 2952; Ledingham KWD, Kilic HS, Kosmidis C, Deas RM, Marshall A, McCanny T, Singhal RP, Langley AJ, Shaikh W 1995 Rapid Comm. Mass Spectrom., **9**, 1522

[3] Grun C, Heinicke R, Weickhardt C, Grotemeyer J 1999 Int. J. Mass Spectrom., **185-187**, 307; Aicher KP, Wilhelm U, Grotemeyer J 1995 J. Am. Soc. Mass Spectrom., **6**, 1059-1068; Weinkauf R, Aicher P, Wesley G, Grotemeyer J, Schlag EW 1994 J. Phys. Chem., **98**, 8381

[4] Ammosov MV, Delone NB, Krainov VP 1986 Sov. Phys. JETP, **64**, 1191

[5] Corkum PB, Burnett NH, Brunel F 1989 Phys. Rev. Lett., **62**, 1259

[6] Augst A, Strickland D, Meyerhofer DD, Chin SL, Eberly JH 1989 Phys. Rev. Lett., **63**, 2212

[7] Dietrich P, Corkum PB 1992 J. Chem. Phys., **97**, 3187

[8] Chin SL, Liang Y, Decker JE, Ilkov FA, Ammosov MV 1992 J. Phys. B: At. Mol. Opt. Phys., **25**, L249

[9] DeWitt RJ and Levis MJ 1999 J. Phys. Chem. A, **103**, 6493

[10] Talebpour A, Yang J, Chin SL 1999 Optics Communications, **163**, 29

[11] Keldysh LV 1965 Sov. Phys. JETP, **20**, 1307

[12] Sheehy B and DiMauro LF 1996 Annu. Rev. Phys. Chem., **47**, 463

[13] Corkum PB, Ivanov MY, Wright JS 1997 Annu. Rev. Phys. Chem., **48**, 387

[14] Yu Hengtai, Zuo T, Bandrauk AD 1998 J. Phys. B: At. Mol. Opt. Phys., **31**, 1533

[15] Codling K, Frasinski L, Hatherly P 1989 J. Phys. B: At. Mol. Opt. Phys., **22**, L321; 1993 J. Phys. B: At. Mol. Opt. Phys., **26**, 783

[16] Cornaggia C, Lavancier J, Normand D, Morellec J, Agostini P, Chambaret JP, Antonetti A 1991 Phys. Rev. A, **44**, 4499

[17] Giusti-Suzor A, Mies FH, DiMauro LF, Charron E, Yang B 1995 J. Phys. B: At. Mol. Opt. Phys., **28**, 309

[18] Graham P, Ledingham KWD, Singhal RP, McCanny T, Hankin SM, Fang X, Tzallas P, Kosmidis C, Taday PF, Langley AJ 2000 J. Phys. B: At. Mol. Opt. Phys., *to be published*

[19] Luk TS, Moriarty RM, Awashti A, Boyer K, Rhodes CK 1992 Phys. Rev. A, **45**, 6744

[20] Hishikawa A, Iwamae A, Hoshina K, Kono M, Yamanouchi K 1998b Chem. Phys. Lett., **282**, 283-291

[21] Shimizu S, Kou J, Kawato S, Shimizu K, Sakabe S, Nakashima N 2000 Chem. Phys. Lett., **317**, 609

[22] Bandrauk AD, Ruel J 1999 Phys. Rev. A, **59**, 2153

[23] Posthumus JH, Giles AJ, Thompson MR, Frasinski LJ, Codling K, Langley AJ, Shaikh W 1996 J. Phys. B: At. Mol. Opt. Phys., **29**, L525

[24] Graham P, Ledingham KWD, Singhal RP, McCanny T, Hankin SM, Fang X, Smith DJ, Kosmidis C, Tzallas P, Langley AJ, Taday PF 1999 J. Phys. B: At. Mol. Opt. Phys., **32**, 5557

[25] Ellert CH and Corkum PB 1999 Phys. Rev. A, **59**, R3170

[26] Posthumus JH, Plumridge J, Taday PF, Sanderson JH, Langley AJ, Codling K, Bryan WA 1999 J. Phys. B: At. Mol. Opt. Phys., **32**, L93

[27] Sanderson JH, El-Zein A, Bryan WA, Newell WR, Langley AJ, Taday PF 1999 Phys. Rev. A, **59**, R2567

[28] Hering Ph and Cornaggia C Phys. Rev. A, **59**, 2836

[29] Graham P, Ledingham KWD, Singhal RP, McCanny T, Hankin SM, Fang X, Kosmidis C, Taday PF, Langley AJ 2000 J. Phys. B: At. Mol. Opt. Phys., *to be published* (letter)

[30] Normand D, Dobosz S, Lezius M, D'Oliveira P, Schmidt M 1996 Inst. Phys. Conf. Ser. No. 154, Multiphoton Processes 1996 Conf. Garmisch-Partenkirchen, Germany

[31] Friedrich B and Herschbach D 1995 Phys. Rev. Lett., **74**, 4623; Friedrich B and Herschbach D 1995 J. Phys. Chem., **99**, 15686

[32] Sukharev ME and Krainov VP 1998 JETP, **86**, 318

[33] Sugita A, Mashino M, Kawasaki M, Matsumi Y, Gordon RJ, Bersohn R 2000 J. Chem. Phys., **112**, 2164

[34] Kumar GR, Gross P, Safvan CP, Rajgara FA, Mathur D 1996 Phys. Rev. A, **53**, 3098

[35] Posthumus JH, Plumridge J, Codling K, Frasinski LJ, Langley AJ, Taday PF 1999 Laser Physics, **9**, 1-8

[36] Henriksen NE 1999 Chem. Phys. Lett., **312**, 196-202

[37] Keller A, Dion CM, Atabek O 2000 Phys. Rev. A, **61**, 023409-1

[38] Friedrich B and Herschbach D 1995 J. Chin. Chem. Soc., **42**, 111-117

[39] Block PA, Bohac EJ, Miller RE 1992 Phys. Rev. Lett., **68**, 1303

[40] Loison JC, Durand A, Bazalgette G, White R, Audouard E, Vigue J 1995 J. Phys. Chem., **99**, 13591

[41] Schmidt M, Dobosz S, Meynadier P, D'Oliveira P, Normand D, Charron E, Suzor-Weiner A 1999 Phys. Rev. A, **60**, 4706

[42] Banerjee S, Kumar GR, Mathur D 1999 Phys. Rev. A, **60**, R3369

[43] Posthumus JH, Plumridge J, Thomas MK, Codling K, Frasinski LJ, Langley AJ, Taday PF 1998 J. Phys. B: At. Mol. Opt. Phys., **31**, L553

[44] Codling K private communication

[45] Normand D, Lompre LA, Cornaggia C 1992 J. Phys. B: At. Mol. Opt. Phys., **25**, L497

[46] Strickland DT, Beaudouin Y, Dietrich P, Corkum PB 1992 Phys. Rev. Lett., **68**, 2755

[47] Posthumus JH, Plumridge J, Frasinski LJ, Codling K, Langley AJ, Taday PF 1998 J. Phys. B: At. Mol. Opt. Phys., **31**, L985

[48] Larsen JJ, Sakai H, Safvan CP, Wendt-Larsen I, Stapelfeldt H 1999 J. Chem. Phys., **111**, 7774; Sakai H, Safvan CP, Larsen JJ; Hilligsoe KM, Hald K, Stapelfeldt H 1999 J. Chem. Phys., **110**, 10235

[49] Friedrich B and Herschbach D 1999 J. Chem. Phys., **111**, 6157

[50] Machholm M and Henriksen NE 1999 J. Chem. Phys., **111**, 3051

[51] Larsen JJ, Wendt-Larsen I, Stapelfeldt H 1999 Phys. Rev. Lett., **83**, 1123

[52] Meshulach D and Silberberg Y 1999 Phys. Rev. A, **60**, 1287

[53] Trebino R, DeLong KW, Fittinghoff DN, Sweetser JN, Krumbugel MA, Richman BA, Kane DJ 1997 Rev. Sci. Instrum., **68**, 3277

[54] Tenner MG, Kuipers EW, Kleyn AW, Stolte S 1991 J. Chem. Phys., **94**, 5197

[55] Brandt M, Greber T, Kuhlmann F, Bowering N, Heinzmann U 1998 Surface Science, **402-404**, 160

[56] Li H, Franks KJ, Hanson RJ, Kong W 1998 J. Phys. Chem. A, **102**, 8084

[57] Alvarino JM, Aquilanti V, Cavalli S, Crocchianti S, Lagana A, Martinez T 1997 J. Chem. Phys., **107**, 3339

[58] Constant E, Stapelfeldt H, Corkum PB 1996 Phys. Rev. Lett., **76**, 4140

[59] Posthumus JH, Giles AJ, Thompson MR, Codling K 1996 J. Phys. B: At. Mol. Opt. Phys., **29**, 5811

[60] Siedman T, Ivanov MY, Corkum PB 1996 Chem. Phys. Lett., **252**, 181

[61] Siedman T 1999 J. Chem. Phys., **111**, 4397

[62] Friedrich B and Herschbach D 1995 J. Chin. Chem. Soc., **42**, 111

[63] Wynar R, Freeland R S, Han D J, Ryu C, Heinzen D J 2000 Science, **287**, 1016

[64] Lubman DM (Ed.), *Laser and Mass Spectrometry*, Oxford University Press, New York (1990)

[65] Vertes A, Gijbels R, Adams F, *Laser Ionisation Mass Analysis*, Chemical Analysis Ser. Vol. 124, John Wiley and Sons, New York (1993)

[66] Ashfold MNR, Howe JD 1994 Ann. Rev. Phys. Chem., **45**, 57

[67] Ledingham KWD, in An Introduction to Laser Spectroscopy, Andrews DL and Demidov AA (Eds.) Plenum Press, New York, pp. 187-227 (1995)

[68] Haefliger OP and Zenobi R 1998 Anal. Chem., **70**, 2660

[69] Kumar GR, Safvan CP, Rajgara FA, Mathur D 1994 J. Phys. B: At. Mol. Opt. Phys., **27**, 2981

[70] Fang X, Ledingham KWD, Graham P, Smith DJ, McCanny T, Singhal RP, Langley AJ, Taday PF 1999 Rapid Commun. Mass Spectrom., **13**, 1390

[71] Castillejo M, Couris S, Koudoumas E, Martin M 1998 Chem. Phys. Lett., **289**, 303

[72] Lockyer NP and Vickerman JC 1998 Int. J. Mass Spectrom., **176**, 77

[73] Nicolussi GK, Pellin MJ, Lykke KR, Trevor JL, Mencer DE, Davis AM 1996 Surface and Interface Analysis, **24**, 363

[74] He C, Basler J, Paul A, Becker CH 1996 J. Vac. Sci. Technol., **A14**, 1433

[75] He C and Becker CH 1996 Current Opinion in Solid State and Material Science, **1**, 493

[76] Becker CH and Hovis JS 1994 J. Vac. Sci. Technol., **A12**, 4

[77] He C, Basler J, Becker CH 1997 Nature, **385**, 797

[78] Ledingham KWD and Hankin et al. RAL Tech report, 1999/2000

[79] Fraser MP, Cass GR, Simoneit BRT 1999 Atmospheric Environment, **33**, 2715; Clark NN, Jarrett RP, Atkinson CM 1999 Journal of the Air & Waste Management Assoc., **49**, 76

[80] Finlayson-Pitts BJ and Pitts JN 1997 Science, **276**, 1045

[81] Atkinson R and Arey J 1988 Environ. Health Perspect., **102**, 117

Chapter 2

Experimental

2.1 Chapter Overview

This chapter is concerned with explaining the linear time-of-flight (TOF) mass spectrometer used in all the experiments performed during the course of the Ph.D and a description of the design, implementation and working parameters will be given. This chapter also details the development of techniques used to generate femtosecond laser pulses with sufficiently high intensities (typically of the order of 10^{16} W cm^{-2}) as used to perform the experiments detailed in the thesis work. The various underlying principles such as pulse-compression, as well as the different components of the laser system will be discussed. The optical layout and experimental design will also be mentioned. Furthermore, the experimental technique, such as chemical sample preparation and procedures for mass spectra acquisition and analysis, will be discussed.

2.2 Femtosecond Laser and Optical Layout

2.2.1 Intense short laser pulse generation – a brief history

The first laser to be developed was the ruby laser in 1960 by Maiman et al., [1]. Initially, the laser was infamously called a 'solution looking for a problem'. However, as the development of lasers progressed, it was realised fairly early on that the new technology could be applied to atomic and molecular physics as well as for analytical chemistry.

The ruby laser produced pulses of fluctuating intensity lasting between a microsecond and a millisecond. The concept of Q-switching was proposed soon after [2, 3], and a Q-switched ruby laser was shown to provide pulses of about 10 nanoseconds (ns, 10^{-9} s). The principle of Q-switching is to increase the loss of the cavity to allow the radiation energy to build up via an increase in the population inversion. Then the loss is removed from the cavity to allow a laser pulse to carry away the energy that has built up. This technique enables much shorter pulses to be generated, and hence higher laser intensities to be produced. It was around this time that the aforementioned fields took advantage of the laser technology and nonlinear optical phenomena were investigated for the first time. Unfortunately, the Q-switching technique is rather limited in the duration of the shortest pulses one can obtain to about a few nanoseconds.

The shortcomings of the Q-switching technique led to the next stage of the development of short pulse generation, that of mode locking. A laser cavity can support a large number of longitudinal modes of the oscillating light, and by mode-locking those modes which are accepted by the gain profile of the lasing medium, one is able to achieve shorter pulses than is possible by employing the Q-switch technique. The duration of the pulse is theoretically limited in mode locking by how many modes the laser cavity can sustain and that the lasing medium can amplify. Consequently, if the lasing medium has a broad gain profile, then from the Fourier transform, the pulse duration that results is shorter than for a lasing medium with a narrower gain or a cavity which cannot sustain as many modes.

There are two types of mode locking: active and passive. Active mode locking is achieved by modulating the index of refraction of the gain medium at the period of a round trip by a photon in the laser cavity. A train of pulses separated by the cavity round-trip time is hence produced. Passive mode locking is achieved by placing a saturable dye absorber within the cavity. Passive mode locking was first demonstrated by Mocker and Collins, [4] and pulses shorter than 1 ns were obtained by DeMaria et al., [5] by passive mode locking a Nd-glass laser, which has a broad gain profile. Pulses of sub-picosecond (ps, 10^{-12} s) duration were first obtained by Shank and Ippen, [6]. With further developments such as a ring dye laser, together with compensation of group velocity dispersion (GVD) in a thin-film dye absorber, a train of 6 femtosecond pulses (fs, 10^{-15} s) was achieved by Fork et al., [7, 8] using 'white' light continuum input pulses. Similar systems with pulse durations between 10 and 100 fs are very sensitive and require frequent careful adjustments. It was discovered [9] that titanium:sapphire (Ti:Al_2O_3) lasers show "spontaneous" dynamic mode locking without having to include a saturable absorber. This occurrence is due to the intensity-dependent refractive index in the Ti:S crystal. Compensation of GVD is essential and pulses of 7 fs duration have been reported [10].

A further recent development makes high-energy femtosecond pulse production routine. The technique was adapted from research conducted by radar scientists during WWII and is termed Chirped Pulse Amplification (CPA). To obtain the high laser intensities required for many applications, one could simply increase the energy of the laser pulse. However, this would exceed the damage threshold of many optical components. This problem is especially critical in the amplifier medium. An unfocussed 10 fs beam, of 1 cm^2 cross-section and 1 μJ pulse energy has a fairly modest intensity of 10^8 W cm^{-2}. Even at this power level the beam will become susceptible to self-focussing and filamentation in the Ti:S crystal.

The technique of CPA has been developed to overcome the above problems and allow high gain amplification of a pulse of femtosecond duration. Many authors [10-22] have now demonstrated this technique, as well as the technology of measuring the temporal characteristics and are able to generate amplified pulses as short as 7 fs [10]. This work is mainly carried out at 800 nm corresponding to an

optical period of 2.67 fs. Since the shortest compressed pulse one can obtain is about 1.5 times the optical cycle of the smallest wavelength component in the pulse spectrum, the theoretical limit is being reached. A gain factor of 10^9 (e.g. nJ to J level) is now routinely achieved. The basic principles of CPA are outlined in figure 2.1. A low-energy femtosecond pulse is stretched (positively or negatively chirped) by a pulse stretcher which consists of either an optical delay line fibre-optic arrangement, or more typically, a grating pair arranged in an anti-parallel configuration. This stretched pulse can then be safely amplified in a regenerative or multi-pass amplifier to many times its initial energy content. A grating pair in a parallel configuration then recompresses it to its original femtosecond pulse-width. The resulting focussed intensities that are achieved by this technique can be of the order of 10^{18} - 10^{20} W cm^{-2}. Such intensities were once the preserve of the 'large' laser facilities such as NOVA at Livermore and VULCAN at RAL. The corresponding laser electric field will be comparable to the Coulombic field that bind atoms together to form molecules. These high intensities can be used to open up new physical regimes to investigation in the field of laser/matter interaction such as relativistic and nuclear physics, as well as attosecond (as, 10^{-18} s) pulse generation at X-ray wavelengths. The time evolution of the laser intensities achievable using Q-switching, mode-locking and CPA techniques is shown in figure 2.2.

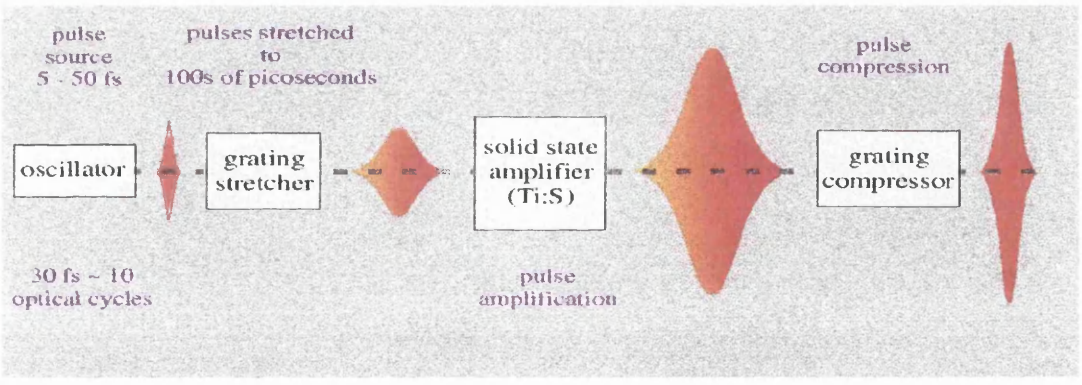

Figure 2.1 The principle of chirped pulse amplification (CPA)

By completely ionising a gas by intense femtosecond laser pulses, it is possible to generate high harmonics. Harmonics up to the 169th stage has been reported [23]. These harmonics are self-mode locking and X-ray pulses of attosecond are possible to generate. Several techniques have also just been developed to measure the phase

By completely ionising a gas by intense femtosecond laser pulses, it is possible to generate high harmonics. Harmonics up to the 169th stage has been reported [23]. These harmonics are self-mode locking and X-ray pulses of attosecond are possible to generate. Several techniques have also just been developed to measure the phase and spatio-temporal characteristics of short (fs and as) pulses and to manipulate them. This allows arbitrary shaping of the pulse to the experimental requirements, such as coherent chemical control. The field of ultraintense, ultrashort laser pulse generation hence makes possible investigation of effects due to relativistic electrons, plasma physics, particle physics and fusion. Attosecond pulse generation is mentioned here only for completeness, and will not be touched upon further.

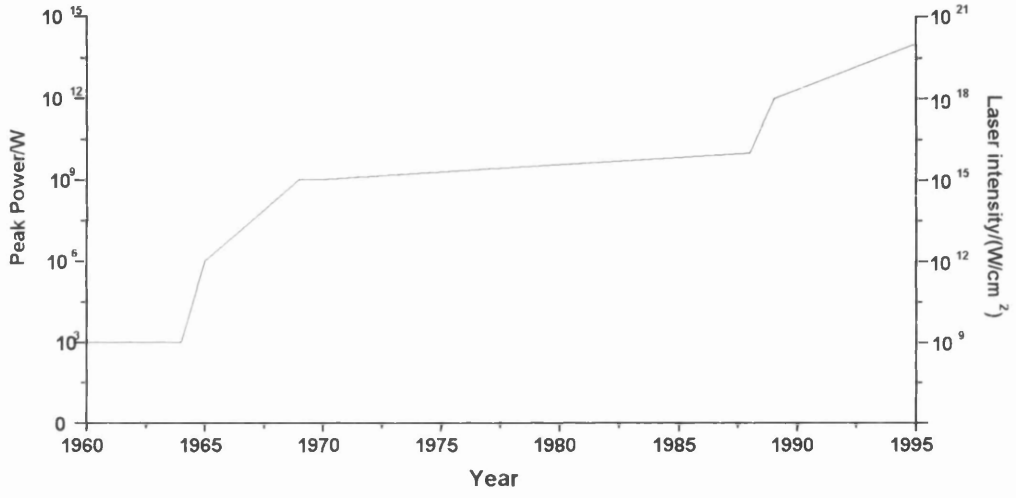

Figure 2.2 The evolution of attainable laser pulse power generation

2.2.2 The Femtosecond Laser System

The laser system used for the experiments detailed in this thesis was the femtosecond laser based at the Central Laser Facility (CLF) in the CLRC Rutherford Appleton Laboratory (RAL) in Didcot, Oxfordshire. This subsequently evolved into the ASTRA laser facility and was relocated to another laboratory also based at RAL. These systems are based on a Nd:YAG laser pumped Ti:S multi-pass amplifier [22, 24] utilising the CPA technique [25].

2.2.2.1 Stage I femtosecond laser system

The laser facility was upgraded during the duration of the Ph.D work reported herein. The stage I laser was used in two experimental runs in November 1997 and August 1998. A schematic of the stage I system is shown in figure 2.3 and is described below. A large-frame Argon ion (Spectra Physics) laser is used to pump a Ti:S femtosecond oscillator (Tsunami, Spectra Physics). The oscillator produces pulses of 50 fs at the characteristic wavelength of Ti:S lasing of 790 nm. The energy per pulse was about 9 nJ.

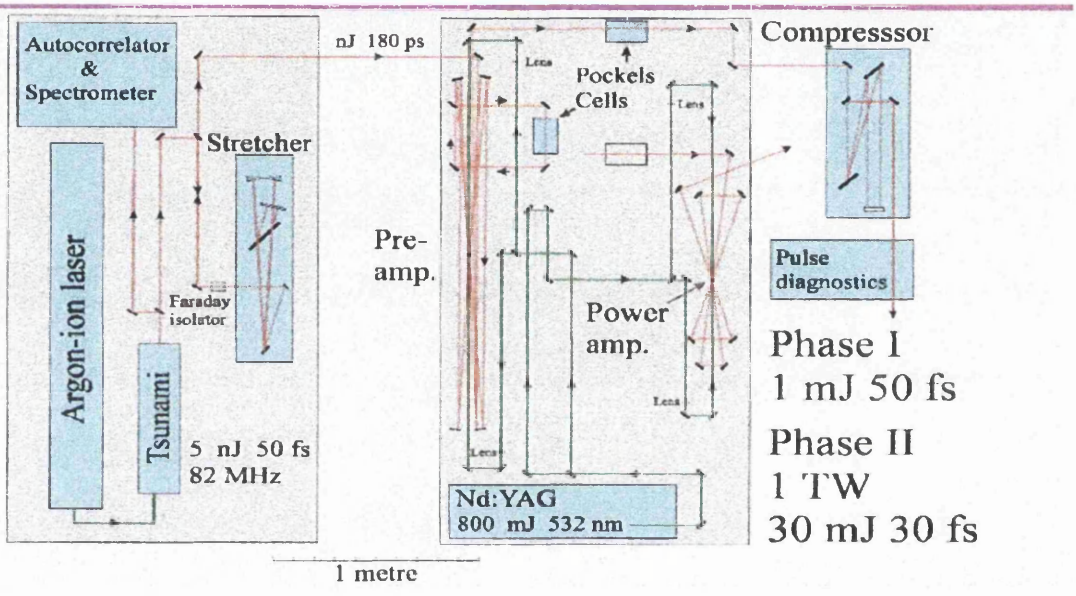

Figure 2.3 Schematic of the RAL stage I femtosecond laser

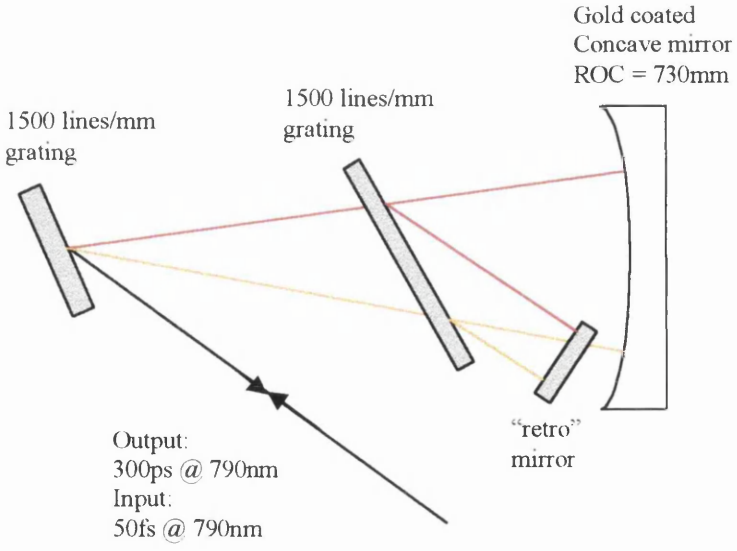

Figure 2.4 All-reflective stretcher

The pulses from the resulting pulse train are subsequently stretched to 200 ps in an all-reflective stretcher, shown in figure 2.4. This consists of two 1500 lines/mm gratings (Spectrogon) arranged in anti-parallel configuration, a large gold-coated mirror of 730 mm radius of curvature (ROC) and a gold-coated flat mirror (Optical Surfaces). The mirrors are gold-plated to increase the reflectivity over a broadband at infrared (IR) wavelengths. The broad bandwidth of the gold mirrors ensure no pulse chirping effects come into play whilst having high (95%) reflectivity. The gratings and mirrors have very high optical quality with $\lambda/10$ and $\lambda/20$ flatness, respectively. In the stretcher design, minimum beam aberration is achieved by retro-reflecting the beam back through the stretcher, as shown. In the laser design implemented at RAL, the beam is expanded to a sizeable diameter and so the retro-reflector is a pair of mirrors arranged in a "V" shape to avoid excessive spatial chirp. The double-pass arrangement through the stretcher also provides a larger degree of pulse stretch via 3rd-order dispersion effects. The pulses thus exit the stretcher with large stretch factors, typically to a pulse duration of 200 ps.

A Faraday isolator is placed between the oscillator and the stretcher to avoid back-reflections disrupting the oscillator. This allows the beam to traverse back through the stretcher along the same path. By rotating the polarisation of the laser beam, the Faraday isolator then allows the pulses from the stretcher to pass to the amplifier 1st stage with energy per pulse of 0.5 nJ.

The 1st stage of the amplifier is a multi-pass confocal amplifier. The amplifying medium is a 7 mm long Ti:S crystal rod (Crystal Systems) with an Figure of Merit (FOM) of 150. The FOM is a measure of the optical quality and degree of doping of the crystal. It is pumped from both ends (longitudinally as opposed to transversely) with 67 mJ from a Nd:YAG laser (Spectra Physics GCR 270-10) operating at the second harmonic of 532 nm. The stretched beam is passed through the Ti:S crystal 5 times using four spherical mirrors of ROC = 2000 mm. It is then directed to a Pockels cell (Leysop) which reduces the repetition rate from 76 MHz to 10 Hz. The pulse is then re-injected into the amplifier for a further 5 passes to increase the pulse energy to 2 mJ. This corresponds to a gain of 4×10^6.

Prior to the compressor the pulse is passed through a second Pockels cell. The Pockels cells together allow one to obtain a bigger gain from the selected pulse and to suppress more efficiently the other pulses in the train, due to the relatively slow rise time of a cell.

The pulse is first expanded to 4 mm in a Galilean telescope before entering the compressor. This is to limit the laser fluence to below the damage threshold of the expensive gratings. The compressor is similar to the stretcher, again comprising of two diffraction gratings with 1500 lines/mm. (The grating density is a compromise, as high groove densities give large stretch factors but uncompensated high-order dispersion and a bigger grating size is required. The throughput is less with small groove densities but high-order dispersion can be more easily eliminated for ultrashort pulse applications). However, the compressor gratings are arranged in a parallel configuration. The temporal characteristics of the compressed pulses are measured using a single-shot 2^{nd}-order autocorrelator. Measurements showed that the pulses were compressed down from 200 ps to the original pulse width of 50 fs from the femto oscillator, at optimal compressor settings.

When the pulses pass through the amplifier for the first five times they are vertically polarised. The pulses are then directed to the Pockel cell, which flips the polarisation by 90°. Therefore, the polarisation must be returned to vertical polarisation prior to re-insertion of the laser pulse to the Ti:S crystal. This is because the polarisation orientation of the pulse to be amplified must be the same as the pump pulse. Furthermore, the Ti:S crystal is birefringent and in the RAL setup the gain is greater when the pulse polarisations are oriented with the vertical axis of the crystal. After the second five passes, the polarisation is changed to horizontal using mirrors for propagation through the compressor. After the compressor, the pulses emerge and mirrors again change the pulse to vertical polarisation.

The final output laser pulses thus have an energy per pulse of about 1 mJ (half the energy is lost through the compressor) and a pulse width of 50 fs at a wavelength of 790 nm. The laser beam was measured to be 1.5x diffraction limited. As the laser beam was focussed by a f/10 spherical mirror inside the TOF vacuum chamber, laser

intensities of greater than 10^{15} W cm^{-2} were achievable. This was corroborated by obtaining a calibration mass spectrum of Argon gas in which the Ar^{5+} ion is present, which is achievable at such intensities.

2.2.2.2 Stage II femtosecond laser system

The upgrade of the femtosecond laser design described above involved replacing the Tsunami femto oscillator with a 20 fs all solid-state mirror dispersion controlled system and pumping the pre-amplifier by a long-pulse (20 ns) frequency-doubled Nd:YAG laser. More importantly, a second power amplifier was installed to further increase the energy gain while maintaining the 50 fs pulse duration, in order to obtain even higher laser intensities.

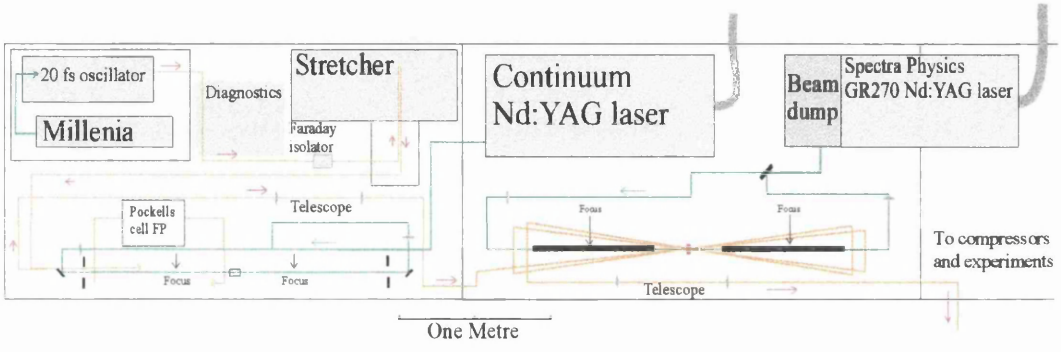

Figure 2.5 Schematic of RAL stage II femtosecond laser system

A schematic of the stage II system upgrade is shown in figure 2.5. The femtosecond laser pulses originate from a Ti:S oscillator controlled via a mirror dispersion technique (Femto, Technische Universitat, Vienna) which is pumped by the second harmonic from a diode-pumped c.w. Nd:YVO_4 laser (Millennia, Spectra-Physics). This generates pulses of 790 nm and of sufficient bandwidth to attain a pulse width of 20 fs, at a rate of 74 MHz.

The pulses from the oscillator are then directed to the stretcher, which is again an all-reflective type to minimise the contribution of high-orders of dispersion and hence maintain pulse fidelity and stretched to 300 ps. This first stage (the pre-amplifier) is essentially as detailed above. The only exception to this is that now the Ti:S amplifier crystal is pumped by the second harmonic from a Nd:YAG (SureLite,

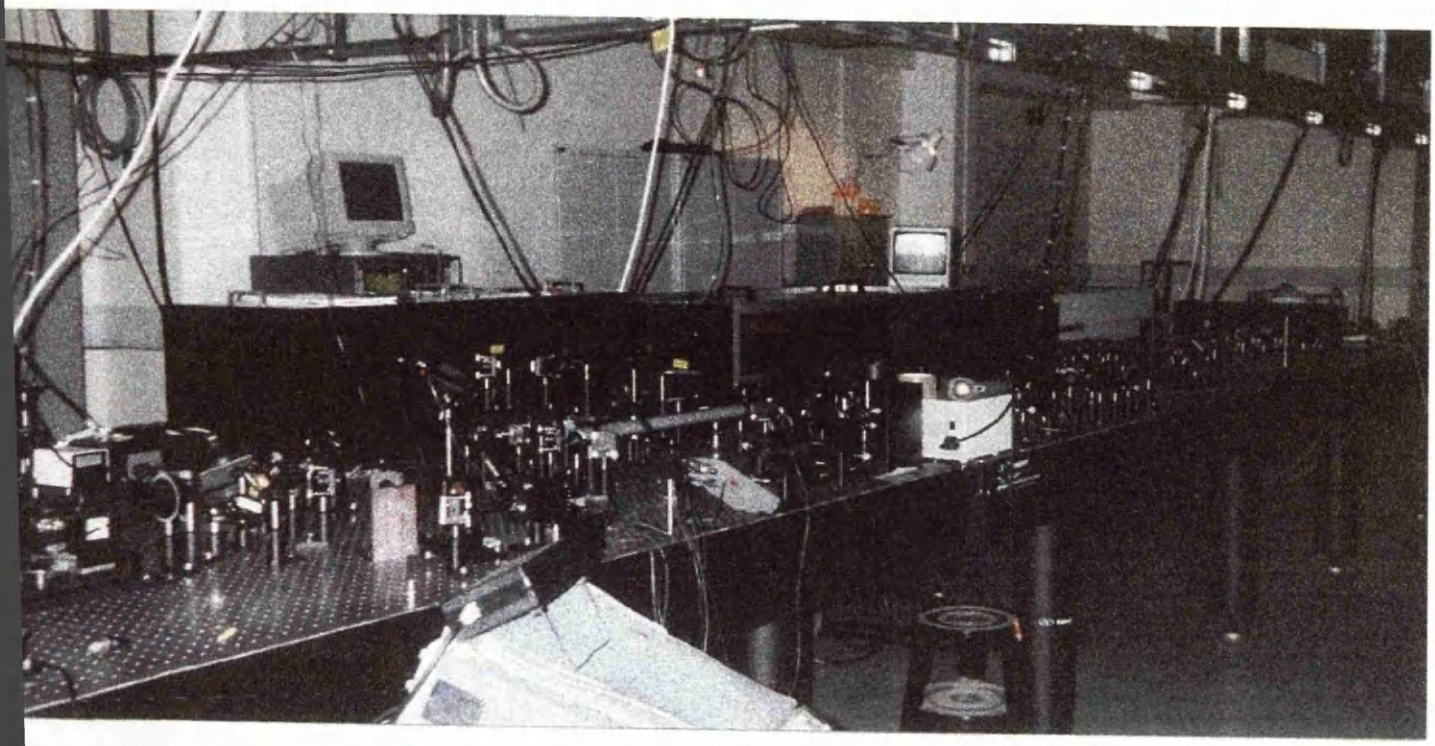

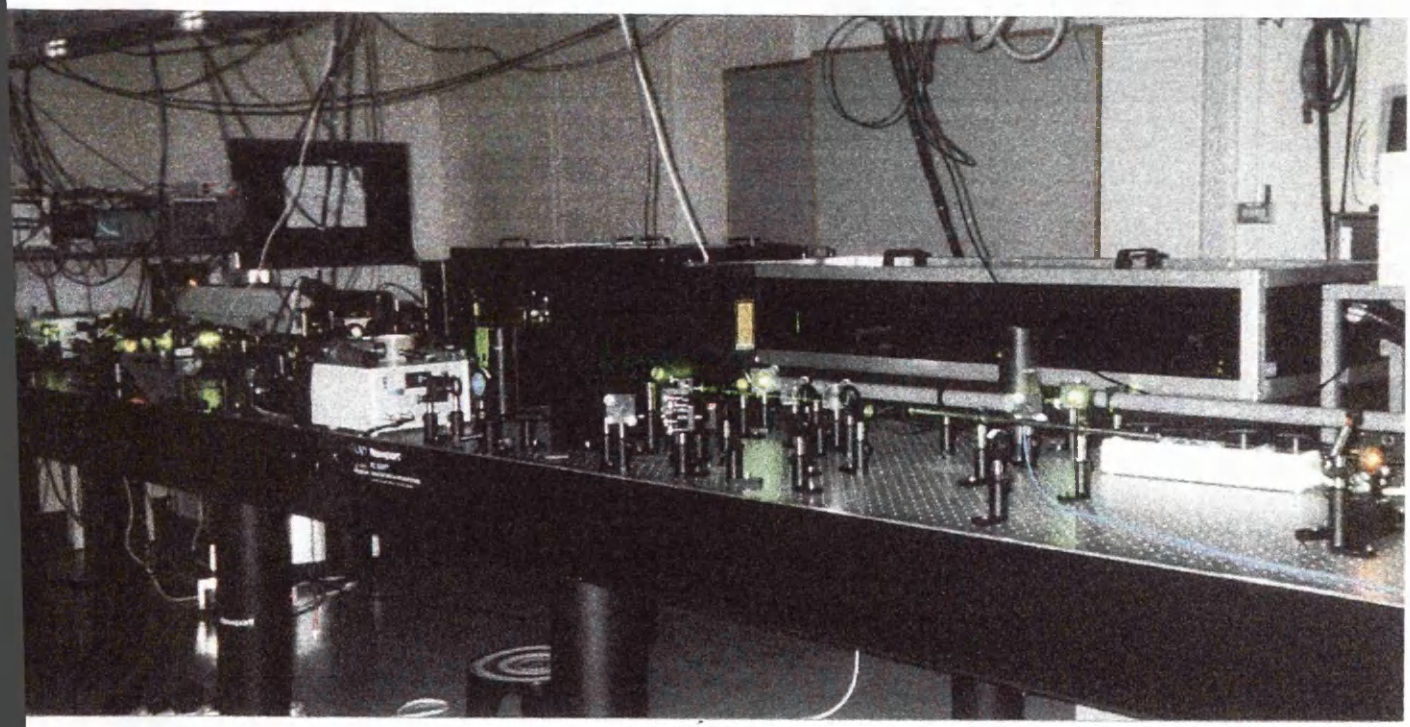

Photographs showing two views of the ASTRA laser facility situated in a semi-clean room. The green pump beams are clearly seen, as is the distinctive orange glow of the first and power amplifiers at centre-left and right of the lower picture, respectively.

Continuum) operating at 10 Hz with an energy of 140 mJ and 20 ns pulse duration. This pulse length of the pump laser is longer than previously and gives improved reliability and stability of the output pulse energy. The pump beam is image-relayed to the crystal. This is to ensure a uniform saturated pump fluence of 2 J cm^{-1}, which also ensures stability of the pulse energy. The output pulse from the first stage has energy of 1-2 mJ at 50 fs, as in the stage I design.

The pulse from the pre-amp stage is subsequently seeded into a power amplifier of a 'bow-tie' design similar to the pre-amp arrangement. The gain medium is a 7 mm long Ti:S crystal (Crystal Systems, FOM = 150) of diameter 10 mm. The crystal is longitudinally pumped from either end with up to 850 mJ from two 532 nm pulses from a Nd:YAG (Spectra Physics, GCR 270-10). The expected amplified pulse energy is near 200 mJ. However, in practice the laser output is usually limited to 110 mJ by parasitic modes in the crystal, which compete for gain at pump energies greater than 700 mJ. Future development will clad the rod in a material of higher refractive index, which should minimise this effect. As the pump beam is imaged onto the end-face of the rod, it necessarily comes to a focus at some point before the crystal. The fluence at the focus is sufficient to ionise the air and so the focal point is placed in a small beam-tube fed with nitrogen gas to prevent the discharge from coating the delicate optics.

The resulting amplified pulses are split by a 50:50 beam splitter and directed into two separate experimental areas, each of which is supplied with 5 mJ per pulse before compression. When the other experimental area was not in use, it was possible to conduct experiments using the full 10 mJ of the laser beam. By measuring the beam divergence of the compressed pulses, the beam was determined to be 2x diffraction limited.

The compressor system was that already in existence as part of the stage I laser and was situated in the experimental area. Thus, the pulse width could be varied to a desired value for an experiment from the 50fs optimum value by simply changing the spatial separation of the gratings. The separation needed to achieve a desired pulse width could be calculated from the formula:

$$p.w = \sqrt{\left[(50fs)^2 + (\Delta t)^2\right]} \qquad \text{(Eq. 2.1)}$$

where Δt is the difference induced in the pulse duration (chirp) and is given by:

$$\Delta t = \alpha(L - L_0) \qquad \text{(Eq. 2.2)}$$

where α is a constant given by: $\alpha.L_0$ = 300 ps (the duration of the stretched pulse) and L_0 is the optimal grating separation when the 300 ps pulse is compressed back to the original 50 fs duration.

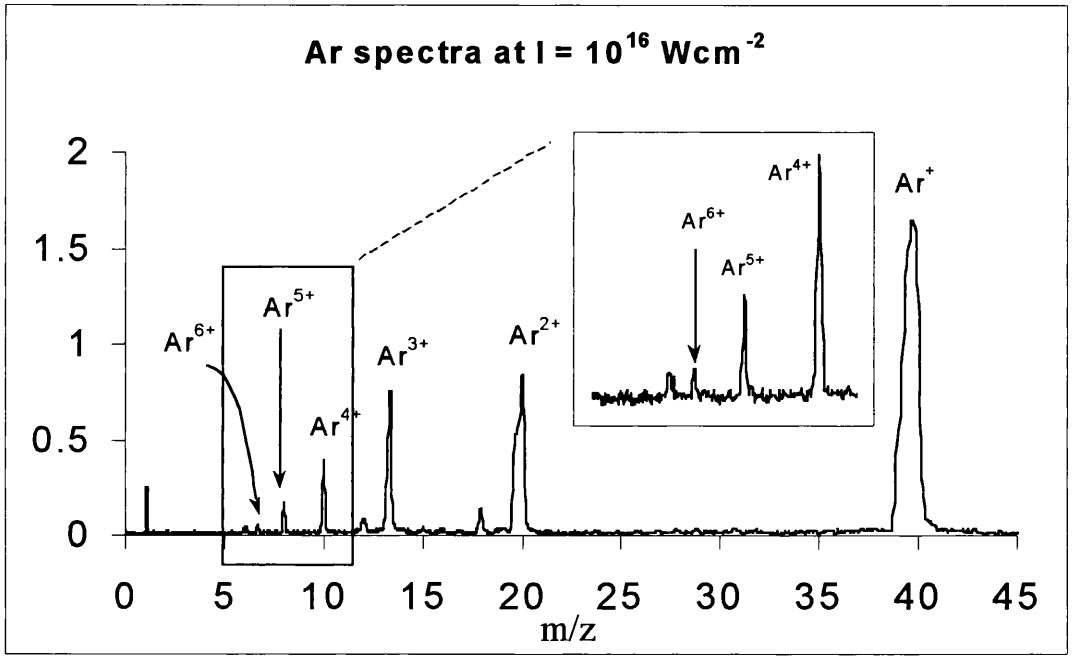

Figure 2.6 Ar spectra taken at a laser intensity of 10^{16} W cm^{-2}, showing Ar^{6+}

When the compressed 50 fs, 5 mJ pulses are focussed in the vacuum chamber of the TOF using a f/3 spherical mirror, laser intensities of about 10^{16} W cm^{-2} were achievable. This was corroborated using an argon calibrant and observing the Ar^{6+} ion signal, shown in figure 2.6. Laser systems capable of generating such intensities have applications not only in molecular dynamics, but also in the fields of astrophysics and nuclear physics. As noted by Bloembergen [26], the blackbody radiative density at temperatures of 10^6 K, such as those found in star interiors, corresponds to 10^{17} W cm^{-2}.

2.2.3 Laser components

This section deals with the laser system components individually.

2.2.3.1 Stretcher/Compressor

In order to achieve stretching of the duration of pulses from the femto oscillator, required prior to amplification (to limit the radiative density in the amplifier medium to below the damage threshold), as well as to recompress back to the femtosecond pulse regime, one needs a method of chirping the laser pulses. Chirping of laser pulses means to change the number of frequency components in the pulse spectrum. For example, up-chirping would increase higher frequency components in the leading-edge of the pulse, and an increase in the lower frequencies in the trailing-edge for down-chirping.

One technique for achieving this is to propagate the pulse down a single-mode optical fibre. The nonlinear refractive index of the fibre induces a phase shift of the frequencies that depends on the instantaneous intensity of the pulse. As the intensity rises along the leading edge, the phase shift increases until the peak and then diminishes as the intensity decreases. The instantaneous frequency shift (chirp) is given by the rate of change of phase-shift. This effect is termed self-phase modulation (SPM). Single-mode fibres have the advantage that all frequencies are chirped in an identical fashion. However, it is more difficult to compress the pulse back to its original duration using this technique, as the stretcher and compressor are mis-matched, i.e. there is a residual chirp after re-compression.

A more reversible way of chirping the pulse is to use an all-reflective stretcher/compressor arrangement. This is the technique used in the RAL system. By proper adjustment of the grating separation and incident angle in the stretcher/compressor, 2^{nd} and 3^{rd} order dispersion can be compensated for.

The stretcher and compressor consist of two diffraction gratings arranged in an anti-parallel and parallel configuration, respectively. The schematics are shown in figure

2.7. This design was first demonstrated by Martinez [13, 27] and shown to provide large, reversible stretch factors. It is important in a femtosecond laser to ensure no angle mis-match in two-grating designs that would distort the output pulse by introducing temporal and spatial chirping that would not be compensated for by the compressor. Small imperfections in the recompression may exist due to an offset from the ideal stretcher/compressor separation and incident angles required to compensate for the amplifier material and other optics in the system.

The laser pulse is incident on the first grating of the stretcher and is reflected at an angle that depends upon the wavelength. Thus the frequency components are spread out spatially. The effect is repeated at the second grating. The effective distance between the second grating and the image of the first grating controls the dispersion. When this distance is made optically negative, this arrangement has exactly the opposite dispersion of the grating compressor, shown in (b). The laser pulse in this stretcher design is retro-reflected and sent back through along the same path, thus providing a greater chirp in the output pulse from the stretcher.

After pulse chirping to about 200 or 300 ps in the system used at RAL and amplification in the saturated regime (to minimise pulse energy fluctuations and maximise energy gain) and in which the chirp is preserved, the pulse can be recompressed by a pair of parallel gratings. Large stretch factors can be achieved from the stretcher, allowing the pulse to be greatly amplified without damage to the gain material. With proper grating separation the compressor can exactly match the stretcher phase function, so that the original pulse width can be recovered. To avoid optical coating damage and phase distortion due to nonlinear index of refraction of the sapphire, the stretch factor is chosen to be greater than the minimum required. The chirp introduced onto the input pulse scales quadratically with grating period.

The gratings in the RAL system have a density of 1500 lines/mm and the spacing period generally depends on the stretch factor required, compensation of high-order dispersion, quality, compactness, size, flatness and diffraction efficiency. High density gratings are efficient and induce large stretch factors but they introduce large high-order dispersion, which may not be able to be compensated for. Low groove

a)

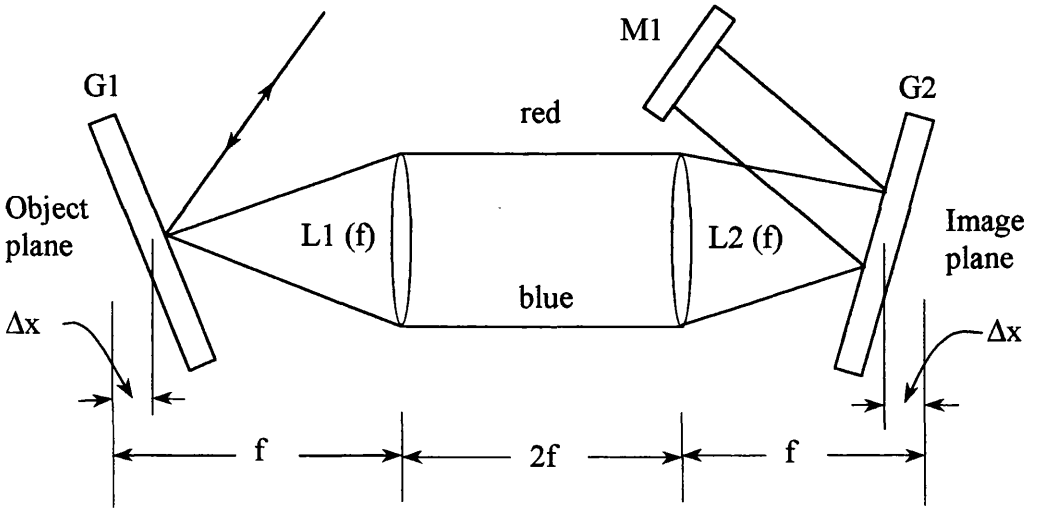

b)

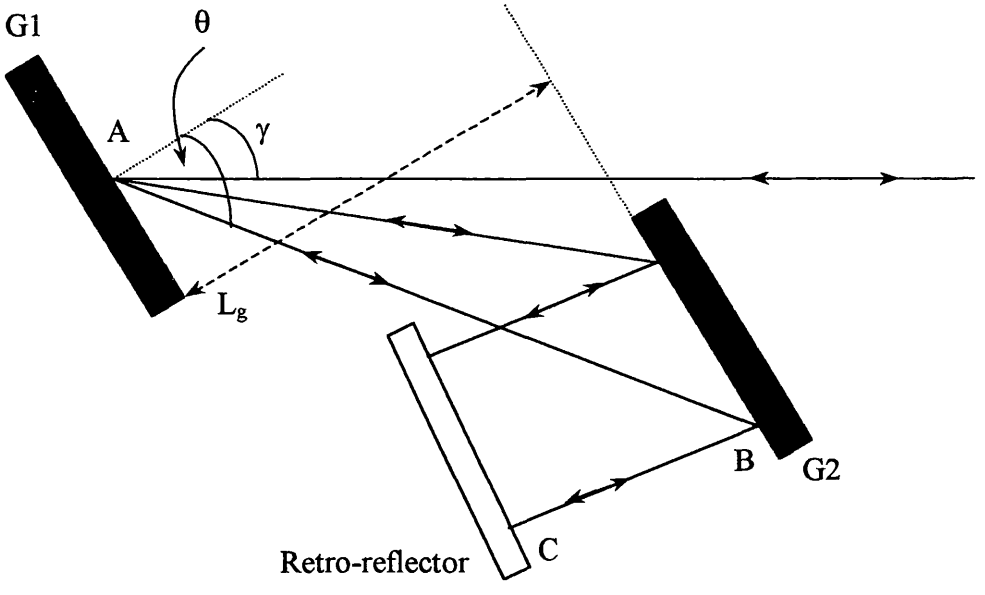

Figure 2.7 Schematic diagrams of a) laser pulse stretcher and b) laser pulse compressor.

densities, conversely, allow compensation up to third-order, with a relatively low residual fourth-order dispersion.

The pulse is also retro-reflected through the compressor to avoid the wavelength-dependent 'walk-off'' and hence minimise spatial chirping of the pulse. As the pulse size is large in the RAL system, the pulse is retro-reflected by a corner-reflector to direct the output pulse above and parallel to the input pulse. Furthermore, the parallelism of the grating faces in the compressor must be carefully aligned to avoid spatial chirping. To ensure good beam fidelity and focussing the grating surfaces are required to be as optically flat as possible (typically $\lambda/4$-$\lambda/10$). To obtain large stretch factors requires a large grating size, as the beam is spectrally dispersed on one of the gratings. However, to manufacture large gratings with the required optical flatness is extremely difficult. Thus, arbitrarily large stretch factors are not practical and it is more difficult to recompress the pulse.

The output pulse width is given by the reciprocal of the chirp bandwidth. Thus, if high-order dispersion can be controlled (up to fourth-order in typical femtosecond laser systems), then the original pulse duration can be recovered. In reference to figure 2.7, the dispersion in the stretcher and compressor is matched if and only if: $L_g = -2(f-s)$, where $s = (f-\Delta x)$ and the angle of the input pulse into the stretcher matches the angle of the reflected beam from the natural of the first grating of the compressor.

2.2.3.2 Multi-pass Amplifier

High-power ultrafast laser systems in existence today, such as that situated at RAL use solid-state materials as the gain medium for high gain at a broad bandwidth. These materials have the advantages of relatively long excited state lifetimes, high saturation fluences, broad bandwidths and high damage thresholds. The medium most in use and in use in the RAL system is Titanium:sapphire ($Ti:Al_2O_3$). As mentioned above, the possibility to generate ultrashort pulses by use of Ti:S lasers via the self-modelocking mechanism of the Kerr nonlinearity of the laser crystal has been established.

The Ti:S crystal has many useful properties which make it an almost ideal high-power amplifier medium in femtosecond laser systems. These include very high damage threshold (8-10 J cm^{-2}), high saturation fluence (0.9 J cm^{-2}), high thermal conductivity (46 W/mK at 300 K), and a peak gain cross-section of $\sigma_g = 2.7\times10^{-19}$ cm^{-2}. These factors allow pulses of energy greater than 1 J to be extracted from a small diameter rod, whilst the gain is sufficient to reach this energy from only 12-15 passes through 3 amplifier stages [28]. Of equal importance is that Ti:S possesses the broadest gain bandwidth of any known laser material (230 nm, centered at 800 nm, shown in figure 2.8) and hence it can support extremely short pulses, minimising gain narrowing or spectral clipping of the pulse. For high gain amplification, it also has a broad absorption spectrum centered at about 500 nm, figure 2.8, making it suitable to pump with the second harmonic of a large pulse-width Nd:YAG laser. The large duration of the pump pulse allows efficient coupling of energy into the crystal and the high gain of the entire bandwidth of the seed pulse.

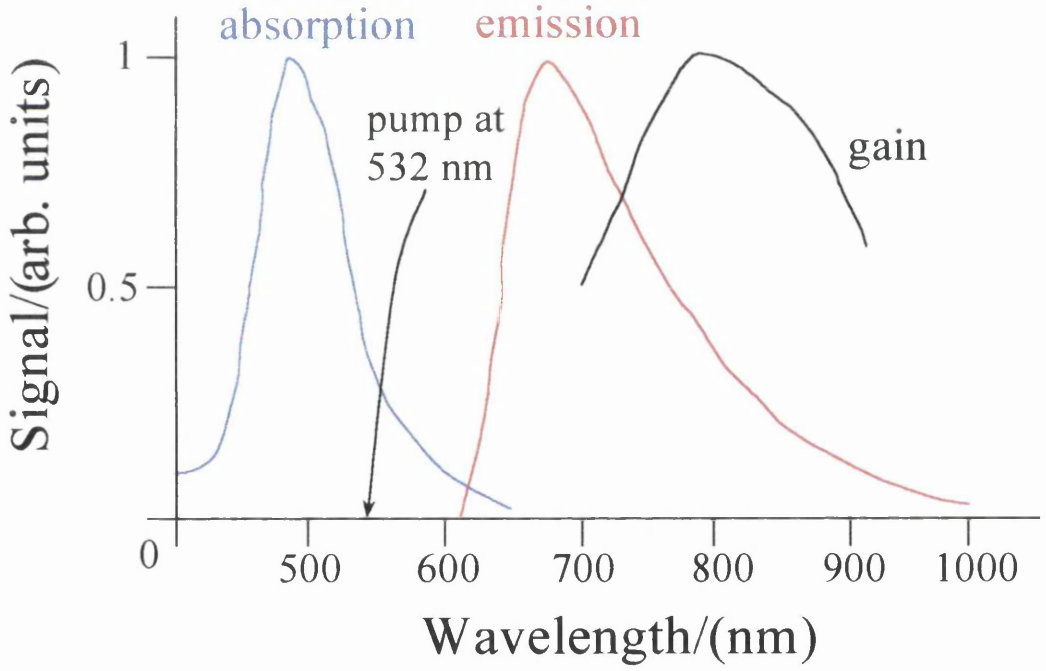

Figure 2.8 Absorption/Emission characteristics of the Ti:S gain medium

As hinted at briefly above, amplification not only increases pulse energy but also has the potential to significantly alter the seed pulse shape and spectrum. This is due to the finite gain bandwidth of the amplifier medium, even in the case of Ti:S. The

spectral narrowing of the input pulse associated with the amplification process is termed gain narrowing. A further consequence of the finite gain bandwidth is that it can blue- or red-shift the pulse depending on the initial offset of the central wavelength of the seed pulse relative to the gain medium. The red wavelengths precede blue wavelengths in the pulse spectrum and the Ti:S gain profile, as shown in figure 2.8, falls more sharply at shorter wavelengths than for longer wavelengths. This leads to an optimum input spectrum whose peak is shifted below the 800nm gain peak of Ti:S.

The Ti:S material has high thermal conductivity. Even so, problems can still arise due to the fact that a beam with high average power levels is focussed to a few mm in diameter in the amplifier to achieve sufficient gain per pass. However, this can lead to thermal lensing (self-focussing), birefringence and stress in the crystal. In the multi-pass amplifier configuration, thermal lensing can build up with successive passes leading to a rapid decrease in the amplified beam size which in turn leads to the pulse reaching saturation fluence before all the energy available can be extracted.

The high power levels of the pulse within the crystal can also lead to nonlinear phase contributions from self-phase modulation, in a similar fashion to propagation in a fibre-optic cable. Since the pulse is chirped in the crystal, this nonlinear temporal phase shift is mapped into the spectral phase. This spectral phase shift is given by:

$$B = \frac{2\pi}{\lambda}\int \frac{\Delta n}{n} dl = \frac{2\pi}{\lambda} n_2 \int_0^L I(t,l)\, dl \qquad \text{(Eq. 2.3)}$$

where n_2 is the nonlinear index (2.5×10^{-16} cm^2 W^{-1} for sapphire), and I (t, l) is the intensity within the crystal. The peak value of this expression is termed the "B" integral of the amplifier system. It is considered desirable to maintain a B integral value less than 1 to eliminate phase contributions that cannot be compensated for by the compressor and self-focussing of the amplified beam within the crystal. Self-focussing causes the crystal to behave as a nonlinear spectral 'filter', as the higher frequencies in the trailing and lower frequencies of the leading 'wings' of the pulse are not as intense and hence experience self-phase modulation to a lesser degree.

This can be overcome by use of a thinner Ti:S crystal, as there is less potential for SPM to build up. Employing a large stretch of the seed pulse can also eliminate self-focussing. In the 1 J amplifier at RAL the seed pulse is first stretched to 600 ps.

There are essentially two basic designs for a femtosecond laser amplifier – a regenerative and multi-pass amplifier, both of which are shown in figure 2.9. In the regenerative (regen) design, as shown in figure 2.9 a, a low-energy chirped seed pulse is injected into the cavity via a time-gated polarisation device such as a Pockels cell and thin-film polariser. It then makes typically 20 passes through the medium and the high energy pulse is subsequently 'switched out' by a second time-gated polarisation rotation. Beam overlap between pump and signal pulse is good in a regen leading to high extraction efficiencies. However, regens have several disadvantages. A relatively low-gain configuration has to be used in a regen, as with higher gains amplified stimulated emission (ASE) can build up quite rapidly and deplete the gain. Furthermore, due to relatively long optical path lengths in the regen cavity and the presence of high refractive index materials in Pockels cells and polarisers, high-order dispersion effects can creep into the pulse, making recompression of ultrashort pulses ($\leq$ 50 fs) difficult.

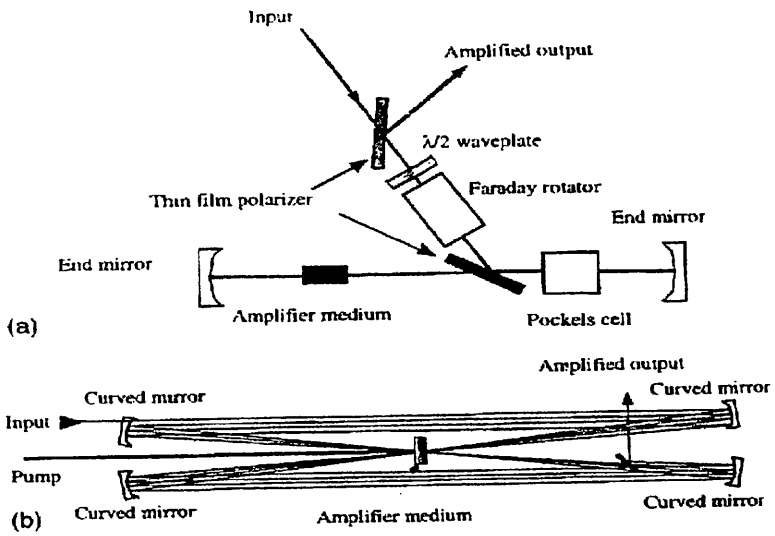

Figure 2.9 Schematic of (a) regenerative and (b) multi-pass amplifier designs

Multi-pass amplifier designs, on the other hand, pass the pulse through the amplifier medium without use of a cavity, as shown in figure 2.9 b. Multi-pass amplifiers have several advantages over regens making it a more practical design in many high intensity lasers, as in the RAL facility. In this amplifier configuration, as there is no cavity as such, the optical path is not a resonator. Thus, ASE can be suppressed to a greater degree while still achieving high gains. A consequence of this is that the gain per pass is higher and so fewer passes are required. This limits the high-order dispersion picked up through the crystal and the nonlinear phase shifts due to the B integral, allowing much shorter pulses to be amplified. The extraction efficiency is lower than in regens, but this can easily be compensated for, if necessary.

2.2.4 Experimental Optical Layout

2.2.4.1 Optical layout for the Stage I laser

The experimental layout for the first series of experiments, using the RAL stage I laser is shown in figure 2.10. The vertically polarised 1mJ femtosecond pulse exits the compressor, passes through an iris, onto a pair of broadband Au-coated mirrors, which are 90% reflective. The pulse is then reflected from a pair of highly reflective Au-coated mirrors and directed into the TOF high-vacuum chamber, via another pair of irises to ensure optimum optical alignment onto the focussing mirror mounted in the TOF. A variable neutral density filter (NDF) is placed in the path of the beam in order to vary the pulse energy and hence the laser intensity at the interaction region. The laser beam alignment into the TOF is aided by using a He:Ne initially, and using a 'nightcam' infra-red viewer, as the 790nm of the laser pulse is just beyond the visible spectrum.

The polarisation of the laser pulse as it propagates through the compressor is horizontal and is converted to vertical polarisation as it exits the compressor, by a pair of mirrors, on its way to the broadband Au-coated mirrors. The polarisation of the laser beam is thus vertically polarised at the interaction region within the TOF.

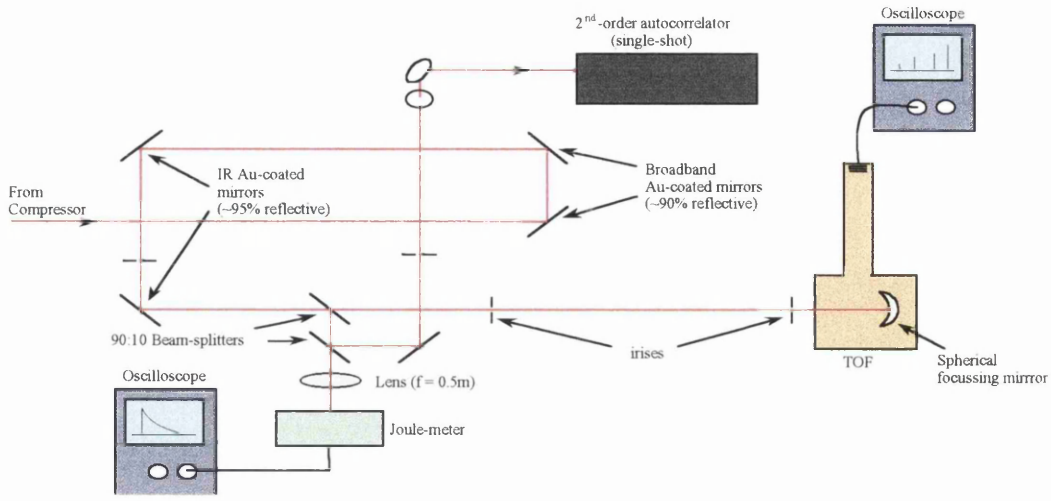

Figure 2.10 Optical layout of the Stage I femtosecond laser system

A Pellicle beam-splitter of 90% transmission is placed in the beam just before entry into the TOF. The Pellicle beam-splitters have the advantages of having broadband characteristics, so do not unduly affect the wavelength spreading of the beam. They also eliminate multiple reflections, which are commonly encountered using thicker glass beam-splitters. They are made of optical grade nitrocellulose and are typically 5 μm thick. The 10% reflected beam is directed to a Molectron J3-09 pyroelectric Joule-meter. The Joule-meter works by having a photosensitive lithium-tantalate crystal, which is rapidly heated by absorption of photons and so becomes electrically polarised. The resulting surface charge is collected and is displayed on a digital oscilloscope (LeCroy 9304, 175 MHz). By calibrating the voltage reading on the oscilloscope with a digital meter, it is possible to convert the voltage into an energy reading. It is considered desirable to always monitor the laser pulse energy to ensure an acceptable shot-to-shot reproducibility, and to be able to calculate the laser intensity at which a mass spectrum is acquired.

A (optional) second 90:10 beam-splitter is placed in the beam-path after the 1st beam-splitter, which directs 10% of the pulse to a single-shot autocorrelator. This device is used to measure the pulse-width of the femtosecond laser and the Gaussian profile of the pulse. The detail of its operation is given below.

2.2.4.2 Optical layout for the Stage II laser

The optical bench layout for the second series of experiments using the stage II design (ASTRA) is shown in figure 2.11. The laser beam comes into the experimental area from the amplification stage vertically polarised. Prior to entry into the compressor, a 90:10 beam-splitter is inserted into the beam path and this reflects 10% of the beam energy into either a Joule-meter, or a photodiode mounted in a beam homogeniser for triggering of the digital oscilloscopes. It is then converted to horizontal polarisation for propagation through the compressor. A further mirror pair converts the pulse back to vertical polarisation after exiting the compressor.

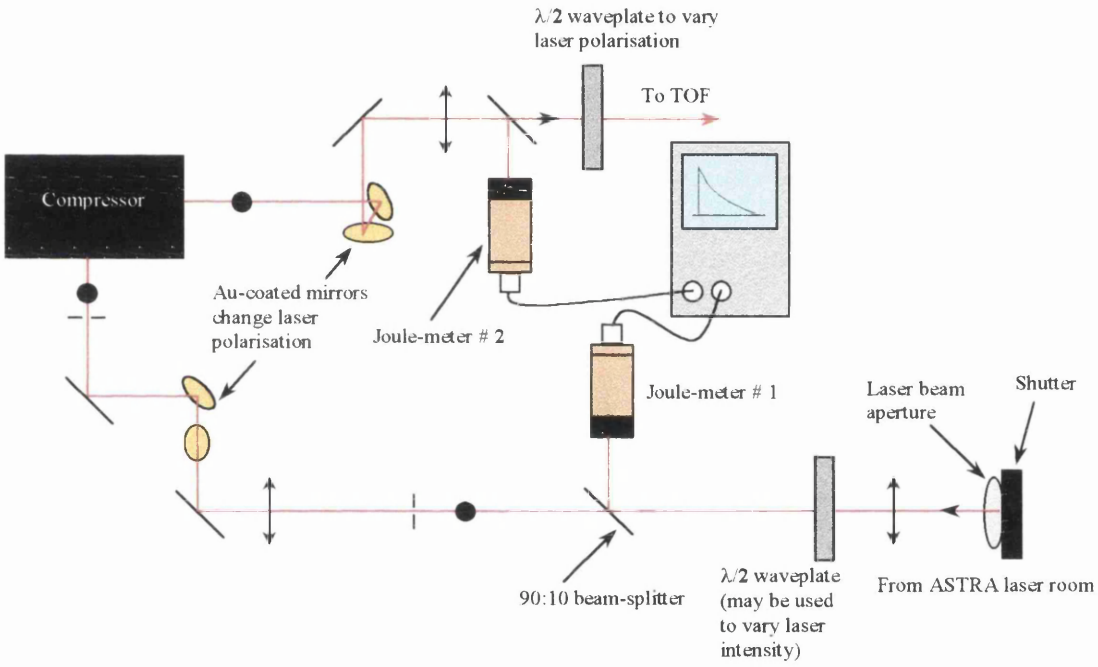

Figure 2.11 Optical layout of the ASTRA (stage II) femtosecond laser system

Because the compressor only allows horizontally polarised light to propagate through it, this property can be used to vary the beam energy into the TOF. This method eliminates nonlinearity in the attenuation process in a NDF, which may also become damaged at the high energies used.

Prior to carrying out polarisation studies, the angle of the λ/2-plate was calibrated to ensure correct polarisation vector orientation. The λ/2-wave plate was inserted

before the compressor arrangement. The waveplate was then rotated until minimum beam energy out from the compressor. This mark corresponds to horizontal polarisation. The wave-plate is then inserted into the path of the beam just before the quartz window of the TOF. This is the best position as it eliminates polarisation-dependent loses through the beam-splitters.

As the laser pulse exits the compressor on its way to the TOF chamber, 10% of the beam is directed via a 90:10 beam-splitter to an Molectron Joule-meter or to a single-shot second-order Autocorrelator to measure the pulse shape and temporal width. The autocorrelator is described in the next section.

2.2.4.3 Single-shot Second-order Autocorrelator

A schematic of the autocorrelator design is shown in figure 2.12. For laser pulses of picosecond duration, the measurement was carried out by fast photoelectronic streak cameras, but the electronic response time is not sufficient for sub-picosecond pulse measurements. Thus, it is not possible to measure the pulse duration by electronic means. Autocorrelation techniques were developed to measure the duration of femtosecond pulses by manipulating the laser pulse to measure itself.

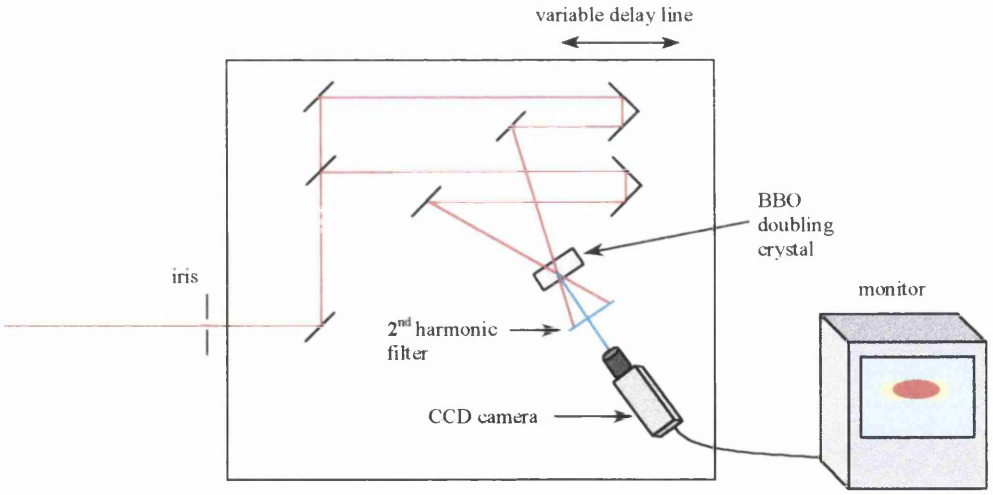

Figure 2.12 A schematic of the single-shot 2nd order autocorrelator

An autocorrelation is a mathematical operation where a function is split into two parts that are delayed with respect to each other, multiplied, and then integrated in time. The pulse is divided by a 50:50 beam-splitter, and one pulse propagates through a variable delay-line. The two pulses are then recombined at a frequency-doubling crystal. For the two pulses entering the crystal, the intensity of the blue light produced depends on the overlap of the pulses in time and space. The detector (Pulnix TM 765 CCD camera) is placed to look only at the blue light in the straight-through position (a filter is used to eliminate pulses of the fundamental frequency), and it integrates the signal for the delay time between laser pulses.

Since the autocorrelation is a function of the delay time between the two pulses, the detected light must be measured for a range of delay times. To shorten the measurement time and simplify the setup, a single-shot autocorrelator is used. In the geometric configuration used, the two pulses are overlapped in the doubling crystal such that the delay time is mapped to the position on the detector. Thus, with a properly calibrated time-to-space mapping on the detector, the autocorrelation can be measured with a single pulse (single shot). A typical second-order autocorrelator measurement of femtosecond pulses is shown in figure 2.13. The multiplicative factor (0.67), shown in the inset, is a constant assuming a Gaussian pulse shape, to obtain the FWHM pulse duration.

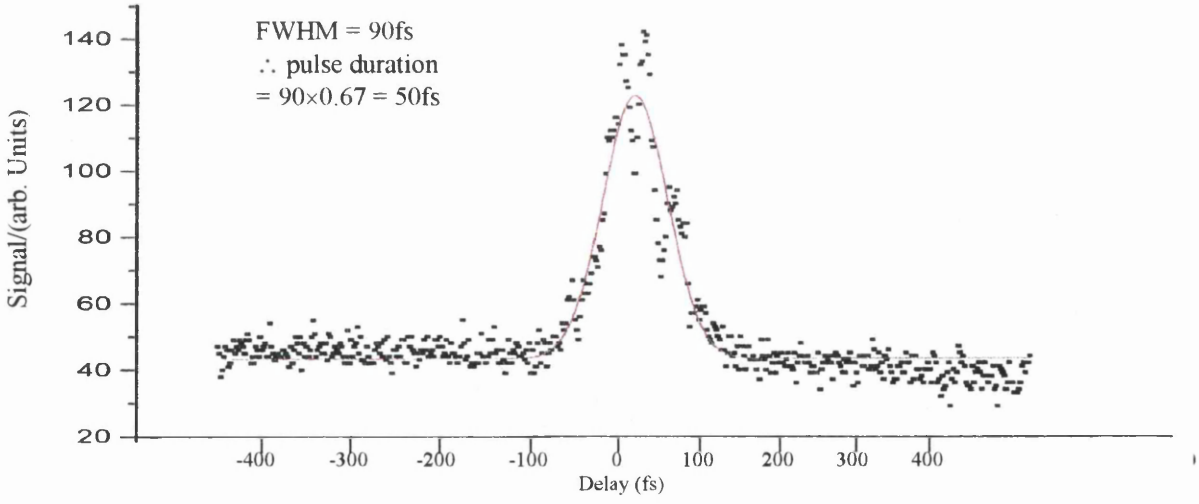

Figure 2.13 Autocorrelation measurement of a 50 fs pulse

There are several problems with 2^{nd}-order autocorrelation techniques, however. For high-power ultrashort pulse lasers it is useful to know the amplitude and phase of the pulse spectrum, which is beyond 2^{nd}-order autocorrelation. Also, it is not possible to measure the pulse contrast ratio or the asymmetry, i.e. the pre-pulse. More importantly, the pulse duration obtained is subject to inaccuracies. The Full Width at Half Maximum (FWHM) that is used to define the duration of a transform-limited pulse, measured using 2^{nd}-order autocorrelation techniques, could be 18, 24 or 45 fs, depending on whether a $sech^2$, Gaussian, or flat-topped pulse shape is assumed. This is assuming no spectral clipping, for a pulse of 40nm bandwidth.

2.3 Linear time-of-flight (TOF) mass spectrometer

2.3.1 General Description

The experiments that are detailed herein were performed using gas-phase samples. The sample is admitted effusively through a hypodermic needle from an inlet line into a high-vacuum interaction chamber. Here the molecular beam diffuses into the chamber and interacts with the intense electromagnetic field of a linearly polarised, femtosecond laser pulse. The interaction volume is hence at the focus of the laser beam, which is the region where the beam waist is a minimum along the Rayleigh length. The laser is focussed by either a f/3, f/5 or f/10 Al-coated spherical mirror. The mirrors are mounted on a rotateable x-y-z vacuum bellows assembly.

The focussing mirrors present a problem in that for a 2x diffraction-limited beam, the spherical mirrors will introduce a spherical aberration and the focus will become 'smudged' in space. Parabolic mirrors may be used to improve the beam quality at focus.

The laser intensities at the focus region in these experiments are sufficient to ionise all molecules investigated to highly charged states. The laser beam alignment is such that the laser/matter interaction region is formed between two ion electrodes – the pusher plate and the 1^{st} ion optic, which are 1cm apart. A 2^{nd} ion optic is set at earth potential. This is the so-called Wiley-McLaren configuration for linear mass

spectrometers, [29]. A schematic of the TOF is shown in figure 4.1. The pusher plate is typically set to 2.5kV and the 1st ion optic is set to 2kV. Thus the ions produced at the interaction spot are produced in an electric field. This extraction field is able to direct the ions into a field-free drift tube, of length 1.2m. An Einzel lens (900V), the ion equivalent of an optical focussing lens, is inserted after the 2nd ion optic to increase transmission to the detector. The ion then falls through a potential difference of approximately 2.25kV before arriving at the detector. The flight time of the ion to reach the detector, t, is dependent on the ion mass-to-charge ratio (m/z). The higher the charge of the ion, the shorter the time to reach the detector. The flight time of an ion of mass m and charge z, is given by the equation:

$$t = l\sqrt{\frac{m}{2zeV}} \qquad \text{(Eq. 2.4)}$$

where l is the ion path length, e is the electronic charge, and V is the potential difference through which the ion falls on its way to the detector.

The precise value of the ion path length is subject to uncertainty. For example, in Coulomb explosion of molecules, which has a propensity to occur at the laser intensities utilised in the experiments detailed herein, the molecule fragments into its constituent atoms. These are ejected with some velocity both towards and away from the detector. The backward-directed atomic ions are then slowed down and directed back towards the detector by the extraction field. The spatial position within the focal region and the intensity at the point of the ions formation give rise to a velocity distribution of the ions detected and further uncertainty in the value of the ion path length.

Furthermore, some ions of a particular mass and charge may be produced slightly later in the laser pulse than others which introduces a temporal 'spread' in an ion peak in the mass spectra. Therefore, this initial spatial/temporal and kinetic energy distribution of the ions limits the resolving power of a practical mass spectrometer, such as the one employed for these experiments. For an ion with m/z ratio, the TOF mass resolution is given by:

$$R = \frac{m/z}{\Delta(m/z)} = \frac{m}{\Delta m} \qquad \text{(Eq. 2.5)}$$

where Δm is the FWHM of the mass peak. The TOF mass resolution is ~100 at 200Da. (1 Dalton = 1 a.m.u), at the operating parameters outlined above.

An electron multiplier (Thorn EMI, Ltd.) is used to detect the ions and is situated at the end of the drift tube (see below). A gain of 2.5 kV is typically applied to the detector, which provides the above mass resolution and good signal-to-noise ratio (SNR). The gain can be increased or decreased as required.

The high-vacuum chamber is pumped to a background pressure of 10^{-8} Torr by a Turbomolecular pump (Balzers TPU 350, 200 l/s) backed by a rotary pump (Edwards). The Turbomolecular pump works in a similar fashion to the jet engine (see below). When samples were introduced into the TOF, working pressures of the order of 10^{-6} Torr were maintained. This pressure is sufficiently low to avoid pressure-broadening or space-charge effects. Factors preventing the optimum working pressure were either leakages or contamination. Alternatively, the system (high-pressure vacuum chamber and/or inlet line) could be 'flushed' with inert Ar gas and/or baked overnight. The system is then 'de-gassed' several times until the desired pressure is attained.

2.3.2 Inlet Line

The sample to be analysed is always in the gas-phase, but the original source of the chemical need not be. For example, CS_2 is a liquid at room temperature, but has a high vapour pressure. Thus a drop of CS_2 is injected into a custom-made glass phial, which is connected to the inlet line via a needle-valve (Swagelok). The sample can then be admitted into the TOF as a gas by opening the needle-valve slowly until the desired operating pressure is attained. The needle-valve allows precise flow control. It is possible, if desired, to analyse solid samples with sufficient vapour pressure in the same way. Most chemical samples however, were initially in the gas-phase and were supplied in a gas cylinder under pressure. These

samples were coupled to the inlet line using a nylon (PTFE) tube inserted into the needle-valve, via a gas regulator. Samples diffused into the high vacuum chamber via a hypodermic needle through the pusher-plate.

For the purpose of sample preparation, an on/off valve situated after the needle valve de-couples the vacuum chamber from the inlet line. This allows the sample to be changed without affecting the vacuum chamber pressure. Residual sample pressure is pumped away by a rotary-pump (Edwards) prior to introduction of a new sample. The PTFE line or glass phial is then pumped for several minutes, to eliminate air contamination. Flushing with Ar or by heating the line with a heat-gun or backing tape can further reduce contamination of the inlet line.

2.3.3 Electron Multiplier

The ions that were produced on interaction of the molecular beam with the laser pulse were detected at the end of a long field-free drift tube by an electron multiplier (E.M) (Thorn EMI, Ltd.). An ion entering the electron multiplier created an 'avalanche' of electrons – a current that was amplified (a gain of 2.5 kV applied to the E.M). This signal was then fed to a digital oscilloscope (LeCroy 9344C, 500 MHz) which allowed the signal to be viewed as a mass spectrum – a measure of the ion mass-to-charge yield as a function of the ions flight-time. Typically, mass spectra were averaged over 300 laser pulses to minimise signals due to small laser intensity fluctuations, and improve the SNR. The digital oscilloscope also allowed the storage of the mass spectra on standard 3.5" 1.44MB floppy discs. Thus, the data can be analysed using a p.c. at a later date.

A schematic of the electron multiplier is shown in figure 2.14. The ions enter the E.M from the right. The grid potentials increase progressively from right to left, so the dynode on the immediate right acts as a cathode relative to that on its left. The first grid is at Earth and the last is at 2.5 kV (the gain on the E.M). An incoming ion strikes a dynode and liberates an electron. The liberated electron accelerates towards the next adjacent grid and knocks free "secondary" electrons from an 'anode'. This process progresses through several stages. This results in an

'avalanche' of electrons, which can be electronically counted. The gain of the E.M can be as high as 10^6, which translates into high sensitivity and ability to count very few ions.

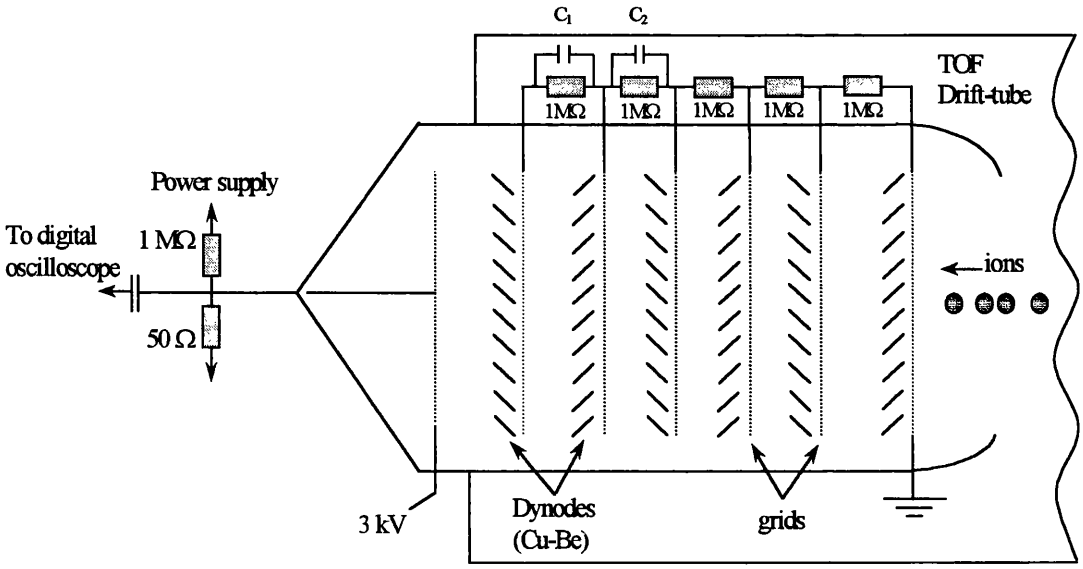

Figure 2.14 A schematic of the electron multiplier

2.3.4 Turbo Molecular Pump

A turbomolecular pump is a high-speed mechanical vacuum pump, essentially comprised of a series of compression stages formed by a rotor rotating at high speed (~90,000 rpm) and a stator, see figure 2.15. In this way, the working principle is similar to an axial-flow compressor. The momentum is imparted to the gas molecules by the fast moving rotor blades. The pumping speed and compression ratio i.e. ultimate vacuum obtained by a Turbomolecular pump is mainly decided by molecular weight of gas to be evacuated, rotational velocity of the pump rotor, the flow channel geometry, total number of rotor and stator blades per stage and total number of stages.

A turbomolecular pump is used to evacuate the high-vacuum chamber of the TOF since it is able to evacuate a vacuum system from atmospheric pressure down to 10^{-8} Torr and produce a clean and hydrocarbon-free vacuum. The pumping rate for the system described here is about 200 l/s. The gas captured in the compression stages is then compressed by the downstream stages, which are equipped with shorter

blades so that the gas is compressed to such an extent that it can be taken over by a backing (rotary) pump. The turbomolecular pump is supported by a backup rotary pump to provide molecular flow conditions and to displace the molecules to the outside atmosphere.

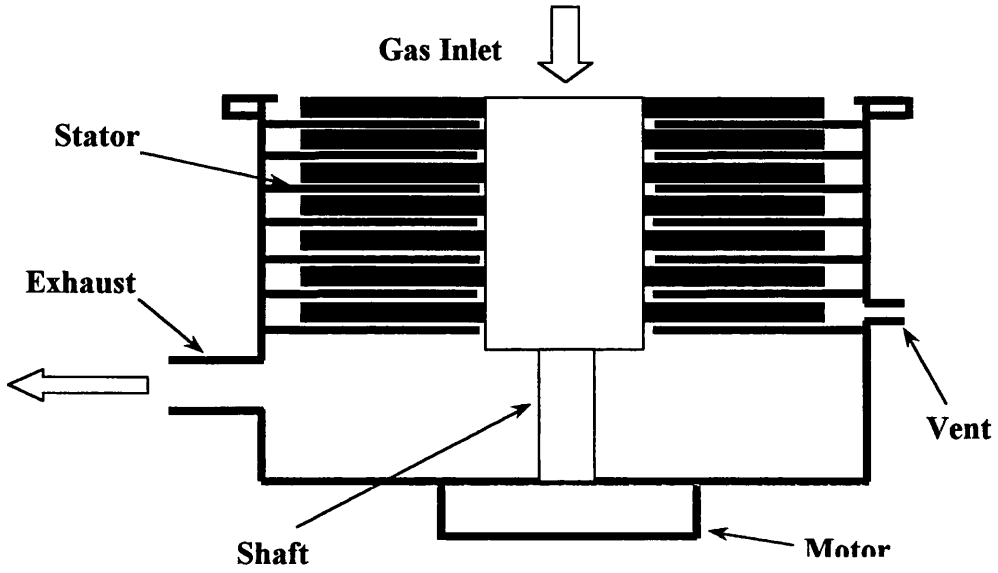

Figure 2.15 A schematic of the Turbomolecular Pump

References

[1] Maiman TH 1960 Nature (London), **187**, 493

[2] Hellwarth RW 1961 Advances in Quantum Electronics, Ed. JR Singer (Columbia University), p.334

[3] Hellwarth RW 1961 Bull. Am. Phys. Soc., **6**, 414

[4] Mocker HW and Collins RJ 1965 Appl. Phys. Lett., **7**, 270

[5] DeMaria AJ, Stetser DA, Heinan H 1966 Appl. Phys. Lett., **8**, 174

[6] Shank CV and Ippen EP 1974 Appl. Phys. Lett., **24**, 373

[7] Fork RL, Shank CV, Yen RT 1982 Appl. Phys. Lett., **41**, 223

[8] Fork RL, Brito Cruz CH, Becker PC, Shank CV 1987 Opt. Lett., **12**, 483

[9] Spence DE, Kean PN, Sibbett W 1991 Opt. Lett., **16**, 42

[10] Zhou JP, Taft G, Huang CP, Murnane MM, Kapteyn HC 1994 Opt. Lett., **19**, 1149

[11] Janszky J, Corradi G, Gyuzalian RN 1977 Opt. Commun., **23**, 293

[12] Shank CV, Fork RL, Yen R, Stolen RH, Tomlinson WJ 1982 Appl. Phys. Lett., **40**, 761

[13] Martinez OE 1987 J. Quant. Elec. (IEEE), **23**, 1385

[14] Knox WH 1988 J. Quant. Elec. (IEEE), **24**, 388

[15] Maine P, Strickland D, Bado P, Pessot M, Mourou G 1988 J. Quant. Elec. (IEEE), **24**, 398

[16] Kmetec JD, Macklin JJ, Young JE 1991 Opt. Lett., **16**, 1001

[17] Rudd JV, Korn G, Kane S, Squier J, Mourou G Bado P 1993 Opt. Lett., **18**, 2044

[18] Barty CPJ, Gordon III CL, Lemoff BE 1994 Opt. Lett., **19**, 1442

[19] Barty CPJ, Guo T, LeBlanc C, Raksi F, Rose-Petruck C, Squier J, Wilson KR, Yakovlev VV, Yamakawa K 1996 Opt. Lett., **21**, 668

[20] Chambaret JP, LeBlanc C, Cheriaux G, Curley P, Darpentigny G, Rousseau P, Hamoniaux G, Antonetti A, Salin F 1996 Opt. Lett., **21**, 1921

[21] Rundquist A, Durfee C, Chang Z, Taft G, Zeek E, Backus S, Murnane MM, Kapteyn HC, Christov I, Stoev V 1997 Appl. Phys. B, **65**, 161

[22] Langley AJ, Girard N, Mohammed I, Ross IN, Taday PF 1999 Central Laser Facility, RAL Annual Report 1998/99, 187

[23] Shon NH, Suda A, Midorikawa K 1999 Phys. Rev. A, **60**, 2587

[24] Taday PF, Mohammed I, Langley AJ, Ross IN, Codling K, Ledingham KWD, Newell WR, Preston S, Riley D, Williams I 1998 Central Laser Facility, RAL Annual Report 1997/98, 179

[25] Strickland D, Mourou G 1985 Opt. Commun., **55**, 447

[26] Bloembergen N 1999 Rev. Mod. Phys., **71**, S283

[27] Martinez OE 1986 J. Opt. Soc. Am. B, **3**, 929

[28] Backus S, Durfee III CG, Murnane MM, Kapteyn HC 1998 Rev. Sci. Instrum., **69**, 1207

[29] Wiley WC and McLaren IH 1955 Rev. Sci. Instrum., **26**, 1150

Chapter 3

Uniform molecular analysis using femtosecond laser mass spectrometry (FLMS)

CHAPTER OVERVIEW

The potential of femtosecond laser time-of-flight mass spectrometry (FLMS) for uniform quantitative analysis of molecules has been investigated. Various samples of molecular gases and vapours have been studied, using ultra-fast (~50 fs) laser pulses with very high intensity (up to 1.6×10^{16} W cm^{-2}) for non-resonant multiphoton ionisation/tunnel ionisation. Some of these molecules have high ionisation potentials, requiring up to ten 800nm photons for non-resonant ionisation. The relative sensitivity factors (RSF) have been determined as a function of the laser intensity and it has been demonstrated that for molecules with very different masses and ionisation potentials, uniform ionisation may be achieved at the highest laser intensities. Universal quantitative laser mass spectrometry of molecules is therefore a distinct possibility.

1 Introduction

The coupling of short-pulse lasers with mass spectrometry permits unambiguous and ultra-sensitive detection and analysis of atoms and molecules, and has become an important analytical tool in many areas [1-4]. The procedure and mechanism of ion production plays a key role in its analytical ability. Generally, preceding detection of ions by a time of flight (TOF) mass spectrometer, a laser ionises the atoms or molecules in samples by resonant (including resonance enhanced) or, as in the case with femtosecond laser pulses used here, non-resonant ionisation. For elements, such ionisation is a simple up-pumping of atomic levels to ionic states. However, due to the larger number of degrees of freedom, ionisation of molecules is often accompanied by and/or competes with molecular dissociation, which leads to the production of fragment ions.

Molecular fragmentation due to multiphoton absorption can occur via two different mechanisms [5-7], known as ladder switching and ladder climbing. These two mechanisms proceed as dissociation followed by ionisation (DI) and ionisation followed by dissociation (ID), respectively. In the first mechanism, the molecule absorbs a number of photons resonantly or non-resonantly to reach a dissociative state below its ionisation level. If the laser pulse length is longer than the lifetime of the state then the molecule can fragment to form neutral moieties. Depending on the laser intensity, these fragments may absorb further photons from the same laser pulse to ionise and/or further fragment. Conversely, for the second mechanism, usually if the laser pulse is much shorter than the lifetime of the dissociative state, then the up-pumping rate may be high enough that the ionisation level is reached. The manifold of ion states can absorb further photons and fragment. Alternatively, the molecule can be pumped, via a series of auto-ionisation levels, to some highly excited state of the molecule, which then dissociates via Coulomb explosion to produce highly charged fragment ions. These two variants result in ionisation before dissociation and hence parent ions are produced and may be detected in these ID processes. The DI and ID mechanisms compete with each other, although ladder climbing becomes more dominant as the laser pulse duration decreases.

Therefore, short pulse and high intensity lasers are likely to suppress the dissociation via neutral molecules, so that the parent molecule may be more readily detected.

Formerly, nanosecond (ns) laser pulses were coupled to mass spectrometers for surface analysis and demonstrated [8, 9] a powerful analytical ability for elements with low ionisation potentials. However, in the ns regime the ionisation efficiency is very poor for elements with high ionisation potentials and for molecules the process of dissociation followed by ionisation (DI) dominates [10] and leads to small or no parent ion production/detection and hence to ambiguous analysis. Therefore, shorter and higher intensity laser pulses are likely to have considerable potential for the chemical analysis and mass spectrometry of molecules and elements with high ionisation potentials.

Ultrafast (ps to fs) pulse lasers generating intense fields of 10^{12}-10^{15} W cm^{-2} and beyond have become increasingly available in research laboratories (with compact footprints), opening up ultrafast/high intensity laser mass spectrometry to extensive investigation. Consequently, scientists in analytical areas, who are trying to take advantage of the great potential of FLMS to overcome the difficulties experienced in the nanosecond regime, are showing considerable interest. A series of experiments [10-18] have been carried out to compare high intensity (up to 10^{15} W cm^{-2}) and short pulse width (ps and fs) with nanosecond laser multiphoton absorption in mass spectrometry, for many different atomic and molecular samples. From these results it has been shown that by using ultrafast intense lasers, the dissociative states of molecules can be bypassed and hence parent ions, allowing wholly unambiguous identification of the molecular species present, are more easily produced/detected and often dominate the mass spectra. Ionisation saturation of species can be reached and it is possible that species with different ionisation energies are ionised with similar efficiencies. Therefore, it is expected that FLMS may be used as a universal ultra-trace analytical technique. This may be achieved if all the molecules of each species present could be completely ionised in a well-defined ionisation volume and the ionisation saturation of each species were reached.

For quantitative surface and material analysis, C.H. Becker and C. He et al. [19-22] have studied some gases (Ar, Kr, NO, Xe, N_2 and O_2) and solid samples (SiO_2, GaAs, SiC and C1154 alloy) using a high intensity (10^{14}-10^{15} W cm^{-2}) 35 ps-laser at 532 nm with time-of-flight mass spectrometry. The results, with the relative sensitivity factors (RSFs) close to unity, showed that the saturation of the multiphoton ionisation and uniform ionisation yields were achieved even for species with widely different ionisation potentials. The possibility of quantitative surface compositional analysis was demonstrated with a powerful ionisation laser. These authors have indicated that the ionisation proceeds via multiphoton processes although at the highest intensities reached, tunnel ionisation begins to play a part.

Using the FORTH (Foundation for Research and Technology – Hellas, Greece) and RAL (Rutherford Appleton Laboratory, UK) laser facilities, the Glasgow group [13, 14, 23-28] have carried out a wide series of investigations on high intensity laser, non-resonance, multiphoton and tunnelling ionisation TOF mass spectrometry. A number of different molecular species have been studied to develop a general ultra-trace analytical technique with ultra-high sensitivity. In this research, laser intensities up to 4×10^{15} W cm^{-2} with pulse widths of 50 – 300 fs were used at wavelengths of 248, 496, 375 and 750 nm. Small to medium mass molecules, e.g. NO, NO_2, CS_2, CH_3I, etc. and some polyatomic and aromatic molecules such as C_6H_5D, C_6H_6, C_7H_8 were studied in this way. It was concluded that under irradiation by ultrafast/intense lasers, the parent ions dominate the mass spectra of all the molecules under study. Infrared laser wavelengths are favoured due to a reduced molecular fragmentation. Furthermore, ionisation saturation for some of the molecular species was achieved.

The motivation for the research detailed in this chapter was to present data demonstrating the general applicability of FLMS for uniform chemical analysis, with a number of molecules of different properties and structure. The TOF mass spectra for a number of molecular species with their corresponding RSFs (a measure of ionisation efficiency) have been investigated using the up-graded high intensity femtosecond lasers ($> 1.6\times10^{16}$ W cm^{-2}) now available at the Rutherford Appleton Laboratory ASTRA facility.

2. Experimental

The basic experimental set-up is shown in figure 3.1. The femtosecond laser and TOF mass spectrometer are described in chapter 2. Briefly, laser pulses of 50 fs are produced from a mode-locked titanium sapphire oscillator that utilises the CPA technique to provide the high-energy ultrashort laser pulses. These pulses are directed into the high-vacuum interaction chamber of the TOF and their energy can be continuously monitored to ensure that each mass spectrum is obtained at the desired laser intensity. Autocorrelation measurements of the 790 nm pulses showed that the pulses were of 50 fs duration. Since transmission through the compressor is polarisation-dependent, a $\lambda/2$ wave-plate is placed before it to control the attenuation of the laser pulse energy. Laser pulse energies up to 10 mJ per pulse can be obtained directly from the fs-laser system. A spherical 10 cm focusing mirror was fixed behind the ion extraction region to allow the laser beam focus to lie very close to the sample entrance hole in the pusher electrode. The intersection space between the focus and the sample stream is defined as the ionisation volume where photoions are produced.

A sample consisting of one species of interest or a mixture, was admitted effusively into a high vacuum system through a needle valve and then into the TOF through a tiny hole in the pusher plate. The mixture was prepared in a specially designed 'mixing manifold' wherein the partial pressures of each species could be controlled and allowed to mix together. The sample inlet system was pumped to a pressure of 10^{-3} Torr by a roughing pump. Ion signals were detected and amplified by a Thorn EMI (Ruislip, UK) electron multiplier which was coupled to a LeCroy (Chestnut Ridge, NY, USA) 9344C digital oscilloscope. The mass spectra were obtained by averaging over a minimum of 300 shots and could be stored on a normal floppy disc.

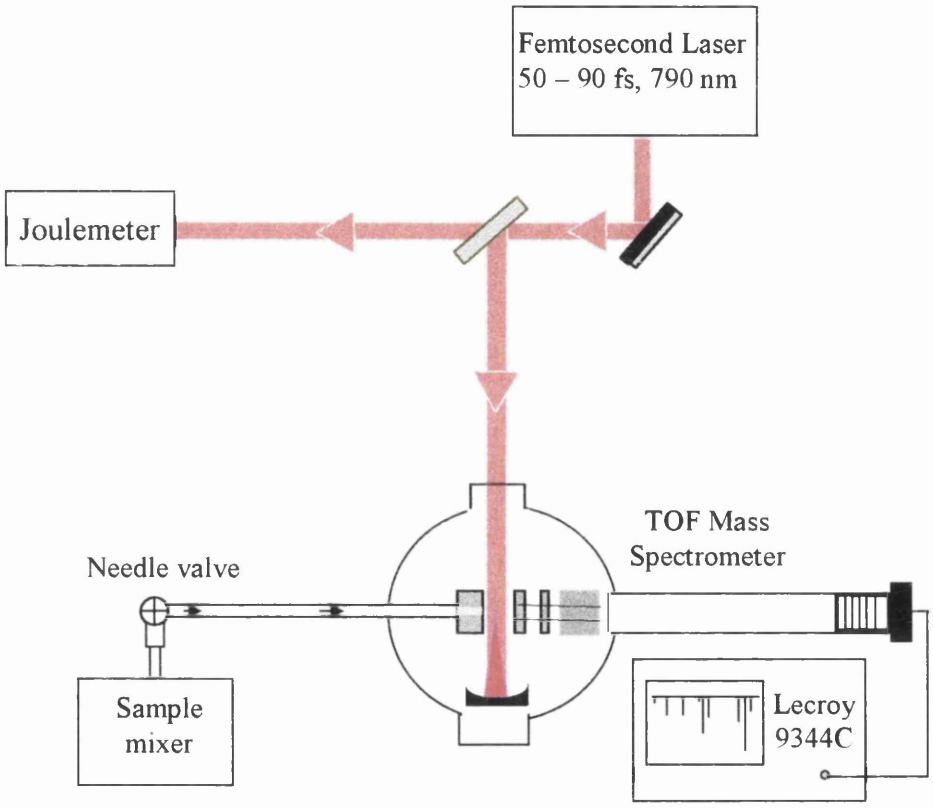

Figure 3.1 Schematic arrangement of the femtosecond laser and TOF MS experimental set-up

3. Results and analysis

The mass spectra for a number of different molecular gases and vapours were measured as a function of laser intensity and compared with the spectra for argon. This was carried out for a mixture of the two gases at equal partial pressures (~2.1×10^{-6} Torr) and for the two gases at the same pressures separately. From these spectra the relative sensitivity factors (RSFs) were calculated for each gas.

These samples are listed in Table 3.1 with their molecular ionisation potentials and the numbers of photons required for ionisation to form parent ions. The relative sensitivity factor is a very important parameter for this analysis [20, 25] that evaluates the quantification capability of the mass spectrometry technique. For a species A in a sample with reference to species B, the RSF is defined as:

$$RSF(A) = \frac{I_A / [A]}{I_B / [B]} \tag{1}$$

Where I_A and I_B are the summed ion signal intensities of species A and B in all charged states, respectively, which are measured by peak area integration in their TOF mass spectra, and [A] and [B] are the concentrations of species A and B in the mixture sample. For a sample comprising a mixture of species at equal partial pressures, i.e. [A] = [B], the RSF is simply written as:

$$RSF(A) = \frac{I_A}{I_B} \tag{2}$$

I_A and I_B are proportional to the photoion populations of these species, and hence a value of unity for RSF demonstrates that similar ionisation efficiencies of the species are achieved, in spite of any difference in ionisation potentials. Such a RSF would represent a complete, uniform detection sensitivity and reliable quantification. It should be noted

Species	1st Ionisation Energy (eV)	No. of Photons
Ar	15.76	10
N_2	15.58	10
N_2O	12.89	9
NO_2	9.79	6
NO	9.25	6
CO	14.01	9
CO_2	13.77	9
H_2S	10.4	7
CH_4	12.6	8
O_2	12.06	8
CS_2	10.08	7
CH_3I	9.54	6
C_6H_6	9.24	6
C_7H_8	8.5	6

Table 3.1 Ionisation energies and photon number required for ionisation for the element and molecular species studied.

that in the case of a molecule, the contribution of fragment ions arising from that molecule to I_A should be taken into account for a proper analysis.

Figure 3.2 (a)-(c) show the mass spectra of a sample of NO mixed with the reference gas Ar at the same partial pressure (2.1×10^{-6} Torr) at laser intensities of 8.3×10^{14} W cm^{-2}, 1.7×10^{15} W cm^{-2} and 4.9×10^{15} W cm^{-2}. In figure 3.2 a, the NO^+ ion signal is far larger than the Ar^+ signal and their peak area integration are 0.1 nVs and 0.005 nVs, respectively. Hence, the RSF for NO/Ar is ~20/1. The I.P is 9.25 eV for NO, requiring six photons for ionisation and 15.76 eV for Ar, thus requiring ten photons for ionisation. Therefore, a laser intensity of 8.3×10^{14} W cm^{-2} is not high enough to achieve similar ionisation efficiencies for the two species. When the laser intensity is increased to 1.7×10^{15} W cm^{-2}, the RSF of NO relative to Ar is 3.2 and the ionisation efficiencies for these species are becoming more similar. At the laser intensity of 4.9×10^{15} W cm^{-2}, the signals from multiply charged parent ions and the fragment ions become stronger. The summed peak area of NO^{2+}, NO^+ and N^+ is 2.1 nVs and that of Ar^{4+}, Ar^{3+}, Ar^{2+} and Ar^+ is 1.8 nVs. Derived from the peak area integration the RSF is 1.17, which is close to unity. At this level of laser intensity or higher a uniform ionisation for these species can be obtained.

Similar results for the N_2 molecule in a sample mixture with reference Ar are shown in figure 3.3 (a)-(c). The I.P of N_2 is 15.58 eV, requiring the same number of photons as Ar for ionisation. They have nearly the same ionisation efficiency. At the laser intensity of 2×10^{14} W cm^{-2}, the RSF of N_2 relative to Ar is 1.08, derived from the peak area integration. When the laser intensity is increased to 9×10^{14} W cm^{-2}, the signals from fragment ions N^+, N^{2+} and N^{3+} become stronger. Two fragment ions are produced from each molecule and hence half of the peak area of the fragment ion is counted for one parent ion. The RSF is 1.04, and as the laser intensity is increased further to 1.7×10^{15} W cm^{-2}, the RSF decreases to 0.9, again close to unity.

Figure 3.4 (a)-(c) show the RSFs as a function of laser intensity, for the molecules CO, CH_4, NO with the presence of Ar in the species respectively. Uncertainties of 11% for

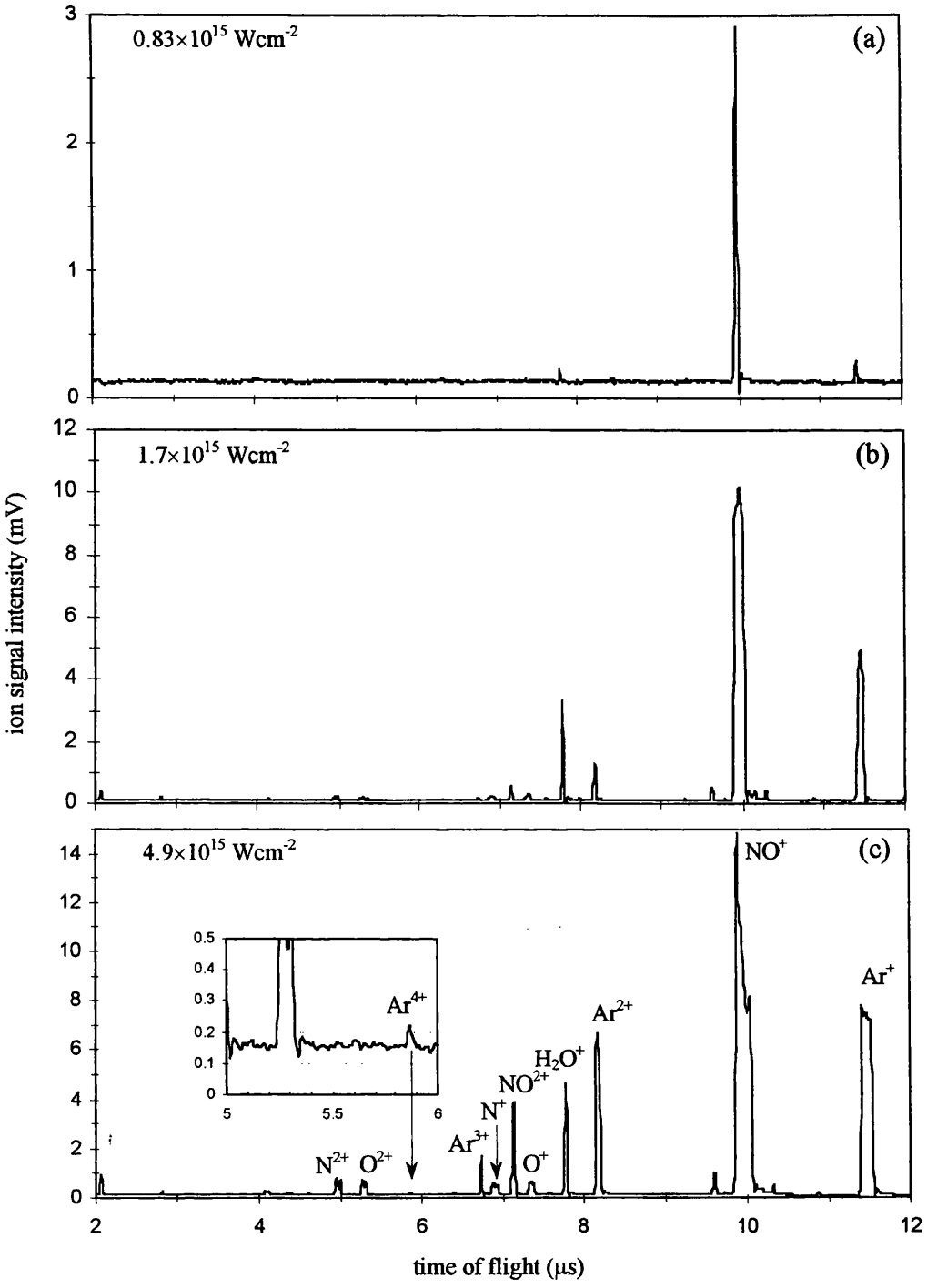

Figure 3.2 Time of flight mass spectra for the molecule NO at laser intensities of (a) 0.83×10^{15} W cm^{-2}, (b) 1.7×10^{15} W cm^{-2} and (c) 4.9×10^{15} W cm^{-2}, respectively

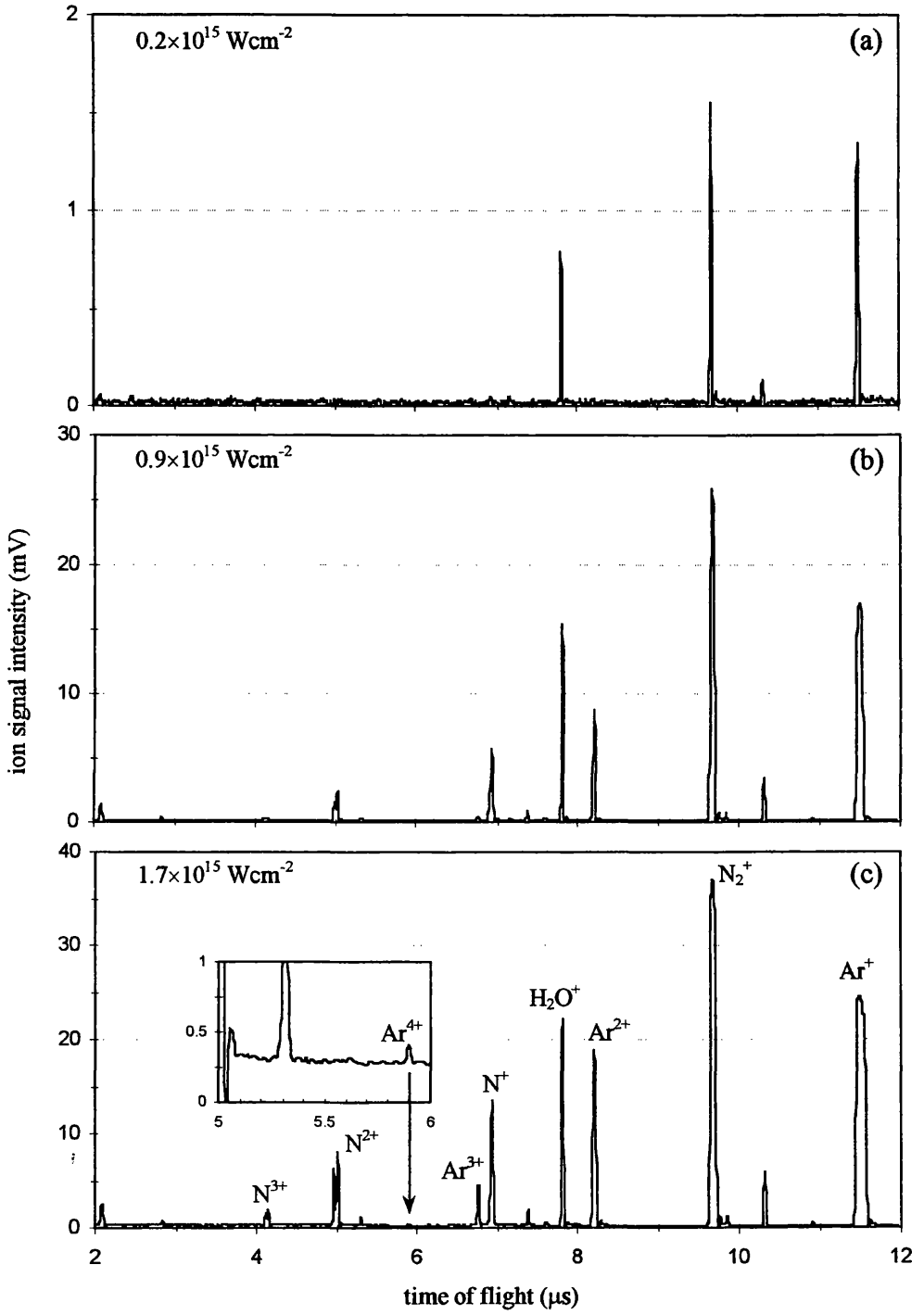

Figure 3.3 Time of flight mass spectra for the molecule N_2 at laser intensities of (a) 0.2×10^{15} W cm^{-2}, (b) 0.9×10^{15} W cm^{-2} and (c) 1.7×10^{15} W cm^{-2}, respectively

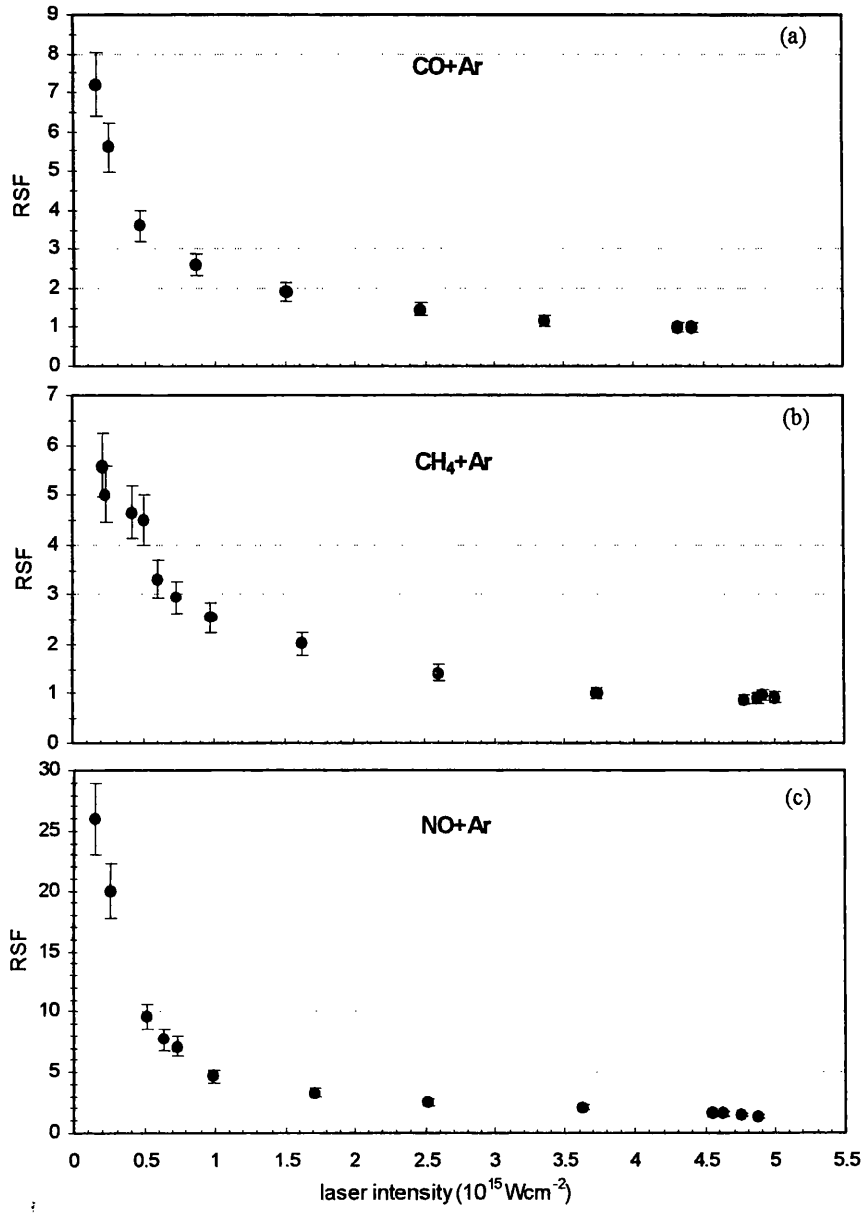

Figure 3.4 RSFs relative to Ar, versus laser intensity, of molecules (a) CO, (b) CH_4 and (c) NO, with the presence of Ar in the mixtures. The error bars indicate the estimated measurement errors of 11%.

the RSFs of each gas were carefully estimated and are shown by error bars in the figures. These uncertainties result from the measurement errors of gas pressures and peak area integration of the TOF spectra, as well as such experimental errors as laser intensity and its fluctuation on a shot-to-shot basis. The sample pressure was 4.2×10^{-6} Torr with the same partial pressures for the two species in each mixture of CO/Ar, CH_4/Ar and NO/Ar. From these figures, it is seen that the RSFs decrease as the laser intensities increase and approach unity when the laser intensities are about 3.5×10^{15} W cm^{-2} for CO, 3.6×10^{15} W cm^{-2} for CH_4 and 4.8×10^{15} W cm^{-2} for NO, respectively. At these laser power levels or higher, uniform ionisation efficiency is achieved and quantification is reliable. Due to the different ionisation potentials of CO, CH_4, NO and Ar: 14.01 eV, 12.6 eV, 9.25 eV and 15.76 eV, respectively, the numbers of photons required for ionisation are different for each, requiring 9, 8, 6 and 10 790 nm photons (equivalent energy 1.57 eV), respectively. At lower laser intensities, the probability of ionisation is different, which make the RSFs greater than unity. The difference between the numbers of photons required for ionisation of NO and Ar is larger than those for CO and Ar and for CH_4 and Ar. As a result the RSFs of NO are higher than the other two at the same laser intensities before the onset of ionisation saturation.

Figure 3.5 (a), (b) show the RSFs as a function of laser intensity, again relative to Ar, for the molecules NO_2 and H_2S, with error bars of 11%. The experimental parameters used for these samples were the same as those in figure 3.4. Similarly, photon numbers required for the multiphoton ionisation of these two molecules (6 and 7 photons, respectively) are much less than that for Ar (10 photons) and so their RSFs decrease as the laser intensities increase. The RSFs were measured to be about 2.4 but since the maximum recorded laser intensity was only 2.6×10^{15} W cm^{-2}, the minimum value for the RSFs had not been reached for these two molecules.

The case of the nitrogen molecule is interesting. This species has a high ionisation potential (15.58 eV) which is very close to the I.P of Ar (15.76 eV), and ten photons are needed to ionise both the N_2 and Ar molecule. Thus, the two species would be expected to have similar ionisation cross-section and ionisation efficiencies. Figure 3.6 (a) shows

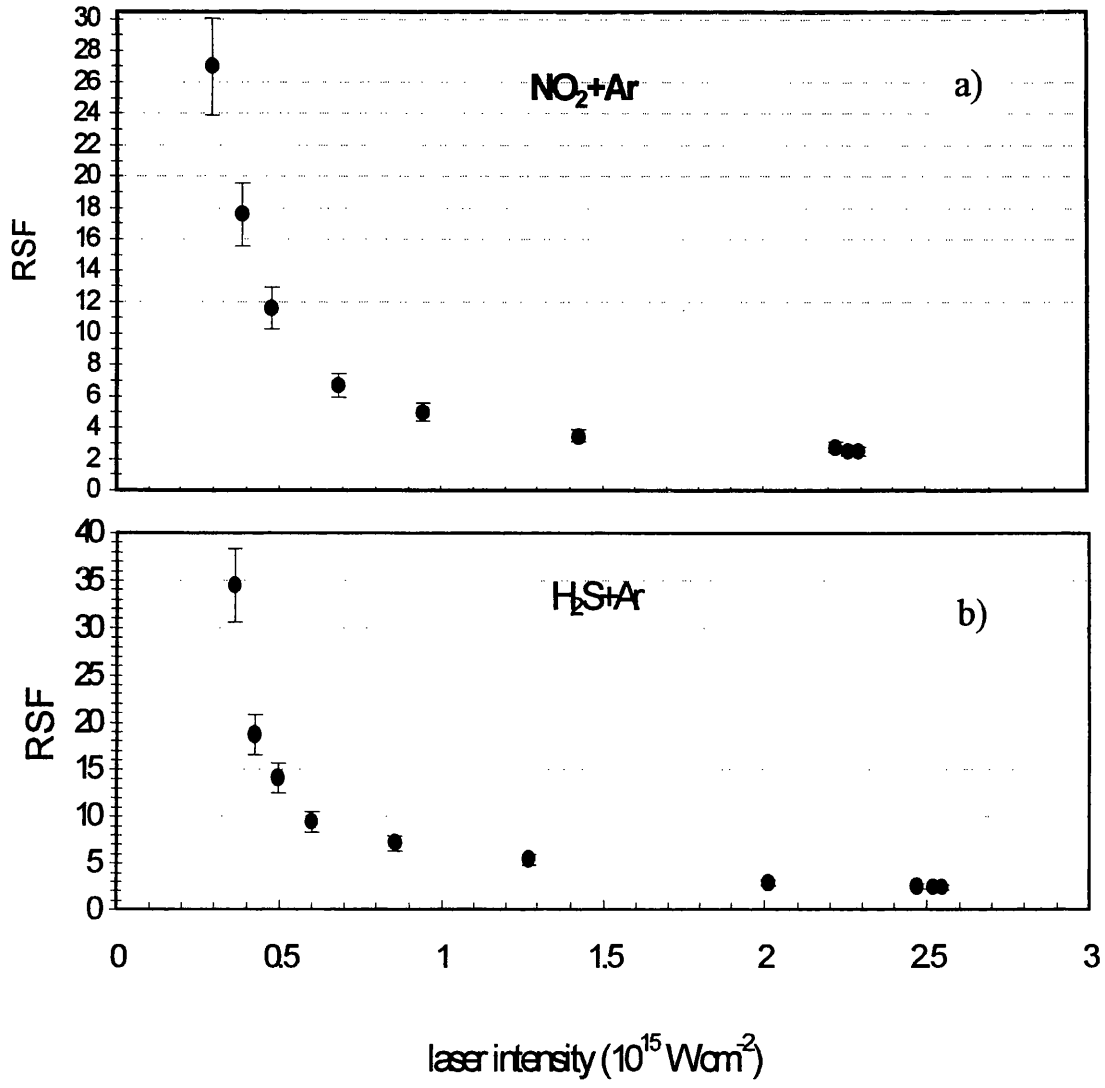

Figure 3.5 RSFs, relative to Ar, versus laser intensity of the molecules a) NO_2 and b) H_2S, with the presence of Ar in the mixture. The error bars indicate the estimated measurement uncertainties of 11%.

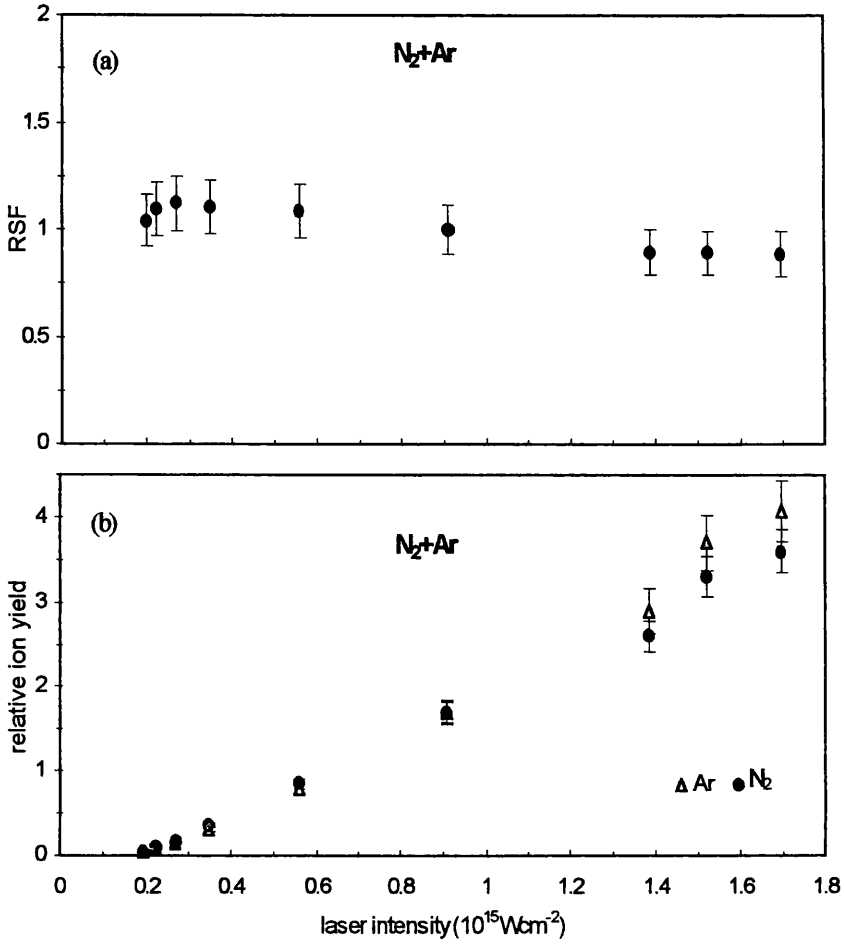

Figure 3.6 RSFs relative to Ar, versus laser intensity of a) N_2 with the presence of Ar in the mixture; (b) the ion yields of species N_2 and Ar versus laser intensity. The error bars indicate the estimated measurement errors of 11%.

that the RSFs relative to Ar versus laser intensity, obtained from the spectra of the mixture sample ($4.2x10^{-6}$ Torr) of N_2 and Ar with the same partial pressures is indeed close to unity throughout the laser intensity range. The RSFs change only slightly as the laser intensity increases, lying close to unity throughout the range. Figure 3.6 (b) shows the ion yields of both of the species as a function of laser intensity, from which it is seen that the ion yields of both species increase slowly. This indicates that the ionisation volume increases as $I^{3/2}$ with increasing laser intensity, indicative of the fact that a sharply defined ionisation volume has not been achieved.

For liquid-phase molecular species, a difficulty arises when the RSFs are measured using a mixture of its vapour with the reference species. Figures 3.7 (a), (b) and 3.8 (a), (b) show the RSFs, with error bars of 13%, of CH_3I and CS_2 relative to Ar versus laser intensity. Figure 3.7 (a) indicates the RSF measured for the gases separately while 3.7 (b) shows the values measured for a mixture of CH_3I and Ar. Only for the separate gases does the final RSF come down to unity as the laser intensity increases. It would appear that, although the vapour pressure of CH_3I was measured to be the same as that of Ar in the mixture, when this is transferred to the TOF, these partial pressures are not maintained. This is possibly due to sticking of the vapour to the walls of the transfer capillary tube and differing pumping speeds of the two species. A very similar behaviour is recorded for a mixture of CS_2 and Ar, with the RSFs being very large when saturation is approached, as shown in figure 3.8 (a), (b). Again, when these gases are separately, figure 3.8 (b), measured at identical pressures, the RSFs approach unity with increasing laser intensity.

In figure 3.9 (a), (b), RSFs relative to Ar of N_2O and CO_2 versus laser intensity are shown with their error bars of 11%. These were measured for when the separate (non-mixture) N_2O, CO_2 and Ar species were used to obtain mass spectra for peak area integration. For the ionisation of these molecules nine photons are required. The RSFs of the two species tend to unity when the laser intensities are about 3.5×10^{15} W cm^{-2} for both CO_2 and N_2O. Thus uniform ionisation has been reached at this intensity. In this figure, the data for laser intensity up to 10^{16} W cm^{-2} is shown. The reason for this is because the laser was

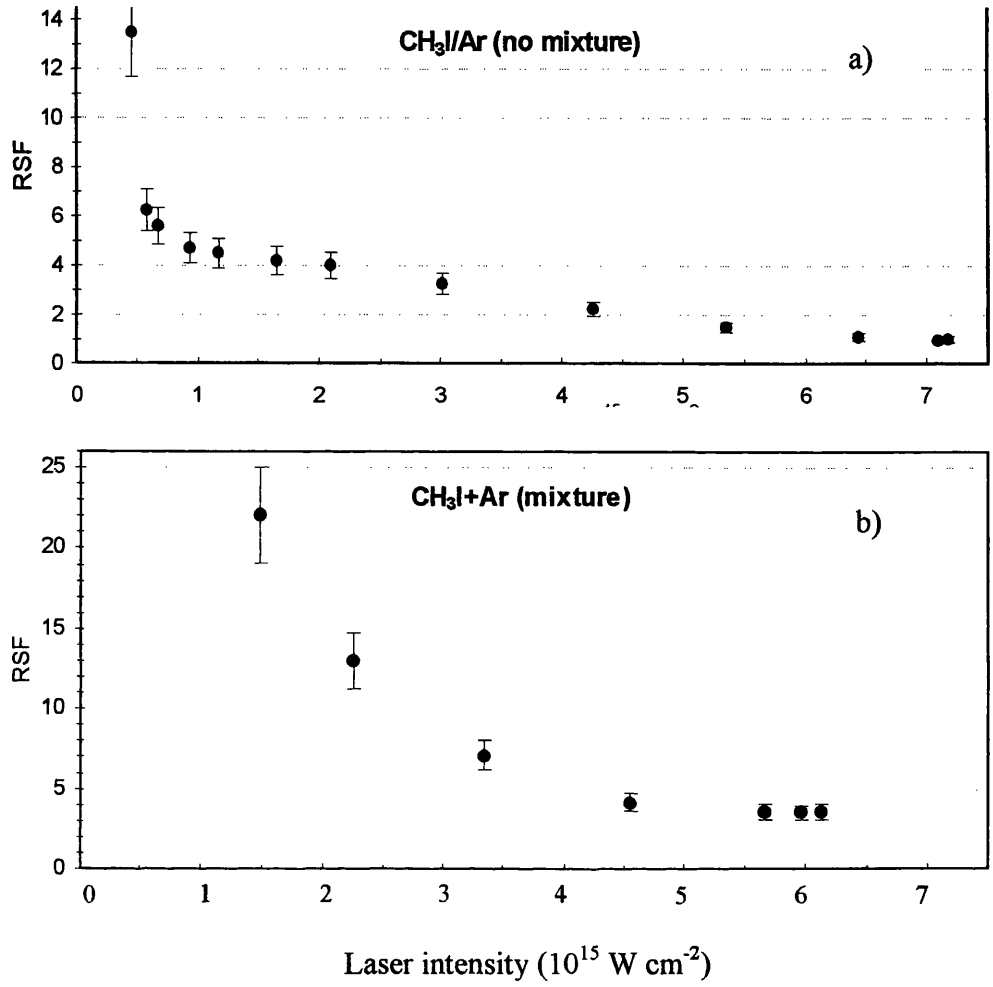

Figure 3.7 RSFs versus laser intensity, of liquid-phase (vapour) molecular samples of CH_3I, relative to Ar, when a) a mixture sample of CH_3I and Ar and b) separate (non-mixture) species measurement was used. The error bars indicate the estimated measurement uncertainty of 13%.

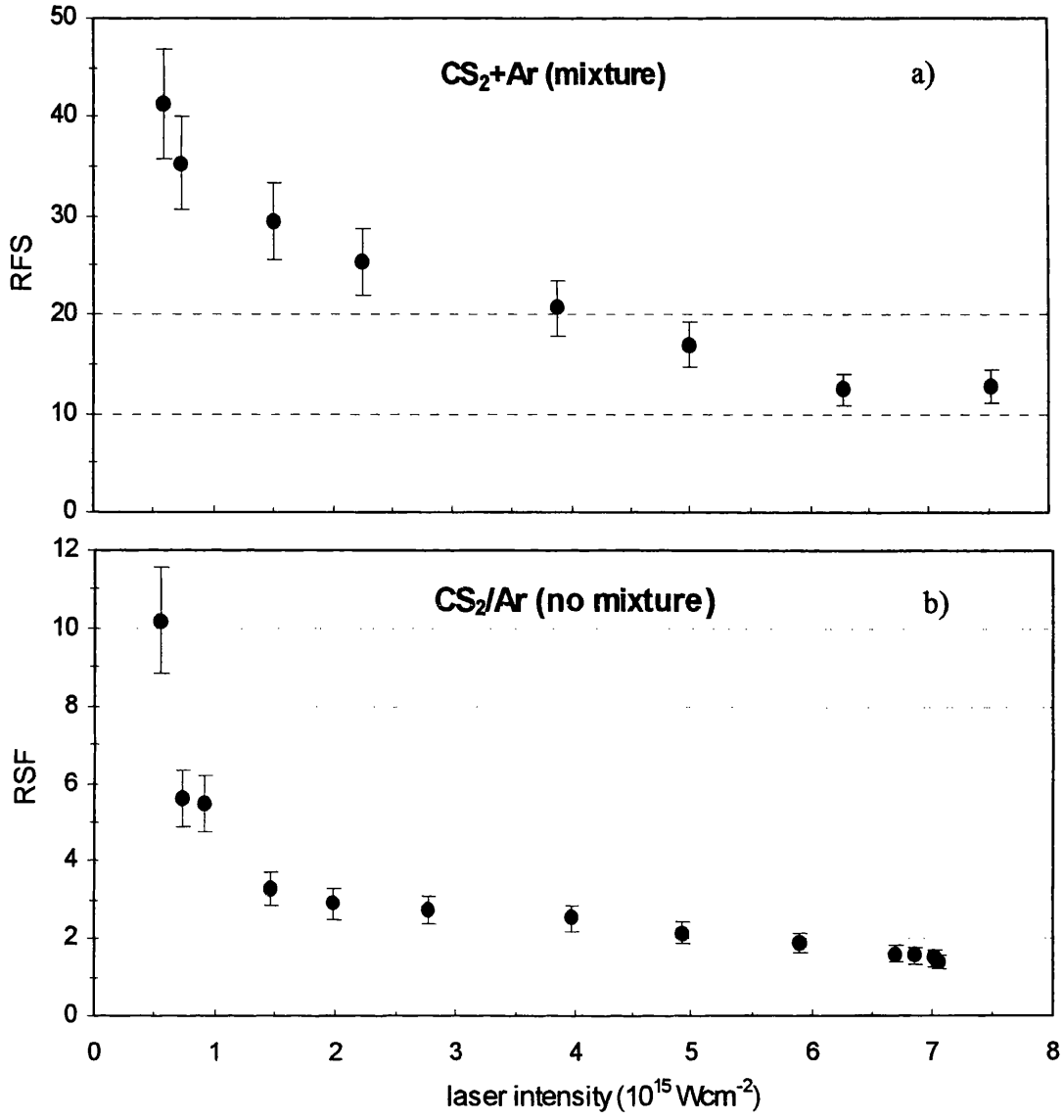

Figure 3.8 RSFs versus laser intensity, of liquid-phase (vapour) molecular samples of CS_2, relative to Ar, when a) a mixture sample of CS_2 and Ar and b) separate (non-mixture) species measurement was used. The error bars indicate the estimated measurement uncertainty of 13%.

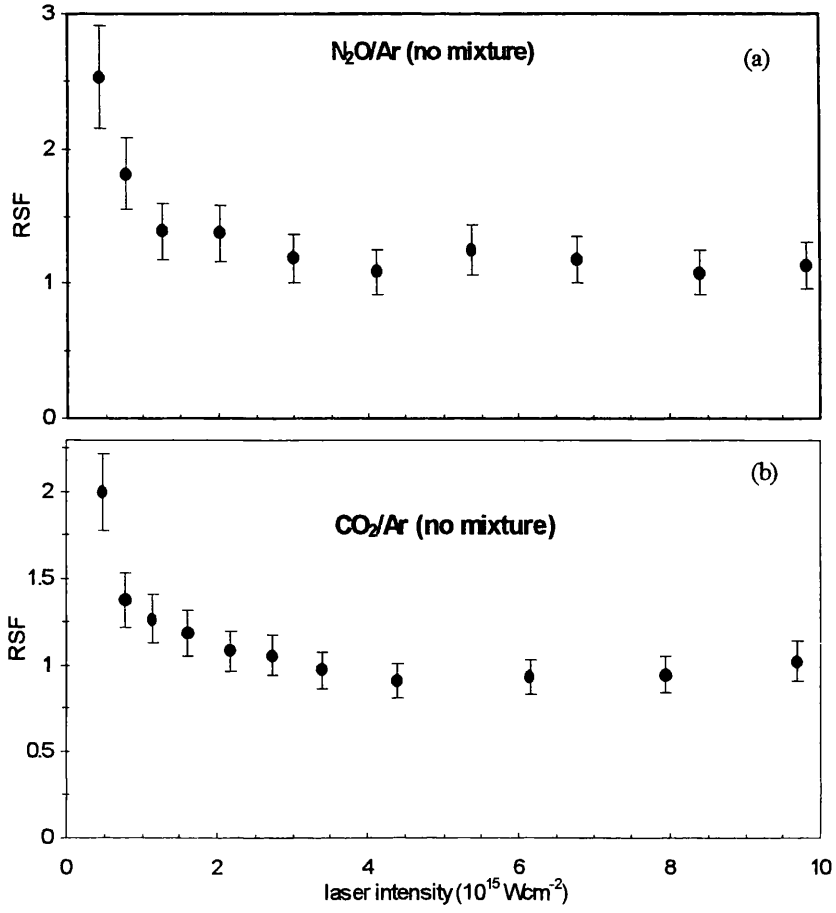

Figure 3.9 RSFs, relative to Ar, versus laser intensity of molecules a) N_2O and b) CO_2. These species had their mass spectra measured separately. The error bars indicate the estimated measurement errors of 11%.

upgraded before this data was taken and intensities up to a few times 10^{16} W cm^{-2} are now available.

Polyatomic molecules were also studied using the fs laser. Figure 3.10 (a), (b) show the RSFs for the molecules C_6H_6 and C_7H_8 versus laser intensity, respectively. The ion yields of the three species C_6H_6, C_7H_8 and Ar were separately measured from their time-of-flight spectra, for the RSF calculations. In figure 3.10 (a), the ionisation saturation is reached at the laser intensity of 7×10^{15} W cm^{-2} where the RSF is unity. In figure 3.10 (b), the RSF of C_7H_8 decreases down to a value close to 1.0 at the laser intensity of about 6×10^{15} W cm^{-2}, where uniform ionisation is reached.

The RSF data for all of the molecules studied in the experiments described in this chapter are presented in Table 3.2. It can be seen that when the gases are irradiated separately the RSFs lie close to unity except for NO_2 and H_2S, where the laser intensity used was not sufficiently high to produce uniform ionisation. If mixtures of gases (particularly vapours) were used then the RSFs were higher than unity. This was due to possible sticking effects and differential pumping speeds between species. It would appear that uniform ionisation efficiency has been demonstrated at laser intensities about 7×10^{15} W cm^{-2} for the gases studied and hence FLMS has considerable potential for quantitative molecular analysis. This work may be expanded for many more different types of molecules, especially those of environmental concern, together with (fs) laser ablation to include solid samples, to further ascertain the generality of the technique.

4. Conclusions

Using a femtosecond laser with high intensity at the wavelength of 790 nm coupled to a TOF mass spectrometer, a series of molecules, namely: CO, CH_4, NO, NO_2, H_2S, N_2O, CO_2, N_2, CH_3I, CS_2, C_6H_6 and C_7H_8, with very different ionisation potentials and molecular structure have been investigated. The detailed analysis of RSFs as a function of laser intensity, up to 1.6×10^{16} W cm^{-2}, has demonstrated that most of the molecules have reached their ionisation saturation status, as shown in Table 3.2. At intensities of

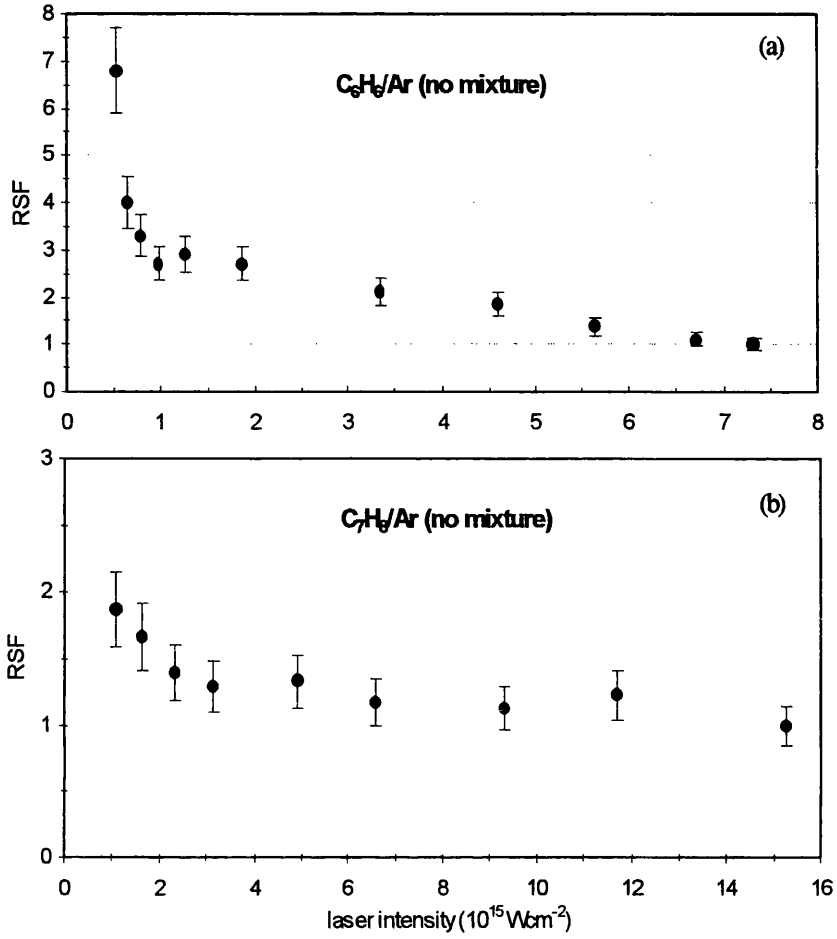

Figure 3.10 RSFs, relative to Ar, of molecules a) C_6H_6 and b) C_7H_8 versus laser intensity, when the mass spectra were measured separately. The error bars indicate the estimated measurement errors of 13%.

Samples (mixing ratio)	Leaking pressure (10^{-6} Torr)	RSF (relative to Ar)	Ionisation status	Laser Intensity (10^{15} W cm^{-2})
CO+Ar (1:1)	4.2	1±0.1	Saturation	4.0
CH_4+Ar (1:1)	4.2	0.9±0.1	Saturation	3.6
NO+Ar (1:1)	4.2	1.2±0.1	Saturation	4.9
NO_2+Ar (1:1)	4.2	2.4±0.3	Non-saturation	2.2
H_2S+Ar (1:1)	4.2	2.4±0.3	Non-saturation	2.2
N_2+Ar (1:1)	4.2	0.9±0.1	Non-saturation	11.7
CH_3I+Ar (1:1)	4.2	3.6±0.5	Saturation	5.4
CH_3I (non-mixture)	3.2	1±0.1	Saturation	6.5
CS_2+Ar (1:1)	4.2	12.4±2	Saturation	6.1
CS_2+Ar (non-mixture)	3.2	1.4±0.2	Saturation	7.0
N_2O (non-mixture)	3.2	1±0.1	Saturation	4.5
CO_2 (non-mixture)	3.2	0.9±0.1	Saturation	4.5
C_6H_6 (non-mixture)	3.2	1±0.1	Saturation	7.0
C_7H_8 (non-mixture)	3.2	1.1±0.1	Saturation	6.0

Table 3.2 Sample parameters, the minimum RSFs and corresponding laser intensity and molecular ionisation status for each sample species.

about 7×10^{15} W cm^{-2}, uniform ionisation efficiencies were reached resulting in RSFs tending to unity and reliable quantification, in addition to unambiguous identification.

It is noted that for liquid-phase molecular species, separate mass spectrometric measurements for the species and its reference gas is essential to avoid the effect of 'sticking' of the liquid-phase molecules on the inlet line and differential pumping rates, in order to obtain true RSF values. Finally, the possibility of reliable, sensitive and quantitative chemical analysis for these types of molecular samples has been demonstrated. Possible future developments could include inclusion of solid and 'real-world' environmental samples to test the generality and practicality of this technique.

In the present chapter, the method of ionisation (multiphoton versus tunnelling) at the high laser intensities has not been elaborated upon, largely because the analytical potential for FLMS has been emphasised and has been the main philosophy of these experiments. However, in a number of previous papers that this group has published recently, it has been shown that at intensities up to 10^{16} W cm^{-2}, the method of ionisation is likely to have a significant tunnelling component [32-34].

References

[1] D. M. Lubman (Ed.), Laser and Mass Spectrometry, Oxford University Press, New York (1990)

[2] A. Vertes, R. Gijbels and F. Adams, Laser Ionisation Mass Analysis, Chemical Analysis Ser. Vol.124, John Wiley and Sons, New York (1993)

[3] M. N. R. Ashfold and J. D. Howe, Ann. Rev. Phys. Chem. 45, 57 (1994)

[4] K. W. D. Ledingham, in: D. L. Andrews and A. A. Demidov (Eds.), An Introduction to Laser Spectroscopy, Plenum Press, New York, pp.187 – 227 (1995)

[5] D. M. Lubman, R. Naaman and R. N. Zar, J. Chem. Phys., 72, 3034 (1980)

[6] J. J. Yang, D. A. Gobeli and M. A. El-Sayed, J. Chem. Phys., 89, 3426 (1985)

[7] L. Zandee and R. B. Bernstein, J. Chem. Phys., 71, 1359 (1979)

[8] C. H. Becker and K. T. Gillen, Appl. Phys. Lett., 45, 1063 (1984)

[9] C. H. Becker and K. T. Gillen, J. Opt. Soc. Am., 2, 1438 (1985)

[10] D. M. Szaflarski and M. A. El-Sayed, J. Phys. Chem., 92, 2234 (1988)

[11] D. Mathur, G. R. Kumar, C. P. Safvan and F. A. Rajgara, J. Phys. B: At. Mol. Opt. Phys., 27, L603 (1994)

[12] K. W. D. Ledingham, H. S. Kilic, C. Kosmidis, R. M. Deas, A. Marshall, T. McCanny, R. P. Singhal, A. J. Langley and W. Shaikh, Rapid Commun. Mass Spectrom., 9, 1522 (1995)

[13] H. S. Kilic, K. W. D. Ledingham, C. Kosmidis, T. McCanny, R. P. Singhal, S. L. Wang, D. L. Smith, A. J. Langley and W. Shaikh, J. Phys. Chem., A101, 817 (1997)

[14] C. Kosmidis, K. W. D. Ledingham, H. S. Kilic, T. McCanny, R. P. Singhal, A. J. Langley and W. Shaikh, J. Phys. Chem. A101, 2264 (1997)

[15] R. Weinkauf, P. Aicher, G. Wesley, J. Grotemeyer and E. W. Schlag, J. Phy. Chem. 98, 8381 (1994)

[16] C. Grun, C. Weickhardt and J. Grotemeyer, Europ Mass Spect. 2, 197 (1996)

[17] K. P. Aicher, U. Wilhelm and J. Grotemeyer, J. Am. Soc. Mass Spectrom., 6, 1059 (1995)

[18] R. Moller, M. Terhorst, E. Niehuis and A. Benninghoven, Org. Mass Spectro. Lett., 27, 1393 (1992)

[19] C. H. Becker and J. S. Hovis, J. Vac. Sci. Technol. A12, 4 (1994)

[20] C. He, J. Basler, A. Paul and C. H. Becker, J. Vac. Sci. Technol. A14(3), 1433 (1996)

[21] C. He and C. H. Becker, Current Opinion in Solid State & Material Science, 1, 493 (1996)

[22] C. He, J. N. Basler and C. H. Becker, Nature, 385, 797 (1997)

[23] C. Kosmidis, K. W. D. Ledingham, H. S. Kilic, T. McCanny, R. P. Singhal, A. J. Langley and W. Shaikh, J. Phys. Chem., A101, 2264 (1997)

[24] D. J. Smith, K. W. D. Ledingham, R. P. Singhal, H. S. Kilic, T. McCanny, A. J. Langley, P. F. Taday and C. Kosmidis, Rapid Commun. Mass Spectrom., 12, 813 (1998)

[25] K. W. D. Ledingham and R. P. Singhal, Int. J. Mass Spectrom. Ion Proc. 163, 149 (1997)

[26] D. J. Smith, K. W. D. Ledingham, H. S. Kilic, T. McCanny, W. X. Peng, R. P. Singhal, A. J. Langley, P. F. Taday and C. Kosmidis, J. Phys. Chem., A102, 2519 (1998)

[27] K. W. D. Ledingham, R. P. Singhal, D. J. Smith, T. McCanny, P. Graham, H. S. Kilic, W. X. Peng, S. L. Wang, A. J. Langley, P. F. Taday and C. Kosmidis, J. Phys. Chem., A102, 3002 (1998)

[28] P. Graham, K. W. D. Ledingham, R. P. Singhal, D. J. Smith, S. L. Wang, T. McCanny, H. S. Kilic, A. J. Langley, P. F. Taday and C. Kosmidis, Proceedings of the 9th Symposium on RIS (1998)

[29] P. F. Taday, I. Mohammed, A. J. Langley and I. N. Ross, Annual Report 1997/1998, Central Laser Facility, Rutherford Appleton Laboratory, p.179

[30] K. W. D. Ledingham, H. S. Kilic, C. Kosmidis, R. M. Deas, A. Marshall, T. McCanny, R. P. Singhal, A. J. Langley and W. Shaikh, Rapid Commun, Mass Spectrom. 9, 1522 (1995)

[31] W. C. Wiley and I. W. Mclaren, Rev. Sci. Instrum. 26, 1150 (1955)

[32] K. W. D. Ledingham, D. J. Smith, R. P. Singhal, T. McCanny, P. Graham, H. S. Kilic, W. X. Peng, A. J. Langley, P. F. Taday and C. Kosmidis, J. Phys. Chem. 1999, accepted for publication

[33] D. J. Smith, K. W. D. Ledingham, R. P. Singhal, T. McCanny, P. Graham, H. S. Kilic, P. Tzallas, A. J. Langley, P. F. Taday and C. Kosmidis, to be published

[34] C. Kosmidis, P. Tzallas, K. W. D. Ledingham, T. McCanny, R. P. Singhal, P. F. Taday and A. J. Langley, to be published

Chapter 4

An investigation of the angular distributions of fragment ions arising from the linear CS_2 and CO_2 molecules

CHAPTER OVERVIEW

The non-linear interaction of the triatomic molecules CS_2 and CO_2 with the intense field of a linearly polarised laser beam of femtosecond (fs) pulse duration, was used to study the ionisation and dissociation of the parent molecule. The fragment ion angular distributions arising from the Coulomb explosion of the parent ions were also measured. For CS_2, the angular distributions of CS_2^+, CS_2^{2+}, CS_2^{3+}, CS^+, CS^{2+}, S^{n+} $(n \leq 6)$ and C^{m+} $(m \leq 4)$ ions are presented for a laser intensity of 1×10^{16} W cm^{-2} at a wavelength of 790nm and pulse duration of 50fs. The angular distributions of the parent molecular ions are all isotropic. The S^{n+}-fragments are peaked along the laser polarisation, whereas the C^{m+}-fragments explode perpendicularly to this. Similar results for CO_2 are also presented for comparison. The S-ion distributions do not narrow as their ionic charge increases, and it is argued that the angular distributions of fragment ions from CS_2 are due mainly to the angular dependence of the ionisation probability. On the other hand, the anisotropies observed for the lighter CO_2 molecule are thought to be at least partly due to alignment via dipole moments induced by the laser, as the O^{n+} angular distributions slightly narrow as their charge increases. The conclusion of these results is that the laser pulse may be too short for the CS_2 molecule to align in the pulse. Angular distributions for S and C ions are also presented for varying laser pulse durations, in the range of 50fs to 300ps. The isotropies increase as the pulse duration increases. The anisotropy of the C ion distribution is a measure of molecular bending prior to dissociation. The dynamics of the ionisation/dissociation mechanism are discussed in the context of the TOF mass spectra and angular distributions recorded for CS_2.

1. Introduction

As theoretical and experimental studies of diatomic and triatomic molecules subjected to intense laser beams [1-13] gain momentum, useful insights are obtained into the dynamical processes involved. The experiments are becoming increasingly sophisticated and include pump-probe analysis of potential energy surfaces [14-16] as well as the alignment and trapping [17-20] of molecules. Indeed, the ability to control the alignment of the overall molecular dipole moment with the laser field can have significant implications in the control of chemical reactions (steric effects) and hence is receiving intense contemporary interest from several groups [19, 21-31].

A dramatic upsurge in short-pulse laser technology, with its concomitant high achievable peak powers, has been observed in the last few years. This has largely been brought about by the development of chirped-pulse amplification (CPA) techniques [32]. Now Table-Top Terrawatt (T^3) lasers are to be found in many university and national laboratories. Thus, the development of these laser sources [32-38] provides pulses with **E**-fields (E) of a magnitude comparable to the internal fields which bind atoms together to form molecules (~0.5 V $Å^{-1}$ = 5×10^9 V cm^{-1}). Furthermore, the pulse durations are shorter than the time scale for nuclear motions to occur (sub-picosecond). Pulses of this magnitude (E = 2.74×10^9 V cm^{-1} for I = 1×10^{16} W cm^{-2}, λ = 790 nm, τ = 50 fs) allow the study of nonlinear phenomena in molecules at intensities sufficient to distort the electron cloud, which leads to a distortion of the internal structure. These distortions may induce a polarisation within the molecule, which in turn interacts with the field. Consequently, this sets up a torque that acts to align the molecules with the field. As the polarisation increases with charge state of the parent ion, this leads to a greater field coupling and hence to more efficiently aligned molecular ions. The alignment of highly charged, transitional states of the parent molecule can be characterised by the angular distribution of the resulting exploding fragments. This has been carried out utilising time-of-flight (TOF) mass spectrometry.

The angular distributions of exploding fragments have been studied for a number of different molecules. Results for NO_2, CS_2, and CCl_4 [27, 28] using pulses of 35 ps

at 532 nm have been reported previously. Other reports have studied CS_2, CO_2, H_2, N_2 and I_2 in the femtosecond regime [17, 39-48]. Anisotropic distributions of fragment ions have been observed to be molecule specific. In cases of triatomic fragmentation in the subpicosecond regime the ejection of the central atom has been observed to be orthogonal to the peripheral atoms, which are ejected parallel to the field, independently of the polarisation orientation. This phenomenon is contrary to Mathur group's study of CO_2 and CS_2 molecules in the picosecond regime [12, 27, 49] where both the central and peripheral ion intensities were maximised along the detection axis.

The rotation of small molecules in intense laser fields has been discussed extensively [3, 17, 27, 39-45]. In an ensemble of molecules with random orientation, those molecules that have their dipole moments oriented with the direction of the laser polarisation experience preferential ionisation. This enhancement, achieved through a lowering of the barrier to ionisation, has been reported [50] to be a result of an extended intramolecular structure induced by the field. Investigating N_2 and CO_2, Hering and Cornaggia [51], using linearly and circularly polarised laser light have found that the enhancement of the ionisation at the critical internuclear distance is independent of the type of polarisation used, as is the kinetic energy of the fragments. For the linearly polarised case, reorientation effects are observed.

Where the electric field is perpendicular to the molecular orientation, the molecule is harder to ionise and fragment. It has been shown by Kumar et al. [27] that dissociation precedes ionisation when a molecule's ionisation energy (IE) is less than 6 eV. It is also known that an increase in molecular size leads to a reduction of the IE and increased fragmentation [52]. The ionisation energy of molecules exhibiting a delocalised electronic system (cf. Benzene) is substantially lower than for those with a localised electronic structure (cf. Cyclohexane). In addition, the field-induced distortion of a bond to twice its equilibrium distance leads to an enhanced ionisation via an electron tunneling mechanism [18, 20, 50]. This apparent lowering of the effective IE at the critical internuclear distance suggests that the tunneling regime will dominate over multi-photon processes in the stretched molecular configuration, further contributing to the enhancement of the ionisation.

By utilising linearly and circularly polarised laser beams, Ellert et al. [44, 45] distinguish between the effects of alignment and preferential ionisation for Cl_2, Br_2, I_2 and O_2. The magnitude of the electric field component along the molecular axis was equal for both polarisations. Measurement of the doubly charged fragments along the TOF axis showed that any alignment effect was negligible for I_2, but started to play a role for Cl_2 and O_2 at laser intensities of 1×10^{15} W cm^{-2} and 80 fs duration. They also observed I_2^{5+} when the laser polarisation was parallel to the TOF axis; however only I_2^{3+} was reached for the perpendicular case. This supports the enhancement of ionisation (and dissociation) hypothesis when the orientation of the molecule coincides with the laser field, vide supra. These observations have also been reported by Posthumus et al. [2, 40] for I_2. The Coulomb explosion of N_2 and SO_2 has been studied using momentum-imaging (ion-imaging) techniques by Hishikawa et al. [3]. It was concluded that the laser field aligned both molecules and that the fragments were ejected with a momentum that increased with the initial charge state.

This chapter reports on an investigation of the angular distribution of fragments ions coming from molecular ions after ionisation/dissociation on interaction with intense linearly polarised laser pulses (5mJ, 790nm, 50fs). These measurements extend the results of previous studies performed at 1×10^{13} W cm^{-2} [26, 27] to an intensity of 10^{16} W cm^{-2}. The angular distributions of CO_2 were also investigated for corroboration of the present results, as the behaviour of this molecule is well characterised under similar laser conditions [43]. Angular distributions for CS_2 at 50 fs, 150 fs, 2 ps and 300 ps pulse widths are also measured. Comparison of these results with previous data for CO_2 in the femtosecond regime and CS_2 in the picosecond regime will be made to elucidate the mechanism responsible for the anisotropic distributions of the fragment ions.

2. Experimental

The experimental arrangement is described in more detail in chapter 2 and shown schematically in figure 4.1. The sample pressure was maintained at ~10^{-6} Torr in order to avoid space-charge effects and pressure broadening of the ion peaks. Ions

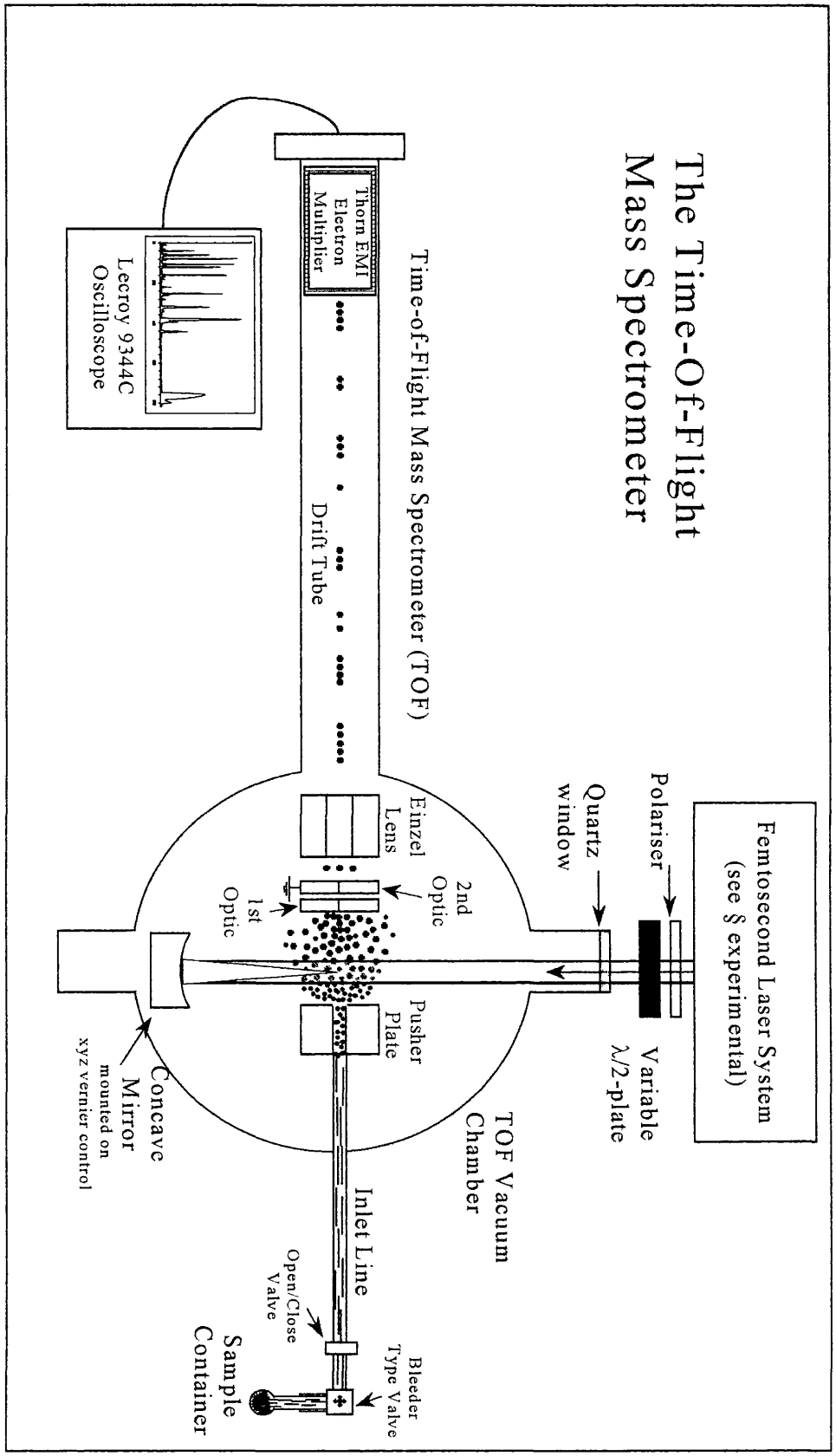

Figure 4.1 Experimental apparatus showing the femtosecond laser system coupled to the linear TOF mass spectrometer. The λ/2-plate, which was used to vary the polarisation angle of the laser pulse in the angular distribution studies, is also shown.

were detected using an electron multiplier (Thorn EMI) connected to a LeCroy (9344C, 500MHz) digital storage oscilloscope. The extraction fields used were of the order of 500 V cm^{-1} and the mass-resolution ($M/\Delta M$) of the TOF system was measured to be 200 at m/z = 100.

The femtosecond laser produces linearly-polarised pulses with energy of ~5 mJ and 50fs duration. The laser beam was then directed into the TOF vacuum chamber using beam-steering optics, where it was focussed using either a f/3 or f/10 spherical mirror mounted on a x-y-z bellows vacuum manipulator. The focus was positioned to maximise the ion signal.

The laser pulse energy was monitored for every shot using a 10% beamsplitter, located prior to the chamber window, and a Joule meter (Molectron). The pulse duration was measured using a second-order single-pulse autocorrelator. The output beam was assumed to have a Gaussian profile; the full width at half maximum (FWHM) was used to define the pulse width. When focussed using the f/3 on-axis mirror the maximum peak intensities were ~10^{16} W cm^{-2}. This intensity was corroborated using a standard argon power dependence [55].

The laser direction through the interaction volume was perpendicular to the direction of the TOF axis as shown in figure 4.1. Horizontal polarisation is defined as being parallel to the TOF axis; vertical polarisation is defined as being orthogonal to this direction. Measurement of the angular distributions of the fragments was achieved by inserting a polariser-$\lambda/2$ wave-plate combination into the path of the beam immediately prior to the quartz window of the target chamber, in order to avoid polarisation-dependent transmission losses through beamsplitters, etc. The $\lambda/2$ wave-plate was then rotated in 10° steps and a spectrum was obtained corresponding to the angle of rotation over typically 300 laser shots. The area under the ion peak of interest was then integrated and plotted against the polarisation vector angle with respect to the reference axis, generating angular distributions.

3. RESULTS AND DISCUSSION

3.1 High intensity TOF mass spectra

Time-of-flight mass spectra of CS_2, recorded using 790 nm laser light at an intensity of 1×10^{16} W cm^{-2}, are shown in figures 4.2 and 4.3 for horizontal and vertical polarisation, respectively. The dominant peaks in both spectra, by peak area, are CS_2^+, CS_2^{2+} and CS_2^{3+}. The peak widths can be seen to narrow with increasing charge. At a sample pressure of $\sim10^{-6}$ Torr pressure broadening of the peaks can be neglected. Consequently, the widths of the peaks are a measure of the energy distribution of the ions. The mass spectra exhibit a broadening in the peak widths, particularly for CS_2^+ and CS_2^{2+}, as the laser intensity increases. This is indicative of an increase in the interaction volume and of a broadening in the initial kinetic energy distribution for the parent ions. Narrower peak widths are observed for the higher charge state species as they are generated only in the highest intensity region of the laser focus. Consequently, they have a higher initial kinetic energy with a narrower distribution. This is consistent with the fragments originating from highly charged (CS_2^{n+} where $n > 3$) transient states of the parent which are themselves only formed in the high-intensity portion of the beam. Furthermore, if the polarisation is vertical then those molecules initially oriented in this direction are preferentially ionised and dissociate. The S-ions are then ejected orthogonally to the TOF axis and hence only those in the low kinetic energy portion of the ion energy distribution can be detected. As the charge of the fragment ion increases, fewer ions will possess sufficiently low kinetic energy to be picked up by the detector. This explains why the S-ion peaks are smaller and narrower in the spectra corresponding to vertical polarisation. The opposite is true for C-ion peaks. This narrowing is observed for the S^{n+} and C^{m+} fragments under both polarisation conditions.

Table 4.1 shows the ionisation energies (in eV) of the atomic constituent fragments from the CS_2 and CO_2 molecules [56]. The large increases in IE for S^{n+} and C^{m+} when n increases from 6 to 7 and when m increases from 4 to 5 accounts for the observation of S^{6+} and C^{4+} ions and the absence of S^{7+} and C^{5+} peaks in the mass spectra for CS_2. At intensities of 1×10^{16} W cm^{-2} the ponderomotive potential produced by the laser is 185 eV. Thus, it is within the capability of the laser at this

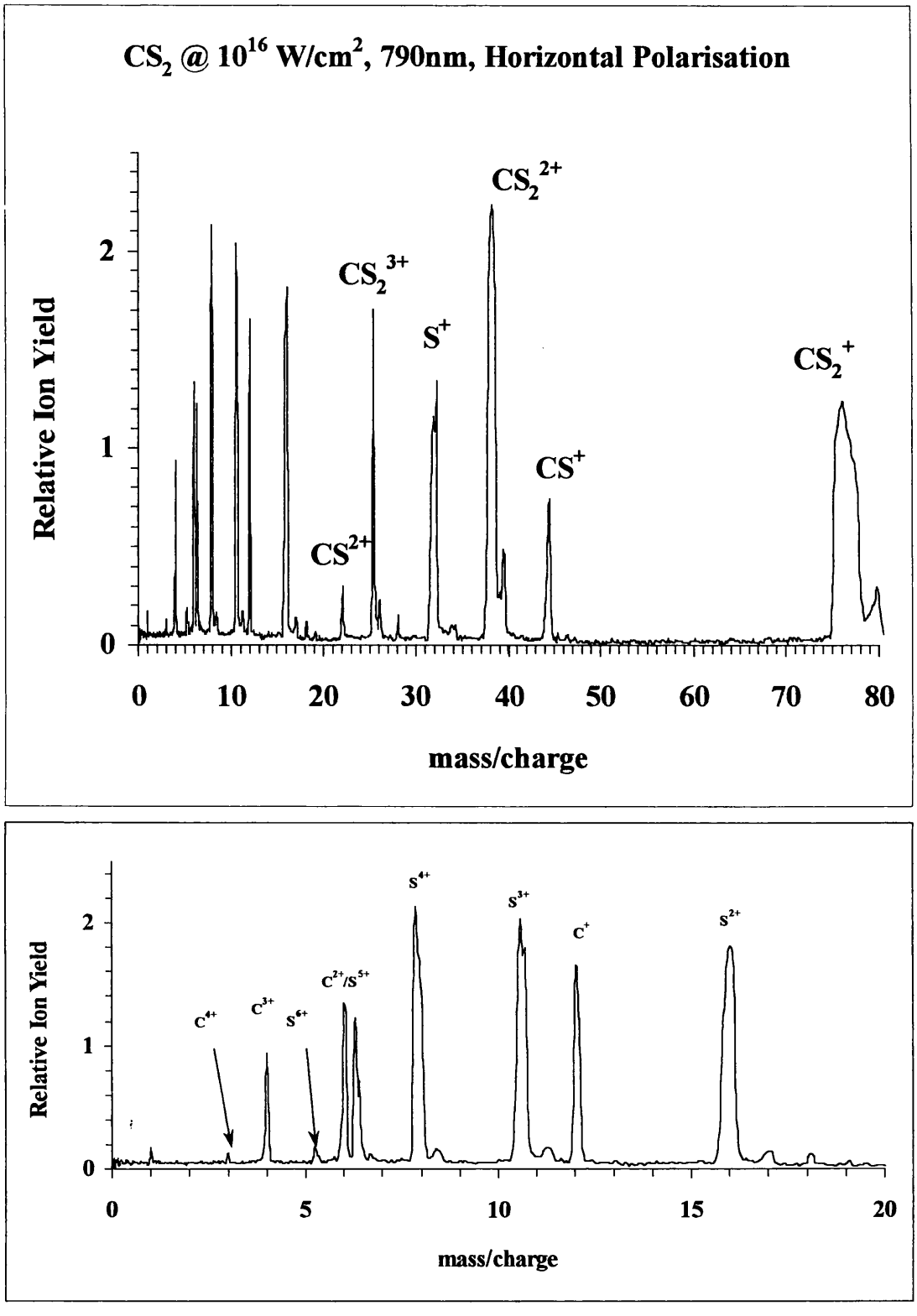

Figure 4.2 TOF mass spectrum of CS_2 recorded using the laser characteristics of 1×10^{16} W cm^{-2}, 790 nm, and 50 fs. The laser polarisation axis was *collinear* with the TOF axis. The lower trace shows an enlarged section of the low-mass region exhibiting broad S^{n+} (n = 2-6) peaks and narrow C^{m+} (m = 1-4) peaks.

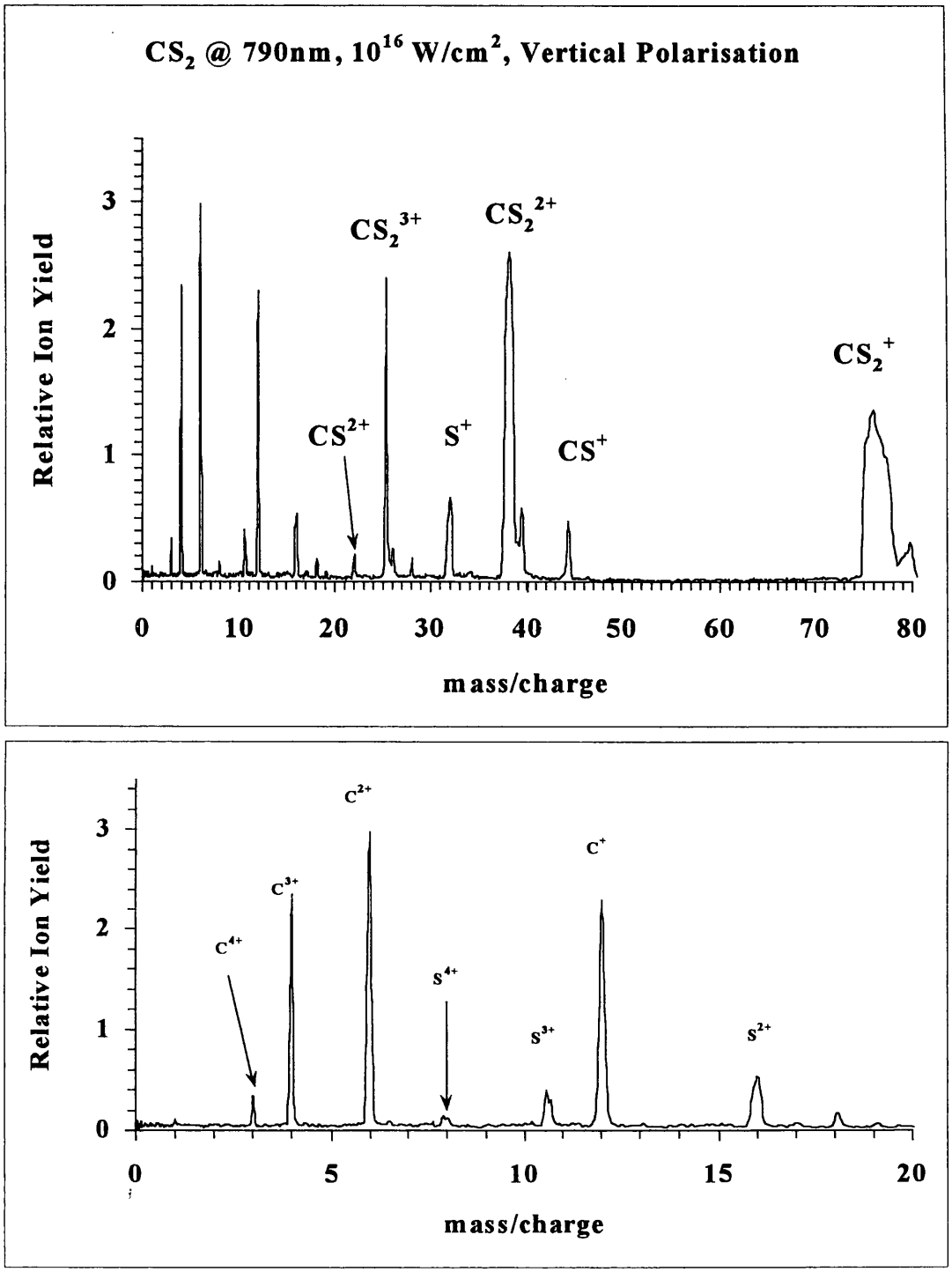

Figure 4.3 TOF mass spectrum of CS_2 recorded using the laser characteristics of 1×10^{16} W cm^{-2}, 790 nm, and 50 fs. The polarisation axis was *perpendicular* to the TOF axis. The lower trace shows an enlarged section of the low-mass region. This region of the mass spectrum now exhibits a reduction in intensity of the S^{n+} peaks, and the C^{m+} peaks are dominant.

n – charge state of atom	S-atom	C-atom	O-atom	Ar-atom
1	10.36	11.26	13.618	15.759
2	23.33	24.383	35.116	27.629
3	34.83	47.887	54.934	40.74
4	47.3	64.492	77.412	59.81
5	72.68	392.077	113.896	75.02
6	88.049	489.981	138.116	91.007
7	280.93	-	739.315	124.319
8	328.23	-	871.387	143.456

Table 4.1 – Ionisation energies of Ar, and atomic fragments from CS_2 and CO_2 [56]

intensity to attain S^{6+}, but not S^{7+}. Similarly, for the carbon atoms C^{4+} is readily obtainable but the remaining electrons in C^{4+} are too tightly bound and so C^{5+} is not attainable at 1×10^{16} W cm^{-2}.

For the case of horizontal polarisation (figure 4.2) the S^{n+} fragment peaks ($n \leq 6$) are often doublet in their structure and broader than the C^{m+} ($m \leq 4$) peaks by a factor of about two. The doublet nature of the fragment peaks is caused by Coulomb explosion where the fragments are directed both towards and away from the TOF detector. Hence the difference in flight time between the forward- and backward-directed fragments is associated with the turn-around time of the initially backward-directed ion in the extraction field. A low detection efficiency associated with the backward-directed ions is apparent from their lower peak intensity in the mass spectra. This is a result of differing finite acceptance cones for the two fragment trajectories. The differences in the two flight times are, within experimental error, independent of charge state as predicted for the Coulomb explosion model; the extraction field acts to reverse the course of the higher charge state fragments more quickly, despite their larger kinetic energies. Thus, the turn-around-times of the backward-directed ions of varying charge states are similar. Furthermore, the peak intensities of the S^{n+}, CS^{+} and CS^{2+} fragments are greater for the horizontal polarisation compared to the vertical case (figure 4.3) for similar laser powers. The maximum charge state reached is also greater in accord with the phenomenon of preferential ionisation observed when the laser field is parallel to the TOF axis. However, the opposite is true for the C^{m+} fragments; the peaks are consistently larger in the spectra for vertical polarisation, although the maximum charge state reached is the same for both polarisation conditions.

3.2 Fragment angular distributions

A polar plot of the CS_2^{n+} ($n \leq 3$) peaks is shown in figure 4.4. The three molecular ions exhibit uniform signal intensity for all polarisation angles (isotropic). The gas-phase molecules have a random orientation with only thermal motion. The isotropy shows that the intact parent ions, ionised up to the triply charged state, are detected with equal efficiency regardless of polarisation orientation. Furthermore, these data

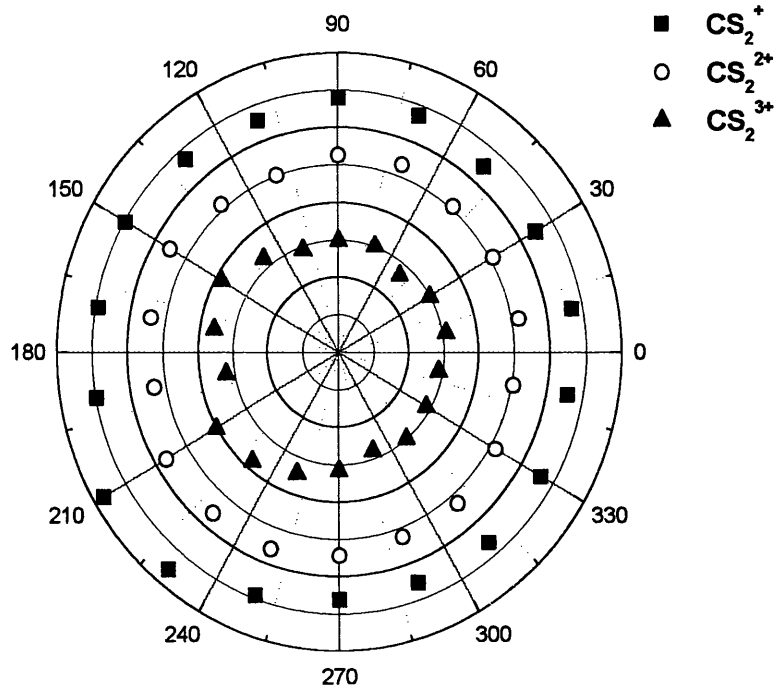

Figure 4.4 Polar plot of the CS_2^+, CS_2^{2+} and CS_2^{3+} parent ions clearly showing isotropic angular distributions. The data points for CS_2^{2+} and CS_2^{3+} are normalised with respect to CS_2^+, for ease of viewing.

are evidence that any instrumentally induced effects play no role on the fragment angular distributions.

The angular distributions of specific fragment ions exhibit a significantly different behaviour to that of the multiply charged parent ions. The angular distributions for the CS^+ and CS^{2+} fragment ions are shown in figure 4.5. In addition to a strong underlying isotropic component CS^+ exhibits anisotropy, whereas the doubly ionised fragment CS^{2+} clearly shows only an anisotropic distribution. The isotropic component arises from the fragmentation of the singly charged parent ion. Bond breaking in CS_2^+ is not a Coulomb explosion process and only imparts a small kinetic energy to the S^+ or CS^+ ions and the neutral counter-fragment. This is termed 'soft' dissociation. The resulting low kinetic energy fragment ions remain within the collection volume of the TOF analyser and are detected efficiently. Conversely, the anisotropic distributions for CS^+ and CS^{2+} are derived from the fragmentation of higher ionised states of the CS_2 molecule resulting in Coulomb explosions. These explosions yield two ionised fragments that may posses sufficient kinetic energy to escape the collection volume of the TOF analyser. The anisotropy in the ion signal is a measure of both the initial direction of ejection and kinetic energy imparted to the exploding fragment ions; those fragments ejected at or near-parallel to the TOF axis are detected with greater efficiency.

The angular distributions for S^{n+} ($n \leq 6$) from CS_2 are shown in figure 4.6. The error bars are typically 10% for the larger peaks and about 30% in the valleys. These arise principally from uncertainties in estimating the baselines of the peaks in the TOF spectra. It is evident from these data that all the fragments are markedly anisotropic, peaking along the parallel direction (0° and 180°). The ion intensities might be expected to decrease for increasing charge state, as they are formed in a smaller interaction volume where the intensity is sufficiently large to produce the highly charged transitional state of the parent molecule from which it explodes. The minimum ion counts for each graph in figure 4.6 are near or equal to zero for all charge states, except S^+. In a similar fashion to CS^+ (figure 4.5), the S^+ distribution has an underlying isotropic component originating from the low-energy fragmentation of CS_2^+ and CS_2^{2+} ions (both isotropically distributed):

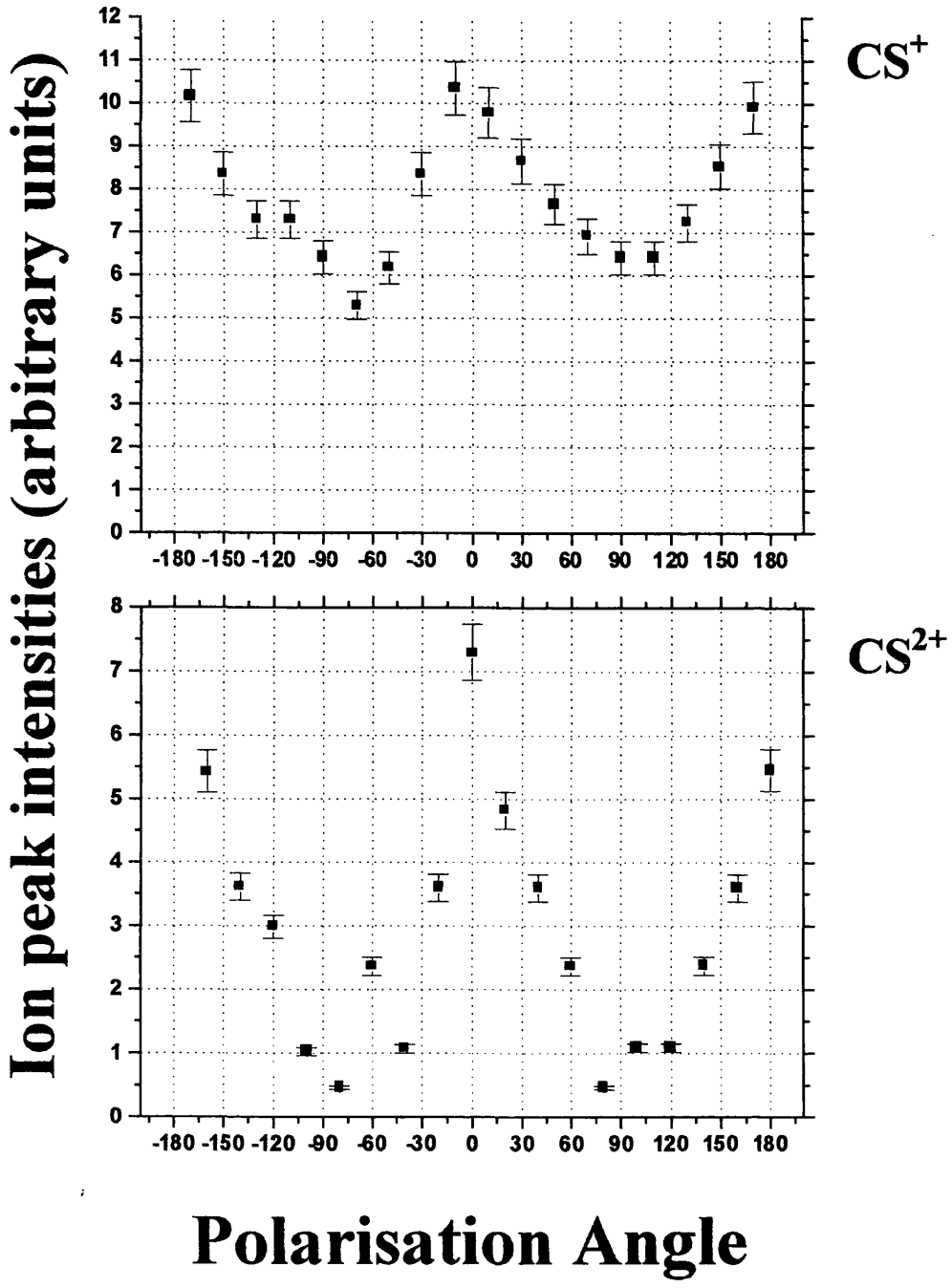

Figure 4.5 Angular distributions for the CS^+ and CS^{2+} fragments. The CS^+ graph shows an underlying isotropic component, while the CS^{2+} fragment distribution is totally anisotropic.

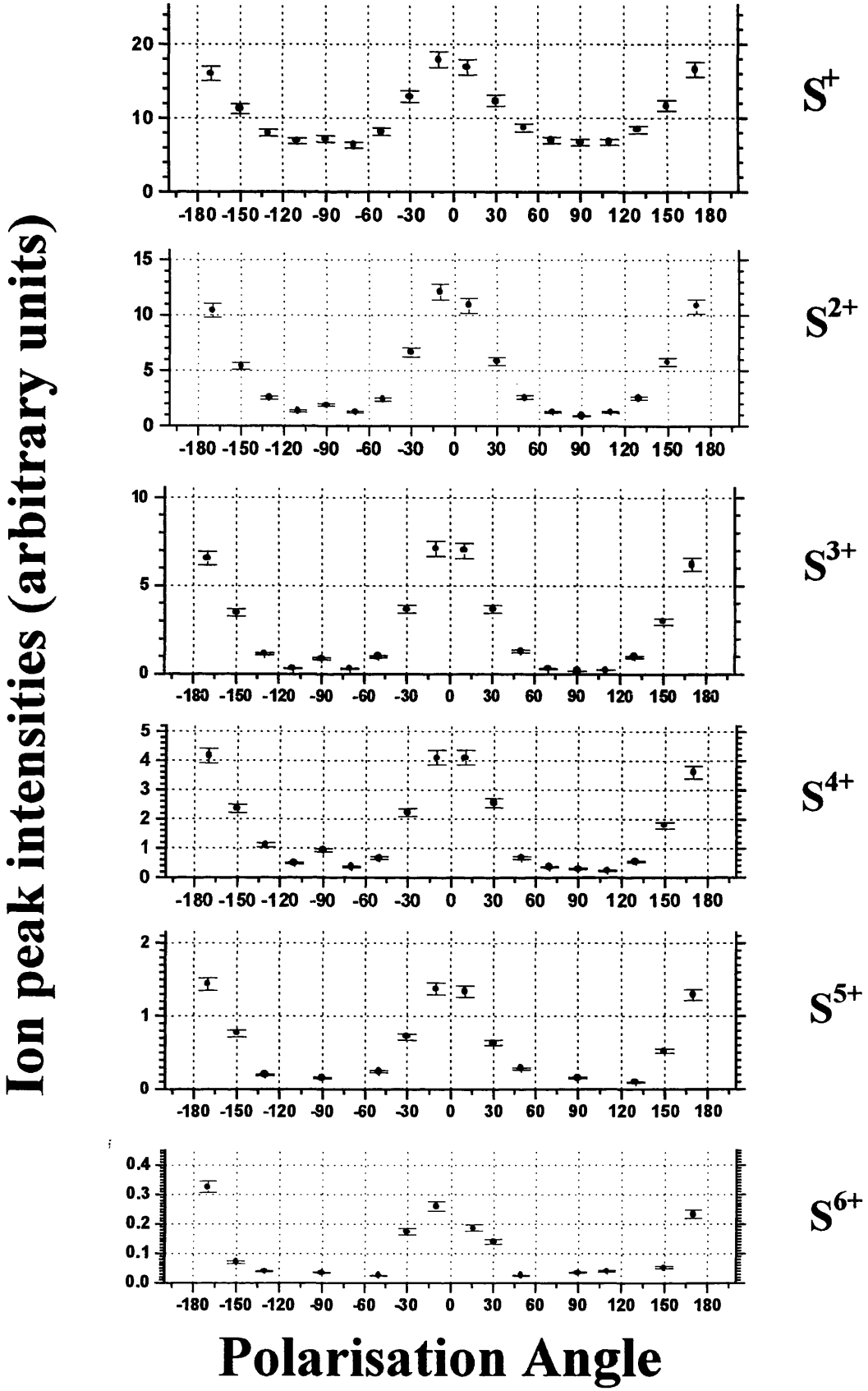

Figure 4.6 Angular distributions for the S^{n+} ($n \leq 6$) fragments from CS_2. The distributions show similar FWHM values, and are anisotropic with a maximum intensity when the polarisation is *collinear* with the TOF axis. The S^+ distribution has an additional isotropic component.

$$CS_2^+ \rightarrow CS + S^+ \quad (1a)$$

$$CS_2^+ \rightarrow CS^+ + S \quad (1b)$$

$$CS_2^{2+} \rightarrow CS^+ + S^+ \quad (2)$$

It is unlikely that the process CS_2^{3+} (isotropic) $\rightarrow$ CS^{2+} + S^+ contributes to the isotropic component of the S^+ ion peak since the CS^{2+} distribution is strongly anisotropic (figure 4.5), although it could contribute to the anisotropic part of the distribution. Processes (1a) and (1b) are likely to have small kinetic energies and hence to be easily propelled by the extraction field to the detector making isotropy more likely. Process (2) is a Coulomb explosion and may impart higher kinetic energies to the fragments contributing towards the anisotropic component. The angular distribution of S^+, in showing both isotropic and anisotropic components, indicates a weak preferential ionisation. This may imply that the CS_2 molecule is not stretched in the field, as an increase in interatomic distance of the molecule has been shown to enhance ionisation [50].

The angle where the maximum ion count occurs is the same for all S^{n+} fragments and is parallel to the TOF axis (0° and 180°). Furthermore, the FWHM value is equal for all S-fragments (~60°) in contrast to the data reported by Couris et al. [57] who observe the distributions to narrow as a function of charge state. If the molecules were aligning in the electric field of the laser beam, one would expect the distributions to narrow for higher charged fragments due to the higher induced dipole moment and hence aligning torque acting on the precursor molecule. Such an effect has been observed for both the light H_2 and N_2 molecules [47, 58]. That this is not the case in the present work indicates that there is little evidence for alignment of CS_2 within the 50 fs pulse, regardless of the transient charge state of the molecule. The FWHM value being equal again supports a preferential ionisation phenomenon and Coulomb explosion along the field direction, with the high kinetic energy ions ejected out from the acceptance angle of the TOF. An alternative explanation for this result, that the molecule aligns *before* ionising is unlikely to occur for non-polar molecules (e.g. CS_2) and the time for electron ejection is much shorter than for rotation of the molecule.

The origin of the anisotropic signal maxima is a result of preferential ionisation occuring when the laser polarisation is efficiently overlapped with the molecular axis of the triatomic parent molecule and the TOF axis. Hence, both ionisation/dissocation and Coulomb explosion are enhanced, apparent through the preferential detection of the CS^{n+} and S^{n+} fragments ejected within ca. ±30° of the TOF axis. Although ionisation is enhanced for parallel-polarisation [40, 45] the CS^+ and S^+ ions with low kinetic energies are created and detected irrespective of the polarisation angle.

Comparison of the angular distributions for S^{n+} and C^{m+} fragments reveals that the molecular structure is distorted by the presence of the laser field. Diametrically opposite behaviour for the ejection of S and C fragments is clearly shown in the angular distributions of figures 4.6 and 4.7. This polarisation-dependent phenomenon arises from the preferential ionisation of those molecules whose molecular axes are pseudo-parallel to the laser field, vide supra. Angular distributions for the C^{m+} ions from CS_2 are shown in figure 4.7. The distributions are maximised along the perpendicular direction (± 90°). A similar underlying isotropic component to that of S^+ and CS^+ is observed for C^+. Furthermore, the FWHM values and angles of minimum ion count are similar for all C^{m+} graphs.

The origin of the diametrically opposite behaviour for C- and S-fragment ions is a result of the molecular geometry in the ion state. The CS_2 ion molecule is slightly bent when excited, with the S-C bonds being at small angles to the electric field of the laser. When the laser field is collinear with the TOF axis, the S^{n+} ions are ejected along the polarisation direction (actually along the bonds) and along the TOF axis resulting in efficient detection. The greatly reduced C^{m+} signal is a result of the fragments being ejected perpendicular to the laser polarisation after Coulomb explosion. The anisotropy of the multiply charged carbon atoms can be traced to the molecular axis being bent such that a momentum transfer from the Coulomb exploding S atoms occurs and results in the C^{m+} ion intensity peak at ±90°. Conversely, when the polarisation is perpendicular to the TOF axis the high-energy S^{n+} ions are lost and detected with reduced efficiency. These differences in the distributions are also observed by Couris et al. [57]. In the perpendicular orientation

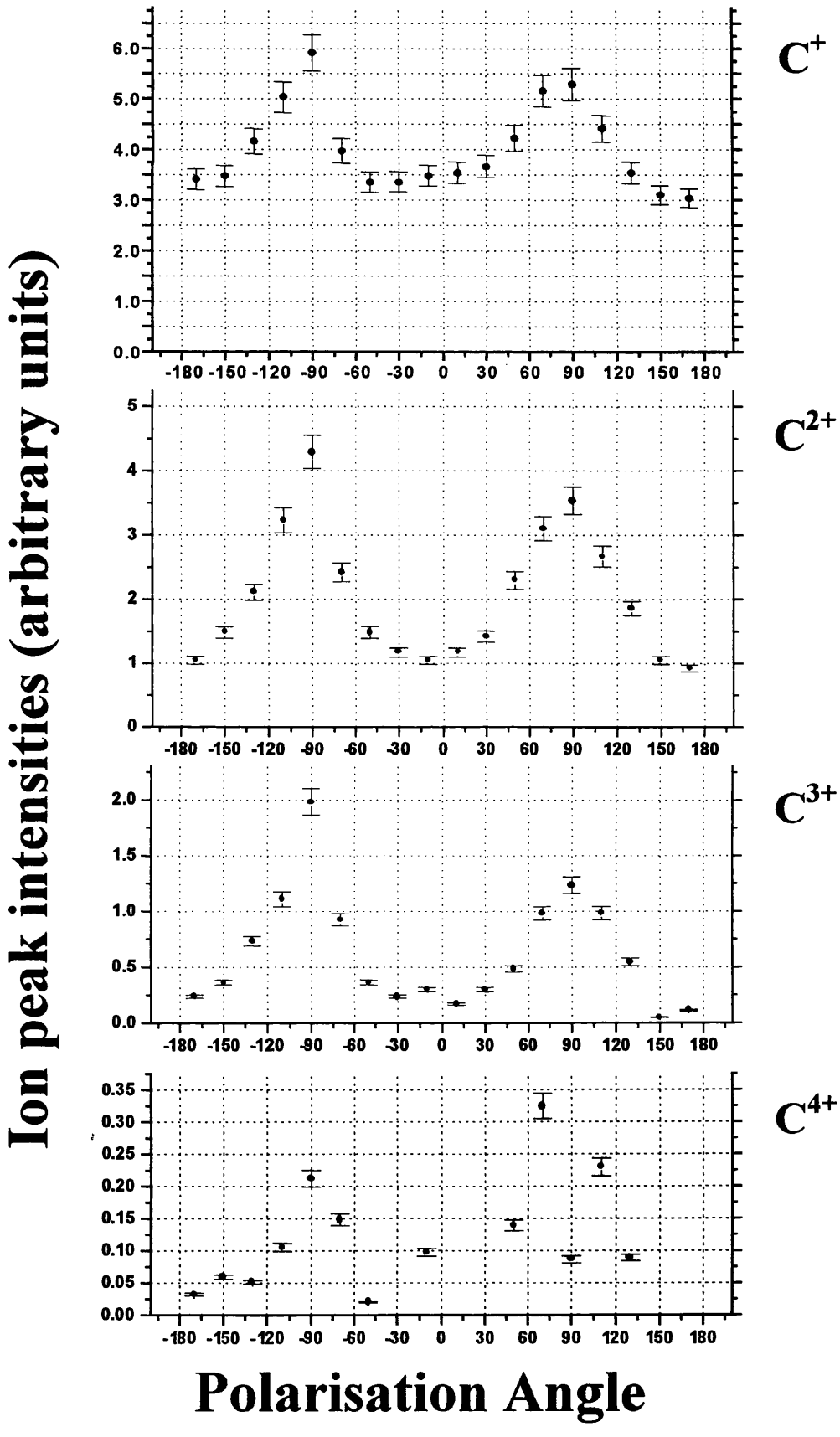

Figure 4.7 Angular distributions for the C^{m+} ($m \leq 4$) fragments from CS_2. These distributions are also anisotropic, but with the maximum intensity when the polarisation is *perpendicular* to the TOF axis. The C^+ distribution also exhibits an additional isotropic component.

of the polarisation, the S-fragments are directed at right angles to the TOF axis with large kinetic energy values depending on the charge-state, and hence large velocities. Thus, highly charged S-fragments are detected with even less probability. The current data presented are in agreement with the work of Couris et al. [46]. A similar result for CO_2 has been obtained under similar conditions here [43]. The orthogonal C^{m+} ion distributions suggests that the molecule structure is being distorted and bent by the intense laser field. The widths of the C peaks are similar in both spectra and do not show signs of splitting.

3.3 Comparative Angular Distributions for CO_2

The angular distributions of O^{n+} ($n \leq 3$) and C^{2+} ions are shown in figure 4.8. The O and C distributions are once again perpendicular to each other and are similar to the S and C fragments for CS_2. Those data are in agreement with that presented in [43]. For both the O^+ and C^{2+} distributions, there is an underlying isotropic component as with CS_2. There is some indication that the O^{n+} graphs narrow with increasing charge-state, which has been attributed to the molecular ions aligning in the electric field of the laser [43]. Alignment of a molecule prior to ionisation would lead to all of the resulting multiply charged products having similar FWHM values.

Alignment of *neutral* I_2 molecules has been reported by Sakai et al. [19] using a non-resonant Nd:YAG laser, coupled to two femtosecond lasers – one to ionise, the second to fragment the molecule. This clarified the interpretation of the anisotropic distributions as either an enhancement or an alignment process. Also, the use of resonant and non-resonant laser beams can induce alignment via the polarizability of both polar and non-polar molecules, and control the molecular orientations and fragment angular distributions; the latter through virtual states, [30, 31]. Furthermore, the molecule must ionise before fragmenting, otherwise all the fragment distributions would be isotropic. It has been quoted by Sanderson et al. [43] that the rotational period of CO_2 in an electric field of 2×10^9 V cm^{-1} is around 15 fs and hence reorientation is likely. The time for alignment of H_2 was also recently determined to be 30 fs through 45° and 80 fs from 90°, at intensities of 1×10^{14} W cm^{-2} [18]. The rotational period of CS_2 is likely to be longer than the value for H_2 and CO_2 due to it's increased moment of inertia.

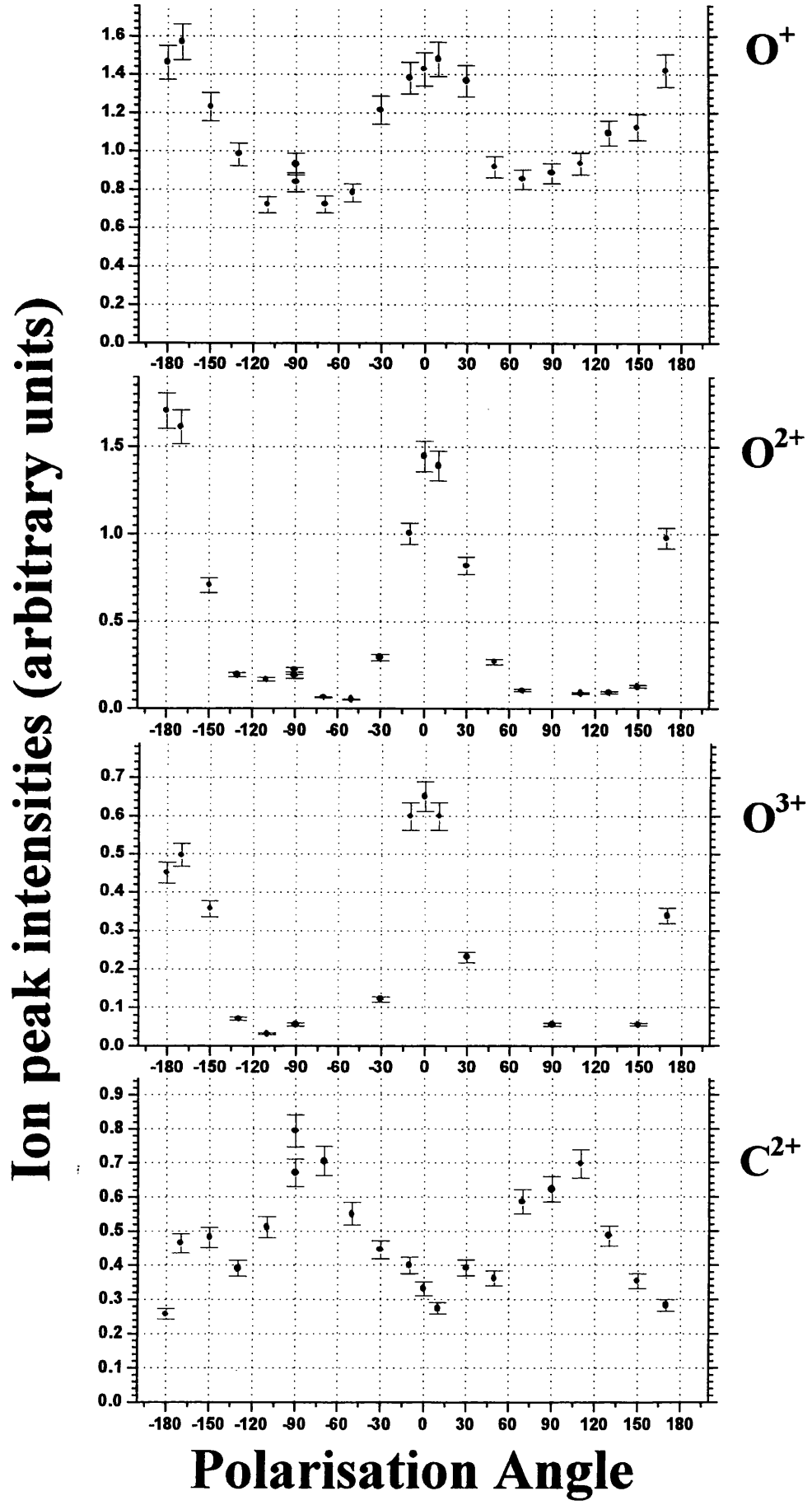

Figure 4.8 Angular distributions for O^{n+} and C^{m+} fragments from CO_2. Similar behaviour to that of the S and C peaks in CS_2 is apparent. The O^{n+} distributions appear to narrow somewhat as the charge *n* increases, suggesting an aligning effect.

3.4 Angular distributions for varying pulse durations

The results presented for CS_2 and CO_2 here are at variance with those presented for these same molecules by Mathur's group [27]. In their work, using a 35 ps laser at 532 nm, the fragment distributions all lie along the TOF axis. This may be due to the longer pulse duration of the laser, allowing the molecule more time to align with the field. Sequential dissociation channels may occur within the time scale of the pulse leading to C-distributions that also peak with parallel polarisation.

In an attempt to elucidate the question of whether the CS_2 molecule can rotate within the laser pulse, angular distributions were carried out at different pulse lengths. Figure 4.9 shows the S^{n+} ($n \leq 5$) distributions for pulse lengths of 50 and 150 fs, 2 ps and 300 ps. The results obtained at 150 fs and 2 ps exhibit little difference from that recorded at 50 fs, although the distributions for the ps pulses seem wider than those for the fs pulses. The isotropic component for 150 fs and 2 ps was slightly larger than for 50 fs. However, the distribution recorded with the longer pulse length (300 ps) became markedly isotropic. A similar finding was obtained for the C fragments. Indeed, the anisotropy shown in the C-ion distributions (figure 4.10) is a measure of molecular bending prior to Coulomb explosion. Thus, the results for 50 fs, 150 fs and 2 ps are largely anisotropic, suggesting a non-linear configuration; the greater the anisotropic component, the greater the degree of molecular bending. The almost complete isotropy in the 300 ps distribution could imply that the laser intensity is insufficient to induce this distortion in the parent precursor. The alignment of CS_2, proposed by Couris et al. [57] to occur at pulse duration of 200 fs, could not be reproduced at 50 fs, 150 fs or 2 ps. Furthermore, the findings of Mathur's group where the C^+ and S^+ ions were both directed along the TOF axis (at 35 ps) could not be corroborated. This orthogonal ejection of peripheral and central ions from triatomic species has been confirmed by numerous groups for molecules such as CO_2, COS and H_2O [43, 57, 59].

As the compressor grating distance is changed, the only laser characteristic to alter is the pulse duration. The energy of the pulse, however, is unchanged. The intensity will hence decrease in proportion with increasing duration. Since any aligning torque acting on a molecule depends principally on the field strength, an increase in

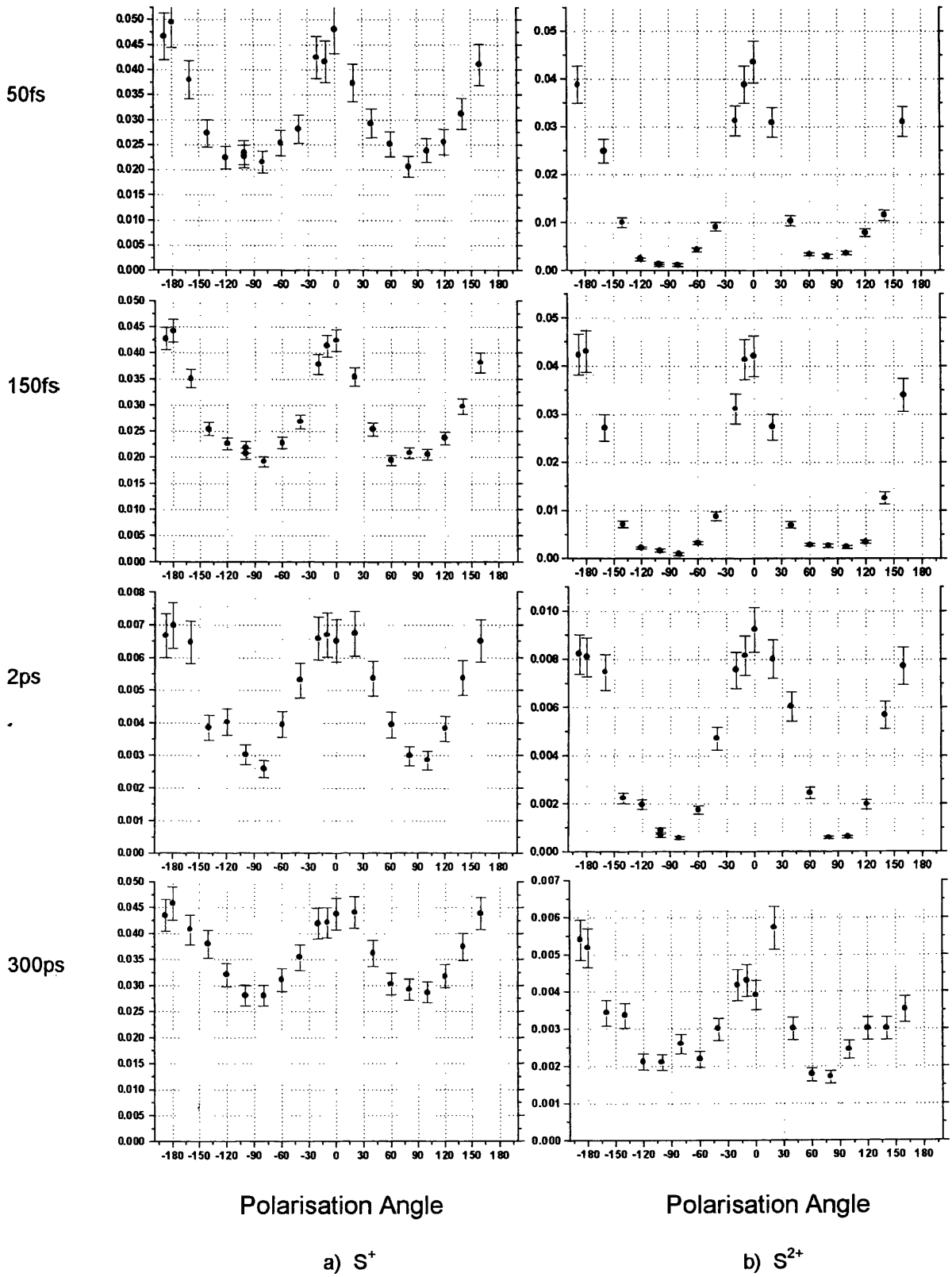

Figure 4.9 Angular distributions for the S^{n+} (n = 1-5) fragment ions arising from the dissociation of CS_2 for different pulse widths of 50 fs, 150 fs, 1 ps and 300 ps. The distribution for the two shorter pulse widths show a similar behaviour to that for 50 fs pulses, but the distribution for the longer pulse width is largely isotropic.

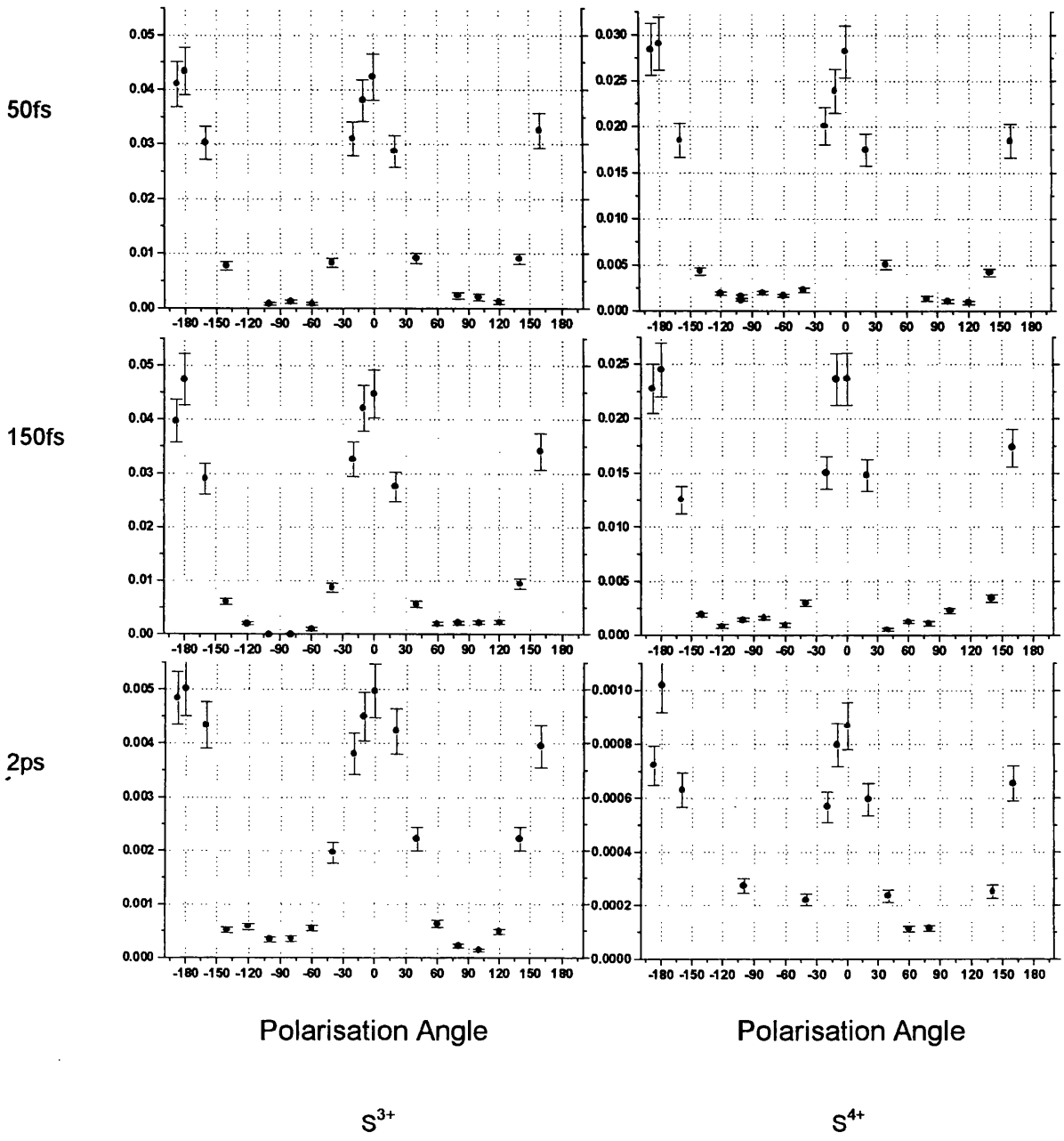

Figure 4.9 Angular distributions for the S^{n+} (n = 1-5) fragment ions arising from the dissociation of CS_2 for different pulse widths of 50 fs, 150 fs, 1 ps and 300 ps. The distribution for the two shorter pulse widths show a similar behaviour to that for 50 fs pulses, but the distribution for the longer pulse width is largely isotropic.

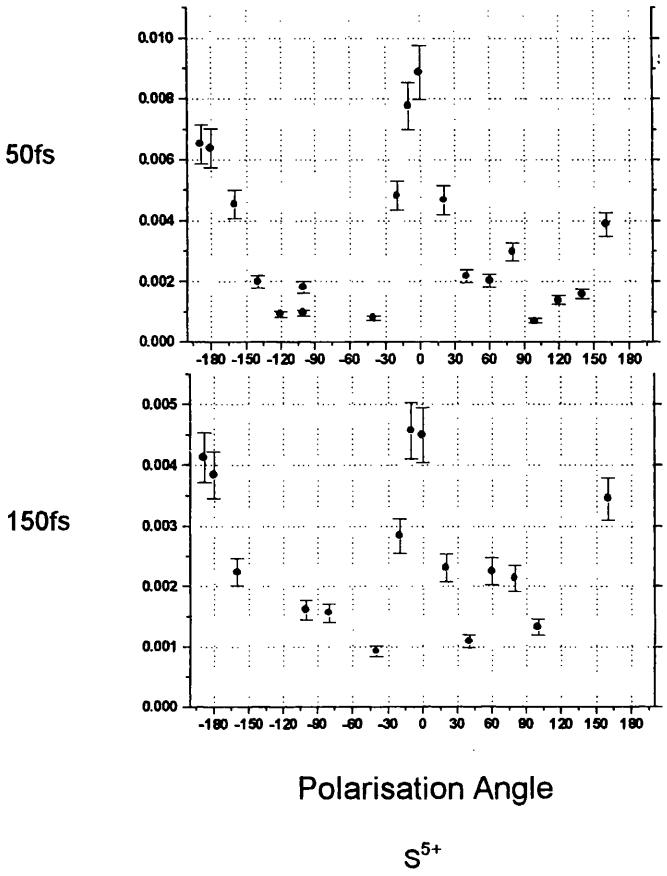

Figure 4.9 Angular distributions for the S^{n+} (n = 1-5) fragment ions arising from the dissociation of CS_2 for different pulse widths of 50 fs, 150 fs, 1 ps and 300 ps. The distribution for the two shorter pulse widths show a similar behaviour to that for 50 fs pulses, but the distribution for the longer pulse width is largely isotropic.

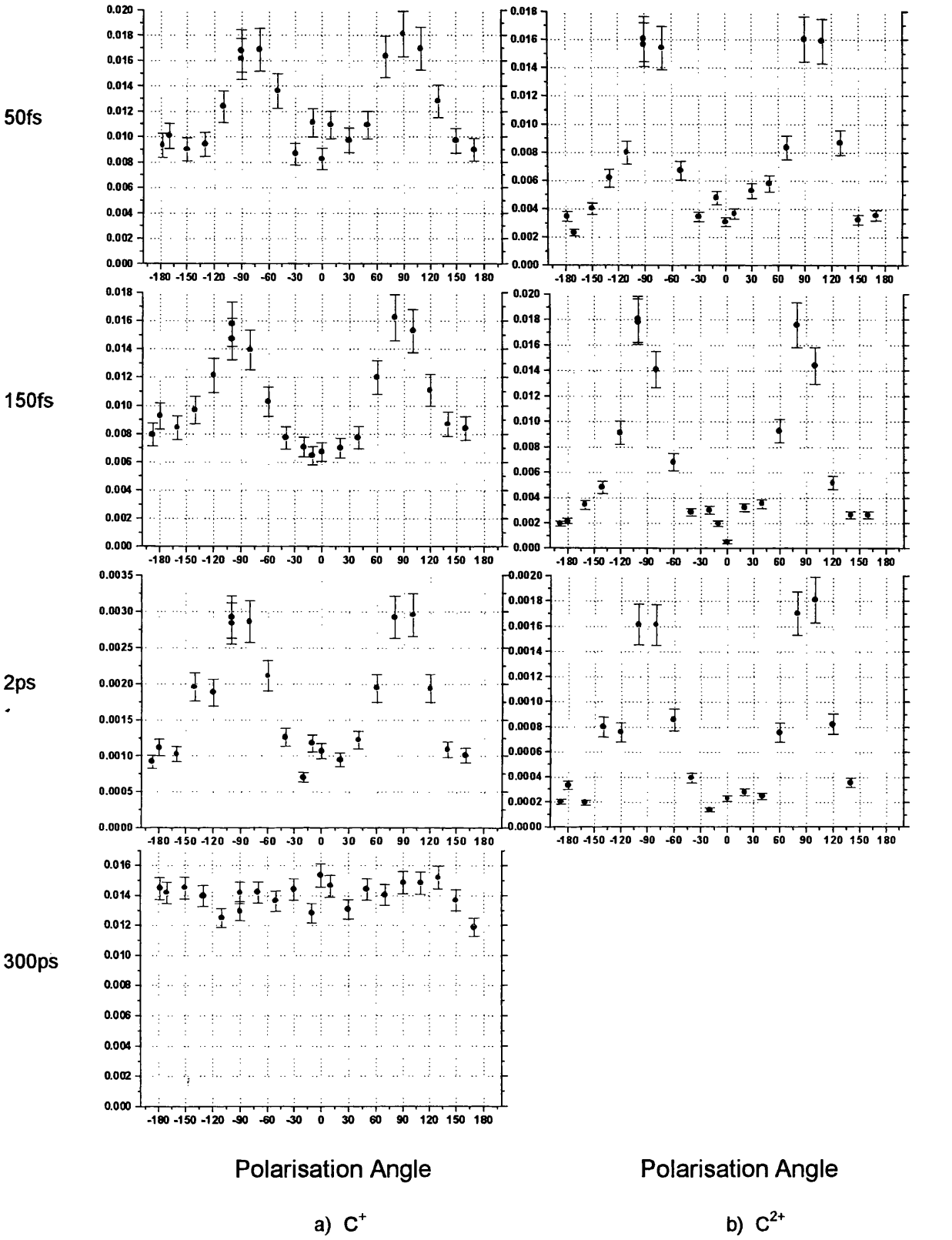

Figure 4.10 Angular distributions for the C^{m+} (m = 1-3) fragment ions arising from the dissociation of CS_2 for different pulse widths of 50 fs, 150 fs, 1 ps and 300 ps. The distribution for the two shorter pulse widths show a similar behaviour to that for 50 fs pulses, but the distribution for the longer pulse width is largely isotropic, indicating a linear molecular structure prior to dissociation.

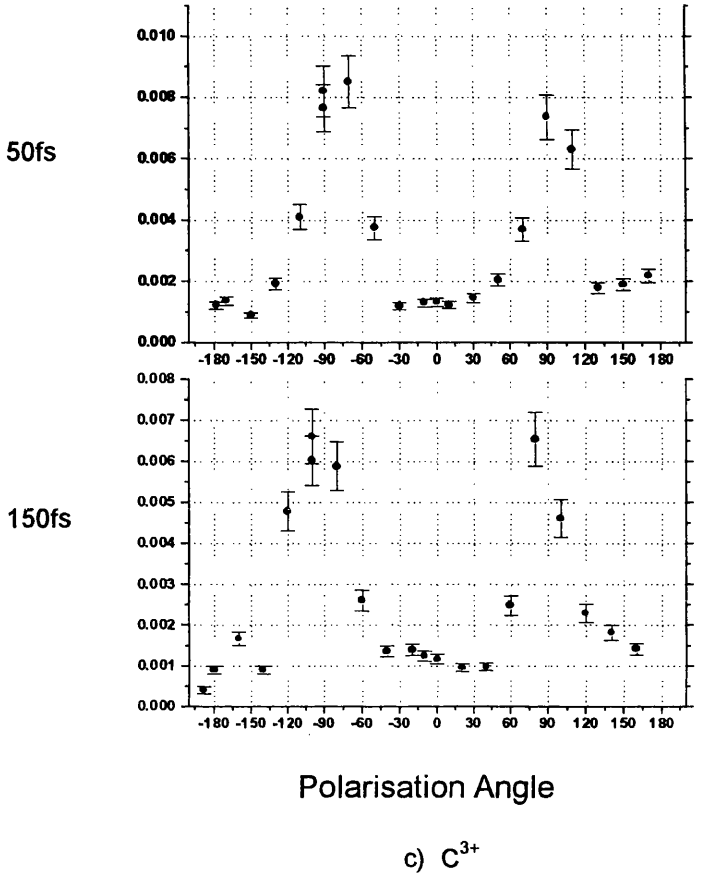

Figure 4.10 Angular distributions for the C^{m+} (m = 1-3) fragment ions arising from the dissociation of CS_2 for different pulse widths of 50 fs, 150 fs, 1 ps and 300 ps. The distribution for the two shorter pulse widths show a similar behaviour to that for 50 fs pulses, but the distribution for the longer pulse width is largely isotropic, indicating a linear molecular structure prior to dissociation.

the pulse duration means that the same torque is allowed to act for a longer time. By comparing the distributions of S-ions of a specific charge as a function of pulse duration (figure 4.9), it can be seen that the isotropic component decreases with decreasing pulse duration. Furthermore, the distribution widths for ps durations seem slightly wider than for fs, which is a counter-intuitive result. It might be expected that the molecule, having more time to align in the field, would result in fragment ions ejected in a direction more closely corresponding to that of the field. However, it is difficult to measure the width of the distributions, as the angular resolution is 20° (corresponding to a $\lambda/2$ wave-plate rotation of 10°). Finally, the ion signal decreases with increasing pulse duration (decreasing intensity), as expected showing that it is laser intensity, and not the pulse energy, that is important to multiply ionise a parent molecule. Specifically, it is the component of the laser electric field that is along the molecular axis that is important in achieving high ionisation and dissociation rates.

4. Conclusions

An investigation of the ionisation/dissociation process of the linear CS_2 and CO_2 molecules has been carried out using 50 fs, 790 nm laser pulses at an intensity of 1×10^{16} W cm^{-2}. For CS_2, the TOF mass spectra reveal that the dominant mass peaks are CS_2^+, CS_2^{2+} and CS_2^{3+}. The S^{n+} fragment peaks are broader than those for C^{m+} fragments, indicating that they possess more energy in the break-up as expected from Coulomb explosions of highly charged CS_2 molecular ions. This is especially obvious in the TOF mass spectra recorded using horizontal polarisation. The maximum charge state attained by S^{n+} (n = 6) is greater than that for C^{m+} (m = 4). This is because the more tightly bound 5+ state in C and 7+ state in S require 392 and 281 eV to ionise, respectively. These energies are not available from a laser beam of intensity 1×10^{16} W cm^{-2} with a ponderomotive potential of only 186 eV.

The angular distributions for the CS_2^+, CS_2^{2+}, CS_2^{3+}, CS^+, CS^{2+}, S^{n+} and C^{m+} ions were analysed by measuring ion peak areas with respect to the polarisation vector of the laser pulse as it was rotated. The CS_2^+, CS_2^{2+} and CS_2^{3+} parent ion distributions are all isotropic. The CS^+, C^+ and S^+ distributions exhibit a significant underlying

isotropic component in addition to anisotropy. All other multiply charged fragments display predominantly anisotropic behaviour. The S^{n+} and CS^{2+} distributions peak for laser polarisations parallel to the TOF axis, whereas the C^{m+} ions are ejected orthogonally. This is accounted for by a field-induced bending of the initially linear CS_2 molecule and subsequent momentum transfer.

The FWHM values for the S^{n+} and C^{m+} peaks are approximately of equal width. It is suggested that the observed anisotropies are not, in fact, due to the alignment of the molecule within the laser pulse. The mechanism responsible for the observed anisotropy is a preferential ionisation of those molecules that have their axes initially oriented with the laser field polarisation vector direction. If this was not the case, all molecules would be ionised with equal probability and an isotropic distribution would result. The isotropic component observed for S^+, C^+ and CS^+ is associated with low energy 'soft' dissociation.

However, the anisotropic distributions observed for the lighter CO_2 molecule are narrower for the higher charged O^{n+} fragments. This cannot be explained purely in terms of preferential ionisation and partial laser-induced alignment of the linear molecule is invoked. Thus, the conclusion drawn for CS_2 (and heavier molecules) is that the initial orientation is responsible for the observed anisotropy, whereas for CO_2 (and lighter molecules) the molecule can be aligned within the 50 fs laser pulse. This is further borne out by results for CS_2 and CH_3I, which show similar degrees of alignment in a nanosecond pulse [19].

Finally, angular distributions are measured for S^{n+} and C^{m+} from CS_2 for laser pulse lengths of 50 fs, 150 fs, 2 ps and 300ps. At the longest pulse length the distribution becomes markedly isotropic for both S and C ions, whereas the two shorter pulse widths are anisotropic and very similar to the results obtained at 50 fs. The anisotropy of the C ions for 50 fs, 150fs and 2 ps is a measure of molecular bending prior to dissociation; whereas the complete isotropy at 300 ps shows that the molecule is linear prior to fragmenting. The distribution width is similar for both 50 and 150 fs, in contrast to a recent report [57]. The spectra corresponding to longer pulse durations also show increased fragmentation over those for shorter pulses. This effect is also observed by Koudoumas et al. [60].

Mass spectra dominated by parent ions of the two molecules studied show the analytical value of femtosecond laser mass spectrometry (FLMS) [61] and allow the study of highly nonlinear processes involved in the intense laser/molecule interaction. Time-of-flight techniques are effective in providing evidence of the Coulomb explosion mechanism through the splitting of the peripheral fragment ion signals when horizontal laser polarisation is employed.

In summary, the orientation of the dipole moment of the molecule with respect to the electric field of the laser is crucial for efficient energy transfer leading to ionisation/dissociation. Molecules that are initially oriented along the direction of laser polarisation contribute most to the observed ion signal through the preferential ionisation process, as mentioned above. Further work has been carried out for other molecules (e.g. H_2S, N_2O, CH_3I) under similar experimental conditions to those used here. The results of this work have been published [62]. It is hoped that this work will lead to a greater understanding of the mechanisms for alignment/enhanced ionisation, and ultimately to steric control of chemical reactions.

References

[1] Vijayalakshmi K, Bhardwaj VR, Mathur D *1997 J. Phys. B: At. Mol. Opt. Phys.* **30** 4065-4085

[2] Posthumus JH, Plumridge J, Thomas MK, Codling K, Frasinski LJ, Langley AJ, Taday PF *1998 J. Phys. B: At. Mol. Opt. Phys.* **31** L553-L562; Posthumus JH, Giles AJ, Thompson M, Shaikh W, Langley AJ, Frasinski LJ, Codling K 1996 *J. Phys. B: At. Mol. Opt. Phys.* **29** L525-L531

[3] Hishikawa A, Iwamae A, Hoshina K, Kono M, Yamanouchi K 1998 *Chem. Phys.* **231** 315-329; Hishikawa A, Iwamae A, Hoshina K, Kono M, Yamanouchi K 1998 *Chem. Phys. Lett.* **282** 283

[4] Lompre LA, Monot P, Auguste T, Mainfray G, Manus C 1993 *Journal de Chimie Physique et de Physico-Chimie Biologique* **90** 1275-1282

[5] DeWitt MJ, Levis RJ 1998 *J. Chem. Phys.* **108** 7739-7742

[6] Talebpour A, Larochelle S, Chin SL 1997 *Laser Physics* 7 851-857

[7] Normand D, Dobosz S, Lezius M, D'Oliviera P, Schmidt M 1997 *I.O.P Conf. Series* **154** 287-297

[8] Ivanov MY, Matusek DR, Wright JS 1996 *Phys. Rev. A* **54** 3235-3244

[9] Cornaggia C 1996 *Phys. Rev. A* **54** R2555-R2558

[10] Chelkowski S, Conjusteau A, Zuo T, Bandrauk AD 1996 *Phys. Rev. A* **54** 3235-3244

[11] Ilkov FA, Walsh TDG, Turgeon S, Chin SL 1995 *Phys. Rev. A* **51** R2695-R2698

[12] Kumar GR, Gross P, Safvan CP, Rajgara FA, Mathur D 1996 *Phys. Rev. A* **53** 3098-3102

[13] Kando AE, Meath WJ 1991 *Molecular Physics* **74** 113-129

[14] Chelkowski S, Bandrauk AD 1991 *Chem. Phys. Lett.* **186** 264-269

[15] Larsen JJ, Markbak NJ, Olesen J, Bjerre N, Machholm M, Keiding SR, Stapelfeldt H 1998 *J. Chem. Phys.* **109** 8857-8863

[16] Stapelfeldt H, Constant E, Sakai H, Corkum PB 1998 *Phys. Rev. A* **58** 426-433

[17] Friedrich B, Herschbach D 1995 *J. Phys. Chem.* **99** 15686-15693

[18] Bandrauk AD, Ruel 1999 *J. Phys. Rev. A* **59** 2153

[19] Sakai H, Safvan CP, Larsen JJ, Hilligsoe KM, Hald K, Stapelfeldt H 1999 *J. Chem. Phys.* **110** 10235

[20] Yu H, Zuo T, Bandrauk AD 1998 *J. Phys. B: At. Mol. Opt. Phys.* **31** 1533-1551

[21] Loesch HJ, Remscheid A 1990 *J. Chem. Phys.* **93** 4779-4790

[22] Zewail AH 1996 *Abstracts of Papers of the American Chemical Society* **211** 153

[23] Vrakking MJJ, Stolte S 1997 *Chem. Phys. Lett.* **271** 209-215

[24] Mainos C 1996 *Phys. Rev. A* **54** 4226-4235

[25] Garrett SJ, Fairbrother DH, Holbert VP, Weitz E, Stair PC 1994 *Chem. Phys. Lett.* **219** 409-415

[26] Mathur D, Bhardwaj VR, Gross P, Kumar GR, Rajgara FA, Safvan CP, Vijayalakshmi K 1997 *Laser Physics* 7 829-838

[27] Kumar GR, Gross P, Safvan CP, Rajgara FA, Mathur D 1996 *J. Phys. B: At. Mol. Opt. Phys.* **29** L95-L103; Safvan CP, Thomas RV, Mathur D 1998 *J. Phys. B: At. Mol. Opt. Phys.* **286** 329-335; Kumar GR, Safvan CP, Rajgara FA, Mathur D

1994 *J. Phys. B: At. Mol. Opt. Phys.* **27** 2981; Kumar GR, Safvan CP, Rajgara FA, Mathur D 1993 *Chem. Phys. Lett.* **217** 626-630

[28] Rost JM, Griffen JC, Friedrich B, Herschbach DR 1992 *Phys Rev. Lett.* **68** 1299-1301

[29] Loesch HJ, Steinkemeier F 1993 *J. Chem. Phys.* **98** 9570

[30] Bandrauk AD and McCann JF 1990 *Phys. Rev. A* **42** 2806; 1992 *J. Chem. Phys.* **96** 903; Bandrauk AD and McCann JF 1992 J. Chem. Phys. **96** 903

[31] Aubanel E and Bandrauk AD 1994 *Chem. Phys. Lett.* **229** 169; 1995 *J. Chem. Phys.* **198** 159; Aubanel E and Bandrauk AD 1995 J. Chem. Phys. **198** 159

[32] Strickland D, Mourou G 1985 *Opt. Commun.* **56** 219

[33] Squier J, Salin F, Mourou G, Harter D 1991 *Opt. Lett.* **16**, 324

[34] Kmetec JD, Macklin JJ, Young JF 1991 *Opt. Lett.* **16** 1001

[35] Rudd JV, Korn G, Kane S, Squier J, Mourou G, Bado P 1993 *Opt. Lett.* **18** 2044

[36] Zhou JP, Huang CP, Murnane MM, Kapteyn HC 1995 *Opt. Lett.* **20** 64

[37] Barty CPJ, Guo T, Le Blanc C, Cheriaux G, Curley P, Darpentigny G, Rousseau P, Hamoniaux G, Antonetti A, Salin F 1996 *Opt. Lett.* **21** 1921

[38] Andre M, Coutant J, Dautray R, Decroisette M, Mainfray G, Manus C, Migus A, Sauteret C, Watteau JP 1991 *Comptes Rendus de L'academie des Sciences serie* **II** 203-209

[39] Graham P, Ledingham KWD, Singhal RP, McCanny T, Smith D, Langley AJ, Taday PF, Cosmidis K 1998 *Resonance Ionisation Spectroscopy (American Institute of Physics Conf. Proc. 9th Int. Symposium*) eds. Vickerman JC, Lyon I, Lockyer NP, Parks JE (Manchester: American Institute of Physics) 331-340

[40] Posthumus JH, Plumridge J, Frasinski LJ, Codling K, Langley AJ, Taday PF 1998 *J. Phys. B: At. Mol. Opt. Phys.* **31** L985-L993

[41] Loison JC, Durand A, Bazalgette G, White R, Audouard E 1995 *J. Phys. Chem.* **99** 13591-13596

[42] Block PA, Bohac EJ, Miller RE 1992 *Phys. Rev. Lett.* **68** 1303-1306

[43] Sanderson JH, Thomas RV, Bryan WA, Newell WR, Langley AJ, Taday PF 1998 *J. Phys. B: At. Mol. Opt. Phys.* **31** L599-L606

[44] Ellert CH, Corkum PB 1999 *Phys. Rev. A* **59** R3170-R3173

[45] Ellert CH, Stapelfeldt H, Constant E, Sakai H, Wright J, Rayner DM, Corkum PB 1998 *Phil. Trans. R. Soc. Lond. A* **356** 329-344

[45] Ellert CH, Stapelfeldt H, Constant E, Sakai H, Wright J, Rayner DM, Corkum PB 1998 *Phil. Trans. R. Soc. Lond. A* **356** 329-344

[46] Couris S, Koudoumas E, Fotakis C 1998 *Resonance Ionisation Spectroscopy (American Institute of Physics Conf. Proc. 9th Int. Symposium)* eds. Vickerman JC, Lyon I, Lockyer NP, Parks JE (Manchester: American Institute of Physics) 331-340

[47] Thompson MR, Thomas MK, Taday PF, Posthumus JH, Langley AJ, Frasinski LJ, Codling K *1997 J. Phys. B: At. Mol. Opt. Phys.* **30** 5755-5772

[48] Bhardwaj VR, Safvan CP, Vijayalakshmi K, Mathur D 1997 *J. Phys. B: At. Mol. Opt. Phys.* **30** 3821-3831; Safvan CP, Vijayalakshmi K, Rajgara FA, Kumar GR, Marathe VR, Mathur D 1996 *J. Phys. B: At. Mol. Opt. Phys.* **29** L481-L487; Safvan CP, Thomas RV, Mathur D 1998 *Chem Phys Lett.* **286** 329-335

[49] Bhardwaj VR, Vijayalakshmi K, Mathur D 1999 *J. Phys. B: At. Mol. Opt. Phys.* **32** 1087-1095

[50] Codling K, Frasinski LJ, Hatherly PA 1989 *J. Phys. B: At. Mol. Opt. Phys.* **22** L321

[51] Hering Ph and Cornaggia C 1999 *Phys. Rev. A* **59** 2836-2843

[52] Aicher KP, Wilhelm U, Grotemeyer J 1995 *J. Am. Soc. Mass Spectrom.* **6** 1059-1068

[53] Ledingham KWD, Kilic HS, Kosmidis C, Deas RM, Marshall A, McCanny T, Singhal RP, Langley AJ, Shaikh W 1995 *Rapid Commun. Mass Spectrom.* **9** 1522

[54] Taday PF, Mohammed I, Langley AJ, Ross IN, Codling K, Ledingham KWD, Newell WR, Preston S, Riley D, Williams I 1997/98 *Central Laser Facility RAL Annual Report* 179

[55] Augst S, Strickland D, Meyerhofer DD, Chin SL, Eberly JH 1989 *Phys.Rev.Lett.* **63** 2212

[56] Lide DR (ed) 1991-92 Handbook of Chemistry and Physics 72nd Ed. (Boca Raton, FL: CRC Press)

[57] Couris S, Koudoumas E, Fotakis C 1999 J. Phys. B: At. Mol. Opt. Phys. **32** L439-L450

[58] Posthumus JH, Plumridge J, Taday PF, Sanderson JH, Langley AJ, Codling K, Bryan WA 1999 *J. Phys. B: At. Mol. Opt. Phys.* **32** L93-L101

[59] Sanderson JH, El-Zein A, Bryan WA, Newell WR, Langley AJ, Taday PF 1999 *Phys. Rev. A* **59** R2567-R2570

[60] Koudoumas E, DeNalda R, Fotakis C, and Couris S 1999 *to be published*

[61] Ledingham KWD, Singhal RP, Smith D, McCanny T, Graham P, Kilic HS, Peng WX, Wang SL, Langley AJ, Taday PF, Kosmidis C 1998 *J. Phys. Chem. A* **102** 3002-3005

[62] Graham P, Ledingham KWD, Singhal RP, McCanny T, Langley AJ, Taday PF, Kosmidis C *to be published*

Chapter 5

The angular distributions of fragment ions from labelled and unlabelled N_2O in intense laser fields

CHAPTER OVERVIEW

The mass spectra and angular distributions of fragment ions arising from Coulomb explosion of highly-charged parent nitrous oxide ions, obtained in the femtosecond regime, are investigated. The N-ion angular distributions from $^{14}N_2O$ show maxima when the laser polarisation is parallel and orthogonal to the time-of-flight (TOF) axis. Measurements with labelled molecules (^{15}N-^{14}N=^{16}O) indicate that the maxima arise from the peripheral and central N-atoms in the molecular structure for parallel and orthogonal polarisation, respectively. The anisotropic distributions may be explained by assuming increased ionisation and fragmentation when the molecular axis is parallel to the laser field. The bond angle prior to explosion is determined to be ~140°, irrespective of the charge-state of the precursor and calculations of the kinetic energies imparted to fragment ions suggest that dissociation occurs at the equilibrium internuclear distance of the neutral molecule.

1 Introduction

Chirped-pulse amplification (CPA) techniques [1] allow the generation of intense, short-pulse laser beams and significant insights into the dynamics of laser/molecular interactions are being obtained using sub-picosecond laser pulses [2-16], especially the ionisation and subsequent fragmentation of molecules in intense laser fields [17-26].

The response of gas-phase molecules in the intense electric fields of such lasers is highly non-linear. The internal structure of the ionised molecule is thus distorted, and the coupling of the laser field with the induced electric dipole moment produces a torque, which *tends* to align the dipole moment along the laser field. The coupling would be expected to be stronger for higher charged states of the molecule, via the increased polarisation, resulting in angular distributions of fragment ions that narrow. Moreover, for large induced dipole moments the molecular ion may stretch beyond the equilibrium nuclear separation, which further increases the polarisation. The ionisation rate increases at this separation, via barrier suppression ionisation (BSI), and the highly ionised molecule undergoes Coulomb explosion [27].

For the initially linear triatomic molecule reported here, Coulomb explosion produces fragment ions that have momentum along the direction of the laser electric field. However, highly charged molecular ions may possess a bent structure and the explosion would result in the central atomic ion moving orthogonally to the laser polarisation direction [28].

The distribution of exploding fragments has previously been measured for a number of molecules. The molecules NO_2, CS_2, C_6H_6 and CCl_4 [15, 25-26] were studied using pulses of 32 ps and 532 nm; while CS_2, CO_2, NO_2, N_2O, H_2, D_2, N_2 and I_2, were analysed in the fs regime [21, 28-44]. For the CS_2 molecule, the ratio of the S-ion yield (of a particular charge state) for horizontal polarisation (laser polarisation being parallel to the TOF axis) to the ion yield for vertical polarisation (orthogonal to the TOF axis) was measured as a function of intensity [37] in the fs regime. The results suggested that CS_2

is *geometrically aligning* [4, 41] with the field. In an ensemble of molecules with randomly orientated dipoles, those molecules that lie along the direction of the laser polarisation are more efficiently tunnel-ionised. It has been argued that this angular dependence of the ionisation probability accounts for the anisotropy observed [4, 34, 43]. However, in the ps pulse regime [15, 24, 26, 42], both central and peripheral ion intensities are maximal along the detection axis. It may be that in a 32 ps pulse the molecules will have more time to align with the field of the laser. This was not observed in experiments performed at 3 ps [29].

On the other hand, Hishikawa et al. [5, 6] studied the Coulomb explosion of N_2 and SO_2 molecules using momentum imaging techniques, from which it was concluded that both are aligned by the laser field and that the fragments are ejected with momentum increasing with initial charge state. Utilising both linear and circularly polarised laser beams, Ellert et al. [34, 43] distinguish the effects of orientation and enhanced ionisation for I_2, Cl_2 and O_2. They also observe I_2^{5+} when the polarisation is along the TOF axis (horizontal) whereas only I_2^{3+} is reached when it is at right angles (vertical). This shows that ionisation is enhanced when the molecular axis coincides with the laser field. This is also observed by Posthumus [4, 30] for I_2.

A comparison between $^{14}N_2O$ and $^{14}N^{15}N^{16}O$ was performed at a laser intensity of 3×10^{16} W cm^{-2}, 248 nm wavelength and 600 fs pulses by Luk et al. [40]. This was to investigate an 'atomic-site dependent production', in which the central ion yield and kinetic energy was found to be different to that for the peripheral N-ion. However, no measurements on the polarisation dependence were performed.

The experiment detailed here, uses both unlabelled and labelled (^{15}N-^{14}N=^{16}O) nitrous oxide to identify unambiguously the origin of the different maxima in the angular distribution of the N-ions resulting from the unlabelled nitrous oxide molecule. Another objective of the present experiment, was to make further comparisons between labelled and unlabelled nitrous oxide in terms of the fragment ion angular dependencies and mass spectra at approximately the same laser intensity as used in [40], but at 800 nm and

shorter pulse durations (50 fs). Finally, by calculating the kinetic energies of the ejected fragment ions in the Coulomb explosion, the bond lengths and angles of the parent precursor ion at the moment of dissociation can be determined.

2 Experimental

For a detailed description of the experimental apparatus, see chapter 2. Briefly, gas-phase samples were admitted effusively from an inlet system into a high-vacuum chamber, pumped to a base pressure of the order of 10^{-8} Torr by a turbomolecular pump. The sample pressures were of the order of 10^{-6} Torr, in order to avoid space-charge effects and pressure broadening of the mass peaks. An extraction field of 500 V cm^{-1} was used to direct ions to the detector. Ions were detected by an electron multiplier connected to a LeCroy 9344C (500 MHz) digital oscilloscope, which allowed real-time observation of the mass spectra obtained as well as their permanent storage on floppy disc.

Gas samples of unlabelled nitrous oxide ($^{14}N_2O$) obtained from BOC gases of 99% purity were used without further sample preparation. Labelled nitrous oxide (99% $^{15}N^{14}N^{16}O$) was obtained from Cambridge Isotopes Inc., USA.

The laser system used is based on a 20 fs Ti:S oscillator pumped by a Spectra-Physics Millenia solid-state laser [47] and utilises the chirped pulse amplification (CPA) technique [1]. Subsequent re-compression of the amplified pulse to 50 fs produces 5 mJ pulses of 790 nm and intensities of 10^{16} W cm^{-2} were achieved when focussed with a spherical on-axis f/3 mirror. The laser repetition rate was 10 Hz.

The laser beam passes through the interaction volume at right angles to the TOF axis. The E-vector rotates in a plane at right angles to the propagation direction, which includes the TOF axis. The horizontal (parallel) direction of the E-field was defined to be collinear with the TOF axis.

To measure the angular distributions of the fragments, a λ/2 wave-plate was inserted into the path of the beam just before the quartz window of the target chamber. A polariser was also used to ensure the polarisation was initially horizontal. The λ/2 wave-plate was then rotated and a spectrum (typically over 300 laser shots) obtained for each polarisation angle, typically in 10° steps. The area under the ion peak of interest was then measured and plotted against the orientation of the polarisation vector with respect to the TOF axis.

3 Results

3.1 mass spectra

3.1.1 Unlabelled nitrous oxide ($^{14}N_2O$)

Mass spectra for $^{14}N_2O$ at horizontal and vertical laser polarisation, for laser intensity of about 10^{16} W cm^{-2}, are shown in figures 5.1 and 5.2, respectively. The N_2O^+ parent ion, at m/z = 44, is the dominant peak and has similar intensity and shape in the mass spectra obtained for both polarisation orientations. This is indicative that the parent ion is produced with negligible kinetic energy [29, 44]. Mass peaks are also present at m/z = 28 and m/z = 30 corresponding to N_2^+ and NO^+, respectively. A small H_2O peak at m/z = 18 is also in evidence. The multiple ionisation of the molecule generally precedes dissociation when using femtosecond (fs) laser pulses [48]. However, only singly ionised parent ions are detected. The multiply charged nitrogen and oxygen ions originate from Coulomb explosion of highly charged parent molecular ions, and are prominent in the mass spectra.

The nitrogen ion peaks have contributions from both the peripheral and central N-atoms. In the peak for N^{2+} in horizontal polarisation, the 'middle' peak is likely due to the low-energy central N^{2+} ion. However, with consideration of the kinetic energy produced as the molecule Coulomb explodes along the laser polarisation direction, the fragments will possess kinetic energy in this direction. Thus, the N-ion peak will mainly arise from the peripheral N in horizontal polarisation and from the central N in the vertical polarisation spectra. The split peaks in the spectra are due to the exploding fragments initially

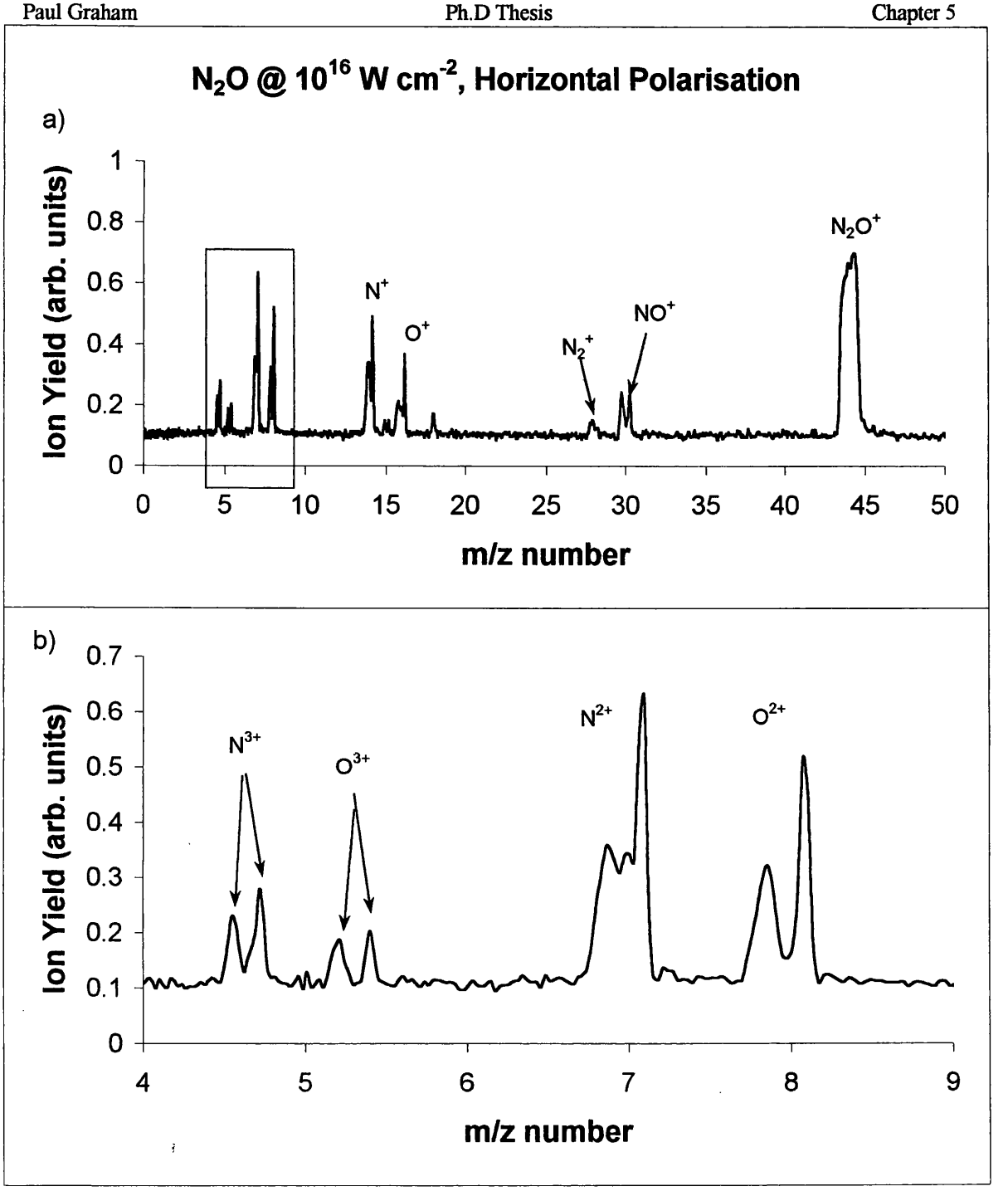

Figure 5.1 a, b Mass spectra of unlabelled nitrous oxide ($^{14}N_2O$) taken for horizontal polarisation at a laser intensity of 10^{16} W cm^{-2}. Fig 5.1 b shows an expanded view of the low-mass region indicating the multiply charged fragment ions.

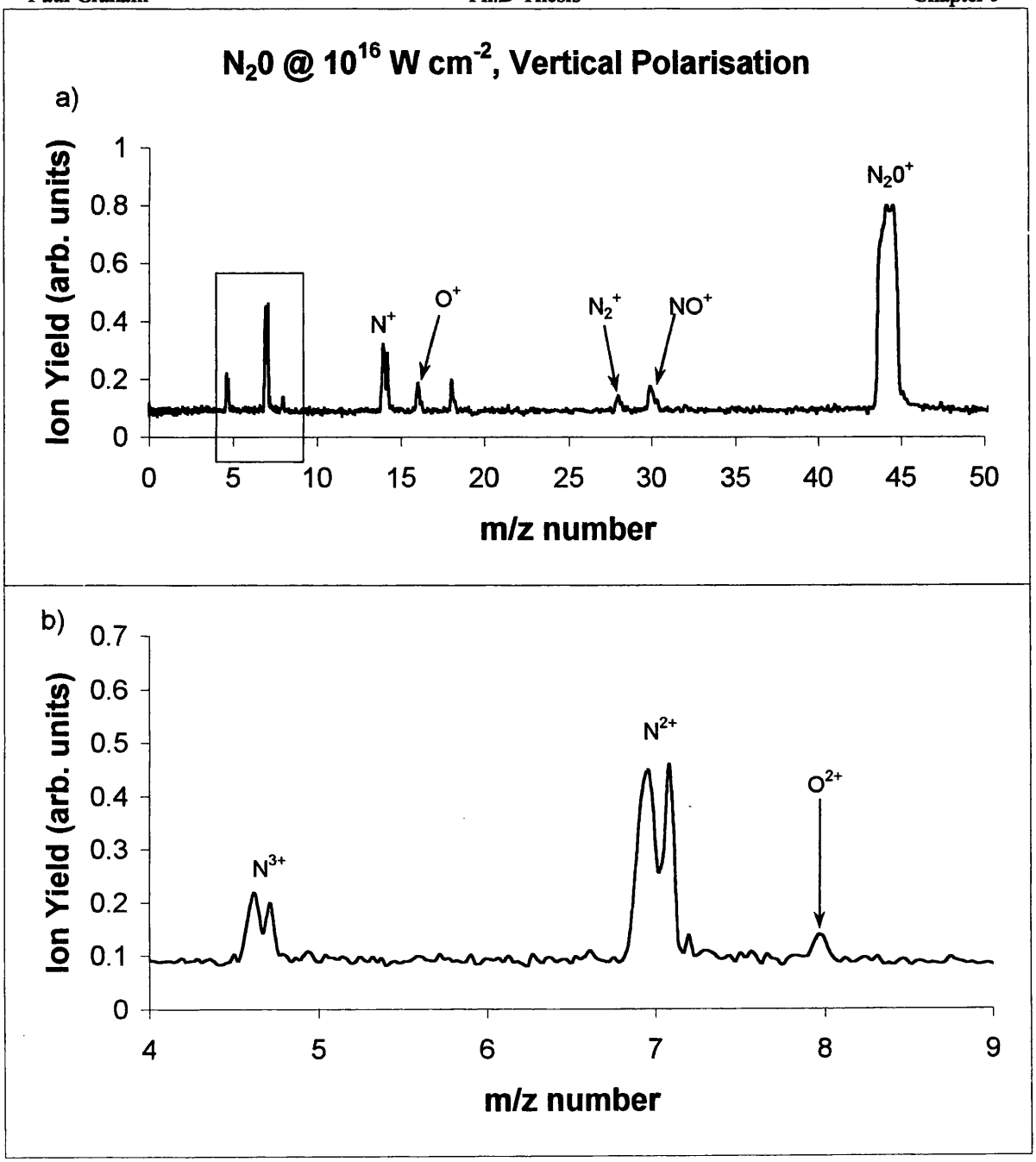

Figure 5.2 a, b Mass spectra of unlabelled nitrous oxide ($^{14}N_2O$) taken for vertical polarisation at a laser intensity of 10^{16} W cm^{-2}. Fig 5.2 b shows an expanded view of the low-mass region indicating the multiply charged fragment ions.

directed towards and away from the detector, and the resulting difference in time of flight can be used to determine the kinetic energy imparted to the exploding ions. The split peaks require some explanation. The broad peak for forward-directed ions and the narrow peak for initially backward-directed ions are a direct consequence of Coulomb explosion of highly charged parent ions and the 'reflectron-effect' of the extraction field. Similar peak shapes are also observed in the spectra presented in Luk et al. [40], who also attribute the peak shapes on an instrumental effect and the kinetic energy imparted to the fragment ions.

The extraction field is insufficient to collect ions possessing measurable kinetic energy in a direction perpendicular to the TOF axis and direct them to the detector. They are hence effectively 'lost' to the detector. This is particularly so for higher charge-states, since the velocity imparted is greater. Only those molecules that explode along the TOF axis will have their fragment ions detected, regardless of polarisation orientation. This is true whether or not they are aligned by the field or initially orientated along the TOF axis. The greater degree of splitting and the observation of higher fragment ion charge when the polarisation is collinear with the TOF axis, is therefore proof that ionisation/dissociation is greatest when the molecular axis lies along the field polarisation.

In the horizontal polarisation spectra, the O-ion peaks are more intense and have greater splitting than in the vertical polarisation spectra. The O^{3+} is missing entirely for vertical polarisation, whilst it is comparable to N^{3+} in horizontal polarisation. The comparison of the N-ion and O-ion yields for horizontal laser polarisation indicates that the N-ion peak is from the terminal N as it is comparable in size to the O-ion peak. However, in the vertical polarisation spectrum, the total absence of O^{3+} and only a weak O^{2+} peak being present indicates that the observed N-ions originate from the central position in the molecule. This conclusion is supported by results obtained using ^{15}N-labelled N_2O, as discussed in the next section.

3.1.2 Labelled nitrous oxide ($^{15}N^{14}N^{16}O$):

The sample of labelled N_2O was quoted as 99% enriched (Cambridge Isotopes Inc., USA) in the form $^{15}N^{14}N^{16}O$. In the mass spectra obtained for horizontal and vertical polarisations, figures 5.3 and 5.4, the parent ion is the dominant peak at m/z = 45. Mass peaks are also seen at m/z = 29 and 30, corresponding to $^{15}N^{14}N^{+}$ and $^{14}N^{16}O^{+}$, respectively. In all mass spectra presented, it can be seen that the NO-ion is bigger than the N_2 ion, particularly for horizontal polarisation, despite the N-N being a triple bond. This is also observed by Luk et al. [40], who conclude that it implies a movement of significant electron density along the molecular axis. The larger NO^{+} peak for horizontal polarisation would seem to support this. However, the m/z = 31 ion peak corresponding to $^{15}N^{16}O^{+}$, which would result when bending of the molecule was sufficient for the two peripheral atoms to bond together, is absent. This is also the case for the results presented in Luk et al. [40]. Such bonding of two peripheral atoms in a triatomic molecule has been previously observed, albeit very weakly, for CS_2 at 375 nm [49]. In the horizontal and vertical polarisation mass spectra, the ^{15}N- and ^{16}O-ion yields from the peripheral positions are similar in intensity but characteristically different from the central ^{14}N-ion peak. The peripheral ion peaks are more split in structure in the mass spectra for horizontal polarisation than for vertical polarisation, reflecting the fact that the molecule dissociates more efficiently along the field direction.

3.2 Fragment Ion Angular Distributions

3.2.1 Unlabelled nitrous oxide ($^{14}N_2O$)

The angular distributions of the fragment ions originating from the unlabelled molecule N_2O are presented in figures 5.5 and 5.6, for 50 fs pulses and laser intensities of about 10^{16} W cm^{-2}. The angular distribution is a measure of the number of ions detected in a narrow 'cone of acceptance' along the TOF axis for a given orientation of the polarisation vector of the laser field with respect to the TOF axis. The distributions for both N_2O^{+} and N_2^{+} are isotropic (not shown). Even though the probability of ionisation is higher if the molecular axis is collinear with the field, the isotropic distribution indicates that these ions are produced with low kinetic energies. The higher kinetic energies upon

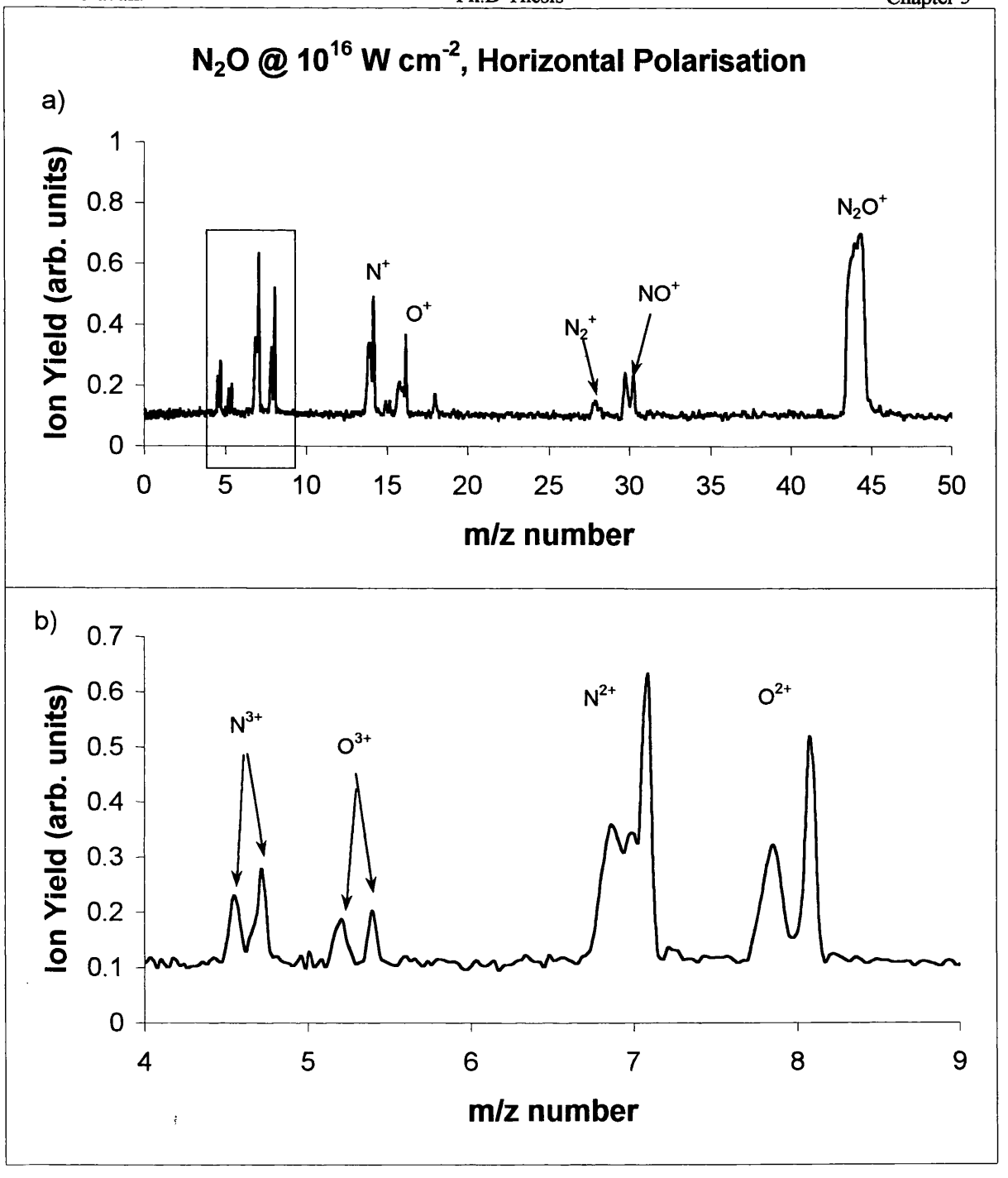

Figure 5.1 a, b Mass spectra of unlabelled nitrous oxide ($^{14}N_2O$) taken for horizontal polarisation at a laser intensity of 10^{16} W cm^{-2}. Fig 5.1 b shows an expanded view of the low-mass region indicating the multiply charged fragment ions.

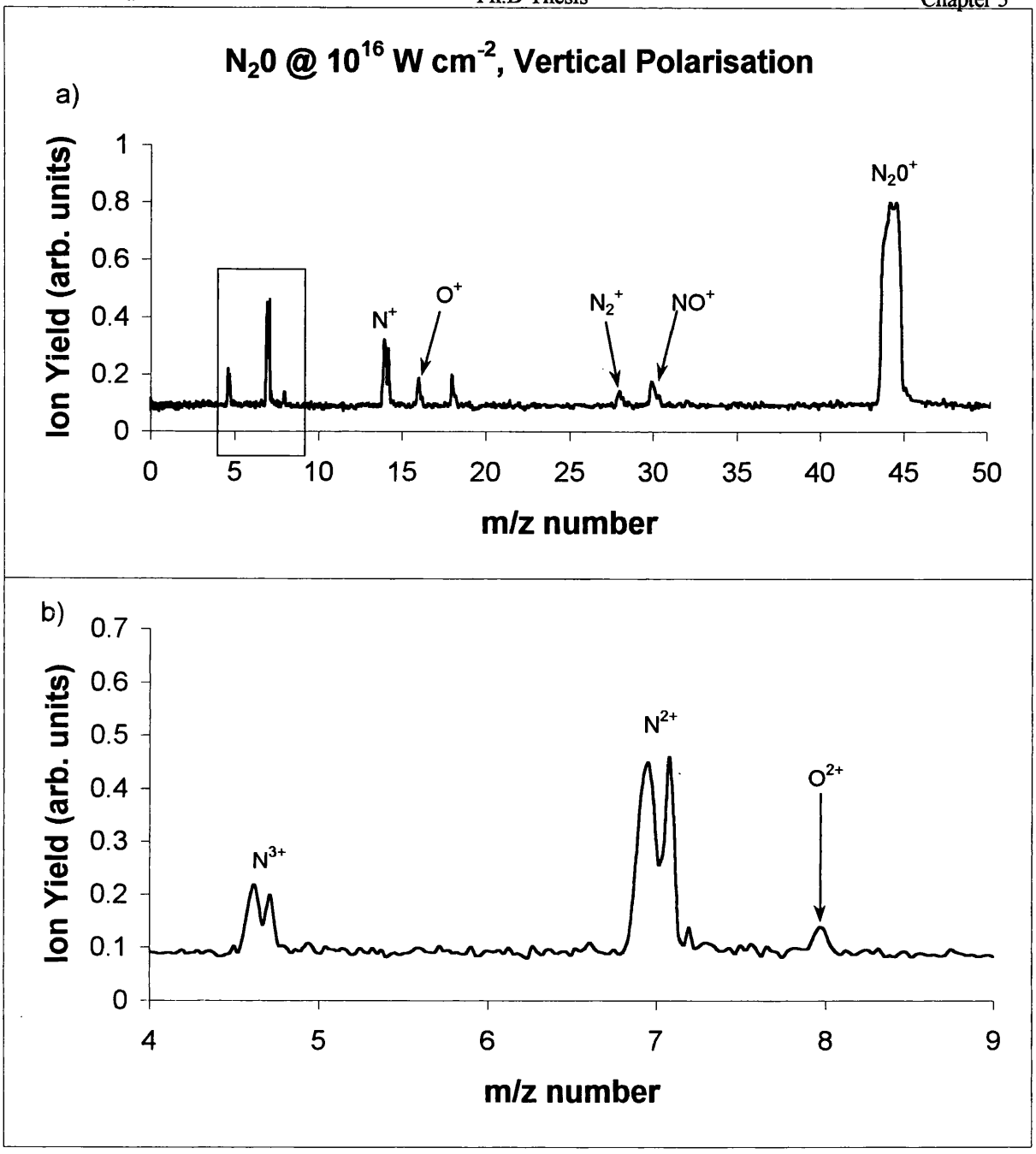

Figure 5.2 a, b Mass spectra of unlabelled nitrous oxide ($^{14}N_2O$) taken for vertical polarisation at a laser intensity of 10^{16} W cm^{-2}. Fig 5.2 b shows an expanded view of the low-mass region indicating the multiply charged fragment ions.

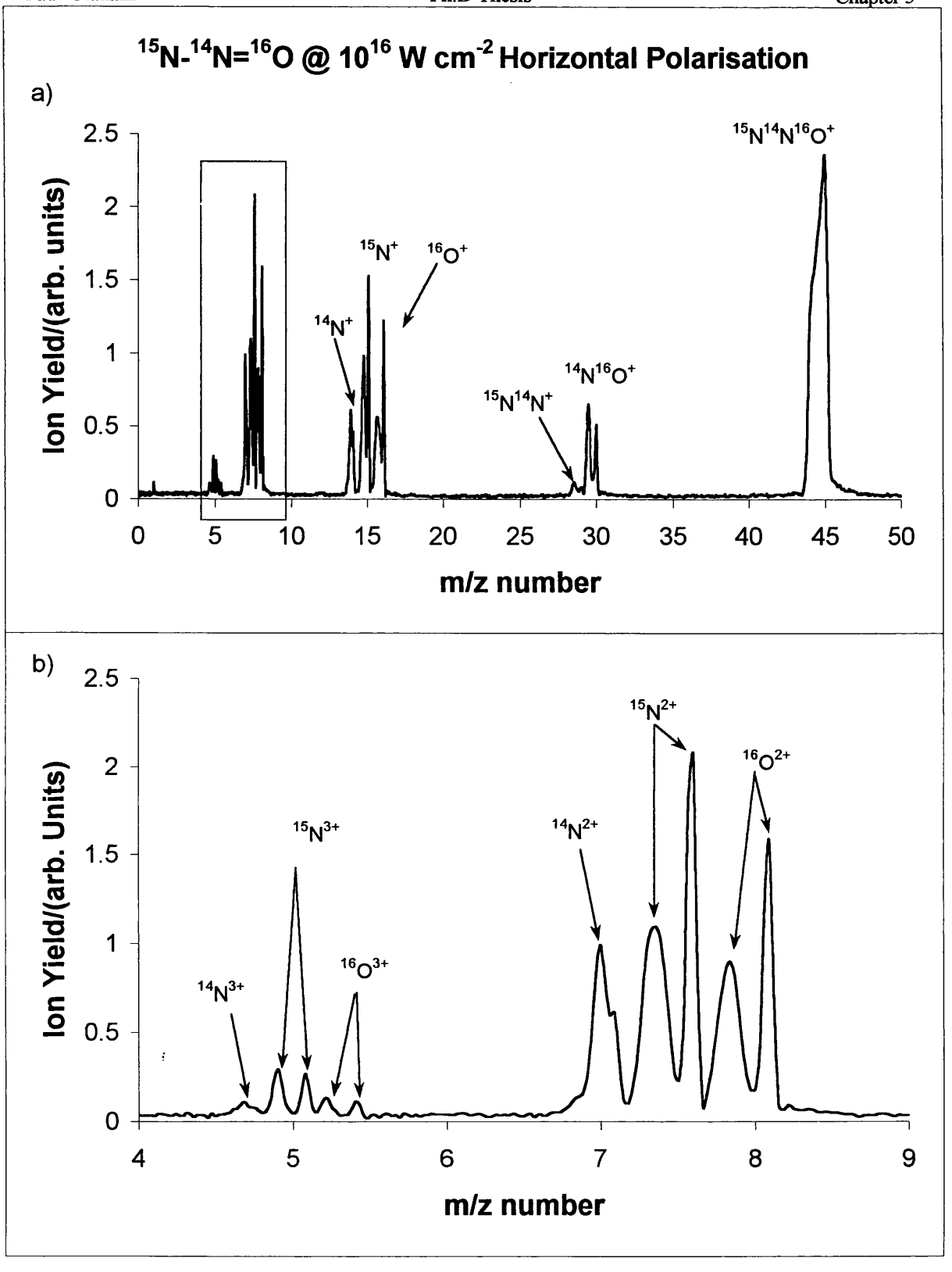

Figure 5.3 a, b Mass spectra of labelled nitrous oxide ($^{15}N^{14}N^{16}O$) taken for horizontal polarisation at a laser intensity of 10^{16} W cm^{-2}. Fig 5.3 b shows an expanded view of the low-mass region indicating the multiply charged fragment ions.

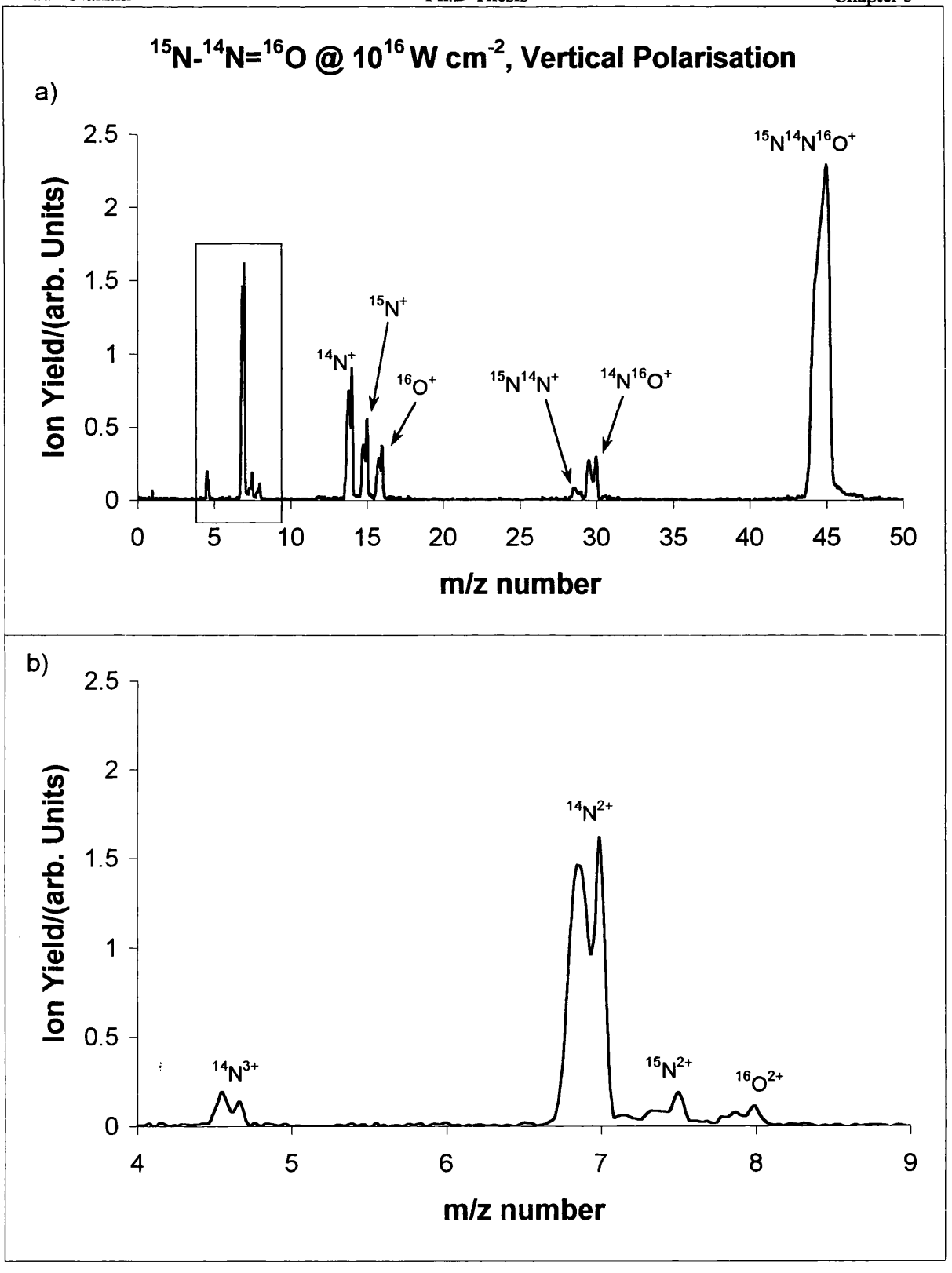

Figure 5.4 a, b Mass spectra of labelled nitrous oxide ($^{15}N^{14}N^{16}O$) taken for vertical polarisation at a laser intensity of 10^{16} W cm^{-2}. Fig 5.4 b shows an expanded view of the low-mass region indicating the multiply charged fragment ions.

dissociation of highly charged transient states, together with the narrow acceptance cone of the TOF system, may result in the observed narrowing of the angular distributions in figure 5.7.

The angular distributions presented generally have an isotropic component that decreases with increasing charge-state of the fragment ion. This is due to two effects. If the ions produced have negligible kinetic energy, then as mentioned previously, the extraction field is sufficient to direct them towards the detector, irrespective of their direction of travel. The second source of isotropy in the distributions is that, at the high laser intensities employed ($\sim 10^{16}$ W cm^{-2}), the laser field is sufficient to tunnel-ionise the molecule even when the molecular axis and the polarisation are orthogonal. Thus, when the polarisation is vertical ($\pm 90°$), molecules oriented along the TOF axis still have a finite probability of ionising and dissociating, resulting in a small peripheral ion count. This probability of ionisation decreases for increasing charge-state of the transient parent ion since the field strength will not be sufficient, reducing the observed isotropic component.

The distributions for NO^+ and NO^{2+} are shown in figure 5.5. Both distributions are peaked in the 0° and 180° directions. These angular distributions are similar to CS^+ and CS^{2+} [29] from CS_2. The NO^+ distribution is anisotropic, but has an underlying isotropic component. The isotropic component of the NO^+ distribution arises from the isotropic parent ion N_2O^+, while the anisotropic component could arise from Coulomb explosion of a short-lived higher charged state, possibly N_2O^{q+} ($q \geq 2$). In comparison, the NO^{2+} is markedly anisotropic suggesting that NO^{2+} originates from a higher charged precursor.

The distributions of the O-fragments are also shown in figure 5.5. It is seen that all are significantly anisotropic, with the lowest charged O^+ distribution having a small isotropic component. The distributions seem to narrow slightly for increasing charge-states. This could arise if N_2O molecules align with the polarisation direction within the 50 fs laser pulse.

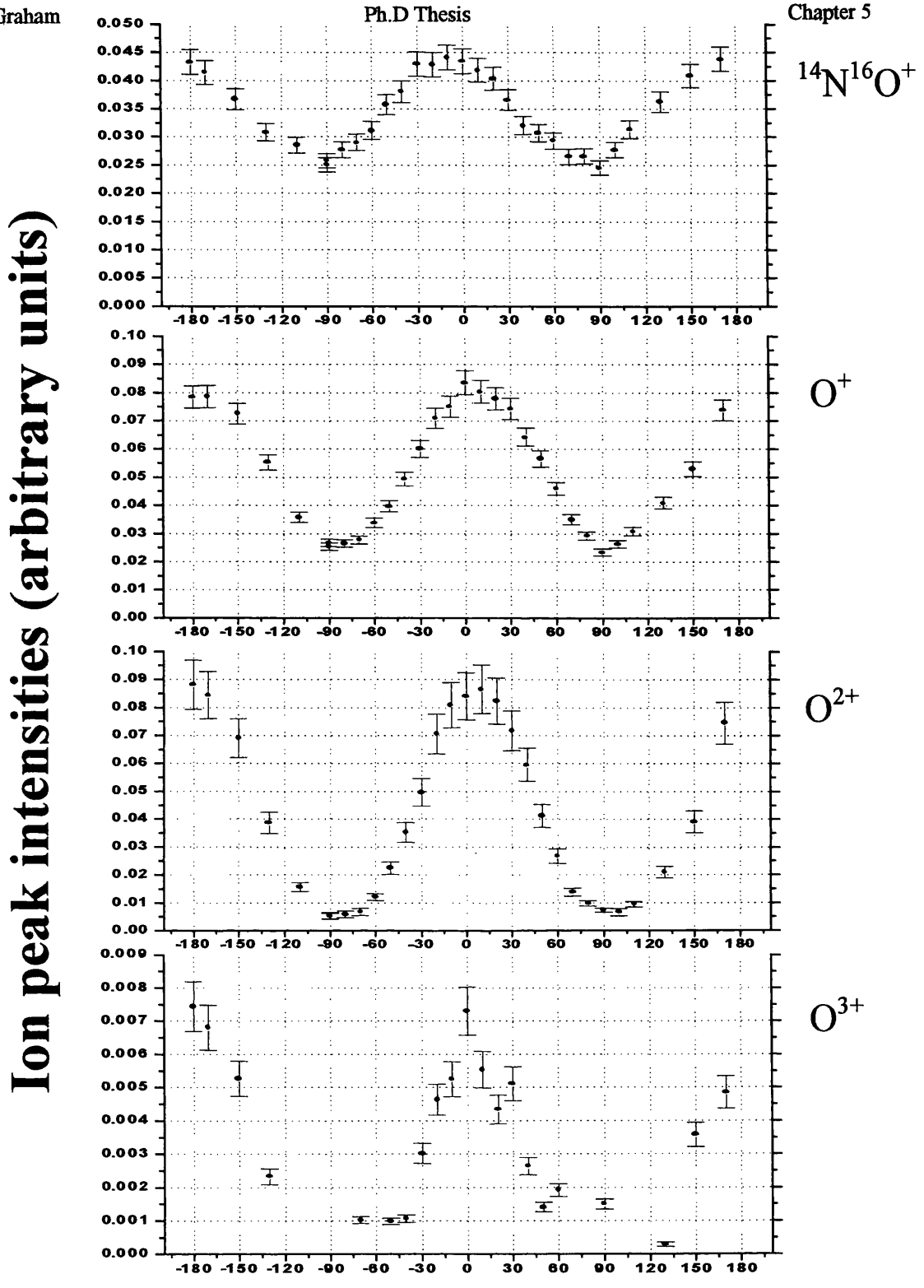

Figure 5.7 The angular distributions of $^{14}N^{16}O^+$ and O^{n+} ($n \leq 3$) ions are shown from labelled nitrous oxide at 10^{16} W cm^{-2}. It is evident that all the distributions resemble that for a peripheral atom from the dissociation of a triatomic, i.e. they peak along the TOF axis direction. The distribution of $^{15}N^{14}N^+$ (not shown) is completely isotropic.

The angular distributions of N^{p+} ($p \leq 4$) are shown in figure 5.6. The distributions show a highly unusual behaviour. All are markedly anisotropic. However, the distributions here are peaked both for horizontal polarisation (the 0° and 180° direction), *as well as* for vertical polarisation (±90° direction), and that this orthogonal contribution increases relatively with increasing charge-state. The two sets of maxima in the angular distributions arise due to the different locations of the nitrogen atoms in the molecular structure N-N=O. The peripheral N-atom is responsible for the peak in the distribution for horizontal polarisation, while the central N-atom is responsible for the peak in the distribution for vertical polarisation. This observation is similar to that for CS_2 where the central C-atom is peaked in the distribution for vertical polarisation [29, 44]. The transient state can achieve a higher ionisation level when the molecular axis and laser polarisation are collinear. Thus, the molecule Coulomb explodes along the direction of the field, and when the polarisation is horizontal the peripheral ions are directed along the TOF axis, and for vertical polarisation it is the central atom that is so directed. The molecule is initially linear. However, as the central N-atom is ejected orthogonally to the polarisation of the laser field, it is surmised that the molecule is being bent in the intense electric field, in the same way to CS_2 [29, 44] and CO_2 [28].

The increasing anisotropy of N-ions, figure 5.6, at ±90° relative to that at 0° and 180° may be a result of the higher kinetic energy of N^{3+} and N^{4+} ions ejected in the perpendicular direction. Thus the probability of detecting them along the TOF axis is reduced compared to that for the central N-ion which is imparted with momentum down the drift-tube, and hence more efficiently detected. The ion yields at ±90° increase relative to those at 0° and 180° with increasing charge-state.

3.2.2 Labelled nitrous oxide ($^{15}N^{14}N^{16}O$)

The angular distributions of fragment ions arising from Coulomb explosion of labelled nitrous oxide ($^{15}N^{14}N^{16}O$) were also studied. The mass peaks at m/z = 29 and 30 correspond to $^{15}N^{14}N^+$ and $^{14}N^{16}O^+$, respectively. The angular distribution of the former peak was isotropic and is not shown here. The distribution of $^{14}N^{16}O^+$ is shown in figure 5.7. The N_2 and NO peak distributions for unlabelled nitrous oxide were also observed to

have similar characteristics. Both fragments come from a two-body breakup. However the NO fragment must be released with sufficient kinetic energy so as to develop an anisotropy in its angular distribution. Thus, it may be that N_2 mainly comes from a 'soft' dissociation and that the NO fragment has a significant contribution from Coulomb explosion of a multiply charged precursor.

The distributions for the O^{n+} ($n \leq 3$) fragment ions originating from the Coulomb explosion of the parent ion are also shown in figure 5.7. A slight narrowing is observed as the charge-state increases. The multiply charged oxygen ions derive from unstable and highly ionised molecules, which have large dipole moments and hence interact more strongly with the laser field. The underlying isotropy of the distribution decreases with increasing charge of the ion indicating that Coulomb explosion becomes increasingly more important for such ions.

The contributions to the N-ion angular distributions arising from the central and peripheral nitrogen atoms are unambiguously determined for the labelled nitrous oxide. The angular distributions of the fragment $^{15}N^{p+}$ ($p \leq 3$) and $^{14}N^{m+}$ ($m \leq 3$) ions are shown in figures 5.8 and 5.9, respectively. The ^{15}N-ion intensity is peaked at 0° and 180° for horizontal polarisation and at ±90° for ^{14}N-ion peaks for vertical polarisation. This is in accordance with previous angular dependence studies on other triatomics [44]. The peripheral $^{15}N^{+}$ ion intensity is non-zero at ±90° indicating that it is ejected with low kinetic energy. This could come about in a weak Coulombic explosion (ionic repulsion) or via an ion/neutral fragmentation pathway.

The central ^{14}N-ion distributions are shown in figure 5.9 and, as already mentioned, peak in the orthogonal direction. The distribution widths seem to be similar for both $^{14}N^{+}$ and $^{14}N^{2+}$, but narrow slightly for $^{14}N^{3+}$. This may be due to higher ejection velocities via an increased Coulomb repulsion or an increase in bond angle with charge state of the parent precursor. The distributions all feature an isotropic component, but this decreases with increasing fragment charge. The angular distributions of these ions mirror those for a central atom in an initially linear triatomic molecule. The anisotropy of the central atom

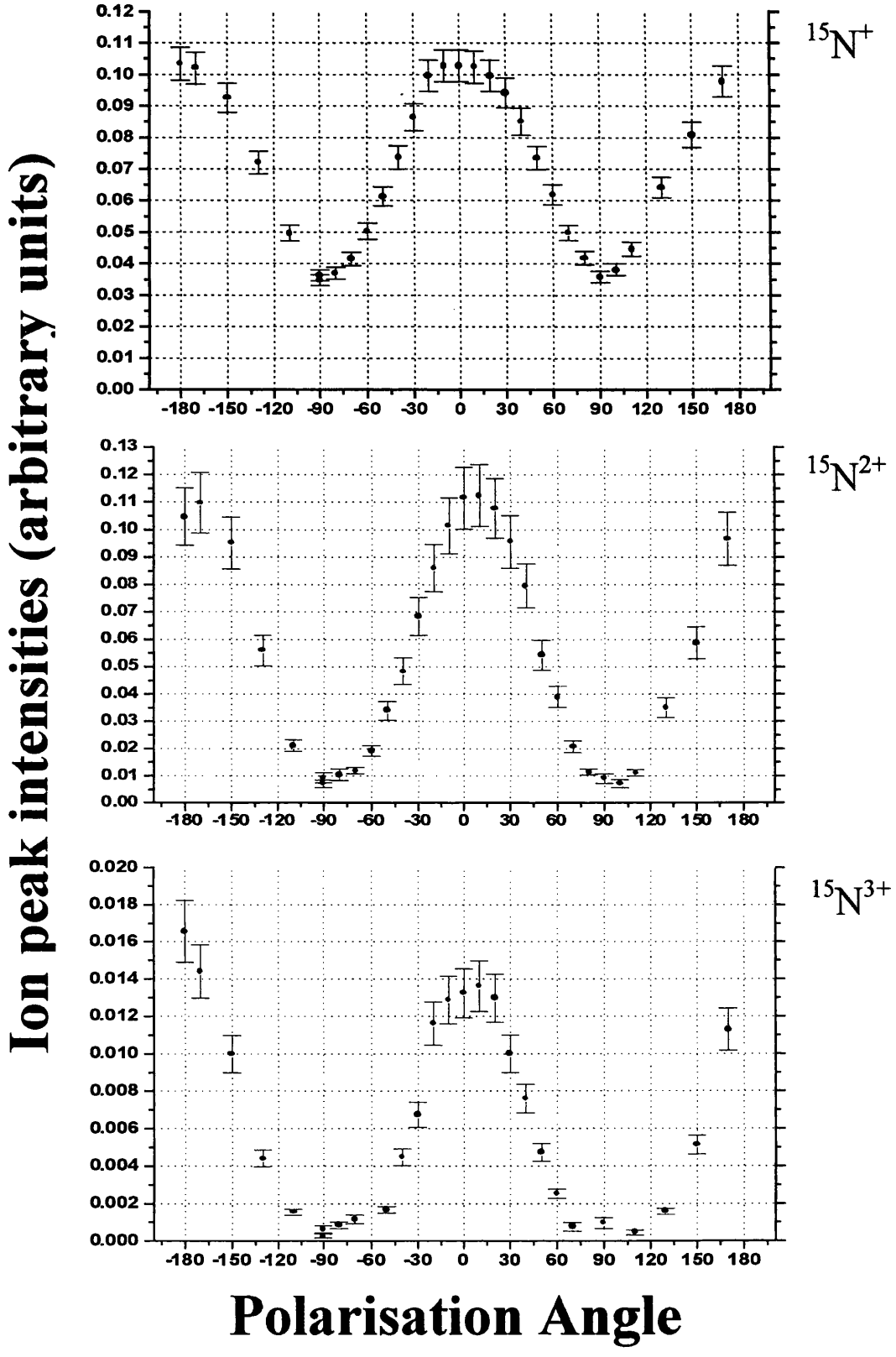

Figure 5.8 The angular distributions of the fragment $^{15}N^{p+}$ ($p \leq 3$) from labelled nitrous oxide are shown. Note that they are characteristic of those of a peripherally placed atom in a triatomic, as expected.

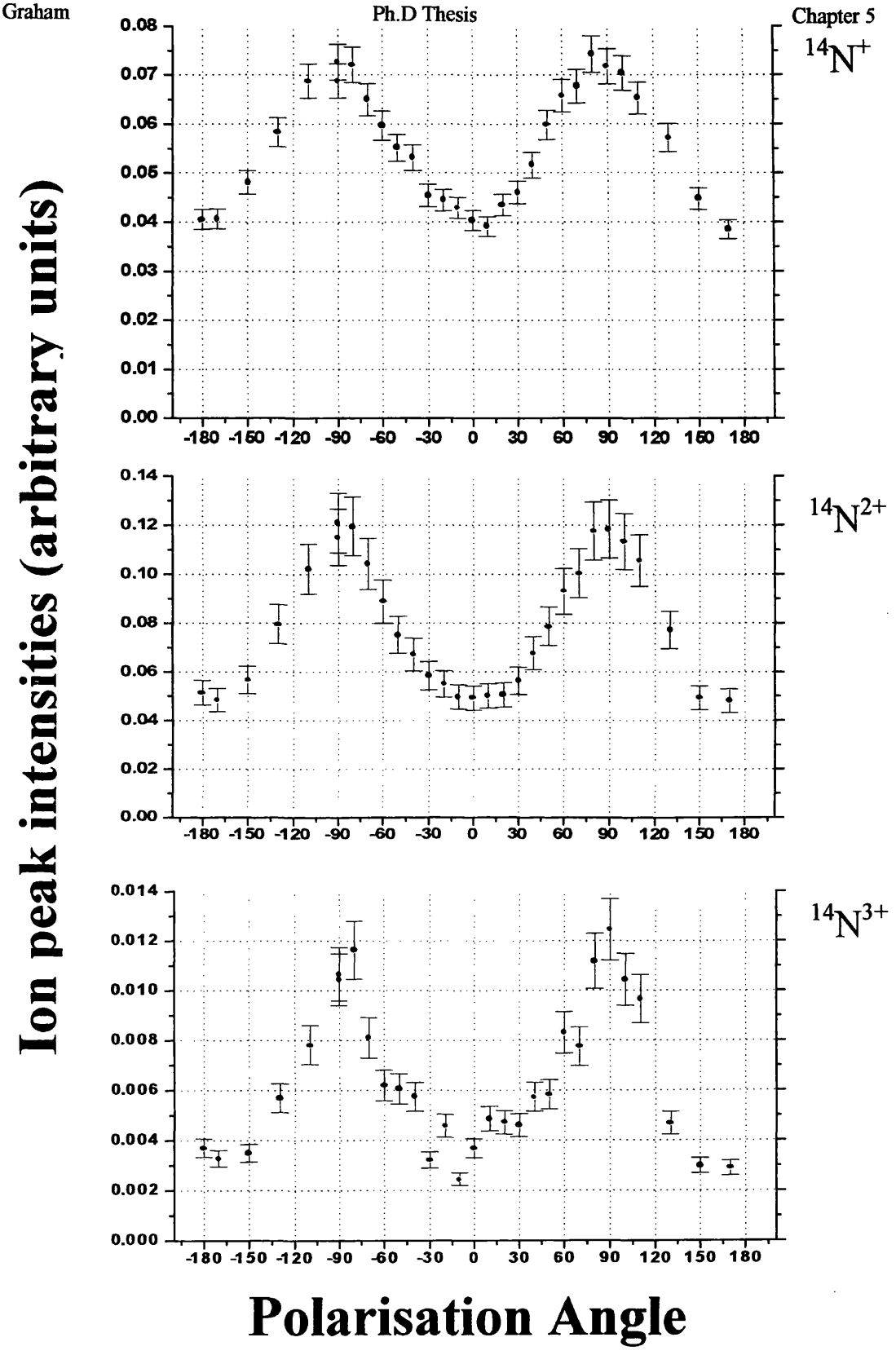

Figure 5.9 The angular distributions of the fragment $^{14}N^{m+}$ ($m \leq 3$) from labelled nitrous oxide are shown. Note that they are characteristic of those of a centrally placed atom in a triatomic, as expected.

of a linear triatomic implies that the molecule undergoes a bending of its structure in the intense field.

By measuring the differences in flight-times of the split peaks in the mass spectra of the ^{15}N- and ^{14}N-ions for the three charge states shown in figures 5.3 and 5.4, the energy imparted to the fragment ions in the Coulomb explosion of the parent was calculated in the parallel and perpendicular directions, respectively. The energy imparted (in eV) to the fragment ions was calculated using:

$$\varepsilon = 9.65x10^{-7} \frac{n^2 E^2 (\Delta t)^2}{8m} \tag{1}$$

where n is the charge state of the fragment ion of interest, E is the extraction field (V/cm), Δt is the difference in flight times of the split peaks (ns) and m is the ion mass (amu). In addition, from conservation of momentum and by taking a ratio of the velocities of the ions of the different charge states in the horizontal and vertical directions, the experimental value for the bond angle 2θ in figure 5.10 prior to dissociation was determined (see below) to be (143±3)°. The experimental kinetic energies for the peripheral ^{15}N ions for three different charge states are shown in Table 5.1. The (n, m, p) designation in Table 5.1 refers to the charge distribution carried away by the fragment ions. For example, (2,2,2) would mean the parent explodes to produce $^{15}N^{2+}$, $^{14}N^{2+}$ and $^{16}O^{2+}$.

The theoretical values for the energies imparted to the different ions were calculated using an invariant bond angle 140° and the bond lengths 1.126 and 1.186 Å, respectively. The total Coulomb repulsion (E_{Coul}) can be calculated using the equation:

$$E_{Coul}(R_{i,j})_{i=1,n} = \sum_{i<j} \frac{14.4 n_1 n_2}{|R_j - R_i|} \tag{2}$$

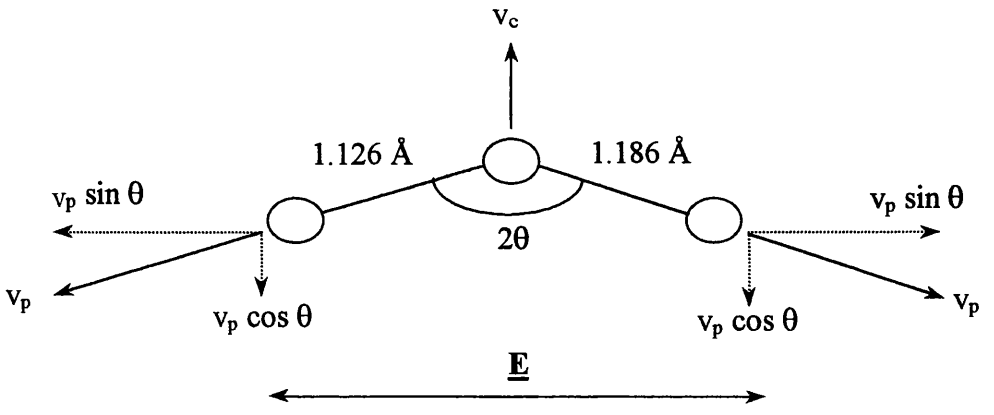

Figure 5.10 Schematic showing the Coulomb explosion process with the fragment ions ejected at velocity v_p for peripheral ions and v_c for the central ion.

Channel	Theoretical kinetic energy/(eV)	Experimental kinetic energy/(eV)	Calculated kinetic energy from ref. [40]
(1,1,1)	12.7	12.8±0.6	16
(2,2,2)	50.2	51.0±2.0	-
(3,2,3)	89.5	87.9±3.0	77
(3,3,3)	114.6		

Table 5.1. Theoretical and experimental kinetic energies for the peripheral $^{15}N^{p+}$ ($p \leq 3$) ions from the (1,1,1), (2,2,2), (3,2,3) and (3,3,3) dissociation channels. The experimental and theoretical energies more closely correspond for the (3,2,3) rather than the symmetric (3,3,3) channel.

where $R_{i,j}$ are the bond lengths and $n_{i,j}$ are the charges of the fragments i and j. These energies can be calculated for all the different charges possible in the Coulomb explosion. The theoretical Coulomb kinetic energy of a specific fragment ion, j, in the Coulomb explosion process is given by:

$$E_j = E_{Coul}\left(1 - \frac{m_j}{M}\right) \tag{3}$$

where E_{Coul} is given by Eq. 2 and is the total amount of energy released in the Coulomb explosion process, m_j is the mass of the fragment ion j, and M is the mass of the parent precursor.

These theoretical fragment ion kinetic energies for a number of different charge states are also given in Table 5.1. This invariance of the bond angle with respect to the charge state is similar to results presented by Cornaggia for CO_2 [12].

3.2.3 Molecular bond lengths and angle

To calculate the kinetic energy imparted to the fragment ions in the Coulomb explosion process, the difference in flight-times between initially forward- and backward-directed ions is measured from split ion peaks in the mass spectra. This time difference is then inserted into Eq. 1, to give the energy in eV.

For example:

To determine the kinetic energy of the doubly charged peripheral $^{15}N^{2+}$ ion:

Time difference, $\Delta t = 0.08$ μs. Therefore, for $\Delta t = 80$ ns and E = 500 V/cm:

$$E_{^{15}N^{2+}} = 9.65x10^{-7}\frac{q^2E^2(\Delta t)^2}{8m} = \frac{(2)^2(500)^2(80)^2}{8x(15)} = 51.47eV$$

From the energy, the velocity imparted can be calculated. As this will be derived from the split mass peaks, this velocity will be that of the component *along* the TOF axis, i.e v_p

sinθ. In the case of $^{15}N^{14}N^{16}O$, there are split peaks for the central ^{14}N ions, so their energy and velocity can be calculated also. The velocity is given by:

$$v = \frac{qE\Delta t}{2m}$$

For the peripheral $^{15}N^{2+}$, $v_p \sin\theta = 25548.9$ m/s, and for $^{14}N^{2+}$, $v_c = 17108.6$ m/s. From inspection of figure 5.10 and the conservation of momentum, the angle 2θ can be calculated. From conservation of momentum $2v_p \cos\theta = v_c$, therefore $v_p \cos\theta = 8554.3$ m/s. Thus, the angle 2θ can be calculated thus:

$$\frac{v_p \sin\theta}{v_p \cos\theta} = \frac{\sin\theta}{\cos\theta} = \tan\theta = \frac{25548.9}{8554.3} = 2.99$$

Hence, the angle θ = 71.5°, and so the molecular bond angle for $^{15}N^{14}N^{16}O$ prior to Coulomb explosion is 2θ = (143±3)°, for the case of doubly-charged fragment ions. Working in similar fashion, it turns out this angle is approximately equal to 140° for all fragment ion charge states observed in the mass spectra.

The correspondence between the theoretical and experimental kinetic energy of the fragment ions suggests that the molecules explode at the equilibrium internuclear distance of the neutral molecule (see figure 5.10). Furthermore, the (3,2,3) channel more closely resembles the experimental kinetic energy of the N^{3+} ion, suggesting it originates from the (3,2,3) rather than (3,3,3) channel. The calculated kinetic energies are similar to those quoted for labelled ($^{14}N^{15}N^{16}O$) nitrous oxide by Luk et al. [40]. They calculate energies of 16 eV and 77 eV for $^{14}N^{+}$ and $^{14}N^{3+}$, respectively.

The conclusion that the ion fragments at the equilibrium distance of the neutral molecule is in contrast with previous studies of diatomic and triatomic molecules [4, 6, 12] and suggests that dissociation occurs before the molecule can elongate to the critical distance, at which the ionisation rate is enhanced [50]. This is supported by Luk et al. [40] in their experiments with nitrous oxide and by Shimizu et al. with benzene [51]. The dissociation occurring at the equilibrium internuclear distances for both nitrous oxide and benzene

may be due to the double and triple bonds in N_2O and the inherently rigid structure of benzene. These features may make it difficult to ionise bonding electrons and hence the molecules do not change their structure significantly prior to dissociation. Further results on nitrous oxide using the covariance-mapping technique by Frasinski et al [52] suggest that the dominant fragmentation channel is $N^{2+}+N^{2+}+O^{2+}$ with a kinetic energy release of 38 eV, slightly less than the values shown in Table 5.1.

4. **Conclusions**

The angular distributions of fragment ions coming from Coulomb explosion of highly charged parent precursor states using linearly polarised femtosecond (fs) laser beams with an intensity of 10^{16} W cm^{-2} of both isotopically labelled ($^{15}N^{14}N^{16}O$) and unlabelled ($^{14}N_2O$) nitrous oxide were measured and presented herein. By comparing the mass spectra and angular distributions of fragments from labelled and unlabelled N_2O, earlier results performed on N_2O where the N-ion yield has maxima for both horizontal polarisation (0°/180°) and vertical polarisation (±90°) can now be explained unambiguously. By measuring the angular distributions for peripherally placed ions, it has been shown that $^{15}N^{p+}$ and $^{16}O^{n+}$ have maxima at 0° and 180° while the central $^{14}N^{m+}$ distribution has maximum ion yield at ±90°. These distribution patterns are therefore in accordance with those measured for peripheral and central fragment ions arising from Coulomb explosion of a triatomic in a femtosecond pulse laser studied by this and other groups. Hence, all initially linear triatomic molecules studied so far behave in the same way in an intense fs linearly polarised laser pulse. In addition, the anisotropy of the ^{14}N-ions provides evidence of the distortion (bending) of the initially linear parent in the intense laser field. The bond angle appears to be about (140±3)° regardless of the ionisation-state of the precursor. Studies of non-linear triatomics such as H_2O [53] and H_2S [44] suggest that the molecule is 'straightened out' in the field of an intense femtosecond laser. This, however does not seem to hold in the case of SO_2 according to both Cornaggia et al. [54] and Hishikawa et al. [6], who calculate the bond angle prior to dissociation to be 130°.

References

[1] Strickland D, Mourou G 1985 Opt. Commun., **56**, 219

[2] Corkum P, Ivanov MY, Wright JS 1997 Annual Review of Physical Chemistry, **48**, 387-406

[3] Vijayalakshmi K, Bhardwaj VR, Mathur D, 1997 J. Phys. B: At. Mol. Opt. Phys., **30**, 4065-4085

[4] Posthumus JH, Plumridge J, Thomas MK, Codling K, Frasinski LJ, Langley AJ, Taday PF 1998a J. Phys. B: At. Mol. Opt. Phys., **31**, L553-L562

[5] Hishikawa A, Iwamae A, Hoshina K, Kono M, Yamanouchi K 1998a Chem. Phys., **231**, 315-329

[6] Hishikawa A, Iwamae A, Hoshina K, Kono M, Yamanouchi K 1998b Chem. Phys. Lett., **282**, 283-291

[7] Lompre LA, Monot P, Auguste T, Mainfray G, Manus C 1993 Journal de Chimie Physique et de Physico-Chimie Biologique, **90**, 1275-1282

[8] DeWitt MJ, Levis RJ 1998 J. Chem. Phys., **108**, 7739-7742

[9] Talebpour A, Larochelle S, Chin SL 1997 Laser Physics, **7**, 851-857

[10] Normand D, Dobosz S, Lezius M, D'Oliviera P, Schmidt M 1997 I.O.P Conf. Series, **154**, 287-297

[11] Ivanov MY, Matusek DR, Wright JS 1996 Phys. Rev. A, **54**, 3235-3244

[12] Cornaggia C 1996 Phys. Rev. A, **54**, R2555-R2558

[13] Chelkowski S, Conjusteau A, Zuo T, Bandrauk AD 1996 Phys. Rev. A, **54**, 3235-3244

[14] Ilkov FA, Walsh TDG, Turgeon S, Chin SL 1995 Phys. Rev. A, **51**, R2695-R2698

[15] Kumar GR, Gross P, Safvan CP, Rajgara FA, Mathur D 1996a Phys. Rev. A, **53**, 3098-3102

[16] Kando AE, Meath WJ 1991 Molecular Physics, **74**, 113-129

[17] Loesch HJ, Remscheid A 1990 J. Chem. Phys., **93**, 4779-4790

[18] Loesch HJ, Steinkemeier F 1993 J. Chem. Phys., **98**, 9570

[19] Zewail AH 1996 Abstracts of Papers of the American Chemical Society, **211**, 153

[20] Vrakking MJJ, Stolte S 1997 Chem. Phys. Lett., **271**, 209-215

[21] Friedrich B, Herschbach D 1995 J. Phys. Chem., **99**, 15686-15693

[22] Mainos C 1996 Phys. Rev. A, **54**, 4226-4235

[23] Mathur D, Bhardwaj VR, Gross P, Kumar GR, Rajgara FA, Safvan CP, Vijayalakshmi K 1997 Laser Physics, **7**, 829-838

[24] Kumar GR, Gross P, Safvan CP, Rajgara FA, Mathur D 1996b J. Phys. B: At. Mol. Opt. Phys., **29**, L95-L103

[25] Rost JM, Griffen JC, Friedrich B, Herschbach DR 1992 Phys Rev. Lett., **68**, 1299-1301

[26] Safvan CP, Thomas RV, Mathur D 1998 J. Phys. B: At. Mol. Opt. Phys., **286**, 329-335

[27] Posthumus JH, Plumridge J, Codling K, Frasinski LJ, Langley AJ, Taday PF 1999 Laser Physics, **9**, 1-8

[28] Sanderson JH, Thomas RV, Bryan WA, Newell WR, Langley AJ, Taday PF 1998 J. Phys. B: At. Mol. Opt. Phys., **31**, L599-L606

[29] Graham P, Ledingham KWD, Singhal RP, McCanny T, Hankin S, Fang X, Smith DJ, Kosmidis C, Tzallas P, Langley AJ, Taday PF 1999 J. Phys. B: At. Mol. Opt. Phys., **32,** 5556-5574

[30] Posthumus JH, Plumridge J, Frasinski LJ, Codling K, Langley AJ, Taday PF 1998b J. Phys. B: At. Mol. Opt. Phys., **31**, L985-L993

[31] Hishikawa A, Iwamae A and Yamanouchi K 1999 J. Chem. Phys., **111**, 9971-8878

[32] Loison JC, Durand A, Bazalgette G, White R, Audouard E 1995 J. Phys. Chem., **99**,13591-13596

[33] Block PA, Bohac EJ, Miller RE 1992 Phys. Rev. Lett., **68**, 1303-1306

[34] Ellert CH, Corkum PB 1999 Phys. Rev. A, **59**, 5 R3170-R3173

[35] Couris S, Koudoumas E, Fotakis C 1998 Resonance Ionisation Spectroscopy (American Institute of Physics Conf. Proc. 9th Int. Symp.) (AIP Conf. Proc. 454) ed. JC Vickerman, I Lyon, NP Lockyer and JE Parks (Woodbury, NY: American Institute of Physics) pp 331-340

[36] Thompson MR, Thomas MK, Taday PF, Posthumus JH, Langley AJ, Frasinski LJ, Codling K 1997 J. Phys. B: At. Mol. Opt. Phys., **30**, 5755-5772

[37] Banerjee S, Kumar GR and Mathur D 1999 Phys. Rev. A, **60**, R3369-R3372

[38] Safvan CP, Vijayalakshmi K, Rajgara FA, Kumar GR, Marathe VR, Mathur D 1996 J. Phys. B: At. Mol. Opt. Phys., **29**, L481-L487

[39] Frasinski LJ, Codling K, Hatherly PA 1989 Science, **246**, 1029

[40] Luk TS, Moriarty RM, Awashti A, Boyer K, Rhodes CK 1992 Phys. Rev. A, **45**, 6744

[41] Bandrauk AD, Ruel J 1999, Phys. Rev. A, **59**, 2153-2162

[42] Bhardwaj VR, Vijayalakshmi K, Mathur D 1999 J. Phys. B: At. Mol. Opt. Phys., **32**, 1087-1095

[43] Ellert CH, Stapelfeldt H, Constant E, Sakai H, Wright J, Rayner DM, Corkum PB 1998 Phil. Trans. R. Soc. Lond. A, **356**, 329-344

[44] Graham P, Fang X, Ledingham KWD, Singhal RP, McCanny T, Smith DJ, Kosmidis C, Tzallas P, Langley AJ, Taday PF Laser and Particle Beams, *to be published*

[45] Ledingham KWD, Kilic HS, Kosmidis C, Deas RM, Marshall A, McCanny T, Singhal RP, Langley AJ, Shaikh W 1995 Rapid Commun. Mass Spectrom., **9**, 1522

[46] Wiley WC and McLaren IH 1955 Rev. Sci. Instrum., **26**, 1150

[47] Taday PF, Mohammed I, Langley AJ, Ross IN, Codling, K., Ledingham, K.W.D., Newell, W.R., Preston, S., Riley, D., Williams I 1998 Central Laser Facility, RAL Annual Report 1997/98, 179.

[48] Ledingham KWD, Singhal RP, Smith D, McCanny T, Graham P, Kilic HS, Peng WX, Wang SL, Langley AJ, Taday PF, Kosmidis C 1998 J. Phys. Chem. A, **102**, 3002-3005

[49] Wang S.L, private communication

[50] Posthumus JH, Giles AJ, Thompson MR, Codling K 1996 J. Phys. B: At. Mol. Opt. Phys., **29**, 5811-5829

[51] Shimizu S, Kou J, Kawato S, Shimizu K, Sakabe S, Nakashima N 2000 Chem. Phys. Lett., **317**, 609

[52] Frasinski LJ, Hatherly PA, Codling K 1991 Phys. Lett. A, **156**, 227

[53] Sanderson JH, El-Zein A, Bryan WA, Newell WR, Langley AJ, Taday PF 1999 Phys. Rev. A, **59**, 4 R2567-R2570

[54] Cornaggia C, Salin F, Blanc CL 1996 J. Phys. B: At. Mol. Opt. Phys., **29**, L749

Appendix – Calculating the bond lengths and angles of N_2O

To calculate the kinetic energy imparted to the fragment ions in the Coulomb explosion process, the difference in flight-times between initially forward- and backward-directed ions is measured from split ion peaks in the mass spectra. This time difference is then inserted into Eq. 1, to give the energy in eV.

Example:

To determine the kinetic energy of the doubly charged peripheral $^{15}N^{2+}$ ion:

Time difference, $\Delta t = 0.08\mu s$. Therefore, for $\Delta t = 80ns$ and $E = 500$ V/cm:

$$E_{^{15}N^{2+}} = 9.65x10^{-7}\frac{q^2E^2(\Delta t)^2}{8m} = \frac{(2)^2(500)^2(80)^2}{8x(15)} = 51.47eV$$

From the energy, the velocity imparted can be calculated. As this will be derived from the split mass peaks, this velocity will be that of the component *along* the TOF axis, i.e $v_p \sin\theta$. In the case of $^{15}N^{14}N^{16}O$, there is split peaks for the central ^{14}N ions, so their energy and velocity can be calculated also. The equation for velocity is given by:

$$v = \frac{qE\Delta t}{2m}$$

For the peripheral $^{15}N^{2+}$, $v_p \sin\theta = 25548.9$ m/s, and for $^{14}N^{2+}$, $v_c = 17108.6$ m/s. From inspection of figure 5.10 and the conservation of momentum, the angle 2θ can be calculated. From conservation of momentum $2v_p \cos\theta = v_c$, therefore $v_p \cos\theta = 8554.3$ m/s. Thus, the angle 2θ can be calculated thus:

$$\frac{v_p \sin\theta}{v_p \cos\theta} = \frac{\sin\theta}{\cos\theta} = \tan\theta = \frac{25548.9}{8554.3} = 2.99$$

Hence, the angle $\theta = 71.5°$, and so the molecular bond angle for $^{15}N^{14}N^{16}O$ prior to Coulomb explosion is $2\theta = 143°$, for the case of doubly-charged fragment ions. Working in similar fashion, it turns out this angle is approximately equal to 140° for all fragment ion charge states observed in the mass spectra.

Chapter 6

On the fragment ion angular distributions arising from a tetrahedral molecule

CHAPTER OVERVIEW

Utilising an ultraintense (10^{16} W cm^{-2}) femtosecond (fs) laser, the interaction of tetrahedral CH_3I with the linearly polarised laser is investigated. Both mass spectra obtained for horizontal and vertical polarisations and fragment ion angular distributions are presented. All fragment ion distributions are anisotropic and peaked along the direction corresponding to collinearity of the laser electric field with the time-of-flight (TOF) mass spectrometer axis. The angular distributions from the dissociation of the parent precursor ions are all of similar widths, which would imply a geometric, as opposed to dynamic, alignment. The distribution for m/z = 18 peak is also measured and shows anisotropy, suggesting that it is due mainly to I^{7+}. There is present in the CH_m group a CH_2^{2+} ion peak that also has a distribution similar to those measured for the other ions. This mass peak is the only multi-charged ion in this group. As the CH_3I molecule is initially tetrahedral, the angular distributions suggest that the molecule behaves as a diatomic, with the fragment ions being ejected along the field direction, with the C-I bond breaking being the dominant dissociation channel. This is the first time that the angular distributions from a tetrahedral molecule have been presented for fs laser pulses only and in the case of CH_3I, for fragments other than CH_3^+ and I^+.

1. Introduction

The ability to control the relative spatial positions and orientations of groups of molecules is important enough to warrant intensive investigation into the various ways envisioned to achieve this. One such technique to align molecules termed the "brute-force" method [1], uses strong static electric fields to align and orient the molecules. The disadvantages of this however, is that this method is only applicable to polar molecules. A more versatile technique is to use intense linearly polarised laser pulses to effect an alignment. The interaction with any permanent dipole moment averages to zero over an entire optical cycle and only the dipole moment induced by the laser field contributes to the alignment. Hence, both non-polar and polar molecules can be manipulated. The alignment is described by a $\cos^n(\theta)$ dependence, where n describes the degree of alignment which increases as the parent charge-state and hence the torque acting on the parent increases. The electric field vector subtends an angle θ with the molecular axis.

Angular distributions of fragment ions that arise from photo-dissociation of the parent ion can be measured as a function of polarisation angle to determine the preferred direction of ejection of fragment ions with respect to the laser field. The resulting distribution may be due to a molecular alignment as described above, in some cases. However, the anisotropy observed in the distributions may alternatively be interpreted as an ionisation-rate dependent upon the angle made with the laser field [2]. In this scenario, the dissociative ionisation is enhanced when the molecular axis is collinear with the laser field. In order to discriminate between these two effects, a non-resonant intense nanosecond pulse from a Nd:YAG laser was used to align neutrals, whilst a fs laser pulse was employed to dissociate the parent (during the ns pulse) and then ionise the fragments for detection [3-5]. In this way, if the fragment ions show an anisotropy it can only be due to the parent aligning with the (ns) laser field. Various molecules such as CS_2 [3, 4], I_2 [3, 5] and CH_3I [3, 4, 6, 7] have been aligned using a nanosecond laser beam and the degree of alignment was somewhat controlled by increasing the intensity of the ns aligning pulse. However, as the rotational period for CH_3I^+ is likely to be of the order of picoseconds, alignment within a 50fs pulse is not thought likely, even with the intense

laser fields used here. This could be determined from a series of angular dependence studies taken at different fs laser intensities. Thus, in this case the anisotropies observed are interpreted to arise from an angle-dependent ionisation-rate, which can also provide a picture of the molecular structure via potential energy curves (i.e a barrier to ionisation).

The anisotropic ionisation rate of molecules can provide a picture of molecular structure (bond length and angles), but in certain conditions it may be possible to spatially align certain classes of molecules, i.e. those of low angular moment of inertia or large polariseability. This allows a degree of control of chemical reactions. For example, Machholm et al. [8] has shown that by using a two-pulse scheme it is possible to control the orientation of a hetero-diatomic as well as its alignment and the dissociation or its reactivity with another reactant would be enhanced in one orientation compared to the opposite orientation. Furthermore, the branching ratio of photodissociation can be controlled using aligned molecules [5]. This is also observed in comparison of mass spectra at horizontal and vertical polarisations for CH_3I as well as other molecules such as CS_2 and N_2O [9, 10].

In the above experiments that utilise ns pulse lasers, both the fragment ion direction and kinetic energy can be determined, through using ion-imaging techniques. For the present case TOF mass spectrometry is used, which can give the direction. If split fragment ion mass peaks exist in the mass spectra, it becomes possible to calculate the kinetic energy also [10]. This information can then be used to determine bond angles and lengths prior to explosion of the parent ion.

The angular distributions of fragment ions from several small molecules have previously been studied in both the ps and fs regime. These studies have looked at the dynamics of both diatomic and initially linear and non-linear triatomic molecules. In the ps regime Safvan et al. [11] shows that angular distributions of fragment ions from CS_2 exhibit anisotropies and also suggests that this is due to pendular states. Also, the data presented in [11] seems to show that under diffuse molecular conditions, the CS_2 is aligned in the 35 ps pulse. The molecular sample is diffuse in the experimental apparatus used here and

alignment of CS_2 could not be repeated in experiments with CS_2 by expanding the fs pulse out to ps durations [9].

Spatial alignment of bent triatomic molecules was also studied by Bhardwaj et al. [12], who looked at H_2O, NO_2 and SO_2, again in the ps regime. The O ion fragment is found to be isotropic, markedly anisotropic and weakly anisotropic, respectively and the results are explained by the parallel and perpendicular components of the induced dipole moments in the bent structure. The bent H_2O molecule was also studied by Sanderson et al. [13] using ion-imaging. It is found that the O ion is isotropic, but is anisotropic once the variation in detector collection volume with ion momentum is taken into account. Furthermore, comparing with Monte Carlo calculations they are able to present data on the bond lengths and angles. The bonds in H_2O seem to stretch in the laser field when the molecular axis is along the field direction and that the H_2O molecule experiences bond angle softening within the laser pulse. The molecule is slightly straightened out in the field compared with the field-free bond angle.

Laser-induced alignment of several diatomic molecules such as H_2, N_2 and I_2 has been studied using pump-probe techniques by Posthumus et al. [14-16]. These experiments show that the lighter H_2 and N_2 molecules are dynamically aligned but that the more rotationally inertial I_2 is not [14, 15]. This is reflected in the $\cos^{22}\theta$ fit to the experimental H_2 data. The molecules that lie along the laser field are also stretched in the laser pulse to about twice the field-free equilibrium internuclear distance, at which point the ionisation rate increases significantly as the barrier to ionisation is lowered [15]. Furthermore, it is shown for H_2 that Coulomb explosion occurs on the leading-edge of the laser pulse and bond-softening occurs on the trailing-edge [16].

This chapter presents data that seeks to extend further the still new and on-going investigation of small molecule-laser interactions. It is the first time that the angular distributions of a tetrahedral molecule have been presented using fs laser pulses only and for fragments other than singly-charged methyl and iodine ions from the CH_3I molecule.

These experimental results extend previous work done [9, 10, 17] for triatomic molecules to more exotic molecular structures.

2. Experimental

The experimental apparatus is described in detail in chapter 2. Briefly, CH_3I vapour was admitted effusively from an inlet system into a high-vacuum chamber to a pressure of about 10^{-6} Torr. Extraction fields of ~500 V/cm were used, and the mass resolution was 200 at 100 Da. Ions were detected with a Thorn-EMI electron multiplier. The mass spectra were obtained and stored using a LeCroy 9344C 500 MHz digital oscilloscope.

The laser system is based on the chirped pulse amplification technique [18] and produces pulses of about 7 mJ of 790 nm at 10 Hz. The laser pulse entered the TOF perpendicular to the effusive molecular beam and was focussed using a f/10 spherical mirror mounted inside the chamber on a x-y-z manipulator. The polarisation of the laser was rotated by placing a $\lambda/2$ wave-plate in the beam, located in front of the quartz window of the TOF vacuum chamber.

3. Results

3.1 mass spectra

Results from the study of the tetrahedral CH_3I molecule are presented for a laser intensity of about 10^{16} W cm^{-2} and 50 fs pulse duration. Mass spectra for polarisations both collinear with (horizontal) and orthogonal to (vertical) the TOF axis are shown in figures 6.1 and 6.2, respectively. The parent ion is prominent in each spectrum, but sizeable fragment ion peaks are also present. The same ion peaks are seen in both spectra, with somewhat greater abundance of lower mass-to-charge fragments for horizontal polarisation. Peaks for I-ions up to I^{6+} and I^{7+} are observed, along with CH_m^+ ($m \leq 3$), H^+ and C^{p+} ($p \leq 3$) peaks. In both the horizontal and vertical polarisation mass spectra, it can be seen that there is a peak at about m/z = 18 and it is thought (see below) that this has a contribution from an I^{7+} ion and possibly a small impurity H_2O parent ion.

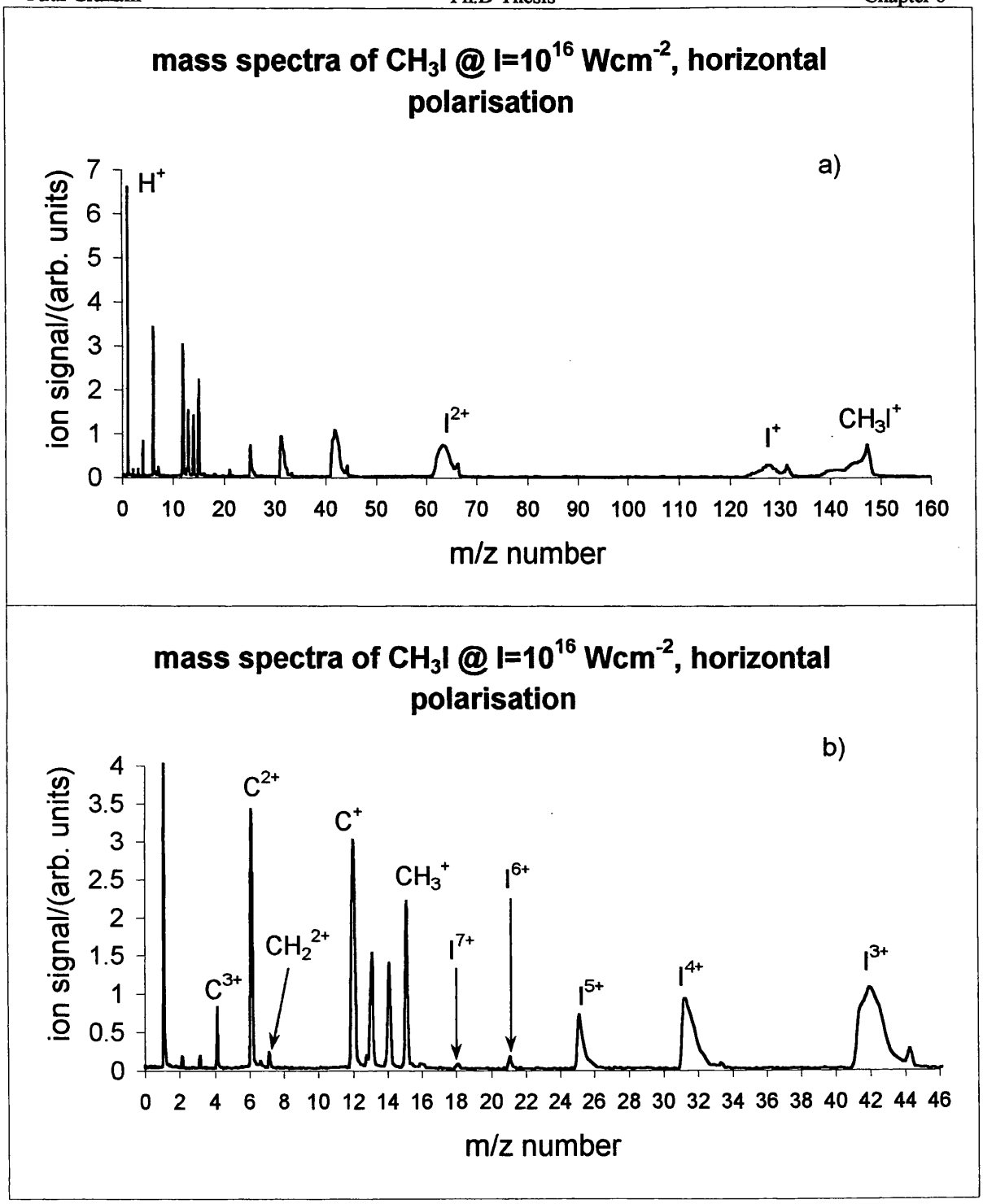

Figure 6.1 Mass spectrum of CH_3I for horizontal polarisation at a laser intensity of 10^{16} W cm^{-2} and 50fs, (a) main spectra and (b) expansion of the low-mass region

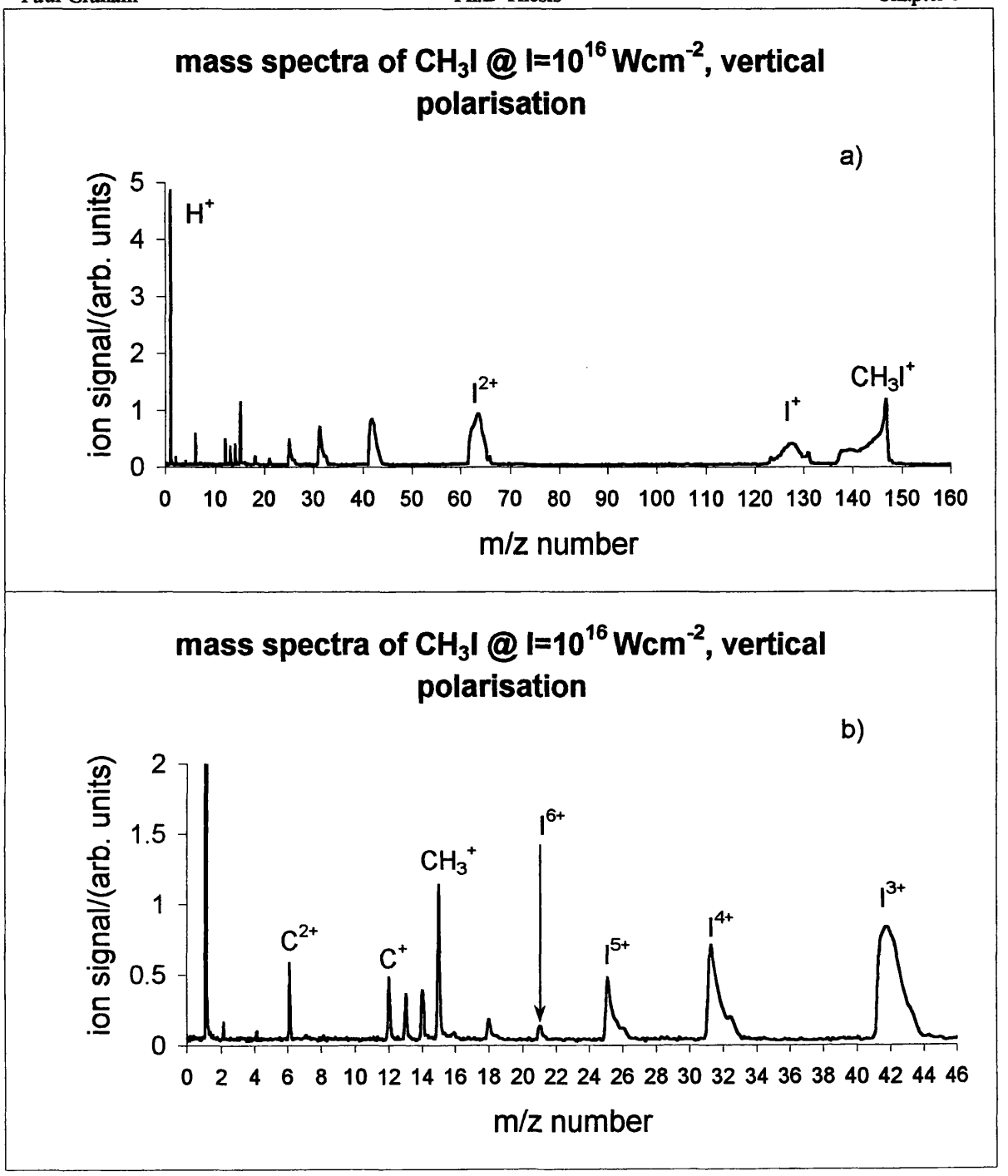

Figure 6.2 Mass spectrum of CH_3I for vertical polarisation at a laser intensity of 10^{16} W cm^{-2} and 50fs, (a) main spectra and (b) expansion of the low-mass region

A peak corresponding to the CH_2^{2+} fragment ion is also present in the CH_m group in the mass spectra. This ion is the only multiply charged fragment observed in the CH_m group, for reasons that are not well understood. Since the pulse duration is only 50 fs, it is unlikely that significant post-dissociative ionisation occurs. Hence, the parent molecule is highly ionised and then Coulomb explodes to produce these multiply charged fragment ions. Although multiply-charged parent ions are not directly observed, their role in the production of I^{n+} ($n \leq 7$) and C^{p+} ($p \leq 4$) is inferred. As expected since there is three per molecule, the H^+ ion peak is the largest in the spectra.

In the mass spectra, figures 6.1 and 6.2, the I^{n+} peaks narrow with increasing charge. This is due to production of the higher charged ions in physically smaller more intense portions of the beam and a narrowing of the acceptance volume of the TOF for highly charged ions imparted with large velocity. However, the dominant mechanism is bond-breaking of the C-I bond, giving rise to I-ions and CH_m ($m \leq 3$) or C and H ions. This may be concluded from the lack of CI^+ ions. Also, mass spectra of CH_3I at lower laser intensities of about 10^{14} W cm^{-2} consist of only the three mass peaks of CH_3I^+, I^+ and CH_3^+ [19]. Studying the photodissociation of state-selected CH_3I using ns-REMPI at wavelengths in the range 340-220 nm and ion-imaging, Eppink et al. [20] determined the C-I bond strength to be 2.41 eV, which is less than twice the photon energy used here.

3.2 Angular distributions

The angular distributions of fragment ions from CH_3I are shown in figures 6.3, 6.4 and 6.5. The parent ion distribution is characteristically isotropic and is not shown. As in the case for the peripheral ions from CS_2 and CO_2 [9] and N_2O [10], the I-ion distributions are a maximum in the direction of collinearity between the polarisation and TOF-axis, (0° and 180°). The ion intensities for I^+, I^{2+} and I^{3+} are similar, whereas the maximum peak intensity drops quickly for the I^{4+}, I^{5+}, I^{6+} and I^{7+} ion peaks. This is due to the very high intensities required to produce these highly charged fragment ions and the small volume and short portion of time of the laser beam where this high peak intensity is reached. Intact parent ions and low-kinetic energy fragment ions with small charge are produced

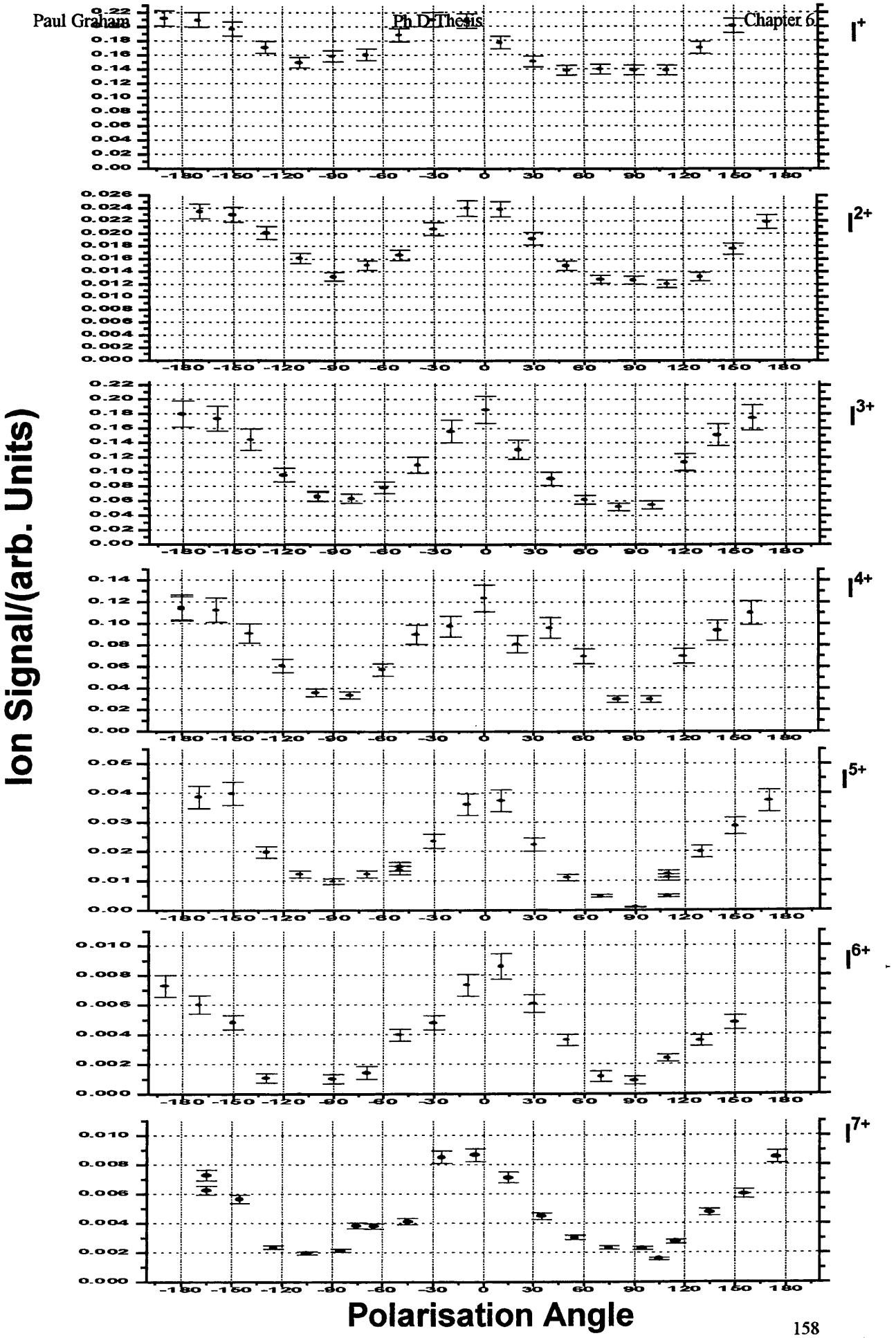

Figure 6.3 Angular distributions of fragment iodine ions, showing a maximum when the laser polarisation and TOF-axis are collinear. The distribution widths are similar and anisotropy increases with charge-state

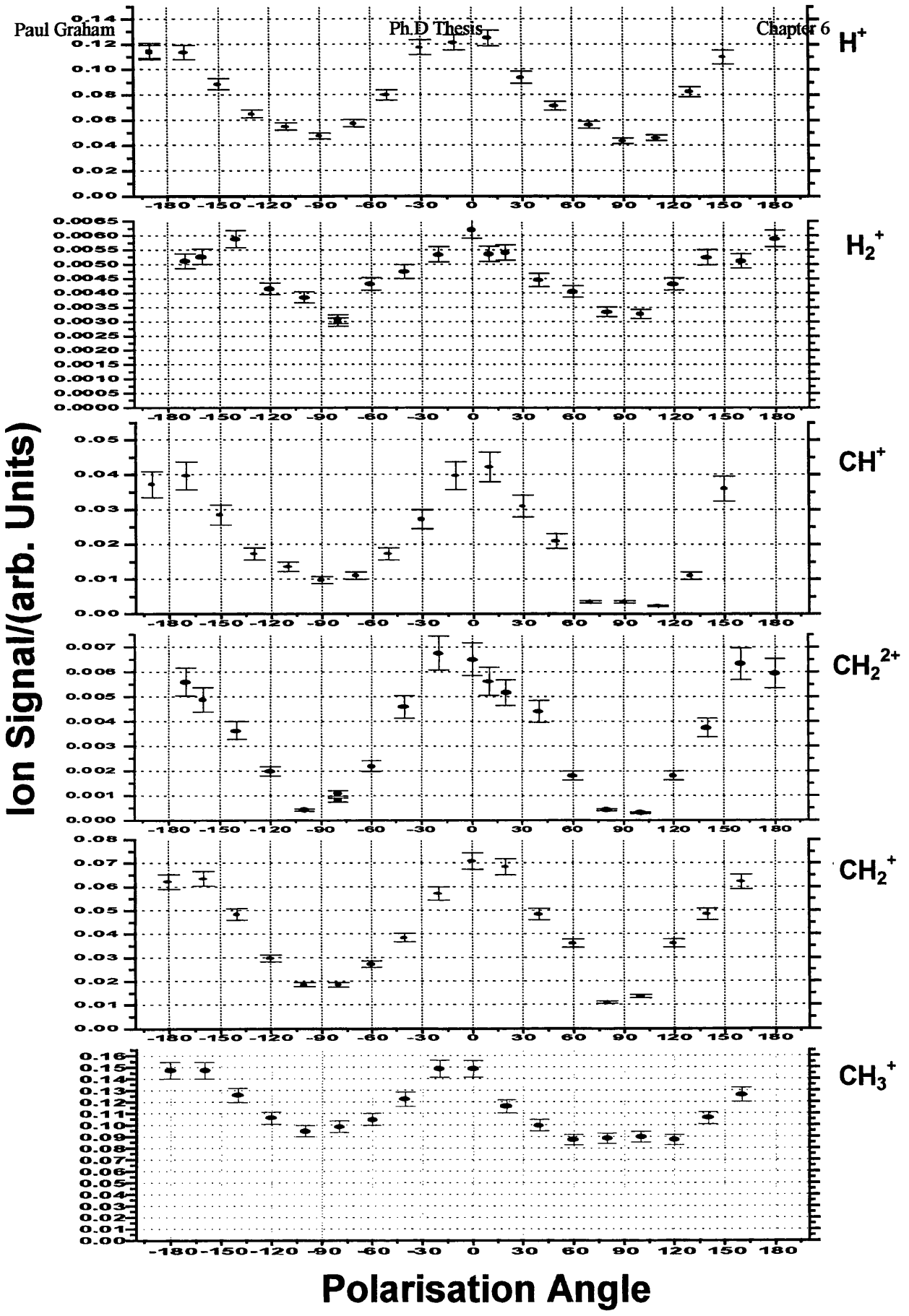

Figure 6.4 Angular distributions of the H^+, CH_m^+ ($m \leq 3$) and CH_2^{2+} fragment ions. These fragment ions are peaked in the direction of collinearity between the laser field and the TOF-axis

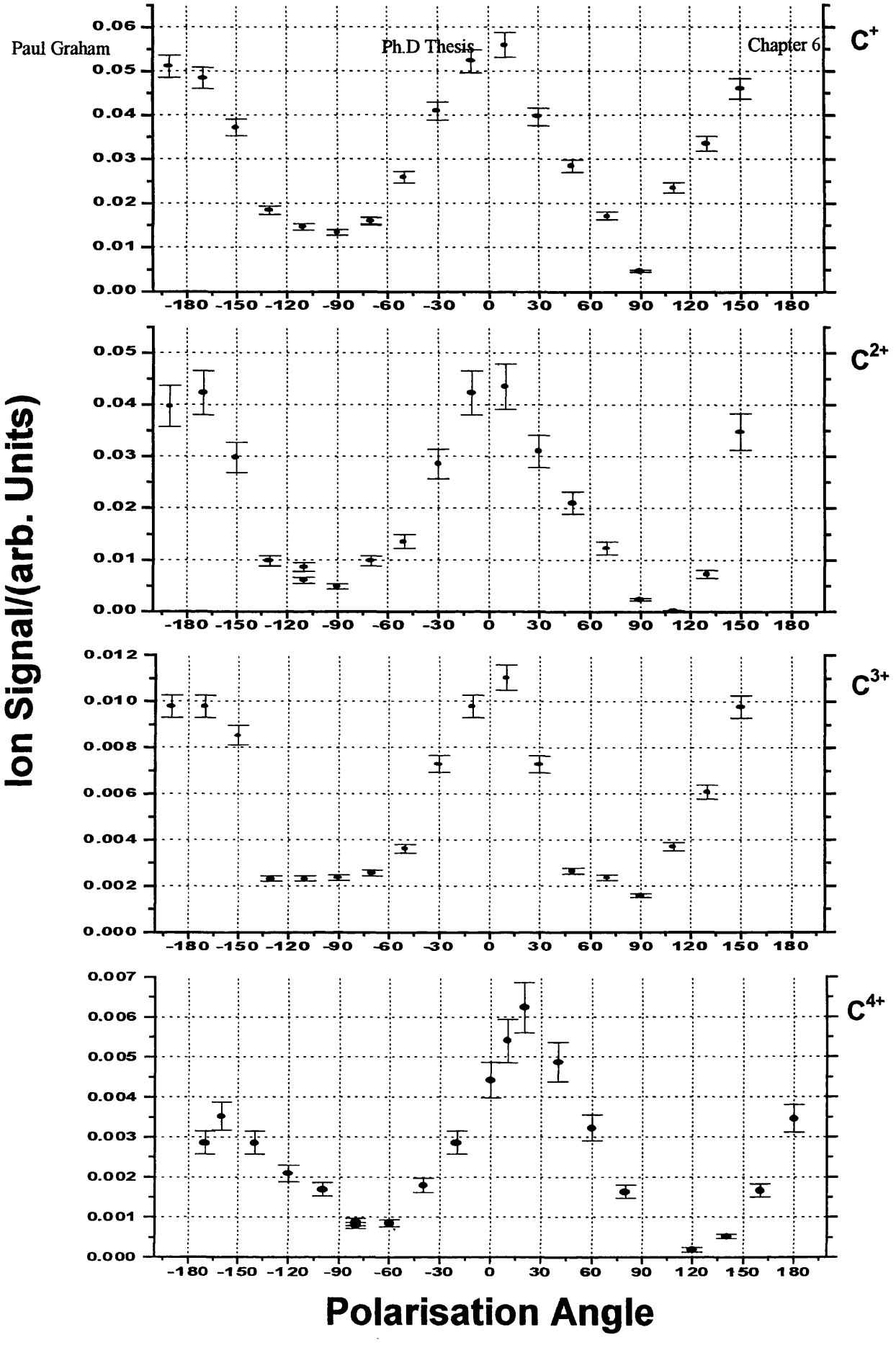

Figure 6.5 Angular distributions of fragment C^{p+} ($p \leq 4$) ions showing a maximum when the laser polarisation and TOF-axis are collinear. The distribution widths are similar and the anisotropy increases with charge-state

in the low-intensity wings, whereas highly charged fragment ions ejected with significant kinetic energy are produced in high-intensity portions of the laser pulse.

All the I-ion distributions are similar in appearance, with comparable widths and the minimum ion intensity occurring at ± 90°. The distributions of I^{n+} are shown in figure 6.3. Due to its large moment of inertia, the CH_3I molecule might not rotate significantly during the 50 fs pulse duration, despite the strong electric field strength of the laser pulse. Thus, the similar widths of the distributions support the hypothesis that the observed anisotropy of the fragment ions results solely from the enhancement of the ionisation and dissociation process when the molecule is initially oriented along the laser polarisation direction. This observation is similar to that described for the CS_2 molecule [9]. Alignment would be more pronounced as the charge-state or polarisability of the parent increases, which would result in a narrowing of the distributions. When the C-I bond orientation is along the TOF-axis, the I-ions resulting from Coulomb explosion are efficiently detected resulting in the maximum in the distribution.

A further feature of the I-ion distributions to note is an isotropic component that gradually disappears as the charge-state increases. This suggests that the lesser-charged fragments are likely to come from 'soft' fragmentation of parent precursors giving rise to low kinetic energy fragments that are within the acceptance volume of the TOF. The higher-charged fragments come from highly charged and unstable transient states of the parent molecule, undergoing Coulomb explosion, which results in higher kinetic energies. This decreases the probability of detecting them when the molecule is orthogonally orientated to the TOF-axis, reducing the isotropy of the distribution. Furthermore, the molecules oriented perpendicular to the laser field will not achieve as high ionisation-states compared to those molecules initially oriented along the field, reducing the ion yield at vertical polarisation. There is a significant anisotropic component to note in the distribution for the m/z = 18 mass peak. This peak could of course be due to a small H_2O impurity ion. However, this anisotropy in the distribution would not arise if this were the case. Thus, this peak is predominantly due to I^{7+} that results from Coulomb explosion of the precursor ion at such high intensities.

Distributions of CH_m^+ ($m \leq 3$), CH_2^{2+}, H^+ and C^{p+} ($p \leq 4$) ions were also measured, as shown in figures 6.4 and 6.5, and their appearance are similar to those for the I-fragments. This is an interesting observation. In neutral CH_3I, the H-C-H bond angle is 111.4° and dissociation of this molecular geometry would result in a broader distribution for H^+ ions, due to the ejection of slow ions, regardless of molecular orientation with respect to the laser polarisation, compared to I^+ ions. It may even result in a distribution that would be a maximum for vertical polarisation. It is postulated that the CH_3I molecule is thus distorted, through a reduction of the H-C-H bond angle in the presence of the intense laser field prior to dissociation, since the hydrogen and iodine distributions are similar in width. Consequently, the molecule behaves as a diatomic with the I-atom at one end. As each of the ions are peaked along the 0°/180° direction, the CH_3I ion may be excited to a state with a structure akin to that of the extreme turning point of an umbrella-mode vibration [7].

Comparing the distributions for the CH_m ions, it can be seen that they become more anisotropic as the H index decreases, i.e. CH is more anisotropic than CH_3 (say). This may be because the CH_3I molecular ion is more violently dissociated when it is highly charged and hence the methyl part is also broken up with greater kinetic energy, accounting for the increased anisotropy. The distribution of CH_2^{2+} is also more anisotropic than for CH_2^+, in similar fashion to all fragment ions of charge greater than or equal to two. That there is a small anisotropy in the distribution for H_2^+ implies that two H atoms can bond together before being detached from the parent precursor, lending support to the CH_3I molecule umbrella mode being excited.

As the C-ion distributions (figure 6.5) are similar to those for the I-ions, being markedly anisotropic with equal widths for all charge-states, this further indicates that the molecule acts as a diatomic, with the detached H-ions having negligible effect. As the charge on both the C and I atoms increase, this will consequently increase the kinetic energy released as the Coulomb repulsion increases in the explosion process.

Conclusion

In conclusion, mass spectra and angular distributions of fragment ions arising from the tetrahedral CH_3I molecules were studied at laser intensities of about 10^{16} W cm^{-2} and in the fs-regime (50 fs). It can be seen in the mass spectra that there is a difference in branching ratio of the fragment ions, i.e. there is a difference in fragment ion yield, between horizontal and vertical polarisation [5]. The ionisation of the parent precedes the fragmentation and that the fragment ions arise either from 'soft' dissociation or Coulomb explosion of the methyl iodide precursor. The lack of multiply charged parent ions shows that the parent ion is unstable for charges greater than one. It is further shown that, for molecules such as CH_3I, the observed anisotropies of the fragment ion distributions most likely arise from an enhanced ionisation and dissociation when the molecular axes are parallel to the laser field. The fragment ions are most efficiently detected along the TOF axis for horizontal laser polarisation. It is postulated that the molecules assume an umbrella-like structure in the intense laser field, prior to dissociation and behaves as a pseudo-diatomic molecule. The I-ion peaks up to I^{7+} are observed for the first time and show a marked anisotropy. The anisotropy observed in the distribution for the m/z = 18 peak proves unambiguously that I^{7+} is produced and detected. Peaks for C-ions up to C^{4+} are also observed. A CH_2^{2+} peak is present and is the only multi-charged ion in the CH_m group. The origin of this ion, and the lack of other multi-charged ions in this group, is unknown. Furthermore, most of the fragment ions possible from the parent CH_3I molecule are present in the mass spectra, with the C-I bond breaking channel dominant. This indicates that the parent ion can access most dissociation channels.

References

[1] Loison JC, Durand A, Bazalgette G, White R, Audouard E 1995 J. Phys. Chem., **99**, 13591-13596

[2] Ellert CH and Corkum PB 1999 Phys. Rev. A, 59, R3170-R3173

[4] Larsen JJ, Sakai H, Safvan CP, Wendt-Larsen I, Stapelfeldt H 1999 J. Chem. Phys., **111**, 7774

[5] Larsen JJ, Wendt-Larsen I, Stapelfeldt H 1999 Phys. Rev. Lett., **83**, 1123

[6] Sugita A, Mashino M, Kawasaki M, Matsumi Y, Gordon RJ, Bersohn R 2000 J. Chem. Phys., **112**, 2164

[7] Samartzis PC, Bakker BLG, Parker DH, Kitsopoulos TN 1999 J. Phys. Chem. A, **103**, 6106-6113

[8] Machholm M and Henriksen NE 1999 J. Chem. Phys., **111**, 7, 3051

[9] Graham P, Ledingham KWD, Singhal RP, McCanny T, Hankin SM, Fang X, Smith DJ, Kosmidis C, Tzallas P, Langley AJ, Taday PF 1999 J. Phys. B: At. Mol. Opt. Phys., **32**, 5557-5574

[10] Graham P, Ledingham KWD, Singhal RP, McCanny T, Hankin SM, Fang X, Tzallas P, Kosmidis C, Taday PF, Langley AJ 2000 J. Phys. B: At. Mol. Opt. Phys., **33**, 3779

[11] Safvan CP, Thomas RV, Mathur D 1998 Chem. Phys. Lett., **286**, 329-335

[12] Bhardwaj VR, Safvan CP, Vijayalakshmi K, Mathur D 1997 J. Phys. B: At. Mol. Opt. Phys., **30**, 3821-3831

[13] Sanderson JH, El-Zein A, Bryan WA, Newell WR, Langley AJ, Taday PF 1999 Phys. Rev. A, **59**, R2567

[14] Posthumus JH, Plumridge J, Frasinski LJ, Codling K, Langley AJ, Taday PF 1998 J. Phys. B: At. Mol. Opt. Phys., **31**, L985-L993

[15] Posthumus JH, Plumridge J, Codling K, Frasinski LJ, Langley AJ, Taday PF 1999 Laser Physics, **9**, 1-8

[16] Posthumus JH, Plumridge J, Taday PF, Sanderson JH, Langley AJ, Codling K, Bryan WA 1999 J. Phys. B: At. Mol. Opt. Phys., **32**, L93-L101

[17] Graham P, Fang X, Ledingham KWD, Singhal RP, McCanny T, Smith DJ, Kosmidis C, Tzallas P, Langley AJ, Taday PF 2000 Laser and Particle Beams, *at press*

[18] Strickland D and Mourou G 1985 Opt. Commun., **56**, 219

[19] CH_3I mass spectra *unpublished*

[20] Eppink ATJB and Parker DH 1999 J. Chem. Phys., **110**, 832

Chapter 7

Conclusions and Future Development

Chapter Overview:

This chapter describes some of the conclusions made based on the results obtained and presented in previous chapters of the thesis. It also outlines the potential future developments, how these may come about through recent advances in ultra-fast laser pulse technology, and any possible future areas of application.

7.1 Introduction

This chapter will detail the conclusions that can be made in light of the experimental data obtained during the course of the author's Ph.D research, presented in chapters 3-6. Further possible developments in the fields of trace chemical detection and identification utilising femtosecond laser mass spectrometry and that of molecular dynamics in intense femtosecond laser beams, based on the experiments performed herein and work carried out by other groups, will be discussed and also highlight possible areas of application.

7.2 Conclusions and Future Work

7.2.1 Trace chemical detection/identification

The field of detecting atoms and molecules using lasers has been on-going for several decades. A variety of detection techniques have been developed including resonance ionisation mass spectrometery (RIMS) and resonance-enhanced multiphoton ionisation (REMPI) for gas-phase samples and secondary ion mass spectrometry (SIMS) for solid-phase samples. These early detection techniques were important for the development of the field but were only partly successful as they relied on nanosecond lasers for the ionisation process. However, nanosecond pulses are long compared to the time-scale of dissociation of the larger and thermally labile molecules that are environmentally important. Hence, oftentimes a parent ion could not be detected at any laser intensity, which is important for the identification of the molecule under investigation.

The development of femtosecond lasers allowed the detection of molecular ions without this problem. The pulse duration is short compared to the dissociation time-scale and so a rapid up-pumping of the molecular states occurs until the ionisation continuum is approached before dissociation can occur. Thus identification is possible, as the parent ion is now detectable.

The utilisation of femtosecond lasers to the ionisation process has made possible the detection technique termed femtosecond laser mass spectrometry (FLMS), which has proved itself in a series of experiments [1, 2] to be very powerful, as it provides

sensitive detection limits as well as being universal. Previous detection techniques such as REMPI utilise the resonance effect when the laser wavelength corresponds to the electronic energy level differences of the molecule. However, this method is very selective and the laser wavelength must be tuned exactly to that required for resonance. If the energy levels are known for the molecule under investigation, this facilitates identification as well as increased sensitivity.

The experiments detailed in this thesis extend those previously performed by He and Becker et al. [3-6] at laser intensities in the range of 10^{12}-10^{14} W cm^{-2} with picosecond lasers. The relative sensitivity factors (RSF – see chapter 3) of a variety of small molecules were measured as a function of laser intensity, using pulses of 50fs duration and laser intensities of the order of 10^{15}-10^{16} W cm^{-2}. The RSFs of all the molecules studied were shown to tend to unity as the intensity was increased. The consequence of this is that the ionisation process within a well-defined interaction region is 100% saturated, i.e. all molecules present are ionised. This gives very low detection limits. Furthermore, the ionisation is able to reach saturation regardless of molecular properties such as ionisation potential and laser characteristics. Therefore, the technique is both sensitive and universally applicable. The parent ion is detectable allowing identification for analytical applications and fragment ions are also present to facilitate elucidation of molecular structure prior to dissociation.

The experimental results shown in chapter 3 are obtained from small molecules in the gas-phase (or vapour pressure in the case of CS_2 and CH_3I liquid samples). The power of the FLMS technique was proved, but further work could be done on other types of samples such as in the solid-phase using laser ablation, for example biomolecules and 'real-world' environmental samples like soil and exhaust particulates. This would also test the limits of applicability of the technique to very massive molecules of interest (e.g. explosives, drugs, hazardous and environmentally damaging chemical species), which are likely to be those most frequently analysed. Thus, if FLMS could be extended to this operating range for both gaseous and solid-phase, it could become the technique of choice for trace chemical analysis, in determining the sample and its concentration. It has been

shown previously [17] that results for molecules as massive as m/z = 3000 can be obtained.

Experiments analogous to those detailed in chapter 3 but with solid-phase samples (polycyclic aromatic hydrocarbons or PAHs) have recently been carried out at the RAL facility, but the results have yet to be analysed. The ablation was performed by a long-pulse (ns) Nd:YAG laser. However, the thermal heating of the sample could be significant with a ns pulse. This may affect the results obtained and lead to dissociation of the parent molecule, especially if it is thermally labile. Therefore, a further evolution of the technique would be to develop a 'pump-probe' set-up whereby a fs laser both ablates and ionises the sample (figure 7.1) to obtain more accurate and reliable results.

7.2.2 Molecular response to intense femtosecond laser fields

The field of manipulating molecules in an external electric field, such as that from an intense laser source is a relatively new one, but it is one that could have far-reaching implications and open up new areas of application. As such, intensive research is being carried out to devise and refine techniques to control the manipulation, and study the molecular responses, of a variety of important molecules in intense laser fields [7-12].

The experiments performed at RAL (chapters 4, 5 and 6) concentrated on investigating the angular distribution of fragment ions that result from the Coulomb explosion of some small molecules, in linearly polarised 50fs duration pulses and a laser intensity range of 10^{15}-10^{16} W cm^{-2}. This laser intensity range is such that the molecule has its electrons stripped off rapidly, and hence is in a highly charged transient state prior to significant dissociation occurring.

For linearly polarised laser beams, those molecules that have the bond axis initially perpendicular to the polarisation vector of the laser field will be ionised to a lesser degree. The molecule behaves in an 'atom-like' way, with effective ionisation potential equal to that required to ionise the molecule in this configuration. Molecules with the bond axis collinear with the polarisation vector will be more efficiently ionised to higher charge-states as the laser field distorts the molecular

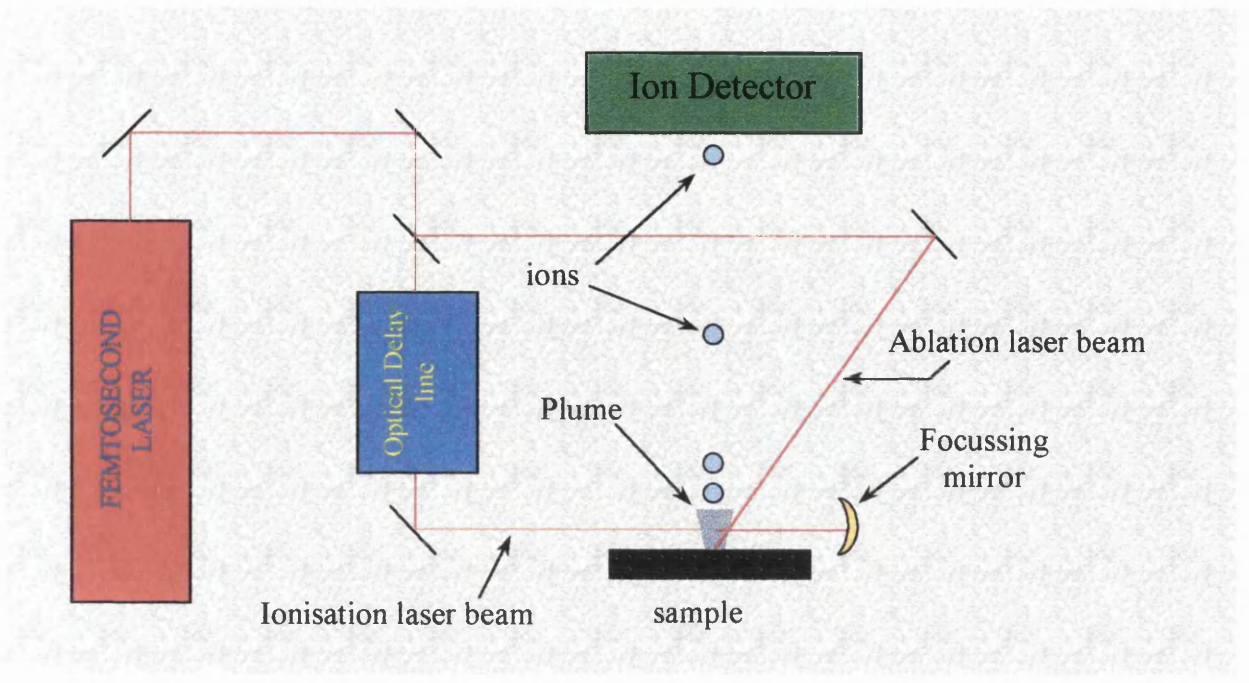

Figure 7.1 A pump-probe experimental set-up, whereby a single fs laser pulse is used to both ablate a sample and ionise the ejected plume for detection of ions in a mass spectrometer.

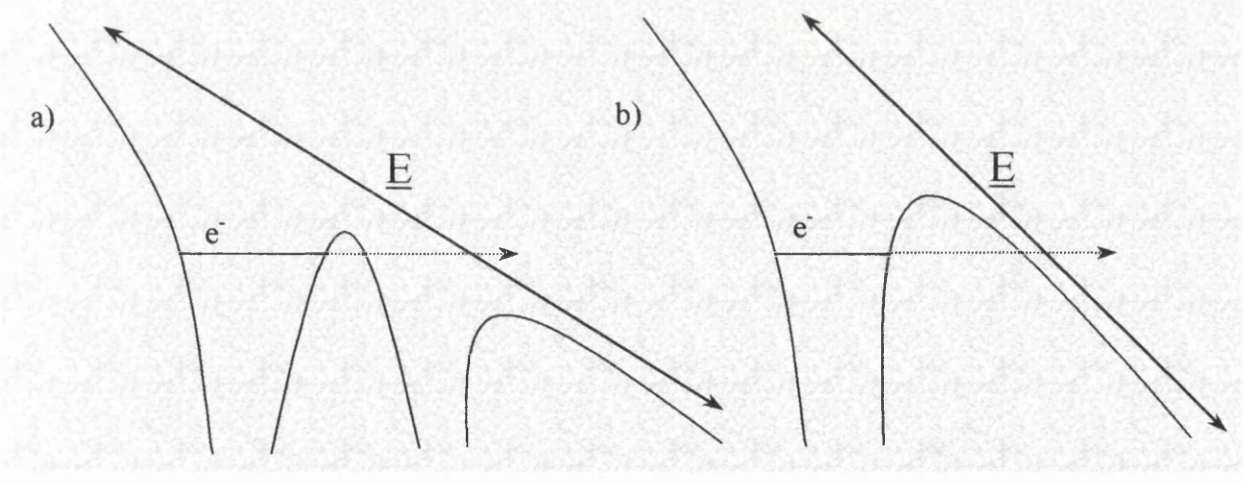

Figure 7.2 The resulting potential energy curves of a diatomic (in this case) when a laser pulse is applied. In a) the intensity is sufficient for electron tunneling to occur; whereas in b), the laser intensity is not sufficient and the electron is unable to tunnel or overcome the barrier to ionisation

potential energy curves sufficiently to suppress the barrier to ionisation (figure 7.2). This can occur while still near equilibrium internuclear distances, or the molecule can elongate in the external field of the laser, which again lowers the barrier. At a critical internuclear distance of typically twice equilibrium, the ionisation rate becomes a maximum and highly ionised states are reached just prior to dissociation. At an elongated internuclear distance, laser-induced electron localisation occurs and the electron can no longer tunnel its way between nuclei. The electron instead climbs over or tunnels through to the continuum. This leads to enhancement of ionisation and is termed charge-resonance enhanced ionisation [13].

The molecular dissociation is also more efficient if the molecule is collinear with the laser field. This is because of the increase in Coulomb repulsion between nuclei when the transient molecule attains a highly charged state. Furthermore, as mentioned above, if the molecule can elongate within the laser pulse, then the electron is localised on one of the nuclei and so no longer binds them together leading to dissociation. This happens more effectively when the molecular bond is along the polarisation vector.

Both the ionisation and dissociation of molecules is hence enhanced if both the molecular bond and polarisation are collinear. This therefore, leads to an anisotropy in the angular distribution of fragment ions. The angular distribution of a majority of fragment ions coming from the molecules studied, show significant anisotropy. This leads to the conclusion that either the molecules within the interaction region show only enhancement of ionisation/dissociation as described above, or that they are also aligned with the laser field, within the pulse duration. It is difficult to distinguish between the two effects from the type of data shown in chapters 4, 5 and 6. Several experiments have been performed to do this, such as aligning neutrals instead of ions with a long-pulse from a Nd:YAG [14], using circularly polarised laser light [15] and using ion-imaging [16].

For the alignment of molecules, one would expect that the torque exerted by the laser field would increase as the parent charge-state increases. This would manifest itself as a narrowing of the fragment ion angular distributions that originate from highly-charged precursor states. However, only several of the distributions from the

lighter triatomics studied show this characteristic. All parent ion distributions and a few fragment ion distributions show total isotropy. This implies that they have negligible kinetic energies as expected for the parent ions, and that the fragment comes from a 'soft' fragmentation. As the charge-state of the precursor molecule and hence the kinetic energy of the fragment ions released increases, the isotropic component of the anisotropic angular distributions decreases.

The Coulomb explosion gives rise to ejected fragment ions possessing high kinetic energies, which gives rise to split peaks of the ion in the mass spectrum. From this splitting the kinetic energies can be calculated. For the triatomic molecules investigated, the molecular bond lengths and angles can be determined. It is found that, contrary to the model of molecular elongation in the intense laser field, the parent ion dissociates at near-equilibrium internuclear distances. Furthermore, for linear triatomics (CS_2, N_2O and CO_2) the molecules are slightly bent when subjected to the intense laser field. The bond angle appears to remain constant for all charge-states. A consequence of this would be that the peripheral atomic ions are ejected along the polarisation direction whereas the central atomic ion would be ejected in an orthogonal direction. As can be seen from the results obtained, this is indeed what is observed. For the initially bent H_2S triatomic molecule however, it is concluded that it is straightened out when subjected to the intense laser field, as the central S ions are all isotropic. This was also concluded for H_2O [18], but does not seem to hold for SO_2 according to both Cornaggia et al. [19] and Hishikawa et al. [20] who calculated the bond angle prior to dissociation to be 130°.

Future research in this field is required to detail the necessary conditions for alignment of certain molecules and to control this degree of freedom. By controlling the orientation of the molecular geometry would enable control of photochemical reaction rates. By aligning with a relatively long-pulse (e.g pico- or sub-picosecond) the alignment process and subsequent dissociation can be probed with shorter femto- or sub-femtosecond pulses.

In collaboration with a d.c static field, an intense laser can be used to control the head vs. tail orientation of a molecule (figure 7.3). This can be used to deposit

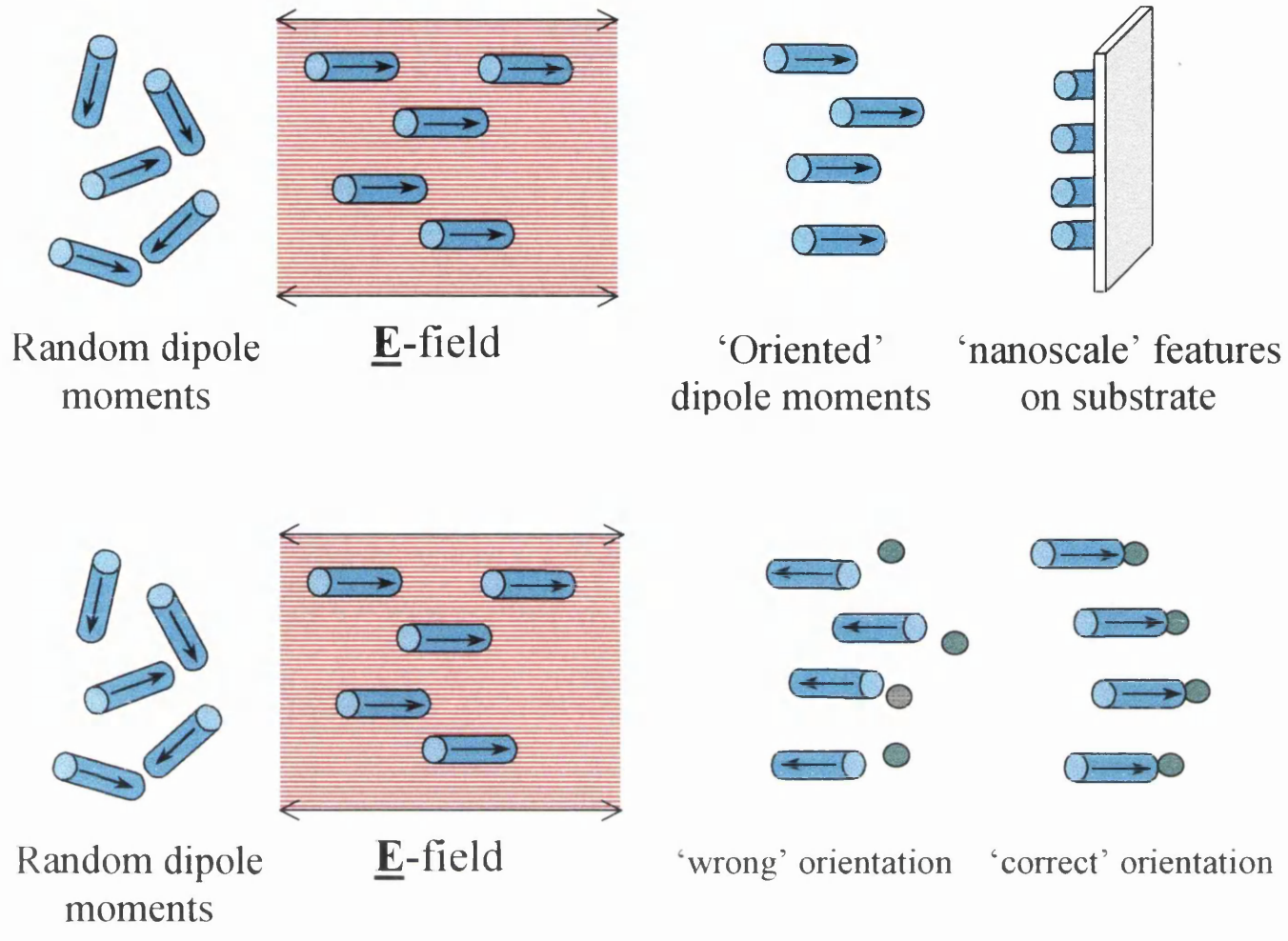

Figure 7.3 Only properly 'oriented' dipole moments can participate in a chemical reaction, e.g. joining with atoms to form molecules

molecular films or nanoscale features on a substrate. This would provide materials with pre-designed mechanical and optical properties and could be important in the field of medicine for designing new drugs. Furthermore, certain chemical reactions progress more efficiently depending on the relative orientations of the reactants involved. Accessing and manipulating the degrees of freedom may also control the evolutionary path of chemical reactions by coherent control, using e.g. shaped ultrashort optical pulses.

References

[1] Fang X, Ledingham KWD, Graham P, Smith DJ, McCanny T, Singhal RP, Langley AJ, Taday PF 1999 Rapid Commun. Mass Spectrom., **13**, 1390

[2] Ledingham KWD, Smith DJ, Singhal RP, McCanny T, Graham P, Kilic HS, Peng WX, Langley AJ, Taday PF, Kosmidis C 1999 J. Phys. Chem., **103**, 2952; Ledingham KWD, Kilic HS, Kosmidis C, Deas RM, Marshall A, McCanny T, Singhal RP, Langley AJ, Shaikh W 1995 Rapid Comm. Mass Spectrom., **9**, 1522

[3] He C, Basler J, Paul A, Becker CH 1996 J. Vac. Sci. Technol., **A14**, 1433

[4] He C and Becker CH 1996 Current Opinion in Solid State and Material Science, **1**, 493

[5] Becker CH and Hovis JS 1994 J. Vac. Sci. Technol., **A12**, 4

[6] He C, Basler J, Becker CH 1997 Nature, **385**, 797

[7] Normand D, Lompre LA, Cornaggia C 1992 J. Phys. B: At. Mol. Opt. Phys., **25**, L497

[8] Strickland DT, Beaudouin Y, Dietrich P, Corkum PB 1992 Phys. Rev. Lett., **68**, 2755

[9] Posthumus JH, Plumridge J, Frasinski LJ, Codling K, Langley AJ, Taday PF 1998 J. Phys. B: At. Mol. Opt. Phys., **31**, L985

[10] Larsen JJ, Sakai H, Safvan CP, Wendt-Larsen I, Stapelfeldt H 1999 J. Chem. Phys., **111**, 7774; Sakai H, Safvan CP, Larsen JJ; Hilligsoe KM, Hald K, Stapelfeldt H 1999 J. Chem. Phys., **110**, 10235

[11] Friedrich B and Herschbach D 1999 J. Chem. Phys., **111**, 6157

[12] Graham P, Ledingham KWD, Singhal RP, McCanny T, Hankin SM, Fang X, Smith DJ, Kosmidis C, Tzallas P, Langley AJ, Taday PF 1999 J. Phys. B: At. Mol. Opt. Phys., **32**, 5557

[13] Bandrauk AD, Ruel J 1999 Phys. Rev. A, **59**, 2153

[14] Sakai H, Safvan CP, Larsen JJ, Hilligsoe KM, Hald K, Stapelfeldt H 1999 J. Chem. Phys., **110**,10235

[15] Ellert C, Corkum PB 1999 Phys. Rev. A, **59**, R3170

[16] Samartzis PC, Kitsopoulos TN 1997 J. Phys. C. A, **101**, 5620

[17] Becker CH and Wu KJ 1995 J. Am. Soc. Mass Spectrom., **6**, 883

[18] Sanderson JH, El-Zein A, Bryan WA, Newell WR, Langley AJ, Taday PF 1999 Phys. Rev. A, **59**, R2567

[19] Cornaggia C, Salin F, Blanc CL 1996 J. Phys. B: At. Mol. Opt. Phys., **29**, L749

[20] Hishikawa A, Iwamae A, Hoshina K, Kono M, Yamanouchi K 1998 Chem. Phys. Lett., **282**, 283